A VERSATILE TURNING CENTRE WITH MULTI-MICROPROCESSOR CONTROL

by

Orhan Behic Alankus, B.Sc., M.Sc.

June 1982

A thesis submitted for the degree of Doctor of Philosophy of the University of London and for the Diploma of Membership of the Imperial College.

Mechanical Engineering Dept
Imperial College
London SW7

ABSTRACT

The advance of microprocessor technology has made possible very high computing power at comparatively low cost. As a consequence in some conventional machines, it has become economic to replace high cost mechanical elements with electrical systems controlled by microprocessors. Essentially, this means that the design of any complex mechanical or electromechanical system needs to be reassessed, machine tools being a good example.

The main objectives in this work were firstly to carry out this reassessment for a machine tool and to analyse the state of the art of machine tool design and secondly the investigation of the existing design techniques and procedures and their use in assessing the design of the machine tool structures and components. While carrying this out, a design methodology was to be developed and applied to produce an optimum outline design for a machine tool which would be versatile enough to make full use of a new multi-microprocessor control system. The overall design was to be low cost and to be suitable for both small workshops and bigger industrial plants. A turning centre with considerable milling and cross drilling capabilities was taken as a basis to satisfy these requirements. In the design, versatility, modularity, standardization and wide use of micro-processor technology are the basic criteria.

The specification is based on a small scale market survey. Reinforced concrete has been chosen for the machine bed on the basis of cost and high damping capacity. The existing static and dynamic analysis methods have been reviewed and detailed reinforcement calculations have been performed using finite element analysis. The stiffness and long term stability of the structure have been considered in detail. Dynamic characteristics of the bed and the bed-slideway assembly have been determined using finite element methods. Existing types of slideways have been reviewed and that best suited for the application incorporated. Drive systems were analysed and a servo drive selection algorithm devised. Hydraulic systems and their microprocessor control were considered in more detail and experiments related to this field carried out. The feasibility of existing tool wear measurement and adaptive control methods are discussed and two routines which are independent of cutting conditions are put forward. Finally, some future research work involving the use of microprocessors in active control of machine tool structures is proposed.

ACKNOWLEDGEMENTS

The author would like to thank Dr R D Hibberd and Dr C B Besant for their constant support, encouragement and irreplaceable supervision throughout the project. He also wishes to thank Emeritus Prof A L L Baker for his help and invaluable advice on the field of reinforced concrete.

The finite element program used during the project was prepared by Mr D Hitchings. The author is grateful to Mr D Hitchings for his help on the use of the program. The author also extends his thanks to Dr C L Tan for his permission to use the BIE program and the valuable help he gave.

The author would like to acknowledge the support and useful advice of Mr G Allerton of Cessna Fluid Power Division and Mr R D Harris of Hydrostatic Transmissions Ltd in the field of hydraulics.

Some of the experimental rigs in this project could not be built without the help of Mr L Eggleston, Mr P Wilson, Mr J Lawrence and Mr T G Thomas. The author very much appreciates their help and support.

The author would also like to thank the Scientific and Technical Research Council of Turkey for sponsoring him throughout the project.

Finally, the author would like to express his thanks to Laura Willis for her immaculate typing.

TABLE OF CONTENTS

Page

Page

Page

LIST OF TABLES

Table *Page*

LIST OF FIGURES

Figure *Page*

Figure *Page*

Figure *Page*

CHAPTER 1

MACHINE TOOL DESIGN

1.1 General

The typical machine shop of the late 1920's was a jungle of leather belts and steam driven line shafts. The scene has completely changed today; however, the change was not revolutionary but rather a result of gradual development of machine tool design influenced by the developments in parallel fields. One example of this is the development of tungsten carbide tools in the late 1920's. Tungsten carbide could remove metal more than five times faster than did the best available tool steel. However, the high removal rates caused problems such as severe vibration and deflection in the machine structures. Overcoming these problems was not simply a matter of strengthening the structure and drive trains. Overall machine design had to be reviewed and designers turned to the now well established automobile industry for help in solving their problems.

The design of gearboxes was one area where technology transfer from automobiles was particularly rewarding. High-strength automotive gears made of hardened nickel-chromium steel were adapted to machine tool drives to make higher speeds and power transmission possible. The higher speeds also caused vibration and chatter in sleeve-bearing supported spindles. So ball and roller bearings,by this time,widely used in automobiles were adapted to machine tool spindles. Lubrication of the new gear boxes was another field where automotive technology was employed.

There were other developments enforced on machine tools by the introduction of tungsten carbide; because cutting speeds are so critical for the efficient operation of carbide cutting tools, a method of quick and simple speed changing had to be developed. The so-called preselector gearbox, introduced in 1934, answered the need. Based on the operation of limited-slip friction clutches, the gearbox was able to change speeds so smoothly in full cut that the point of change could not be detected on the workpiece. The tremendous cutting power of carbide tools presented machine designers with an unusual problem: disposing of the swarf. To solve this problem, chip breakers were developed, and the cutting-tool angles were adjusted in such a way that chips flowed away at right angles. In addition, machine beds and guideways had to be redesigned to be rigid under heavy cutting loads while still allowing free passage of potentially damaging swarf. The solution was a bed with a deep inverted vee section, protected by accurately fitted covers. Also, guideways were machinedand finished on precision grinding machines instead of being scraped by hand.

The second biggest spur on the machine tool design came during the Second World War. The aircraft industry had requirements that could not be satisfied by common mass-production techniques. The industry generally relied on small batch production, required high accuracy, and used unusual metals that required special machining techniques.

The solution to this problem came with development of the copying principle. The use of templates or master forms to control movement of a cutting tool is an old idea. However, the technique is difficult to apply to heavy-duty metal cutting because such machining imposes heavy loads on the tracing stylus. Hydraulic or electrical control systems developed in the early forties were used successfully to solve this problem.

After the war, the emphasis was on automation. One of the most important consequences of this concept was that it fostered the development of powered control systems. With the emphasis on automation, hydraulic and pneumatic systems became faster, stronger and more reliable. However, it was the electric limit switch that really blossomed during this era. As automation grew, limit switches were applied to such tasks as controlling motion, preventing double feeds and pile ups, and shutting down machines when necessary.

Automation eventually led to the development of large transfer systems. With this development came the requirement for a variety of standardized, quick-change tooling systems. They also triggered the development of control systems that indicated when each tool should be replaced.

The next big step in machine tool design came with the introduction of Numerical Control (NC) and Computer Numerical Control (CNC).

The effect of NC and CNC on machine tool design is described below.

1.2 NC and CNC: Their Effect on Machine Tool Design

The idea of numerical control is to make machines directly 'understand' the numbers which actually define the dimensions of the workpieces. Numerical control as it is known today was developed by John Parsons who conceived of a way to produce helicopter-blade templates by calculating air foil coordinates on an electric tabulator, and then feeding the data points manually to a boring machine. His ideas were developed further at the Massachusetts Institute of Technology Servomechanisms Laboratory and the first practical commercial NC systems were introduced in 1955. The system was based on a paper tape that fed calculated positioning data to a so-called "computing director." The director converted the input into time-controlled electrical command signals that were recorded on magnetic tape. This tape was run through a control unit that commanded servo-mechanisms to position the cutting head, with motion verified through feedback circuits (18). The use of complicated control circuits in these systems has caused some downtime problems associated with control failures. This led to the development, 1968, of a control concept called Direct Numerical Control (DNC).

In DNC, a computer controls the machine tool directly, bypassing punched tape input. Because large computers were about 30% more reliable than the in-machine controls, this arrangement provided the reliability required. Furthermore, the computer could be time shared, and could therefore operate more than one machine at a time.

Meanwhile, a concept called Computer Numerical Control (CNC) was being developed. First introduced in 1970, CNC uses one standard control for different types of machine tools; software adapts the control to specific machine requirements. In CNC, each machine contains its own computer. The advantage of CNC is that it does not require the large software expense of DNC, therefore it is more economical.

Development of NC and CNC have created some new problems for machine tool designers. The existing machine tools were not versatile and robust enough to make the full use of NC and CNC. It had long been known that milling machines, for instance, could perform a number of different jobs if only the proper tool were installed.

The introduction of NC has enabled the multi-function machine tools - machining centres - to be implemented. However, the development of machining centres was not easy; it required extensive work on tool changers, holders and storage arrangements.

When numerical control was first implemented on machine tools, it was found that a manually operated machine tool produced better parts than a numerically controlled machine tool of the same construction. The reasons for this observation were quite obvious. A manually operated machine tool has an intelligent source for error compensation namely the operator. The NC machine tool can only compensate for an error that is detected and communicated to the control unit. Structural compliance, vibration and other aspects of mechanical design cannot be easily or economically monitored. For this reason, an NC machine is designed to be stronger, stiffer and to perform to a more accurate standard than its conventional counterpart.

Also, the NC machine elements must be capable of performing accurately under high accelerations and decelerations. Mechanical inaccuracy such as backlash, wind-up and deflection which tend to produce instability, must be reduced to levels not required for manually operated machines. Additionally, it is very important to decrease the friction in drive systems and slideways and to have a constant coefficient of friction. All these requirements have triggered the use of some special machine elements such as recirculating ball screws or machine slides using low friction materials or rolling element linear bearings.

After the basic problems were solved at least to a reasonable degree, the next step was the introduction of an optimisation process to improve the operational characteristics of NC and CNC machine tool systems. Two distinct methods of optimization are 'adaptive control' and 'machinability data prediction.' Although not yet fully developed the intention of these methods is to ensure that the machining operations are carried out under the optimum conditions and also to monitor and in some cases to compensate for process variables such as workpiece-tool air gaps, material property variations, wear and tool deflection.

Another very important effect of NC and CNC is on the machine tool shapes. The importance of thermal deformation in the new high accuracy machine tools coupled with the high metal removal rates has forced the designers to find ways of easy chip removal. This for example has led to slant bed design for turning centres.

These developments in machine tool design could not take place if it were not for the recent advances in electronic technology. The huge NC controls of 1950s based on vacuum-tube technology have in less than twenty years shrunk to a single cabinet. Development in medium-scale and large-scale integration has continued and after the introduction of mini-computers, it has led to the so-called third industrial revolution, - microprocessors -.

1.3 Microprocessors and Their Effect on Machine Tool Design:

The microprocessor can be regarded as a universal integrated circuit (IC): an IC with fixed circuitry, but capable of being adapted by any user to meet the needs of his particular application. This flexibility creates an immense market which makes it ideal for mass production resulting in cheap products. Today it is possible to find microcomputers which are more powerful than a mini-computer for only a fraction of the price.

Therefore it will be possible to arrive at a cheaper system simply by replacing the minicomputers in the CNC machine tools with microcomputers. But the advantages gained by microcomputers are more far-reaching than that.

The classic minicomputer approach used in CNC machine tools has been to have a central powerful computer which performs many tasks on a time division basis (figure 1.1). However, the evolution of microcomputers has made distributed processing control an economic proposition. The distributed processing system avoids the monolithic software packages associated with a centralised system

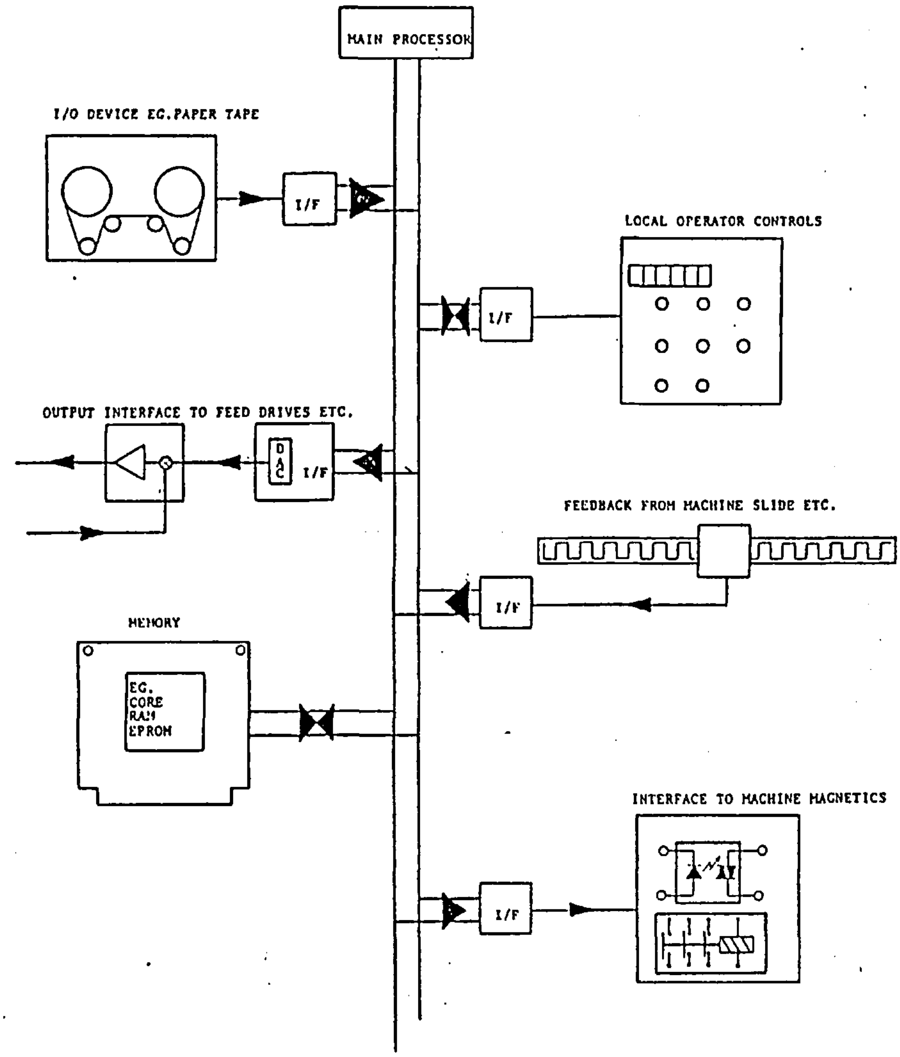

Figure 1.1 Minicomputer approach for CNC machine tools

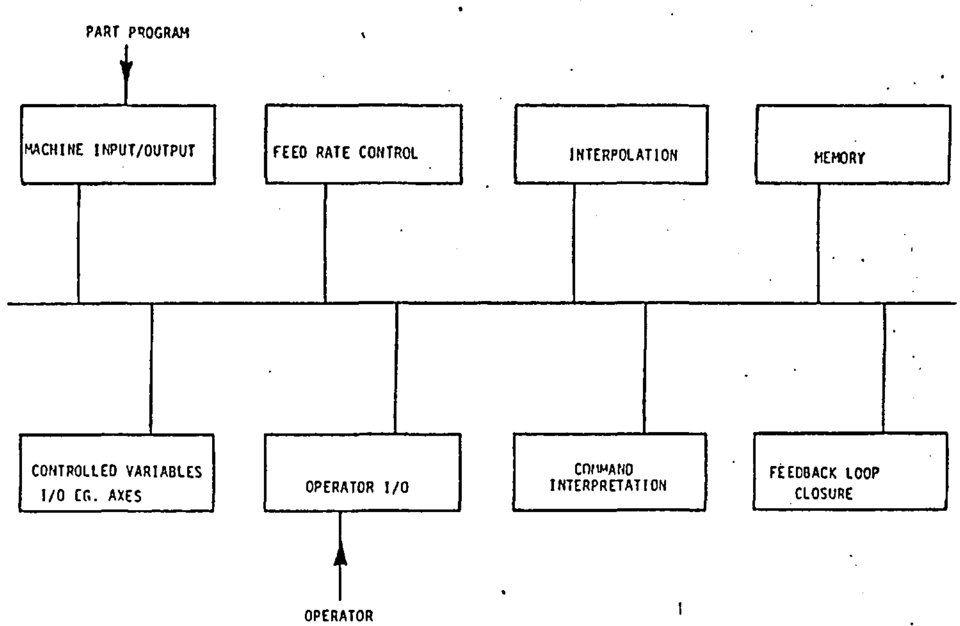

Figure 1.2 Distributed control system

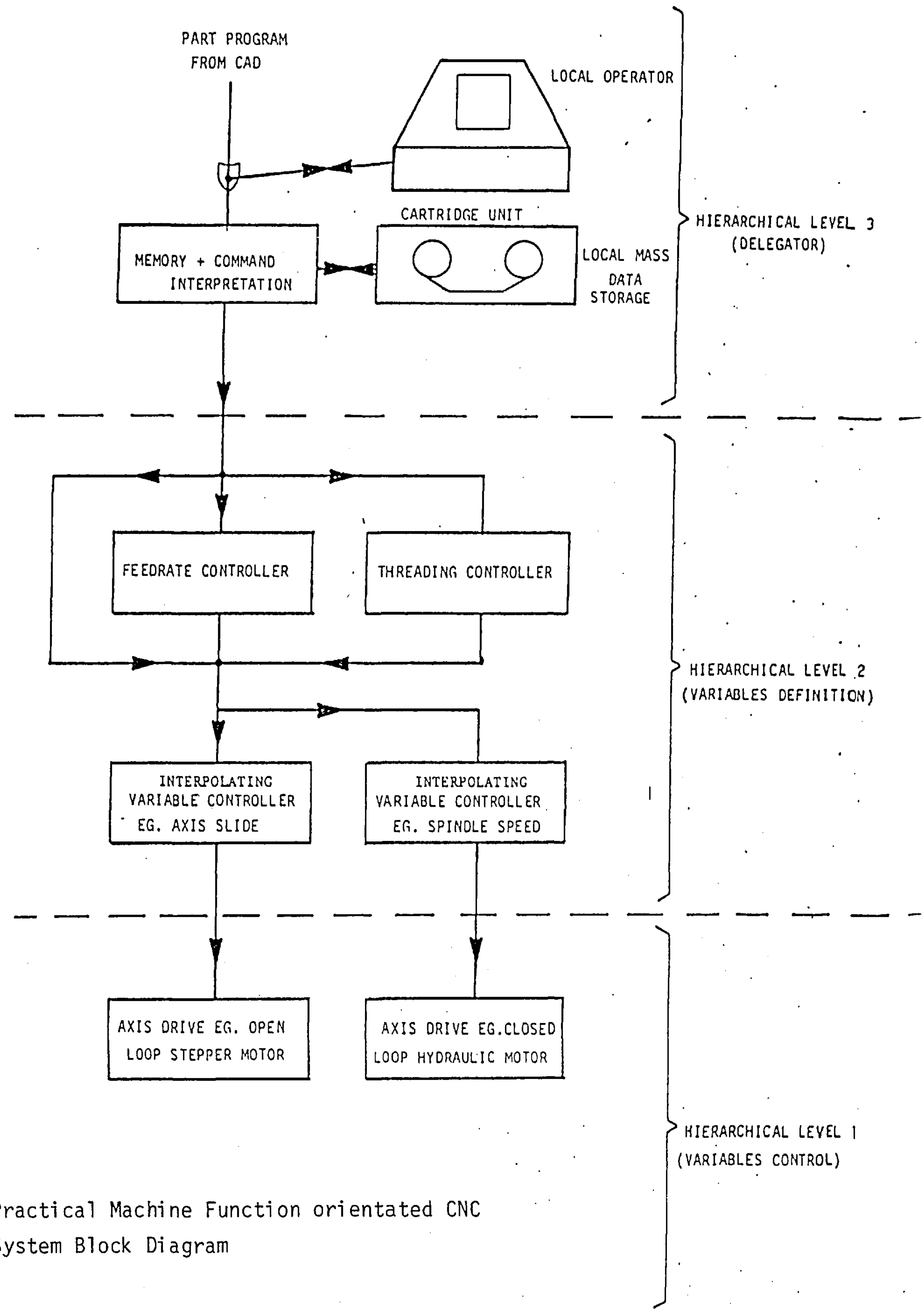

Fig. 1.3 Practical Machine Function orientated CNC System Block Diagram

thus resulting in low software development costs. The modularity of a distributed processing system stems from the smaller quantisation units of computing power used within it and which are often based on low cost 8 or 16-bit general purpose microprocessors. One method of dividing the control tasks in a distributed control system is to allot for each control task its own hardware environment such as interpolation, feedrate, loop closure etc, and then the appropriate software can be written (figure 1.2). However, with this approach, it may be seen that considerable inter-element dialogue is required during typical machining operations leading to a wide interconnecting bus with complex contention handling logic. Furthermore, the addition of another axis to the machine tool has implications for every element requiring software and possibly hardware changes.

The second method of segmenting the control tasks is to allot a hardware and software environment to each machine variable (such as slide position, spindle speed etc) (19). Each variable must have its own support functions, such as feedrate, interpolation and loop closure. The method lends itself to a very versatile system - so called hierarchical structure - (figure 1.3). With this hierarchical structure, inter-unit dialogue need take place only at the beginning and end of machinery operations. The interconnecting bus is only used for the distribution of feedrate synchronising in formation during a cut. Addition of a machine variable such as an additional axis would only have minimal impact on other elements resulting in a very modular and versatile system.

It is very natural that such a versatile and economic control system is going to have its impact on the design of a CNC machine tool. First of all, a modular control system encourages the design of modular machine tools. With a modular machine tool, although the basic structure is the same, it is possible to obtain several machine tools with different functions by simply changing the modules. The control system being modular as well will make the achievement of this flexibility easier.

The second impact of microprocessors on machine tool design emerges from its cheapness. Automating as many functions of machine tools as possible becomes a viable proposition. The flexibility of microprocessors allow the building of sophisticated control algorithms in an economic way to compensate for some of the drawbacks of the mechanical systems. The addition of damping into the longitudinal motion of roller or ball slideways by using a state variable control system is one of the examples to this kind of approach (91).

As microprocessors are a recent innovation, their effect on machine tool design is not yet apparent in the industrial market. Most of the possibilities of using microprocessors with machine tools still lie undiscovered. In Chapter 8, active control is described as a possibility to eliminate chatter. In Chapter 9, the possibility of having a high accuracy with a less rigid structure by controlling the slideway deflections is pointed out. Such complicated control tasks can only be carried out through the use of fast versatile and low cost microprocessors. Compensation techniques adaptive control and calibration can be performed with microprocessors in a more feasible way. With the applications of such techniques, it is possible that machine tools of the future will look quite different.

1.4 Requirements and the Design Process:

The general requirements for a machine tool as stated by Koenigsberger (2), are as follows,

1) Within permissible limits the specified accuracy of shape, dimensional accuracy and surface finish of the components produced on the machine must be obtainable consistently and as far as possible, independently of the operator's skill.

2) The operational speeds and rates of metal removal provided by the machine must be in accordance with the latest developments in materials and tools and therefore ensure the possibility of high productivity.

In addition, the design must be such as to enable it to cope with future developments in these matters in order to prevent the machine from becoming obsolete in a short time

3) In order to be competitive in operation, the machine must show a high technical and economic efficiency.

The above requirements are stated in a very general form. A CNC machine tool has got to satisfy the above requirements as well as many others. The requirements that must be satisfied by a CNC machine tool are given below in more specific terms.

1) The structure of the machine tool should have high static and dynamic rigidity with high damping characteristics in an effort to eliminate vibration.

2) The fundamental machine tool design must be correct, ie, slides moving in a straight line, repeatable positional accuracy of slides and indexing tables, high rotational accuracy and rigidity of spindle, etc.

3) It must be capable of providing high spindle speeds and feedrates with an infinitely variable range to make the selection of optimum feeds and speeds possible.

4) Non-linearities in the mechanics must be brought down to a minimum, ie, minimum backlash in drive systems, low friction on slideways, no stick-slip

phenomena.

5) It must be compatible with Flexible Manufacturing Systems (FMS), ie, the machine tool must be versatile, should be able to cope with high swarf removal rates, its control system should be easily adaptable for intermachine communication, etc.

6) Floor to floor time must be minimised.

7) It must have high reliability with minimum possibility of breakdowns.

8) The drive systems should have as high efficiency as possible while keeping to high metal removal rates.

9) Maintenance of the machine tool must be easy, down-time should be kept to a minimum.

10) It should occupy a low floor space.

11) It should have the necessary safety measures, collision must be avoided.

12) It should have low noise levels.

13) Application of adaptive control should be considered. Compensation techniques (for tool wear or mechanical inaccuracies) should be employed.

14) Thermal effects should be minimized.

As seen from the above requirements the design of a CNC machine tool calls for a careful consideration of many different subjects. Therefore, it requires a systematic and well organised approach. In figure 1.4, the design process implemented in this particular work has been given.

A design process for a machine tool, should start with a market survey. The specifications and the approximate desired cost of the machine tool emerges from the market survey. After the analysis of the general requirements and of the system the machine tool is going to be a part of, the shape and the specifications of the machine tool are finalised. Then the design process is mainly carried along on four basic fields: structure, slideways, drives and adaptive control. In every field, the state of the art is considered in detail and the optimum combination is tried to be achieved.

The subsections of the design process are explained thoroughly in separate chapters. In the following sections a small scale market survey is described and specifications are determined. Then, the alternative shapes for the structure is considered and a selection is carried out. In Chapter 2, alternative materials for machine tools are reviewed and concrete is chosen for its cost effectiveness and high damping properties. The

DESIGN PROCESS

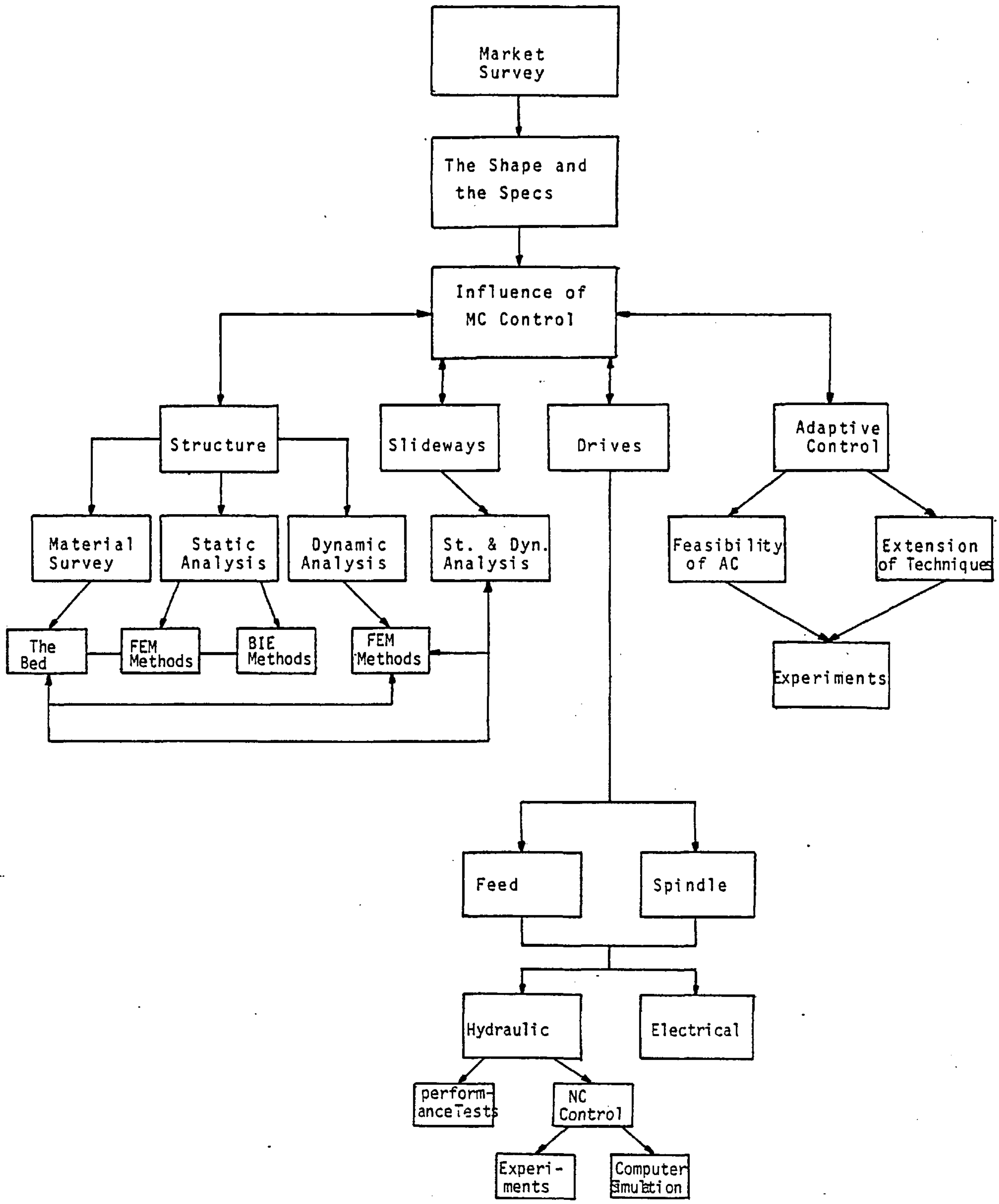

Figure 1.4 Design process for machine tools

cement composition for good short and long term stability is determined. In Chapter 3, a detailed reinforcement calculation using finite element methods is carried out. Creep and shrinkage properties are checked. In Chapter 4, a dynamic analysis of the structure, again, using finite element methods is performed and the shape of the structure is finalised. In Chapter 5, alternative slideways are analysed qualitatively and quantitatively by finite element methods. In Chapter 6, the alternative drive systems are reviewed and a method for servo drive selection is devised. In Chapter 7, hydraulic systems are analysed in more detail and the experiments performed are described. In Chapter 8, the feasibility of adaptive control and the existing tool wear methods are discussed and an algorithm independent of cutting conditions is proposed. Finally, Chapter 9, summarises and concludes the overall work and gives suggestions for future research.

1.5. Market Survey and Specifications

Market research is an essential element in the establishment of the specifications for a new machine tool. Firstly, the home market for the proposed type of machine should be examined because it is desirable that the home market should provide a reasonable base. Reports on home market are being published by some governmental bodies or by some journals (15). Statistics for foreign countries should also be analysed for a complete survey. The next step is to determine the share of the market which the new machine is likely to attract, and then the specification/cost relationship should be refined by analysing sales and service comments on current similar machines and discussing the new specification with selected potential customers. Finally, the market survey should indicate probable sales volume. Despite the difficulties the best estimates possible should be produced at this stage, so that a periodic review of the situation during the project can indicate if the trend is favourable or adverse as internal and external factors become clearer or change.

In parallel to the market survey, the refining of the specification is to be carried out. The usual steps for specification refinement can be summarised as the analysis of workpiece statistics, operational research and ergonomic analysis, analysis of cutting conditions and cutting tools. The procedures market research and specification refinement are given in a flow diagram form in figures 1.5(a) and 1.5(b) respectively.

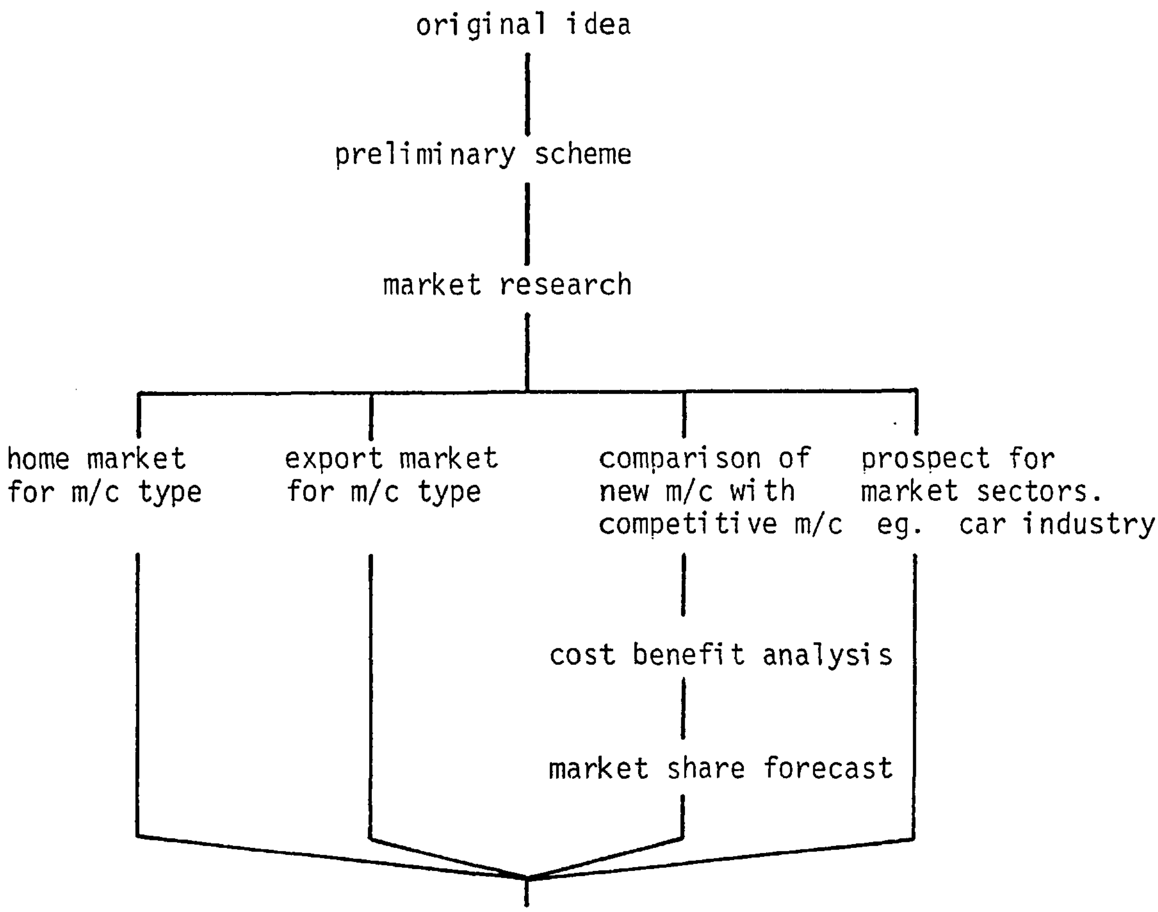

a) · Market Survey Procedure

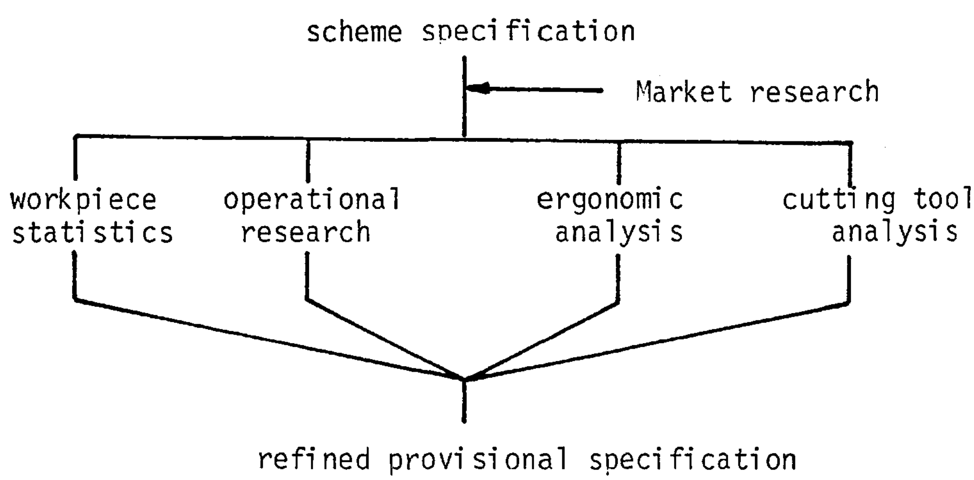

b) Refinement of machine specification

Fig. 1.5 Market Survey and Specification Refinement.

As seen above, a thorough market survey requires a good collaboration of many departments in a company. In this project the market survey has necessarily been carried out on a less sophisticated level.

The market research carried out in this work is described below in steps leading to the final specifications of the machine tool.

1. Firstly, the objectives should be set. The main objective is to analyse the state of the art of machine tool design and produce an optimum design which will be versatile enough to make full use of the versatile microprocessor control system. The overall design should be low cost and should be suitable for both small workshops and bigger industrial plants. A turning centre with considerable milling and cross drilling capabilities was considered to be a good tool to achieve these objectives. For the machine, to be marketable in big factories as well as small workshops, it must be at the border of the so-called "high performance" machines which is usually accepted to be around 10 - 15 hp. (22).

2. After the initial idea and the preliminary scheme, the next step is a market survey. Market survey has been carried out by referring to some papers, (6), (8), (15), or some reports (20), and by visiting CNC exhibitions and by talking to machine tool companies.

Ref No	Manufacturer	No of Axis	No of Turrets	No of Tools	Swing over bed mm	Turning length mm	Spindle power kw (hp)	Capacity		Accuracy µm	Spindle speed range rev/min	No of spindle speeds	Feed range mm/min	Number of feeds
								Bar	Chuck					
1	Boley													
	BDA	2	1	12	250	500	12		75	1	0-5000	inf	0-5000	inf
	BDN	2	1	12	300	500	11		80	1	50-6000	inf	0-10000	inf
2	Butler													
	NC550	2	1-2	4-8	500	1000	9		90	12	50-2215	inf	0-7500	inf
3	Churchill													
	Computurn 200	2	1-2	4-10	500	1500	15				45-2000	inf	0-5000	inf
4	Citizen Cincom													
	E32	2-3	1	16	250	700	5.5	25			175-4000	inf	1-2047	inf
	F2S	2	1	10	250	700	3.7	25			200-7000	inf	1-2047	inf
5	Donobat													
	Danumeric-2	2	1	8	500	500	11		60		30-3000	inf	0-10000	inf
6	Fanuc													
	FL300	2	1	5	300	500	5				135-4500	inf	1-10000	inf
7	Gildemeister													
	NEF 280	2		2	300	700	5.5		60	1	71-3550	9*3	0.01-245*	
	GD 160,200	2	1	12	300	500	15		100	1	-5000		2400/16000	

Table 1.1 Characteristics of some existing turning centres

Ref No	Manufacturer	No of Axis	No of Turrets	No of Tools	Swing over bed mm	Turning length mm	Spindle Power kw (hp)	Capacity		Accuracy µm	Spindle Speed Range rev/min	No of Spindle Speeds	Feed Range mm/min	Number of Feeds
								Bar	Chuck					
8	Hitachi Seiki													
	3NE-300	2	1	12	300	500	7.5				100-4000	inf	0-10000	inf
	3NE-600	2	1	12	500	500	11				20-3150	inf	0-10000	inf
9	Matra-Kitato													
	Variant 5	2	1	4-10	250	500	15				320-2500	inf		
	Variant 15	2	1	4-10	250	1200	15				25-2500	inf		
10	Nakamura-Tome													
	TMC-2	2	1	12	250	400	7.5				190-4500	inf	0-10000	inf
	TMC-3	2	1	12	250	500	11				100-4500	inf	0-10000	inf
11	Norton						7.8 (11)		150		10-4000	inf		
12	Pontiggia (PPL)													
	Galaxy	2	1	14	300	400	10		210		10-4500		0-10000	inf
13	Sicme													
	450 CNC	2-4	1-2	8-16	500	1500	15-22	65	200					

Table 1.1 (cont.d)

Ref No	Manufacturer	No of Axis	No of Turrets	No of Tools	Swing over bed mm	Turning Length mm	Spindle Power kw (hp)	Capacity		Accuracy µm	Spindle Speed Range rev/min	No of Spindle Speeds	Feed Range mm/mm	Number of Feeds
								Bar	Chuck					
14	Strojimport SPT 16N SS 50NC	 2 2			 250 500	 500 1700	 11 11				 -3150 -1800			
15	Takisawa TX-110D SX-210D	 2 2	 1 1	 10 8	 300 500	 400 500	 7.5 15				 100-3500 100-3200	 inf inf	 0-9000 0-9000	 inf inf
16	Traub TNO	 2	 1	 16	 300	 500	 705-22		 90	 1	 50-3150	 35	 0-4000	 4000
17	Tsugami	2	1	12		220	5.5 (7.4)	45	165		70-3550	inf	0-6000	inf
18	Wöest-Alpine Weipert WNC 490	 2	 1	 4-8	 500		 15		 100		 14-2800			
19	Warner & Swasey ISC-250	 2	 1	 12	 300	 400	 15		 150		 56-2558	 inf	 0-7620	 inf
20	Weiler Primus NL	 2	 1	 8			 10.5 (14.2)	 42	 130		 56-4000	 inf		

Table 1.1 (cont.d)

Ref No	Manufacturer	No of Axis	No of Turrets	No. of Tools	Swing over bed mm	Turning Length mm	Spindle Power kw (hp)	Capacity		Accuracy µm	Spindle Speed Range Rev/min	No of Spindle Speeds	Feed Range mm/min	No of Feeds
								Bar	Chuck					
21	Weisser, Eugen													
	Junior-CNC	2	1	4	500	1700	7.5-11		100		26-2000	24	0-8000	inf
	Hector-CNC	2	1	4	500	2000	11-15		110		28-1400	18	0-8000	inf
22	White - BSA						15 (20)	50	150		50-4500	inf		
23	Yamazaki													
	Microslant 15	2	1	12	380	510	11 (15)	45	150	1	41-4100	inf	0-10000	inf
	Slan-turn 15	2	1	12	380	1000	11 (15)	56	210	1	20-4000	inf	0-10000	inf
	Dyno-turn 2L-57	2	1	12	500	370	7.5 (10)	52	210	1	18-3000	inf	0-9000	inf

Table 1.1 (cont.d)

The survey has shown that there is a definite market in NC machines of relatively low cost, but with an effective range of performance and flexibility to meet a wide variety of requirements. At the same time, such machines must be simple to understand, operate and maintain.

In an effort to determine more detailed specifications for the machine tool, the existing turning centres with a power range of 7.5 hp - 20 hp have been analysed and their characteristics have been tabulated (table 1.1). The conclusions from this analysis are given below.

a) max. number of axis: 4 (only two machine tools have four axis control; most have only two axis control)

b) No. of turrets: usually one, a few machine tools have two turrets.

c) No. of tools: usually twelve, a few machine tools go up to 16.

d) Average swing over bed: 360 mm.

e) Average turning length: 750 mm.

f) Average capacity: bar: 45 mm.
chuck: 130 mm.

g) Max. accuracy: 1μm.

h) Spindle speed: Maximum spindle speed is 7000 rpm and the maximum spindle speed range is about 200 to 1. Most of the machines have infinity variable speeds.

i) Feed rate: Maximum feed rate (rapid traverse rates) is 10 m/min. It is infinitely variable.

3. The most encountered sizes and the competitive specifications met during the survey and summarised in 2, can be taken as a base to determine the specifications of the machine tool. Also keeping the objectives of the project in mind, the following specification and criteria can be laid down for the machine tool.

i) The general requirements mentioned in section 1.4 should be followed.

ii) The turning centre must have some heavier milling and cross drilling capabilities.

iii) As many variations as possible must be offered on the basic machine to cater for the individual requirement of each customer (it must be possible to use it as a 2, 3 or 4 axis machine tool).

iv) During the design, the effect of microprocessors should be kept in mind.

v) The resulting machine tool should have as low cost as possible.

vi) During the design, the following specifications should be aimed at,

turning spindle power:	15-20 hp
milling spindle power:	2-3 hp
number of turrets:	1-2
number of tools:	12-16
swing over bed:	300 mm
turning length:	900 mm
capacity: bar:	50 mm
chuck:	200 mm
accuracy:	10 μm
spindle speed:	20-4000 rpm (standard) infinitely variable
	35-7000 rpm (optional) infinitely variable

feed rate: 0-10 m/min infinitely variable.

The accuracy requirement of the machine tool is set at 10 μm rather than the more competitive accuracy level of 1 μm, because it was considered that very high accuracy levels would place stringent requirements on the stiffness of the structure, increasing the overall cost and weight. Also the market survey showed that 10 μm is an acceptable level of accuracy. Besides, it will be possible to improve this through compensation techniques as outlined in section 1.4.

1.6 Alternative Designs and Selection:

Determining the shape and configuration of a machine tool is a difficult task. The first step in tackling this problem should be to lay down the functional and non-functional requirements for the shape of the machine tool. These are listed below. They should be considered in the light of the specifications obtained from the market survey.

1. Easy chip removal
2. Low space occupation
3. Rapid and easy loading and unloading
4. Minimising cutting time
5. Non interference of the tool slides
6. A good distribution of forces
7. Good accessability for maintenance
8. Visible cutting region
9. Easy manufacture and assembly
10. Low cost and weight
11. Correct ergonomically and aesthetically pleasing.

The method which will be followed to choose the right shape for the machine tool will be to choose a shape starting from the first requirement, then refine it as the other requirements are considered. At the end, it might be necessary to review all the requirements from the beginning to confirm the final selection. During the process, it is rewarding to use creative, thinking and brain storming techniques (21).

The first requirement, easy chip removal, suggests the use of an either vertical or inclined bed with an angle of around 60^{o}. Horizontal beds are very bad for chip removal. The second requirement strengthens this view, because inclined or vertical beds also take less space.

The third requirement, rapid loading and unloading, can be used to determine the position of the headstock. If loading and unloading is solely to be performed by a robot, the headstock could almost be placed anywhere. However, in today's conditions, especially when the machine tool is also aimed for small workshops, the loading by human beings should be considered. Then ergonomic reasons fix the height of the headstock to between 80 and 120 cm. It also suggests that the headstock should be on the left hand side for ease of loading. If a robot is employed for loading and unloading, inclined bed may not be a very good solution, because the only way a robot can reach to the headstock is from the front, which rules out the possibility of an operator approaching the controls for the purposes of checking. The safety problems associated with this situation can partly be solved by the use of specialised loading robots. Another solution can be to make the headstock movable so that it can slide along two slides and come to the end of the bed. This solution makes it possible that the robot is placed to the end of the machine tool away from the front part so that the supervisor can check the controls, if necessary, without stopping the operation. Use of a sliding headstock can however conflict with requirement four. Because, in this case usually the cutting tool is stationary and the blank is moving with the headstock. However, the headstock assembly will be much heavier than the saddle assembly and this will result in smaller feedrates with smaller accelerations, increasing the cutting time. Therefore, moving headstock idea can be discounted at this point, and it can be suggested that for safety reasons either remote control panels are to be used or specialised robots should be employed. Requirement four also dictates that simultaneous cutting is desirable. This includes turning and drilling at the same time. For two and three axis machines drilling is done by the end turret. In that case, if standard right handed drills are to be used, with the headstock on the left hand side the sense of rotation should be anti-clockwise. Criteria five, non interference of the slides, can be used to determine the number of slideways. For three axis and four axis machines the best solution is two use four slideways, two for the lower and two for the upper slides. The requirements outlined after the market survey already dictated the use of a separate slide for the milling head. Because turning and milling can not be done at the same time, the two slides can be placed on the same guideways, however necessary measures should be taken to clear the headstock. Requirement six creates a conflict when the sense of rotation is determined on the basis of using right hand drills. Anti-clockwise rotation will cause the main cutting force to act in the direction as to lift the slide from the guideways. In order to solve this problem, either the headstock should be on the right hand side or left hand drills should be used. An analysis of the existing machine tools shows that in almost all of them the headstock is on the left. Therefore, it can be assumed that with time, left-hand drills will be quite common and also their price will be cheaper. For this reason, the headstock will be allowed to remain on the left-hand side, however, a thorough market survey about the employment of left-hand drills should be carried out before the final decision. However, such a market survey will not be attempted here. This requirement also suggests that vertical beds can increase the overhang in the slide assemblies, decreasing the stability of the structure. Therefore, inclined beds are to be preferred. Requirement seven can be used to determine the angle of the inclined bed. From the chip removal point of view, the preferred angle would be above 60^{o}. However, at this angle it might be difficult to reach to some parts of the slide. 70^{o} brings the slide more forward with a better accessibility. However, the angle depends on the overall design and should be treated as such. 60^{o}-70^{o} appear to be reasonable solutions. The design chosen also fulfils requirement eight. Requirement nine is to be considered in the light of component design and in the arrangement of slides. Requirement ten low cost and weight, would decrease the number of slides to three.

Weight requirements also necessitates careful design of the structure with a high strength to weight ratio. Finally, the design should be checked for <u>requirement eleven</u>, appearance and ergonomics.

At this stage, a review of the requirements can be performed. It is seen that the position of the end turret can conflict with <u>requirement one</u>, easy chip removal. This can be solved by locating the end turret into a recess in the structure, however because this will decrease the strength of the structure such a configuration can be discounted.

The above discussion is summarised in figure 1.6. As a conclusion, the shape and configuration as shown in figure 1.7 is reached. The design is also quite versatile as the objectives set forward in the previous section dictated. The versatility of the configuration is illustrated in figure 1.8.

A FIRST REVIEW

Requirement 1 - Easy clip Removal

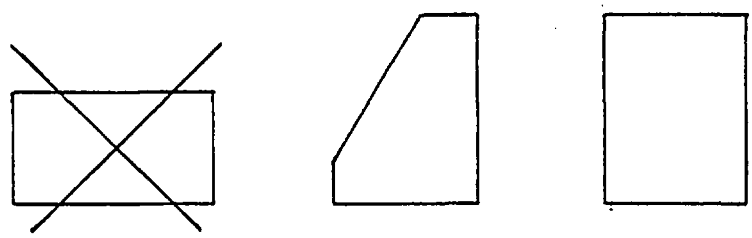

Requirement 2 - Low Space Occupation

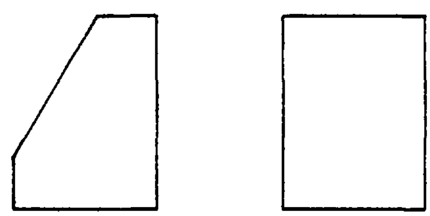

Requirement 3 - Rapid Loading and Unloading

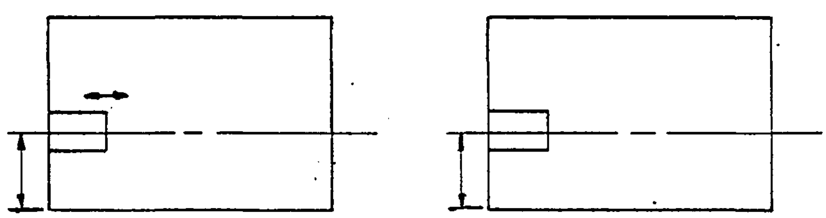

Requirement 4 - Minimizing cutting time

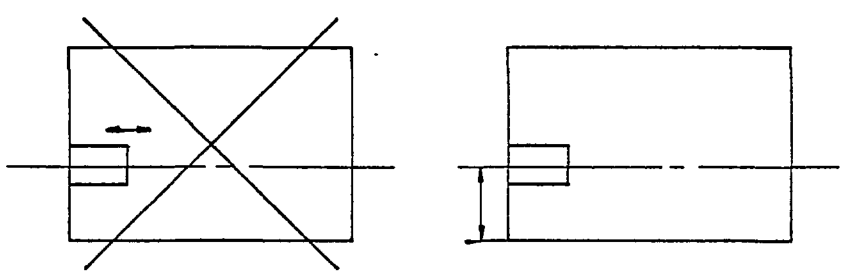

Requirement 5 - Non-inteference of slides

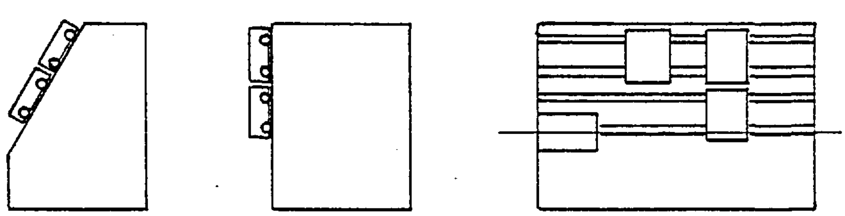

Figure 1.6 Alternative designs and selection procedure

Requirement 6- A good distribution of forces

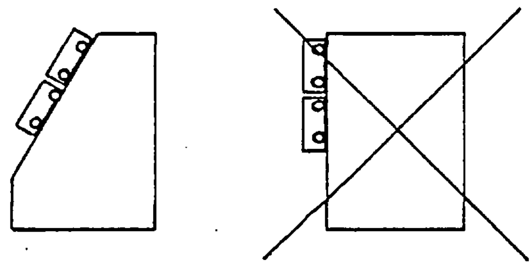

Requirement 7, 8, and 9 - Maintenance, Cutting region, assembly

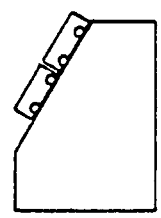

Requirements 10 and 11 - Cost, weight, ergonomics

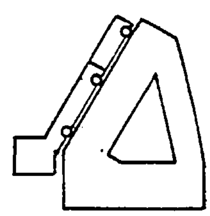

B -. SECOND REVIEW

Requirement 1 -

Requirements 6, 9 and 10.

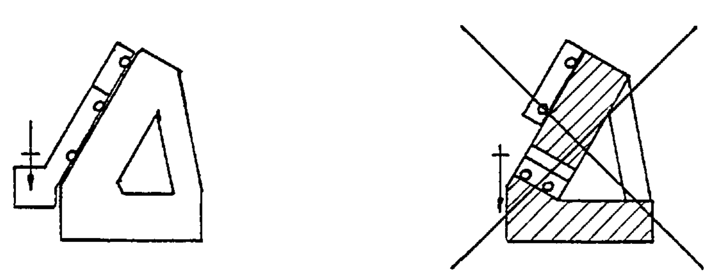

Figure 1.6 (cont.d)

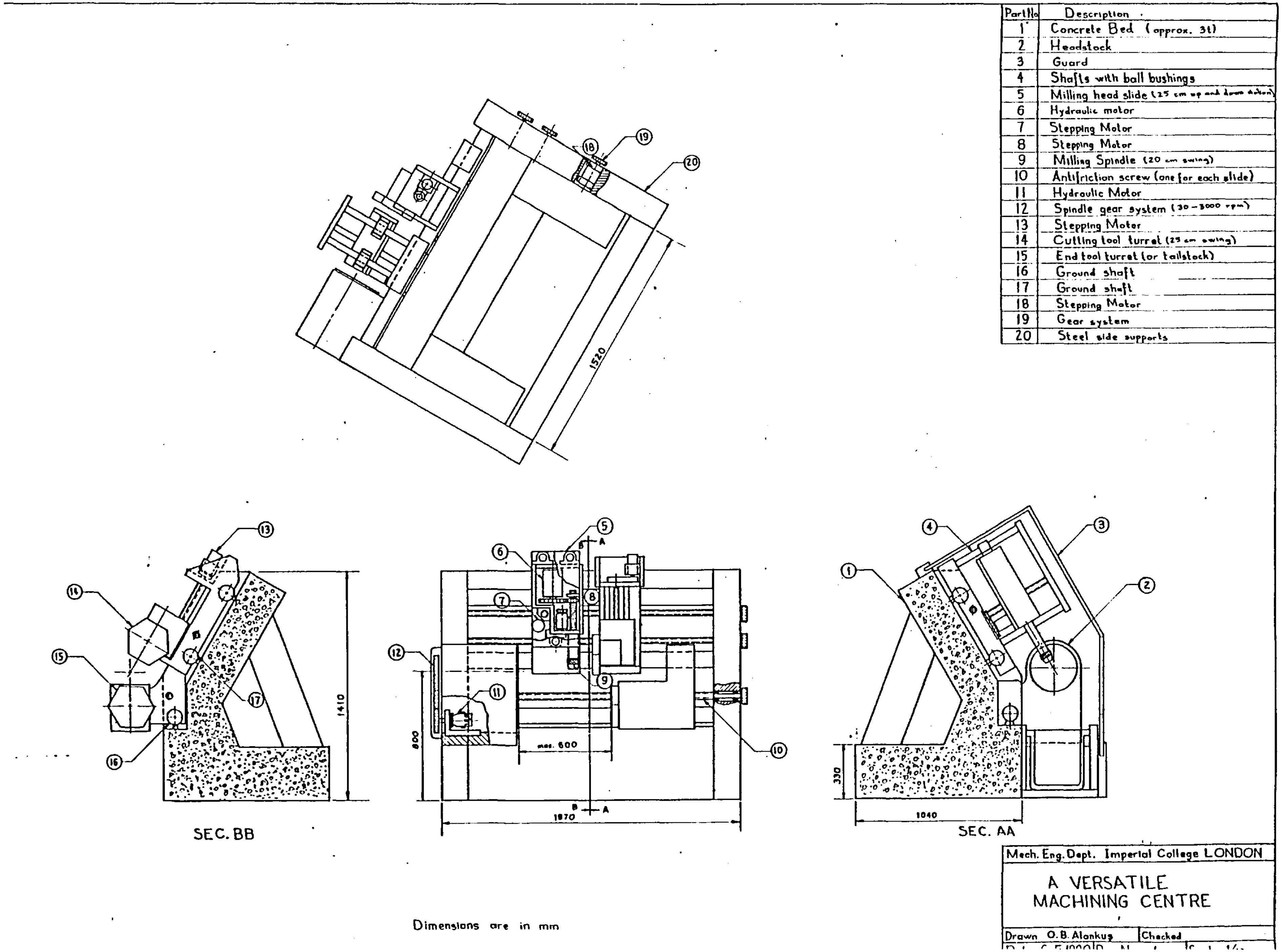

Figure 1.7 The proposed machine tool

1. A TWO AXIS MACHINE

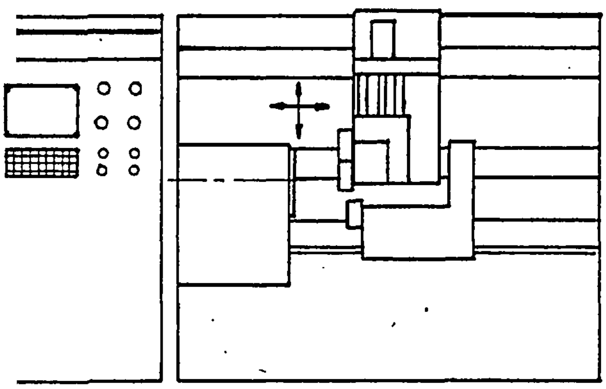

2. A THREE AXIS MACHINE

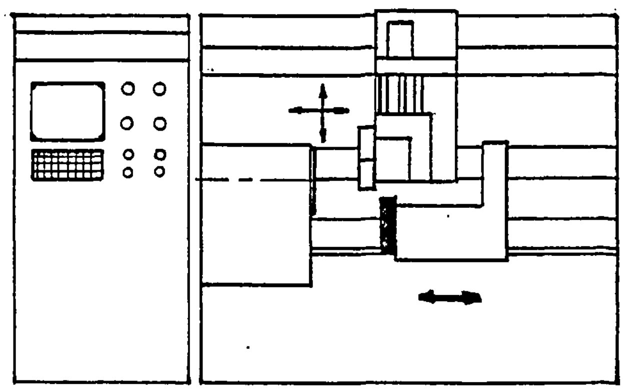

3. A FOUR AXIS MACHINE

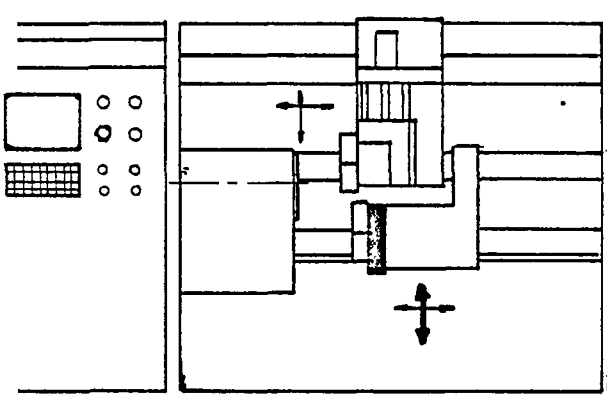

4. FOUR AXIS WITH HEAVY MILLING

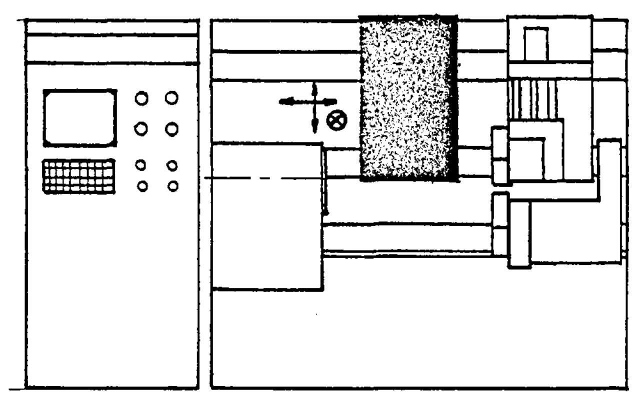

5. A LIGHT MILLING AND DRILLING MACHINE

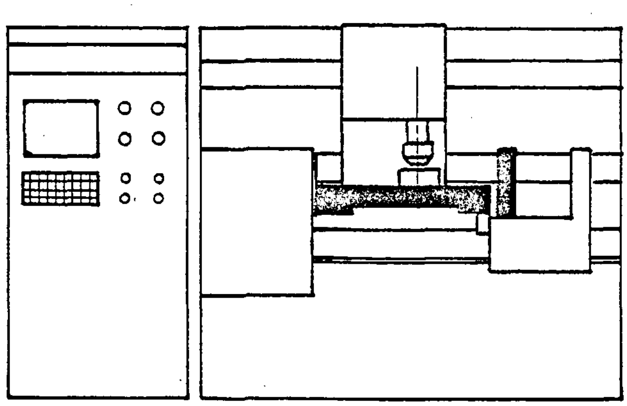

Figure 1.8 Five different configurations of the proposed machine tool

CHAPTER 2

MACHINE TOOL MATERIALS

2.1 Introduction

The main requirement for the structure of a machine tool is that it maintains the correct relative positions of the units and parts mounted on it, over a long period of service and under all the specified working conditions. To maintain accuracy (which is a part of the above requirement) under the influence of cutting forces and the moving weights of machine tool elements, the structure must have high static and dynamic stiffnesses.

In order to achieve high static stiffness and also to minimize torsional vibrations, a "closed box" structure is usually preferred in machine tools. Open box structures are sometimes deliberately used to achieve easy alignment, for easier chip removal and to provide a means of removing the cores of the cast iron beds. A stiff concrete foundation is then usually provided. This does not give high dimensional stability, and usually involves costly excavation of the floor to keep the working height low.

Besides the shape and configuration of the machine tool, the material type used for the structure also plays a very important role in achieving a successful design for the structure. The requirements for a machine tool material are listed below and their implications are discussed.

1. High modulus of elasticity: This ensures a high static and dynamic stiffness.

2. High internal damping: This decreases the amplitude of vibrations and increases the decay rate. Good internal damping characteristics are especially important for high accuracy machine tools.

3. Good long term dimensional stability: The material should be resistant to creep so that permanent strains, resulting from either internal residual stresses or imposed loads, should be too small to affect the accuracy of the machine tool.

4. Low thermal coefficient of expansion: This is important to minimize the thermal deflections, because thermal deflections can seriously affect the accuracy.

5. The material should be resistant to abrasive wear so that it will not be affected by swarf. Also a low coefficient of friction will be useful, because it will prevent lubricants and swarf from sticking to the surface.

6. The overall cost for the material and the production process should be low.

2.2 Common Machine Tool Materials

The most common machine tool materials are examined below. The main physical properties of the materials considered are listed in table 2.1.

1. Cast Iron:

From early times cast iron has been the most commonly used material for machine tool structures. The advantages of cast iron can be listed as follows:

i) It may be cast into complex and intricate shapes.

ii) It can easily be machined and can be hand-scraped and lapped to a high degree of accuracy.

iii) It has good damping properties.

iv) It has reasonably good anti-friction properties helped by the graphite contained in it.

v) Very good long term dimensional stability can be achieved by subjecting castings to a special long cycle stress relief annealing treatment.

It does, however, have several disadvantages,

i) The time and cost taken to produce a finished casting are high.

ii) It is vulnerable to rust.

Material	Modulus of Elasticity lbs/in^2 (N/mm^2)	Density lbs/in^3 (N/mm^2)	Logarithmic decrement	Coefficient of Thermal Expansion $^{o}C^{-1}$	Thermal Conductivity Wm^{-1} K^{-1}	Tensile Strength lbs/in^2 (N/mm)
Cast Iron (Grade 17)	$17 * 10^6$ (117000)	0.260 (7.21)	0.003 (at 1000 Hz)	$12 * 10^{-6}$	75	33400 (230)
Mild Steel (Weldments)	$30 * 10^6$ (207 000)	0.286 (7.93)	-	$12 * 10^{-6}$	80	66 800 (460)
Hydraulic concrete 1: 1½:3	$3.5 * 10^6$ (24 000)	0.0827 (2.29)	0.02 (20-1000Hz)	$9 * 10^{-6}$	0.1	580 (4)
Epoxy concrete	$5 * 10^6$ (33 000)	0.0901 (2.5)	6.02 (20-1000 Hz)	$12 * 10^{-6}$	0.5	3630 (25)

Table 2.1 The properties of the basic machine tool materials

iii) The energy used to melt the iron before casting is high.

The production process consists of manufacture of patterns, forming of sand moulds, casting, shot blasting, rough machining, heat treatment, finish machining, priming, filling, undercoat paint, rub down and topcoat paint. Most manufacturing stages involve the moving of the component either in or outside the factory and transport costs are high.

2. Mild Steel:

Since the 1950's mild steel weldments have been used more and more as a machine tool structural material. Its advantages can be listed as below,

i) it has high stiffness and strength

ii) it allows the use of thin sections, whereas with cast iron the wall thickness is limited by the accuracy of casting.

However, it has some disadvantages:-

i) the material damping is low

ii) friction is high and cast-iron or composite insets have to be used to reduce friction in slideways.

iii) Manufacturing times are long, although less than with cast iron.

iv) It is very vulnerable to rust.

v) Long term dimensional stability has not been verified to the same degree as cast iron.

vi) Fatigue characteristics of welded steel are not good. However, stress levels in the structure are usually low; therefore, fatigue should not create any problems.

3. Hydraulic Concrete:

Hydraulic concrete is a mixture of cement, water and the aggregates sand and gravel. Concrete is usually reinforced with steel as it is very weak in tension. The manufacturing sequence is as follows:

- Reinforcing iron is placed in the mould. Metal guides and reference parts must be attached to the reinforcement.

- the component is cast and vibrated to consolidate the concrete. It is then unpacked from the mould, rendered and primed to prevent oil entering the concrete. Hydrocarbons cause concrete to break down

- At least 40 days curing and hardening of the new casting must be allowed. A large shrinkage occurs.

- Reference areas are machined as with cast iron or steel beds.

- The surfaces are 'filled' and pointed. Covering also serves to reduce growth and shrinkage with varying humidity. Areas exposed to mechanical loads, ie falling swarf, have to be covered with sheet metal.

- Assembling of additional components on the machine is carried out as on traditional cast iron or welded steel beds.

The main attractions of concrete are its low cost and very good damping properties. Also, it is possible to cast large beds and columns on site thereby avoiding high transport costs.

4. Epoxy Concrete

It is a new material especially developed for high precision machine tools by the Precision Engineering unit of Cranfield Institute of Technology (27).

It is a mixture of the binding agent reaction resin and the hardener together with carefully selected and mixed aggregates. Its main advantages are as follows,

i) It has good damping properties, better than traditional concrete.

ii) It can take both compressive and tensile forces; therefore, in most cases, steel reinforcement is unnecessary.

iii) It hardens without measurable shrinkage, provided suitable binding agents and aggregates are used.

iv) It does not expand and contract with changes in humidity; it is impervious to the effects of mineral oils and mineral emulsions.

v) It has a high long-term stability if it is processed correctly with the correct fillers.

vi) The manufacturing time is quite short (one or two days).

vii) Metal components can be cast directly into the bed, provided that the right formulation of synthetic resin is used so that no distortion occurs after alignment ie during casting and curing.

From table 2.1, it is seen that hydraulic concrete and epoxy concrete have considerably better damping characteristics than cast iron. One disadvantage they have is their low modulus of elasticity; however, this can be compensated for by thickening the walls which also has the beneficial effect of considerably increasing panel natural frequencies.

Usually, because of the low density of concrete, thickening the walls will not cause too large an increase in the overall weight. Also, because of the ease of production two types of concrete are considered to be better machine tool materials than cast iron and steel. A comparison between hydraulic concrete and epoxy resin concrete, shows that epoxy concrete because of its short manufacturing time is more desirable. Its ability to take tensile forces will not be an advantage in this case, because the forces involved for a 15 hp machine tool will very probably create higher stresses than epoxy concrete alone can take. Therefore, some reinforcement will be necessary. Reinforcement is also useful to increase the overall stiffness of the structure. Consequently, it is necessary to use steel reinforcement in epoxy concrete structures as well as in hydraulic concrete ones. However, epoxy concrete as a material is more expensive, therefore up to date, it has only been applied to very high accuracy machine tools eg. grinding machines.

The above discussion shows that hydraulic concrete can be considered as an excellent material for machine tools. Although, it is desirable to have a direct cost comparison between a reinforced concrete structure and a cast-iron one, it will not be attempted here, because the costs involved very much depend on the particular design and where the structures are being made and also on the facilities of the machine tool company. However, in general, it is accepted that because of the lower cost of the material and the manufacturing process, reinforced concrete structures will be cheaper than an equivalent cast-iron structure. It is also possible that reinforced concrete structures can be prepared on site thereby eliminating part of the transportation costs.

Although, hydraulic concrete appears to be an attractive material for machine tool structures, its properties can change considerably according to the mix. Therefore, it is necessary to analyse the effects of each ingredient of concrete carefully. In the following section concrete and reinforcement are discussed in general terms. The discussion of thermal properties of concrete together with creep and shrinkage characteristics is treated in Appendix A.

2.3 Concrete and the Reinforcement

Concrete is a general term for conglomerates made artificially from cement, with sand and broken stone or similar materials described generally as fine and coarse aggregate. These ingredients, mixed together with water, form a plastic mass which sets on standing into the hard solid material known as concrete.

Of the various types of cement available and suitable for making concrete, Portland cement is by far the most commonly used. By modifying the compound composition, it is possible to manufacture different types of portland cement having variable characteristics with regard to rate of hardening, rate of heat evolution and resistance to attack by sulphate waters. Five types of portland cement are defined by ASTM C150 (26). Their typical physical-chemical characteristics are given in table 2.2.

Aggregates make up about 70% of the total volume of concrete and, therefore significantly influence the cost economy and the properties of concrete. The physical properties of concrete that can be affected by aggregate characteristics include unit weight, workability, modulus of elasticity, strength, shrinkage, creep, thermal behaviour, and durability. Characteristics of some common aggregate types have been shown in table 2.3 (26). There are two main groups of aggregates: fine and coarse. Regarding size of aggregate the maximum size permissable for a job should be used, because it is generally more economical and also the drying shrinkage of concrete will be reduced and strength increased.

Water is another ingredient of concrete. It must be clean and free from harmful materials such as clay, loam and acids. For a suitable concrete mix, the amount of water as well as the amount of aggregates should be correctly proportioned. For a concrete to be dense and

ASTM C150		Compound composition %				Fineness cm^2/g	Compressive Strength % of Strength of type 1 cement			
Type	Description	C_3S	C_2S	C_3A	C_4AF	Wagner	1 day	7 days	28 days	3 months
I	General purpose	50	24	11	8	1800	100	100	100	100
II	Moderate heat of hydration and moderate sulfate resisting	42	33	5	13	1800	75	85	90	100
III	High early strength	60	13	9	8	2600	190	120	110	100
IV	Low heat	26	50	5	12	1900	55	55	75	100
V	Sulfate resisting	40	40	4	9	1900	65	75	85	100

Table 2.2 - Types of Portland Cement

free from internal voids there has to be sufficient cement to fill the voids between the fine aggregate particles to make a dense mortar and sufficient mortar to fill the voids between the coarse aggregate particles. In all the "nominal concrete mixes" the volume of coarse aggregate is given as twice the volume of fine aggregate. (25). Permissible working stresses for several mixtures are given in table 2.4. Strength of concrete is affected to a great extent by its water content. It is shown in the literature that as the water/cement ratio goes down, the strength of concrete increases. However, a low water content usually results in a dry mixture which impairs the workability of fresh concrete (25).

However successful a concrete mixture is, as mentioned above, concrete is very weak in tension. Therefore, it has to be reinforced if it is used as a structural member. The reinforcement has normally to be one of the following.

i) Rolled steel bars or hard drawn steel wire complying with B.S. 785 (1938).

ii) Cold twisted steel bars complying with B.S. 1144 (1943).

iii) Steel fabric complying with B.S. 1221 (1945). The permissible stresses in steel reinforcement is given in table 2.5.

Rock Types	Specific Gravity (dry)	Absorption and Porosity	Potential Alkali Attack	Durability	Typical Shape
Igneous					
Granite	2.52-2.99	Very low	Insignificant	Good	Equidimensional
Rhyolite	2.30-2.70	Low to moderate	Deleterious	Good	Equidimensional
Andesite	2.22-2.79	Low to moderate	Deleterious	Good	Equidimensional
Basalt	2.21-3.11	Low to moderate	Insignificant	Good	Equidimensional
Sedimentary					
Sandstone	1.60-2.68	Low to high	Insignificant	Good to poor	Equidimensional to platey
Limestone	1.74-2.76	Low to high	Insignificant	Good to poor	Equidimensional to platey
Shale	1.54-3.17	Moderate to high	Insignificant	Satisfactory to poor	Platey
Chert	1.81-2.65	Low to moderate	Deleterious	Good to poor	Equidimensional

Table 2.3 - Characteristics of Common Aggregate Types

Table 2.4 Permissible stress for portland cement mixtures

cement fine coarse Nominal mix (by volume)	compression		Shear	Bond	
	direct	Due to bonding		Average	local
1 : 1 : 2	7.6 *	10	0.9	1.0	1.5
1 : 1½ : 3	6.5	8.5	0.8	0.93	1.4
1 : 2 : 4	5.3	7.0	0.7	0.83	1.3

Table 2.5 Permissible stress in steel reinforcement

Designation of stress	Permissible stress		
	Mild steel to 8.5 785 with no guaranged yield stress		All steels with a guaranteed yield stress
	Bar sizes	Stress N/mm^2	N/mm^2
Tension	Up to and including 38mm	138	Half the guaranteed yield stress but not more than 206
	Over 38 mm	124	nor, in shear reinforcement more than 38
compression	up to and including 38 mm	124	Half the guaranteed yield stress but not more than 158
	over 38 mm	110	

* units are in N/mm^2

2.4 Discussion:

In this chapter, the most common machine tool materials have been reviewed and it has been seen that reinforced concrete is an attractive machine tool material because of its low cost and high damping. However, when designing the structure with reinforced concrete, a lot of attention needs to be given to the concrete mix so as to have a workable, a high strength and creep and shrinkage resistant concrete with good thermal properties. The design of reinforcement is also very important for a good creep and shrinkage behaviour.

In the last section, and also in appendix A, the properties of reinforced concrete have been analysed. Here, they will be reviewed from the point of view of choosing the right mixture for the concrete. As seen in table 2.2 there are basically five types of cement. The general purpose cement should be satisfactory for machine tool structures. Although moderate heat of hydration properties can be attractive, it is thought that the heat of hydration produced by general purpose cement will not be high enough to cause cracking due to thermal strains. Turning to the selection of aggregates, it must be remembered that as the volumetric content and modulus of elasticity of aggregates increase, the creep and shrinkage decrease. The aggregates should have low thermal conductivity and thermal diffusivity, and also its thermal expansion coefficient must be near to that of the cement used for low thermal strains. Additionally, the percentage of fine aggregate by weight should be low for good creep and shrinkage properties. Water content is similarly important. A low water content is desirable because it gives a low thermal coefficient and high strength concrete with good shrinkage and creep properties. However, the water content must be high enough to obtain a workable mixture.

From the above discussion, the properties and the proportions of the concrete mix can be chosen as follows,

Cement: General Purpose

Aggregate: Granite or Limestone (according to the availability and price)

Nominal mix (Cement: fine aggregate: coarse aggregate) 1:2:4

Water/cement ratio by weight: 0.55

(reference (26))

CHAPTER 3

STATIC ANALYSIS OF THE STRUCTURE

3.1 Introduction:

In the previous chapters, the specifications and the shape of the machine tool have been established and the material for the structure chosen. In this chapter, after an evaluation of the cutting forces acting on the structure, stress and deformation calculations for the structure are carried out. The steel reinforcement for the concrete structure will be determined from the results of these calculations.

In the past, the only accepted method of analysis prior to manufacture of the actual machine was "model analysis" (20). However, with this method while it is sometimes possible to deduce an improved structural form, this is by no means simple and the manufacture of a number of models to investigate alternative designs is generally quite impractical.

The limitations of physical model techniques have led to the development of mathematical models representing a variety of mechanical structures. In all the mathematical models, the first step is to subdivide the real structure into simple elements such as beams and polygonal plates, these elements being interconnected at specified nodal or station points only. Relationships between the forces and displacements at these nodal points are then derived in the form of element matrices; the manipulation of these element matrices giving the required information about the whole structure. There are two main types of matrix methods, (20), (31).

a) Flexibility Method

The flexibility method, in which the structural deformations are expressed as a function of the applied forces, as in equation (3.1), has two serious disadvantages when applied to large highly redundant structures.

$$\{\delta\} = F \{P\} \qquad (3.1)$$

where

$\{\delta\}$ is the displacement vector,

$\{P\}$ is the load vector,

and

F is the flexibility matrix

Firstly, the formation of a redundant flexibility matrix can be extremely time consuming as it is necessary to first eliminate each redundancy by cutting the structure. The second disadvantage is that a flexibility matrix is generally fully populated requiring a large fast random access memory in the computer.

b) Stiffness Method

In a displacement or stiffness formulation, the applied force is given as a function of the nodal displacements as in equation (3.2),

$$\{P\} = S \{\delta\} \qquad (3.2)$$

where S is the stiffness matrix and {P} and {δ} are as defined above,

Neither of the two disadvantages mentioned in flexibility method exists since a redundant stiffness matrix for a complete structure is formed by simply adding the small individual element stiffness matrices into the appropriate locations. However, with this method, matrix manipulation might present some difficulties because it is the displacement which is usually required and the applied loading which is usually known.

Several mathematical models have been developed up to now. In Leuven, Manchester and Aachen Universities, the model is based on uniform section beam like elements (33). The model used in Birmingham University can incorporate masses into the model as well (33), (39). More recently, with the advances in finite element techniques, mathematical models based on finite elements have been implemented (31), (32).

During the last few years a new numerical tool has been developed: the boundary integral equation method. The method has been successfully applied in several fields of engineering and has proved to be more efficient than finite element method in most cases. In the following sections, the Boundary Integral Equation (BIE) method will be investigated together with the Finite Element (FE) method and some comparisons between the two methods will be made.

3.2 FE and BIE Methods:

Finding the stresses and deformations of a machine tool structure is an elastostatic problem. The differential equations for such a problem can be written as follows (43),

$$\frac{\partial \sigma_{i1}}{\partial X_1} + \frac{\partial \sigma_{i2}}{\partial X_2} + \frac{\partial \sigma_{i3}}{\partial X_3} + X_i = 0 \quad (3.3)$$

$i = 1, 2, 3$

where σ shows the stresses and X the body forces.

After the manipulation of eqn. (3.3) together with strain displacement relations and Hooke's Law, the following equations can be obtained

$$\frac{1}{1-2\mu}\left(\frac{\partial^2 u_1}{\partial x^2{}_i} + \frac{\partial^2 u_2}{\partial x_i \partial x_2} + \frac{\partial^2 u_3}{\partial x_i \partial x_3}\right) + \nabla^2 u_i + \frac{1}{G} X_i = 0 \tag{3.4}$$

$$i = 1, 2, 3 \quad \left(\nabla^2 \equiv \frac{\partial^2}{\partial x_1{}^2} + \frac{\partial^2}{\partial x_1{}^2} + \frac{\partial^2}{\partial x_3{}^2}\right)$$

$$\frac{d u_i}{dn} + \frac{\partial u_1}{\partial x_i} n_1 + \frac{\partial u_2}{\partial x_i} n_2 + \frac{\partial u_3}{\partial x_i} n_3 + \frac{2\mu}{1-2\mu}$$

$$\left(\frac{\partial u_1}{\partial x_1} n_i + \frac{\partial u_2}{\partial x_2} n_i + \frac{\partial u_3}{\partial x_3} n_i\right) = \frac{1}{G} t_i \tag{3.5}$$

$$i = 1, 2, 3$$

where

- u shows the displacements
- n shows the unit vector perpendicular to the surface
- t_i is the traction vector defined as $t_i = \sigma_{ij} n_j$
- μ is the Poissons's ratio

and G is the shear modulus

Equation (3.4) can be used to evaluate the deflections whereas the equations (3.5) are used to evaluate the stresses. There are several methods of solving these equations. However, only the FE and BIE methods will be analysed here, because they are the most suitable methods for this application.

In case of FE methods, variational formulation is usually used where minimization of the partial differential equations for equilibrium of the body is carried out. The body is divided into simple elements and some simple variation of functions and geometry over each of them, is assumed. For example, in constant strain triangles linear variation of displacement but with constant strain and stress over each element is assumed while in quadratic elements quadratic variation of strains is the assumption. After the "mesh generation", the next step is to obtain the elemental stiffness matrices and then add them together to obtain the global stiffness matrix. The last step is to solve the resulting system of equations and hence evaluate the nodal displacement values.

In case of BIE method the analytical formulation involves the transformation of the governing partial differential equations applicable to the whole domain, into an integral relationship between boundary values of unknown functions. Hence, only the boundary need be modelled reducing the dimensionality of the problem. Also, because there is no interior discretisation, it is capable of providing results with higher resolution than FE method.

In the following sections, the results of the FE analysis will be given and a comparison between FE and BIE methods will be carried out.

3.3 Finite Element Analysis of the Structure

The first step in static analysis is the calculation of the weight and the centre of gravity of the structure and the determination of the number of supports for a stable structure. Detailed analysis is given in appendix B. The second step involves the cutting force calculations. The machine tool designed here incorporates turning, milling and drilling operations. The forces due to these operations should be calculated and then their components acting on the machine tool bed via the slide-way, headstock and turning turret connections should be estimated. This analysis is explained in appendix C.

After those initial calculations, the structure is ready to be analysed. For the structure, two alternative beds were designed as outlined in appendix B. The stiffer bed weighed nearly 3 tons. The lighter bed is just 2 tons and therefore is to be preferred, provided that the stiffness is acceptable.

In this section, the stiffnesses of these two structures will be compared by using finite element analysis. Before attempting this, the meshes for two different structures have to be prepared and checked for convergence.

After the convergence check and stiffness comparison the stress calculations carried out by the FE method can be used for reinforcement calculations. In the FE analysis, the structure will be assumed to be homogeneous. The

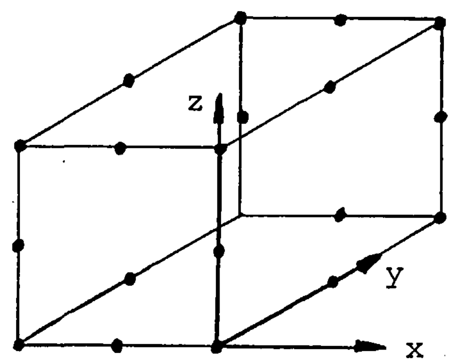

20 Nodes

Figure 3.1 The three dimensional brick element

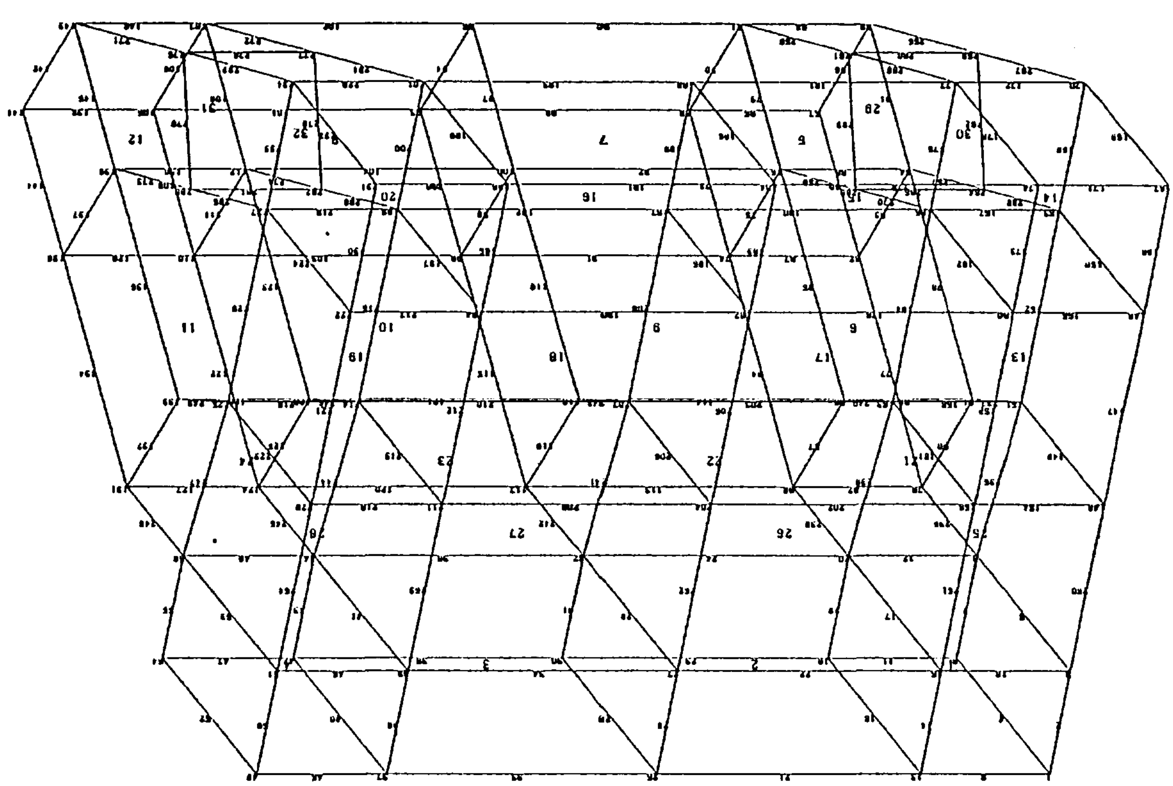

a) Coarse mesh

Figure 3.2 Two FE meshes for the heavier structure

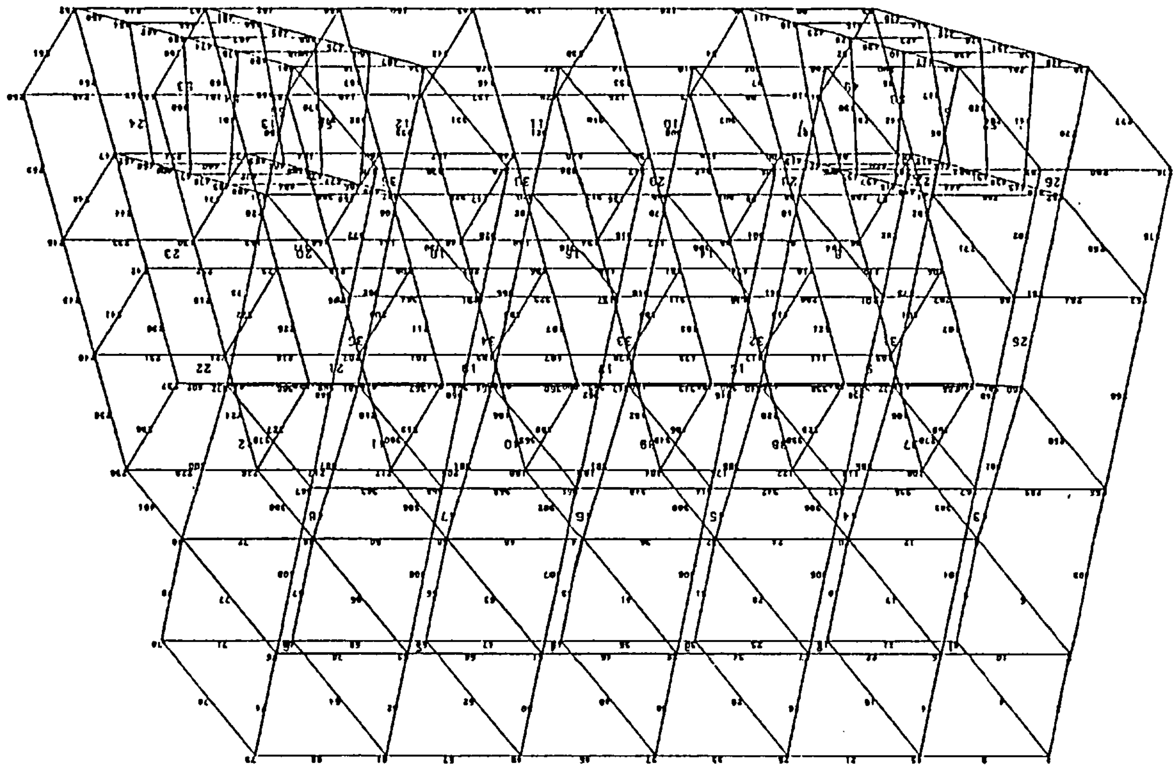

b) Fine mesh

Fig 3.2 (cont.d)

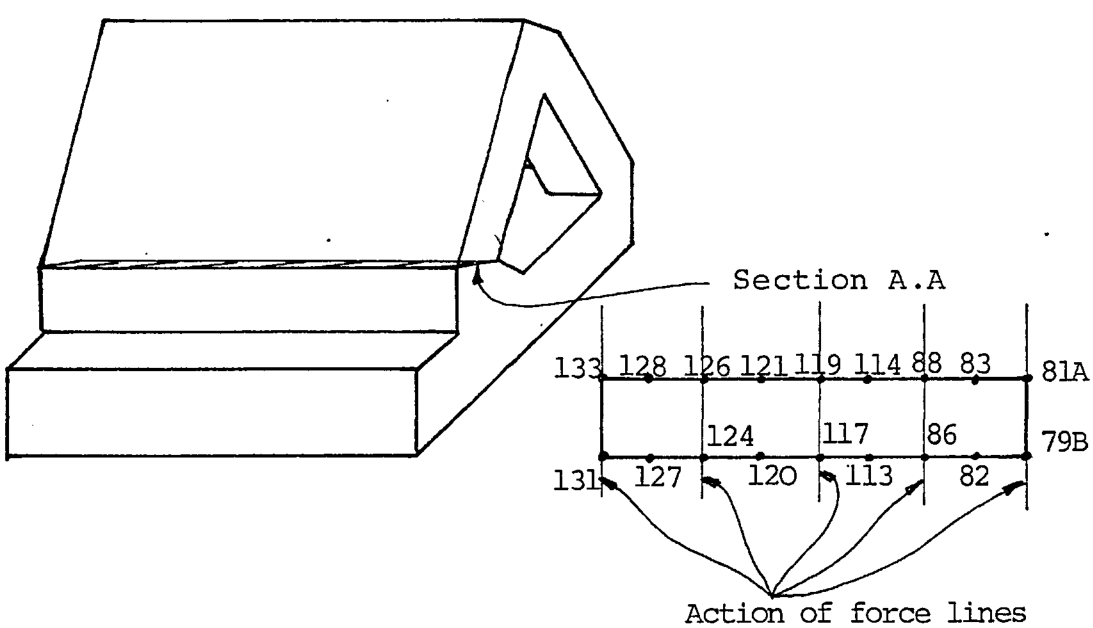

Figure 3.3 The cross section and the nodes where the convergence check is carried out

modulus of elasticity and the density of the concrete is taken as $2.11*10^5$ kg/cm^2 and 0.0024 kg/cm^3 respectively.

As the first step, two different meshes one coarse and the other finer are prepared for the heavier structure. The element used is a 3-D brick with twenty nodes as shown in figure 3.1. The two meshes are shown in figure 3.2. The first mesh has 286 nodes (858 degrees of freedom), while the second mesh has 489 nodes (1467 degrees of freedom). For the analysis a general purpose finite element program which was developed at Imperial College (51) was used. The displacement and stress calculations for the first mesh requires 274.4 secs on CDC 6600 computer. For the second mesh, the time requirement was 661.2 secs. In the analysis point loads are applied onto the nodes according to the force configuration shown in figure C.8. In the program four-point Gauss Integration Equations are used (44).

In order to check the convergence of the results stress and displacement points on several nodes are compared. The nodes where the comparison is carried out are shown in figure 3.3. A.A is a typical cross section used in the reinforcement calculations.

In figure 3.4 the largest stress component is compared for the two different meshes along the line where the nodes 81 to 133 are placed. The figure suggests that although there is some deviation, stress curves are following each other consistently. Deviation between the results can be calculated

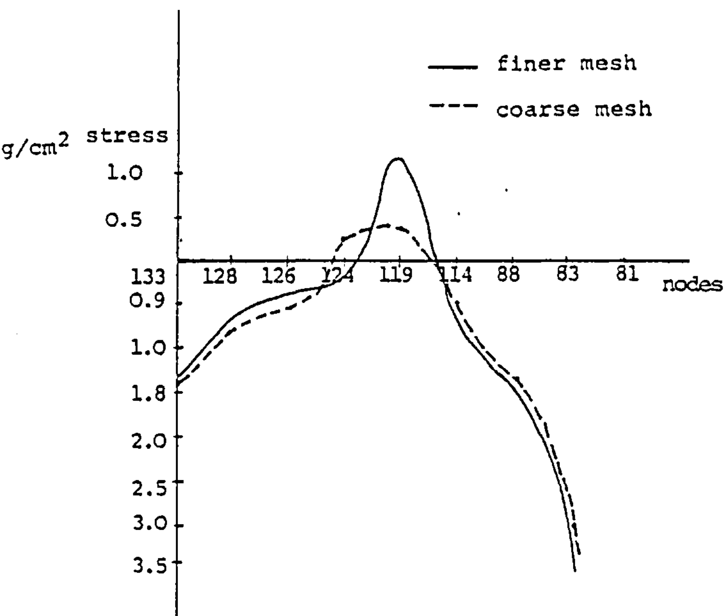

Figure 3.4
Stresses compared for the two meshes

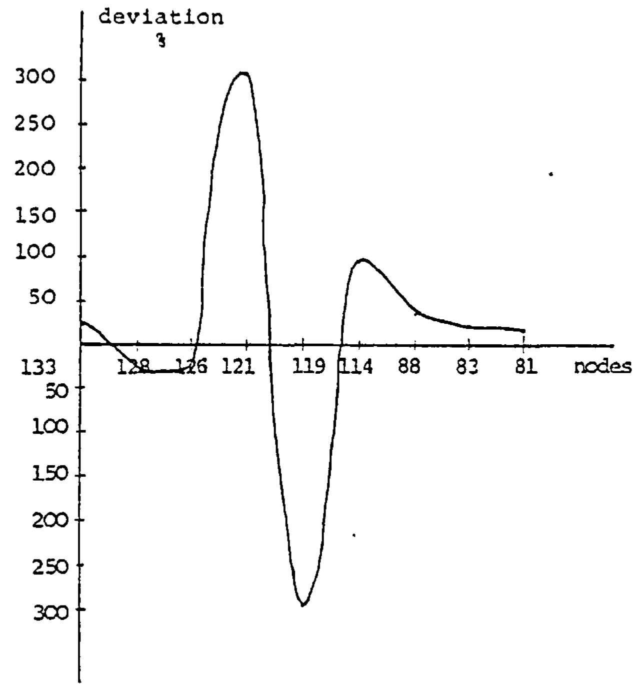

Figure 3.5
Deviation of the stress between the meshes

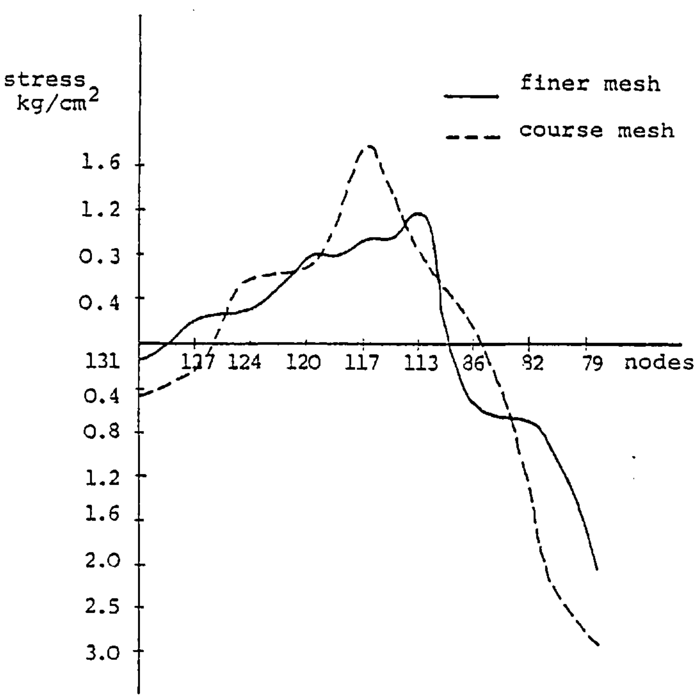

Figure 3.6 Stress compared for the meshes along the line B

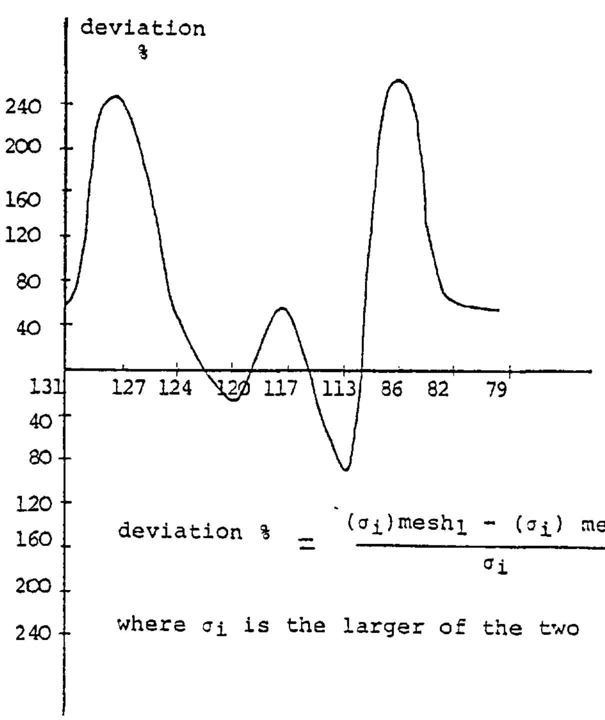

$$\text{deviation \%} = \frac{(\sigma_i)\text{mesh}_1 - (\sigma_i)\text{ mesh}_2}{\sigma_i}$$

where σ_i is the larger of the two

Figure 3.7 Deviation of the stress for two different meshes along the line B.

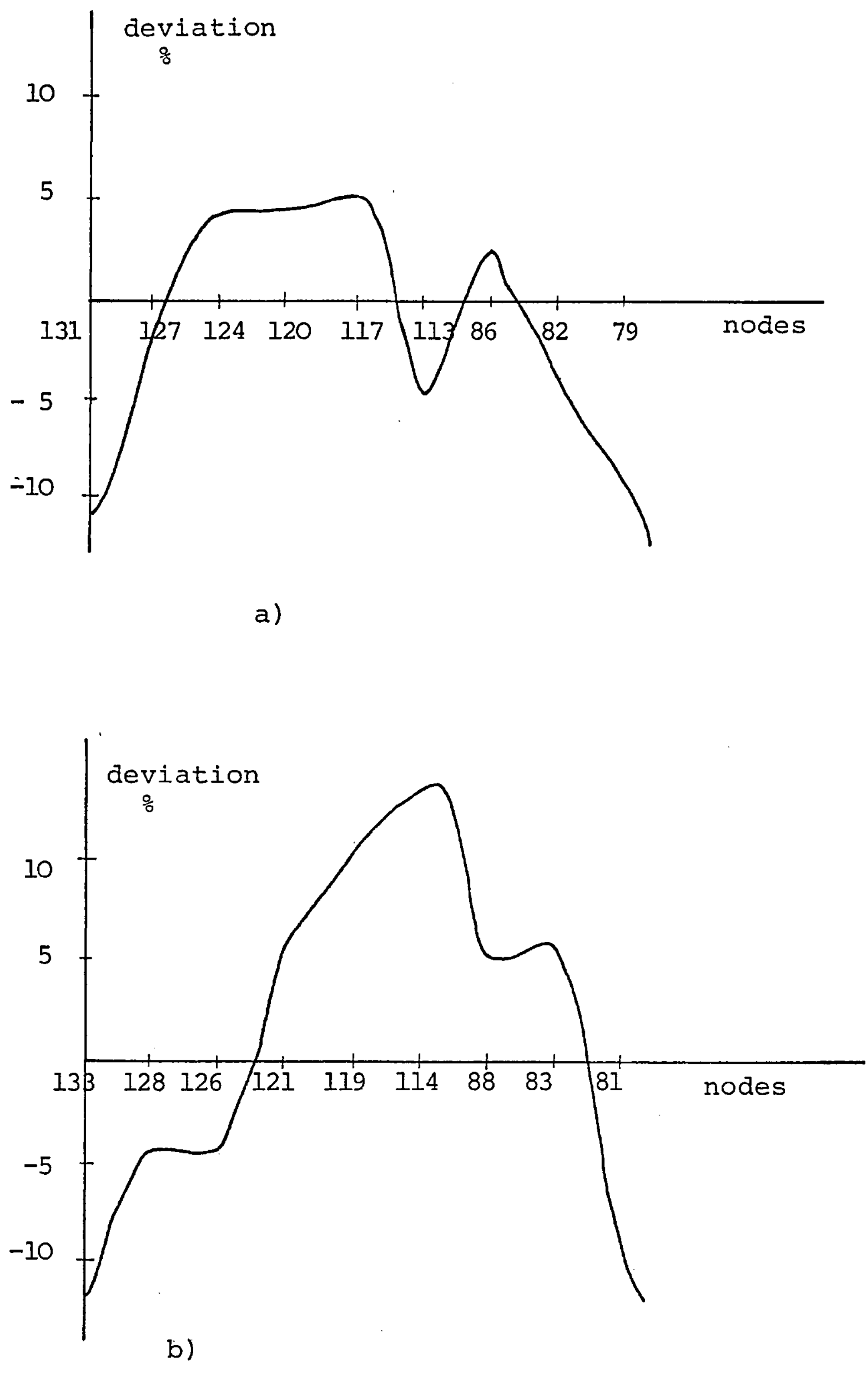

Figure 3.8 Deviation of displacements for the two different meshes

and plotted as shown in figure 3.5. The same calculations can be carried out for the line where the nodes 79 to 131 are placed. The graphs are shown in figures 3.6 and 3.7. Again the stress curves indicates that the results are consistent. However, when the deviation curves figure 3.5 and 3.7 are analysed, it is seen that at some points deviations can reach 300%. At a first glance this may suggest that the results from the two different meshes are in conflict. However, when the deviation curves are analysed together with the stress curves, it will be seen that the point where the deviations are high correspond to low stress points. At higher stresses, the error is between 20 and 80%.

The above analysis does suggest that the results have converged. As a final check, deviation of the displacements between the two different meshes are calculated and plotted in figure 3.8 a and b. The graphs show that the average deviation is below 10%. This close agreement confirms that the results have converged. Therefore, further analysis can be based on the results , obtained from the finer mesh, treated with a factor of safety.

In the light of the results for two different types of meshes, the mesh for the lighter structure can now be prepared. The mesh is shown in figure 3.9. It is based on the finer mesh and it has 411 nodes (1233 degrees of freedom). Displacement and stress calculations required 420 secs on CDC 6600 computer.

In order to carry out a stiffness comparison, the displacements normal to the surface along the two lines as shown in figure 3.10 are tabulated in table 3.1. The sign convention for the displacements is shown on the figure. From table 3.1, it is seen that, especially along z-direction, the stiffness of the lighter structure is 2 to 3 times less than the stiffness of the heavier structure. However, if it is considered that these deflections correspond to cutting forces when the full power of the machine tool is utilised, the deflections in the lighter structure will be seen to be still permissible. Average deflection being around 8 μm is still below the accuracy limit of the machine tool. Moreover, this accuracy limit is aimed at lower spindle powers. Additionally, when the structure is reinforced it will further decrease the deflections. Therefore, at this point, the lighter structure can be considered a feasible solution. The final decision should be made after the reinforcement calculations and dynamic analysis.

For the analysis, finite element method was used. However, as pointed out in section 3.2, BIE is a promising alternative for many engineering problems. In most cases, the resolution of BIE is greater than FE methods and the cost lower. However, for machine tool application, BIE method has not been checked against FE. In the next section, the two methods will be compared for structural analysis.

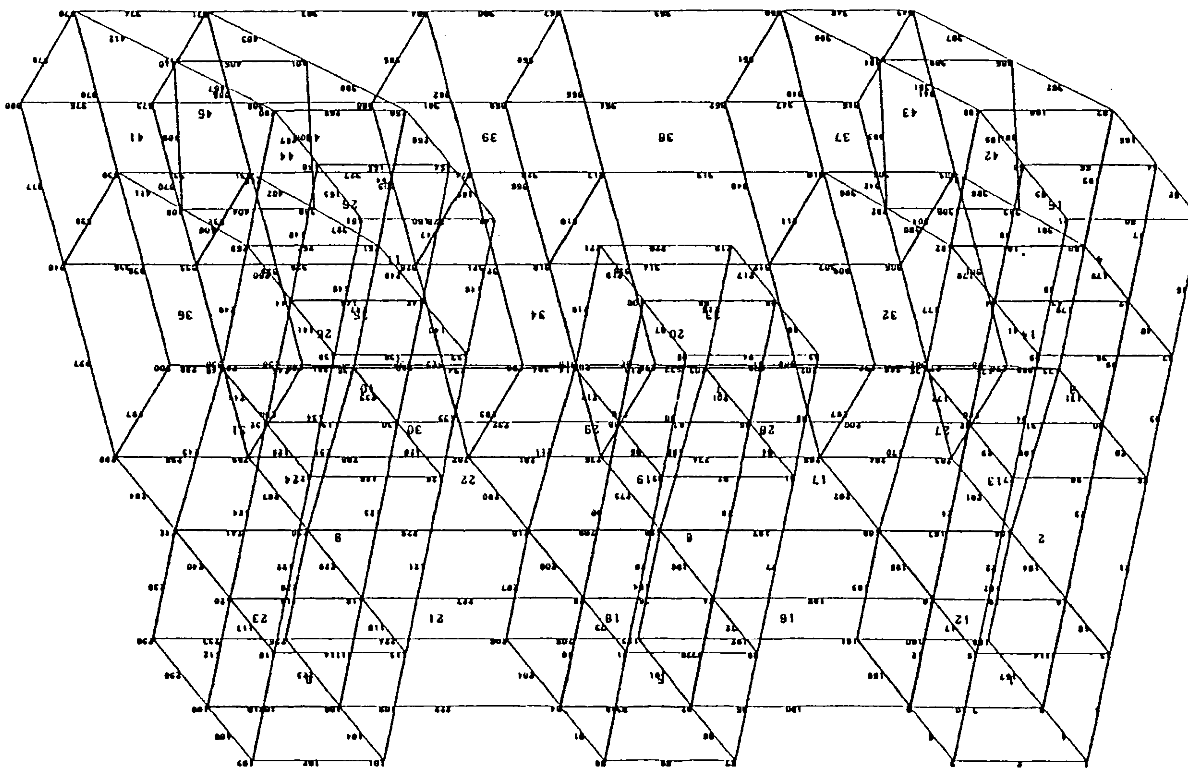

Figure 3.9 Finite element mesh for the lighter structure

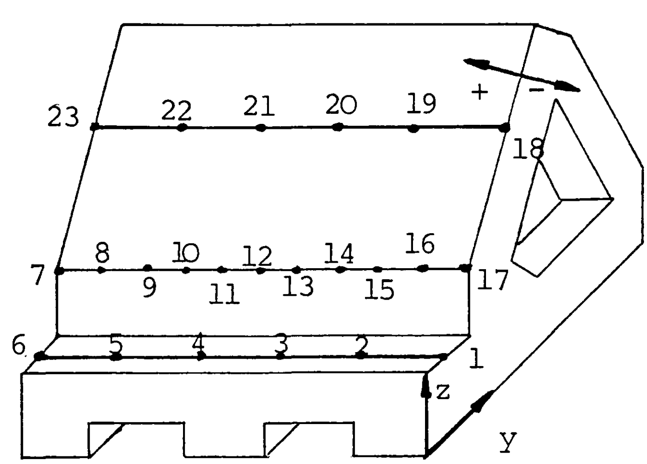

Figure 3.10 The points at which the displacements are compared

Table 3.1 Deflections on two different structures

	Light (cm)			Rigid (cm)		
	y * 10^{-3}	z * 10^{-3}	perp. to plane *10^{-3}	y*10^{-3}	z*10^{-3}	perp.*10^{-3}
1		-0.2355			-0.4042	
2		-0.3210			-0.537	
3		-0.3915			-0.1198	
4		-0.9637			-0.115	
5		-0.344			-0.2161	
6		-0.1286			-0.2161	
7	-1.043	-1.350	-1.57	-0.1227	-0.6131	-0.2
8	-0.7263	-1.073	-1.168	-2.2808	-0.5366	-0.0251
9	0.4490	-0.9203	-0.848	-0.411	-0.4743	+0.1188
10	0.1282	-0.7584	-0.49	-0.5516	-0.3967	+0.279
11	-0.1472	-0.6289	-0.442	-0.6078	-0.3737	0.339
12	-0.1658	-0.6103	-0.162	-0.5845	-0.3652	0.323
13	-0.1587	-0.555	-0.14	-0.5622	-0.3221	0.326
14	0.5164	-0.5408	-0.315	-0.4676	-0.291	0.259
15	0.4869	-0.5077	-0.676	-0.3059	-0.2254	0.152
16	0.4573	-0.5137	-0.653	-0.2336	-0.2018	0.101
17	0.6131	-0.5394	-0.8	-0.1514	-0.1913	0.0355
18	1.129	-1.699	-1.827	-0.7403	-0.6132	0.3345
19	0.8757	-1.202	-1.36	-0.649	-0.4494	0.3374
20	0.3932	-0.7079	-0.7145	-0.7222	-0.1261	0.5624
21	0.3673	-0.6615	-0.6488	-0.6556	-0.8067	0.5274
22	0.7253	-0.7468	-1.001	-0.4063	-0.1617	0.271
23	1.049	-0.8491	-1.333	-0.2145	-0.2145	0.7851

3.4 BIE Method Compared with FE

For the comparison, a computer program developed at Imperial College by C L Tan (43) was used. A mesh for the more rigid structure was prepared. Mesh preparation is similar to FE mesh preparation except that in BIE surfaces instead of volumes are considered. Each surface is taken separately and divided into elements; the continuity of elements from one surface to another should be satisfied.

The prepared mesh is shown in figure 3.11. In the mesh, smaller elements are used around the regions where stress concentration is expected. In the mesh preparation, it was assumed that the point loads can be converted into equivalent surface tractions, and nodes have been provided at the points where the loads act. The mesh have a total of 91 elements and 233 nodes. From the previous experiences, a problem with this mesh size was estimated to take around 800 secs on a CDC 6600 computer. It is longer than the time taken for the finer mesh of the finite element problem (661 secs). Again, from the previous experiences and from the comparison of the two meshes, it was decided that BIE would give better results, because stress concentration effects can be considered in more detail with BIE mesh than with FE. In a BIE analysis it is possible to have a much more rapid change in element size than in an FE

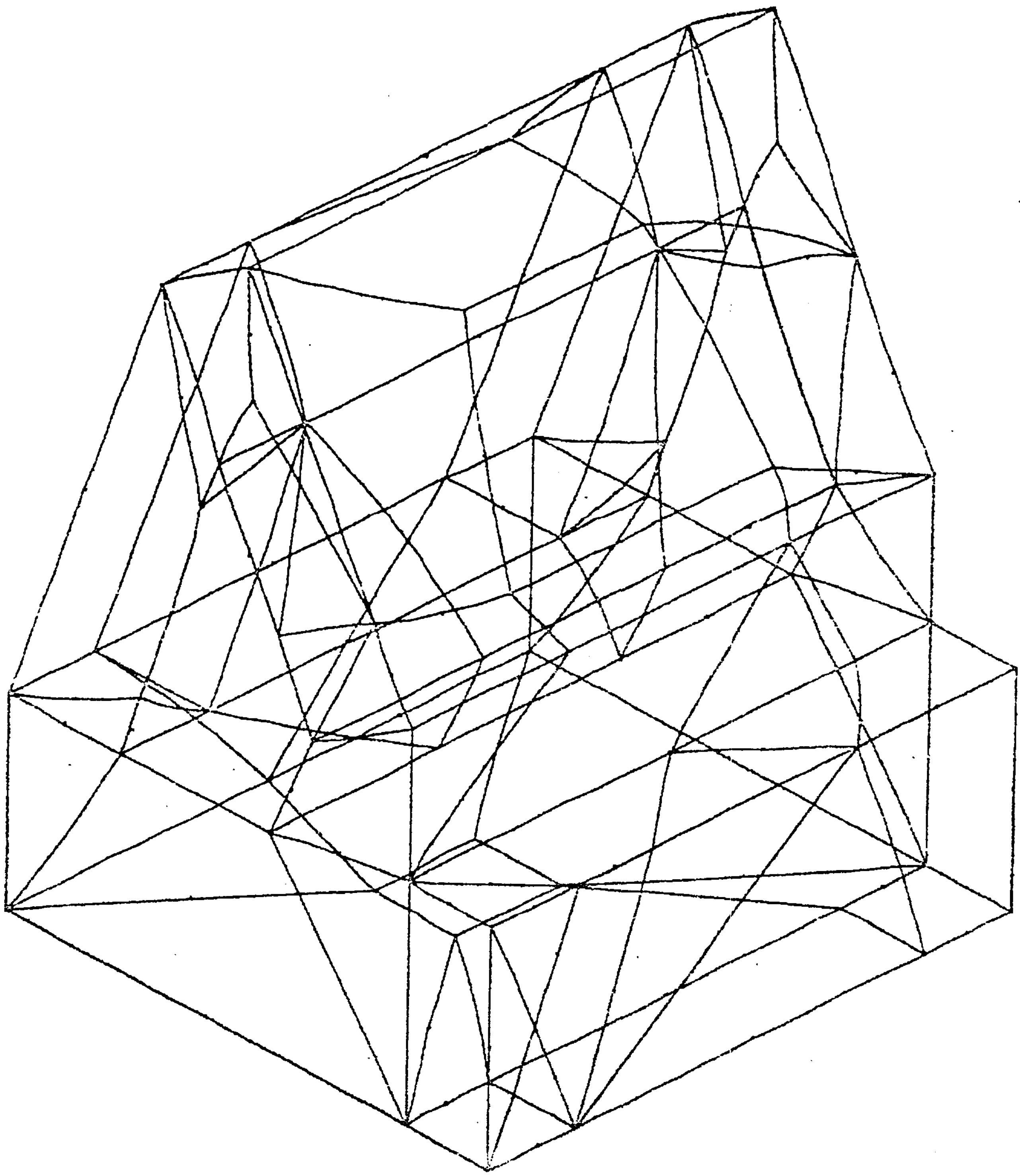

Figure 3.11 BIE mesh for the more rigid structure

analysis and hence stress concentrations can be considered more closely.

This problem was not actually solved on the computer, because little could be achieved with the solution. There are two main reasons for this. Firstly, an analytical solution for the problem does not exist, so it will be impossible to compare the results against a theoretical solution. Secondly, conversion of the point load idealisation used for FE to surface tractions for BIE is a very difficult process. Therefore, it would be impossible to determine if the deviations from the FE results are due to the inaccuracies in the conversion or due to the methods themselves. Therefore, for a direct comparison of the two methods, two further problems with known theoretical solutions were tackled. In these problems, pressure loading was preferred to point loads because it can more readily be simulated for both methods.

The first problem solved is a simple Cantilever beam in tension. FE mesh has 1 element and 20 nodes while the BIE mesh has 6 elements and 20 nodes. In the analysis, Poisson's ratio was used as 0.0, because then the effect of the end constraint on the theoretical results will be negligible. The results show that FE method gives exactly the same results as theoretical solution (figure 3.12). For BIE, although there is some deviation from the theoretical results, it is only 0.1%. Therefore, the results are acceptable. The time required for BIE solution on a CDC 6600

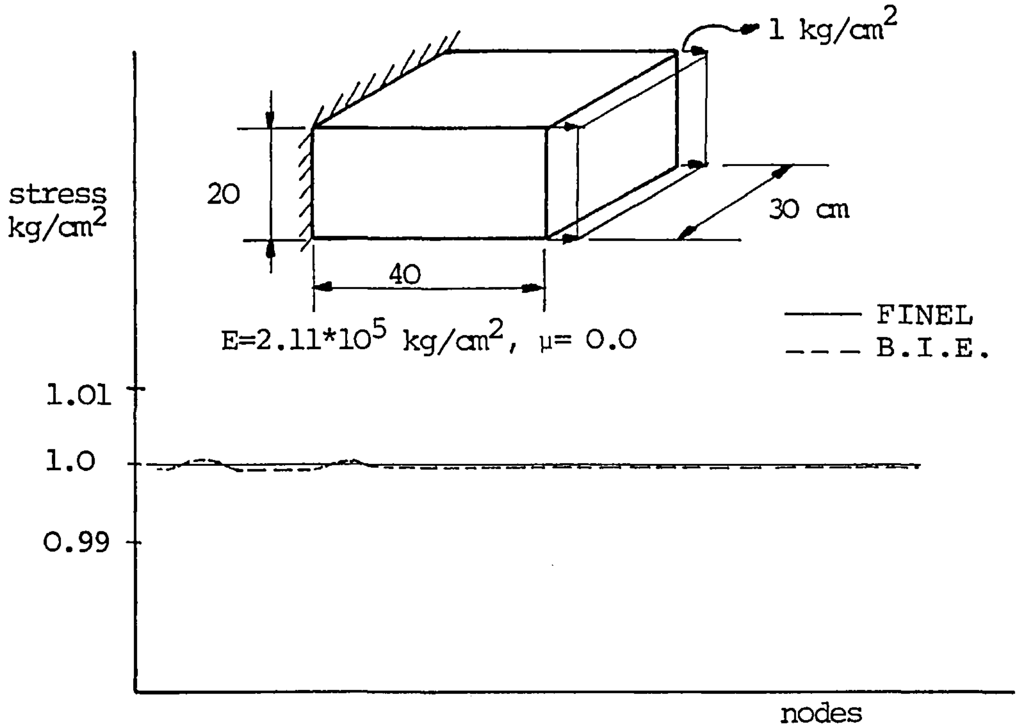

Fig 3.12 FE and BIE methods compared for a cantilever beam in tension

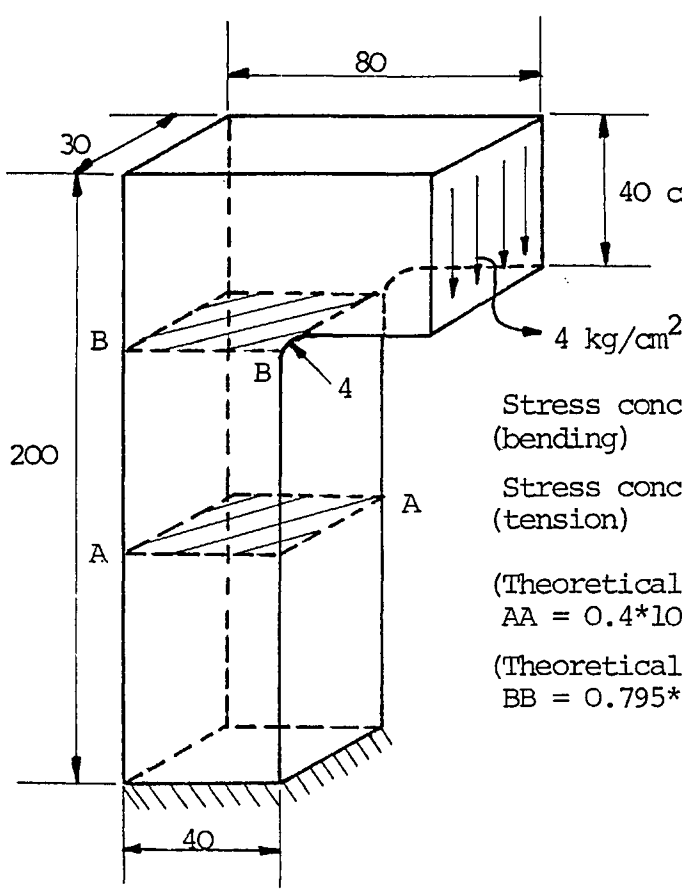

Stress conc. factor (bending) = 1.94

Stress conc. factor (tension) = 2.42

(Theoretical stress) AA = $0.4*10^3$ kg/cm^2

(Theoretical stress) BB = $0.795*10^3$ kg/cm^2

Fig 3.13 Stress concentration problems solved for comparison computer is 6.13 whereas the time for FE is 13.13 secs. It is seen that for this simple problem, BIE is much more effective. With almost the same level of accuracy, the computing time is half of the FE analysis.

Secondly, a more complicated problem was analysed. The stress concentration problem is shown in figure 3.13. The theoretical stress concentration factors and the stresses at the sections of interest are indicated in the same figure. Mesh prepared for BIE has 44 elements and 120 nodes whereas for FE it has 64 elements and 453 nodes. The two meshes are shown in figure 3.14. Both problems are solved on the same computer; the time taken for FE solution was 591 secs whereas for BIE, it was 243 secs. The results obtained from the two solutions are plotted in figure 3.15. Around section A.A, FE results and theoretical results coincide exactly wheras for BIE the deviation is around 3%. At the stress concentration region, deviation for BIE results is around 5% and it is 7% for FE. The comparison suggests for a similar level of accuracy, the time taken for BIE analysis is less by a ratio of 2.4 than that of FE analysis.

If a quick decision were reached based on the last two examples, it would be very much for the favour of BIE method. However, the first example on the actual machine tool structure showed, there are some cases where the BIE method is not so economical. The cost advantage of BIE

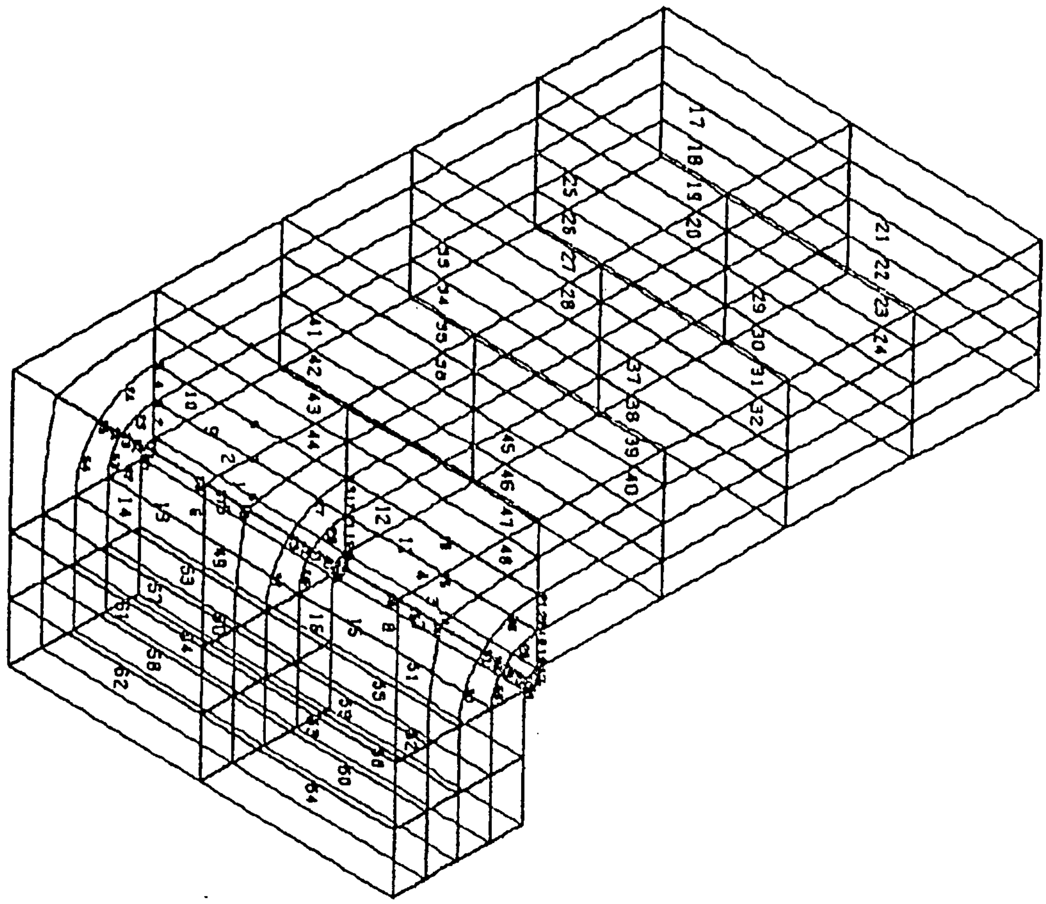

a) FE mesh

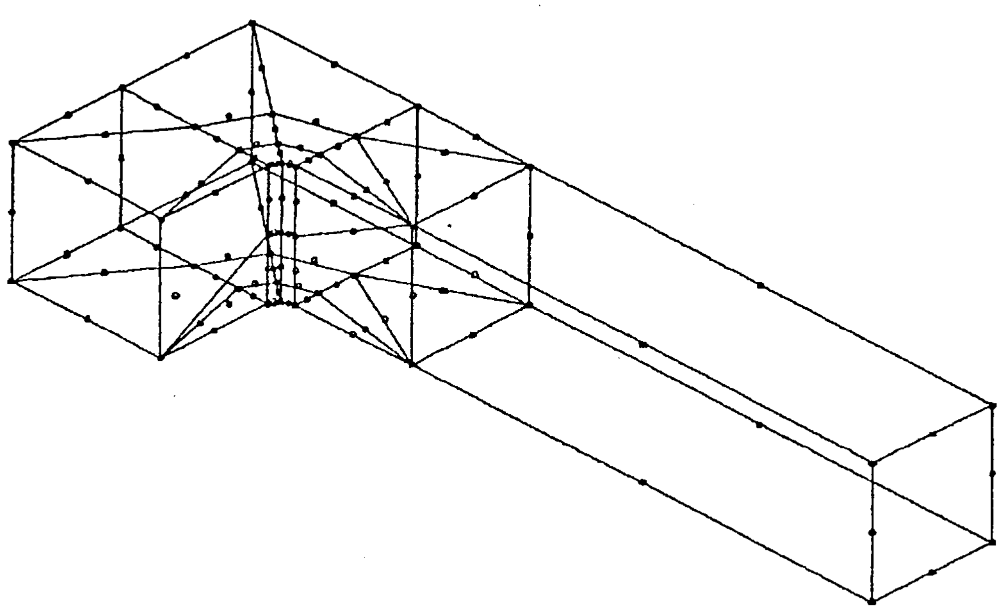

b) BIE mesh

Figure 3.14 BIE and FE meshes for the stress concentration problem

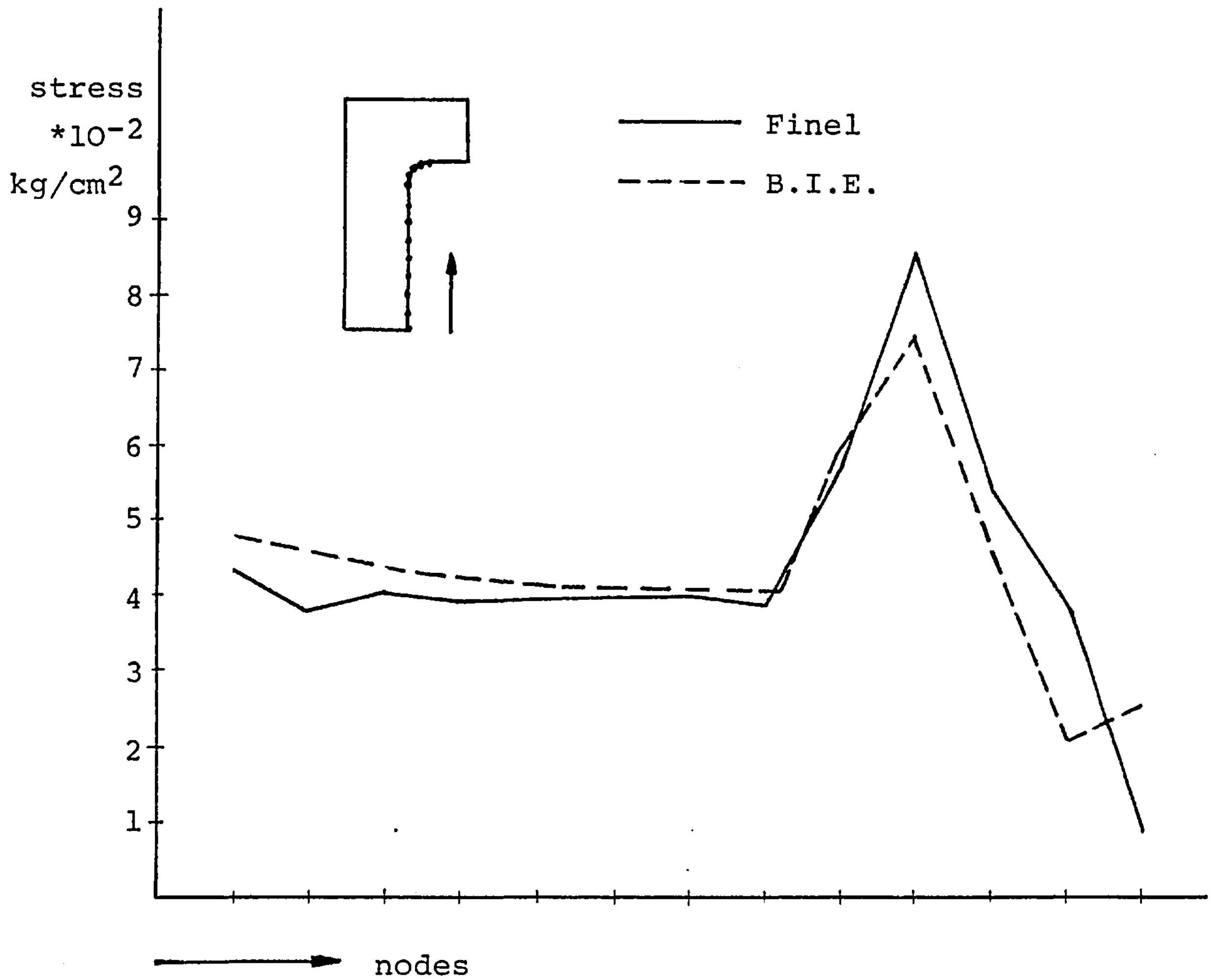

Figure 3.15 F.E. and B.I.E. methods compared for stress concentration.

method decreases as the surface to volume ratio increases. In the first example, because of the high surface to volume ratio and because of the large number of point loads BIE method was less advantageous. Also in plate and simple beam analysis, BIE methods do not show any advantage over FE methods. However, in structural problems where the surface to volume ratio is not excessive, it will be possible to decrease the number of point loads by distributing them as pressure loads. Therefore, in such structural problems, BIE methods will be advantageous.

3.5 Reinforcement Design

In section 3.3, deflection and stress configuration of the structure were determined through finite element analysis. If the stress values given in figure 3.4 and 3.6 are investigated, it will be seen that stresses are actually low and a small amount of reinforcement will be satisfactory to accommodate for these stresses. Therefore, the governing factors in the reinforcement design is not so much the stress, but good creep behaviour and control of deflections. In appendix A, influence of reinforcement on creep and shrinkage behaviour of concrete was analysed. There, it was suggested that for good creep behaviour, reinforcement should be symmetric and compression steel should be used. Using compression steel is also necessary as a safety feature, because the loads can be cyclic and compression and tension sides can change. Therefore, in the analysis doubly reinforced sections will be used.

Reinforcement calculations will be performed according to the stress analysis results, and necessary changes will be made to ensure smaller deflections. For doubly reinforced sections the general method of calculation is indicated in figure 3.16 (25). In the figure, the design is based on the bending stresses. The shear stresses can also be calculated and the steel area can be checked against the shear stresses by using the following equation,

$$\frac{M_r}{bd_1{}^2} = Q \qquad (3.6)$$

where Q is the shear stress. However, the shear stresses are usually small, so the governing design criteria is the bending stresses.

In case of finite element method, the stresses on a section are calculated directly. So the overall tensile force acting on a section can be found directly and once this is found, the following equation,

$$\frac{F_T}{f_{st}} = A_{st} \qquad (3.7)$$

gives required steel area.

In the analysis, fatigue should also be taken as an important factor. The following are usually suggested for

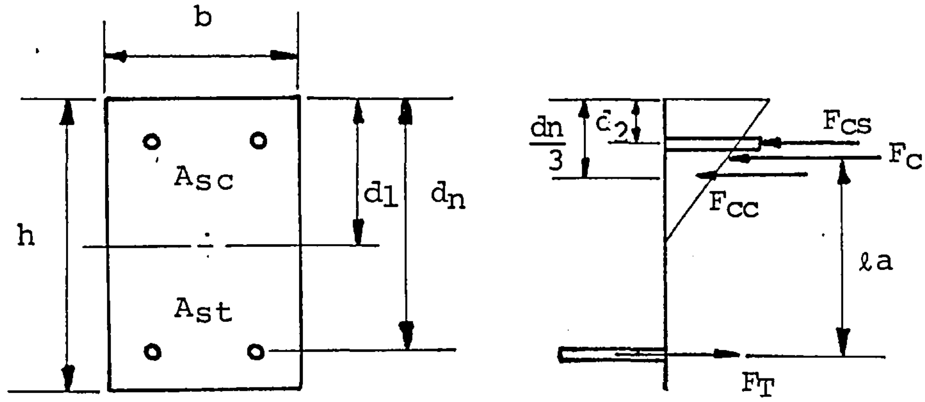

$$\ell a = d_1 - \frac{bd_n^3 + 6A_{sc}\ (m-1)\ (dn-d_2)\ d_2}{3bdn^2 + 6A_{sc}(m-1)\ (dn-d_2)}$$

where $m = \frac{E_s}{E_c} \simeq 7.5$

$M_r = A_{st} \cdot f_{st} \cdot \ell a$

where M_r is the bending moment on the section

A_{st} is the required tension steel area

f_{st} is the allowable stress of the steel

and E_s and E_c are the modulus of elasticies for steel and concrete respectively.

Fig. 3.16 Calculation of the steel area for doubly reinforced sections.

good fatigue behaviour (25), (34).

i) High ductility steel should be used in reinforcement.

ii) Bar bends should be avoided in the highly stressed sections.

iii) Tack welds should be avoided, properly executed butt-welded joints or full penetration fillet welds are to be preferred.

iv) The fatigue strength of concrete is about 0.55 times its static strength.

v) Design stress for steel should not exceed 140 MN/m^2 (1400 kg/cm^2).

The calculations for the reinforcement can be carried out using these rules together with those required to ensure good creep behaviour. In the calculations, a factor of safety of 2.5 is recommended to account for uncertainties and fatigue failure.

Detailed reinforcement calculations were carried out for both the stiffer and the lighter structures; some sample calculations and obtained results are given in appendix D. The results are summarised in tables D.3 and D.4. Here, table D.4 is repeated for convenience and the results are summarised in table 3.2. Also in the same table, percentage area of steel for the relevant cross sections is included.

In BS code CP114 (clause 313), the economic percentage of steel reinforcement (when both concrete and steel are stressed to the full permissible values) is given. For a nominal mixture of 1:2:4 and for 140 MN/m^2 tensile stress reinforcement, the economic percentage is around 1%. This figure can be taken as a guide to assess the reinforcement. As seen in table 3.2, percentage areas of steel are much less than the economic percentage suggesting a lightly reinforced structure. However, before determining the final reinforcement, the effect of creep and also the deflections should be taken into account. As mentioned earlier, symmetric reinforcement should be used to ensure good creep behaviour. The most critical sections from the point of view of deflections are the section A.A, B.B for the upper plane and section C.C for the base. Columns, that support the inclined plane, also play an important role. Therefore, steel areas around these sections should be increased.

With the guidance of the above discussion, a reinforcement schedule for the structure was prepared. It is shown in figure 3.17. The percentage areas of steel is given in table 3.3. The figures show that the structure is still lightly reinforced, however, considerable increase in the percentage area of steel is achieved around the regions critical for deflections. It can be noted that sections

Table 3.2 Tensile steel areas required at several sections of the lighter structure.

	A (tensile) (cm^2)	% area
section A.A	8.313	0.28
section B.B	1.2	0.085
section C.C	0.91	0.06
section D.D	0.19	0.03
section E.E	1.6	0.23
section F.F	0.19	0.03
section G.G	0.4	0.065
column	0.6	0.15

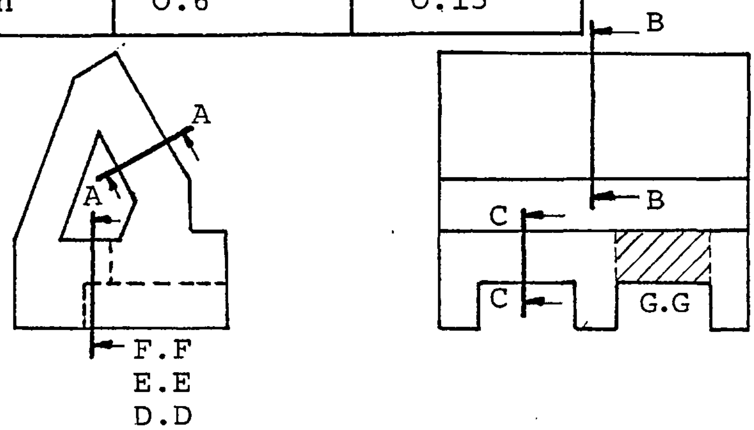

Table 3.3 Percentage areas of steel for the final reinforcement

	A (tensile) cm^2	% area
A.A	11.31	0.38
B.B	4.6	0.33
C.C	3.39	0.22
D.D	3.14	0.45
E.E	3.14	0.45
F.F	3.14	0.45
G.G	1.6	0.27
column	2.2	0.55

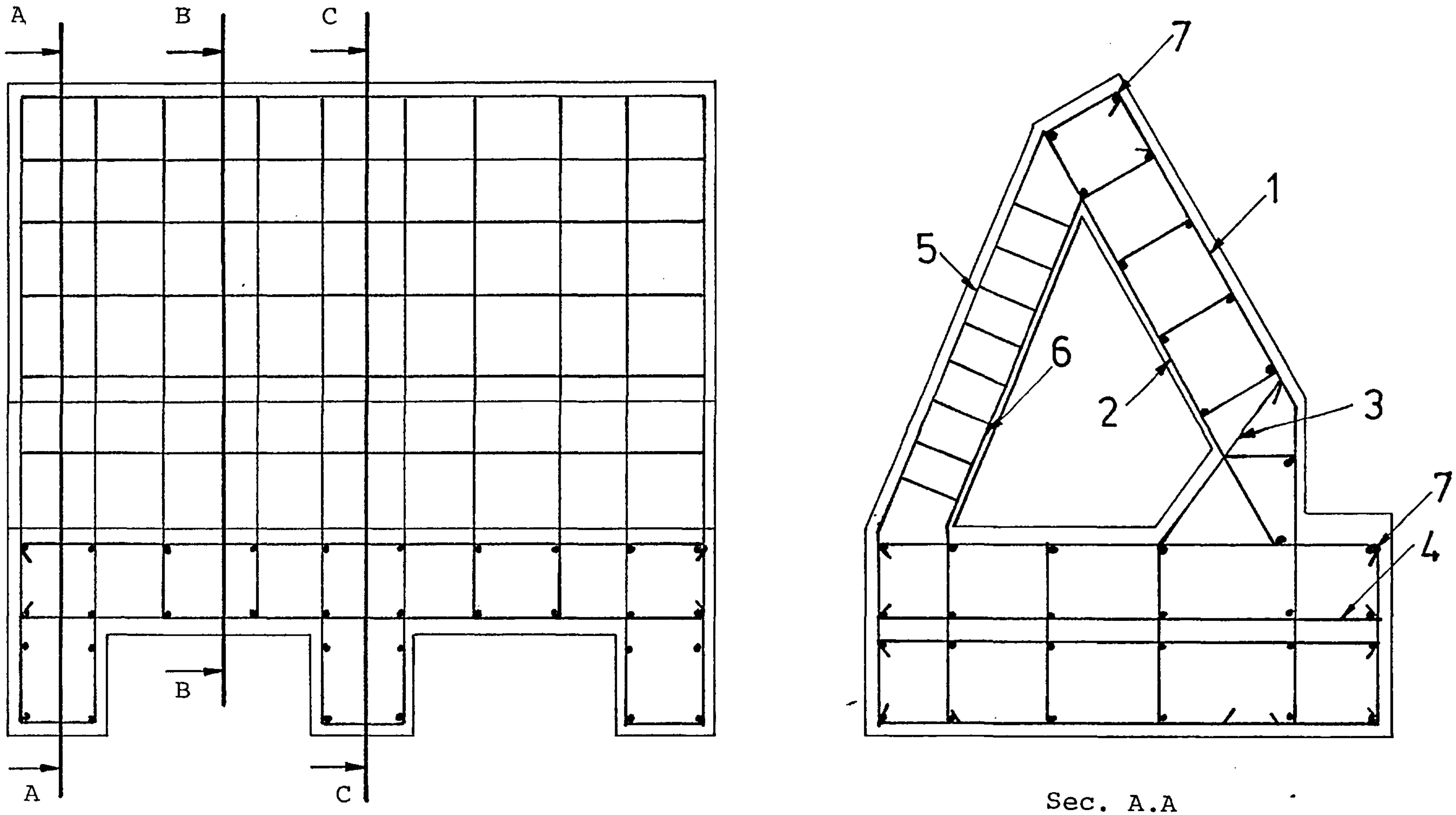

Figure 3.17 Reinforcement for the lighter structure

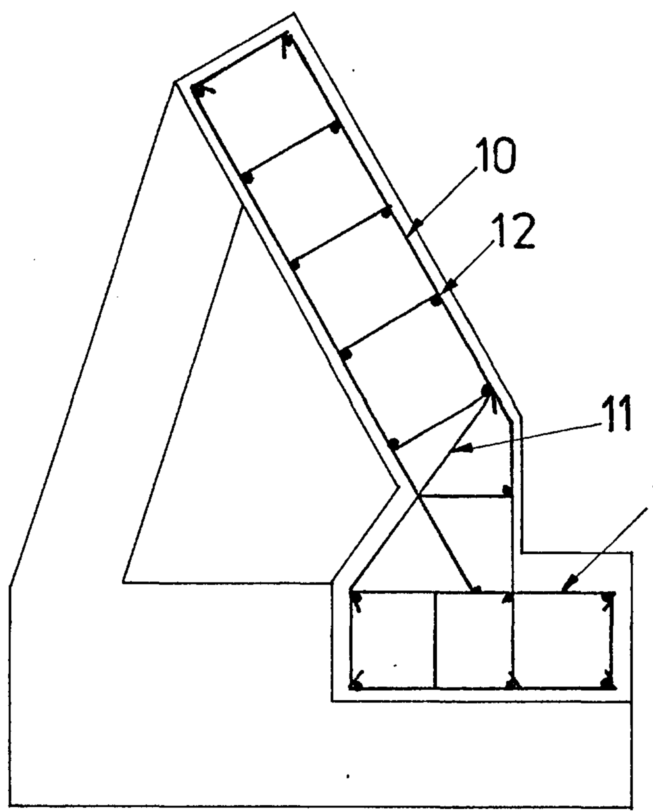

sec. B.B

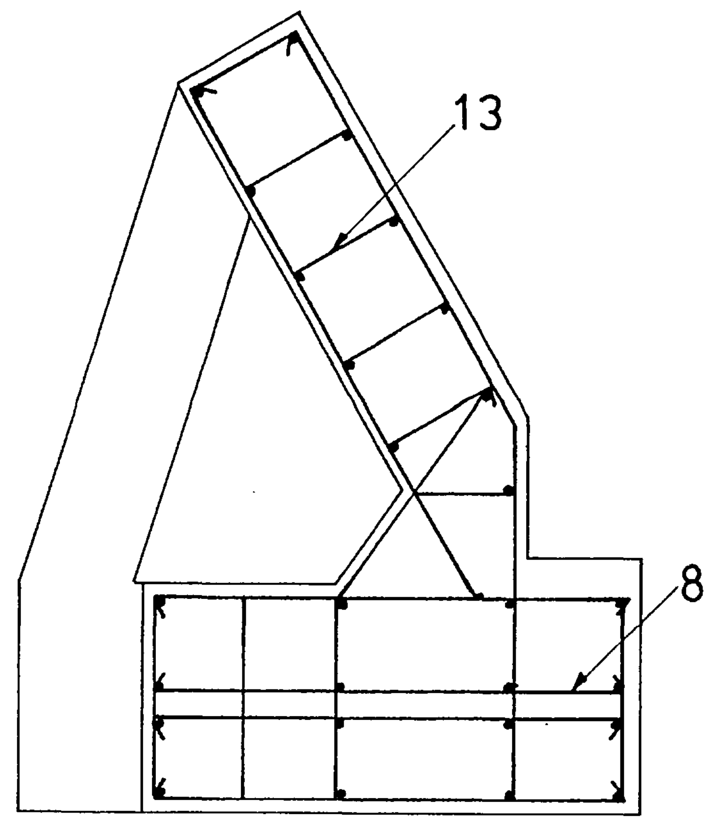

sec. C.C

Figure 3.17 (cont.d)

Figure 3.17 (cont.d)

Bar mark	Type & Size	Total number	Length (cm)	Shape
1	R 12	6	153	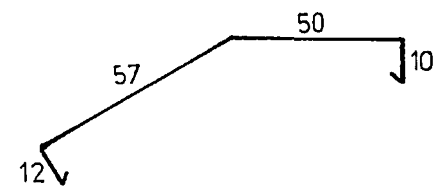
2	R 12	10	111	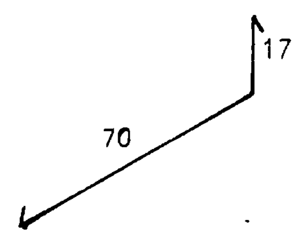
3	R 12	6	112	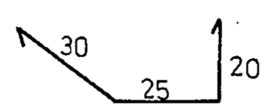
4	R 10	24	100	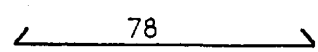
5	R 12	40	150	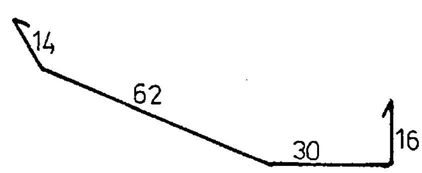
6	R 12	4	130	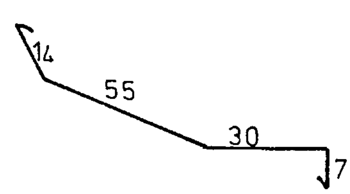
7	R 12	10	130	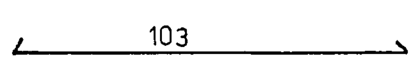

Figure 3.17 (cont.d)

Bar mark	Type & Size	Total number	length (cm)	Shape
8	R 10	8	88	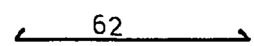
9	R 10	8	58	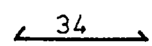
10	R 10	4	150	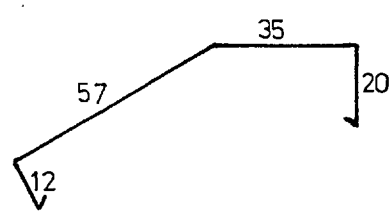
11	R 12	4	86	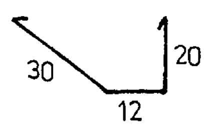
12	R 10	7	130	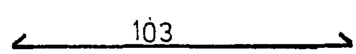
13	R 8	6	38	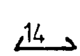

D.D, E.E and F.F although not critical for deflections have a considerable amount of reinforcement. This was the result of the symmetricity considerations.

3.6 Inserts and Attachments:

An important consideration during the design of the bed is the placement of the inserts and attachments on the structure. These are necessary for the connection of the machine tool component onto the bed.

There are two main possibilities for the configuration of attachments. The first is to cast separate plates into the concrete to provide fixing locations for the assemblies and bearings. The second approach is to use a large steel fabrication to carry most of the machine tool components. The second method may result in a heavier structure because of the fabrication, and a separate fabrication decreases the modularity of the machine tool and increases the cost. For these reasons, the first method will be adopted. So separate plates will be cast on the relevant locations. The locations of the plates are shown in figure 3.18. The steel attachments will have anchorages welded with full penetration fillet welds to the reinforcing bars. Detailled calculations are carried out in appendix E. A typical example and the dimensions as obtained in appendix E are shown in figure 3.19.

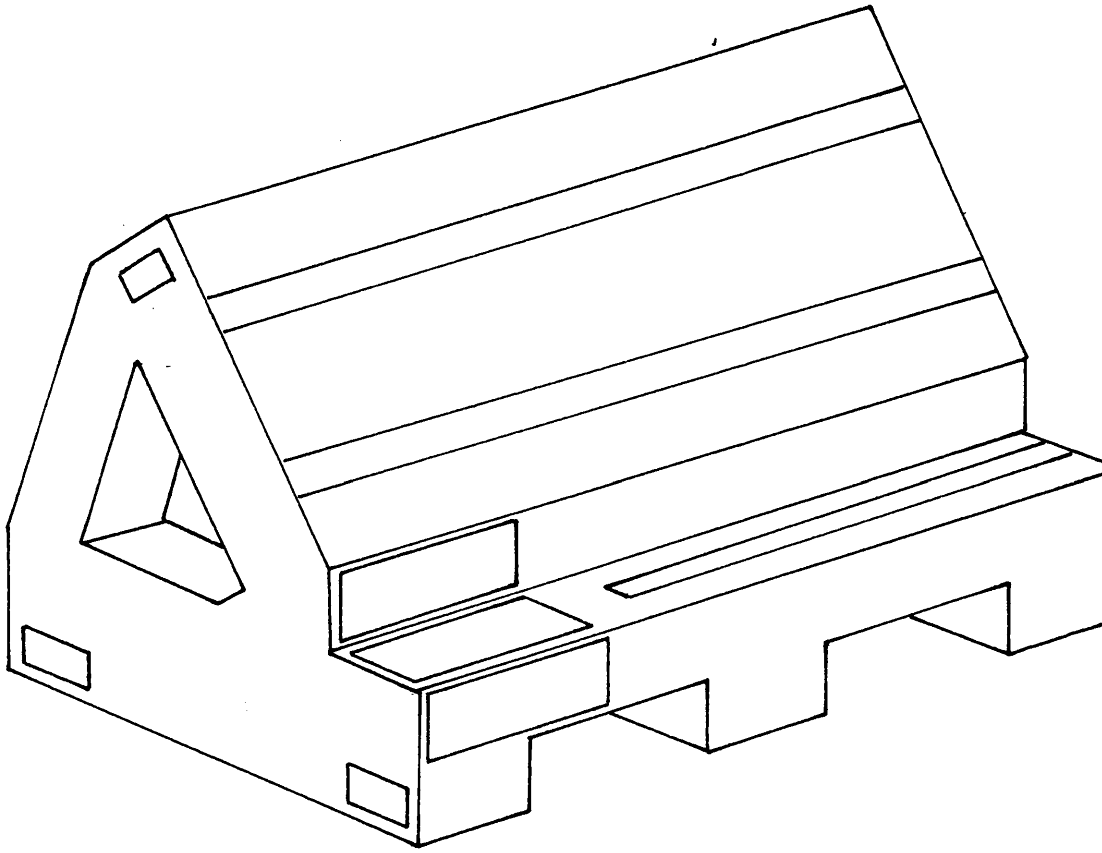

Figure 3.18 The location of the plates in the machine tool structure

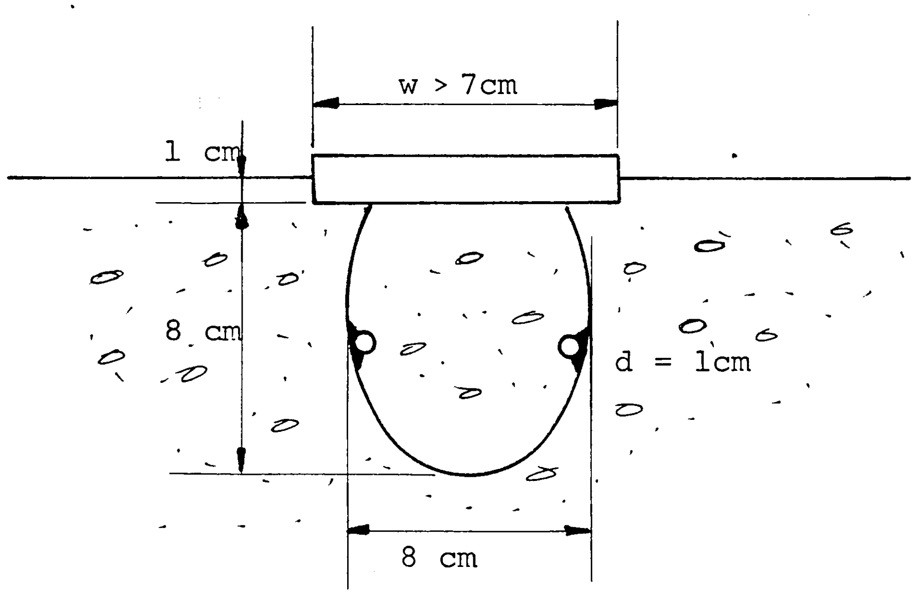

Figure 3.19 A typical attachment

3.7 Discussion and Long Term Stability of the Structure

The deflection and stress analysis was performed only for load case a) of fig C.2 which is the case where the cutting is carried out by the upper turret and the total load is supported by the tailstock. In this section, the other load cases will be considered and then an assessment of the reinforcement and long term stability of the structure will be carried out.

Firstly, the other load cases should be assessed to see how critical they are. As seen from fig C.2, case b) corresponds to the case where cutting without tailstock is carried out with the upper turret involved. Case c) is exactly the same as case b) except this time lower turret is employed in cutting. When the forces given on table C.2 are analysed, it is seen that for case b) all the forces acting on the inclined plane are the same as case a). Therefore, for the inclined plane the most critical loading case is a) or b) For the lower plane, near to the base, the most critical case is c). Indeed, some analytical calculations to find out the approximate bending moments on several sections of the structure were carried out for cases a) and c). They should give the extreme cases for the inclined plane and the lower plane. The results are tabulated in table 3.4. As seen from the results in case c), the moments along section c.c are much higher than in case a).

Table 3.4 Moment Comparison between force cases a) and c)

	Case a Moment kg cm	Case c Moment kg cm
sec A.A	18000	5000
sec B.B	27000	21000
sec C.C inclined plane	14000	20000
sec C.C lower plane	91000	123000

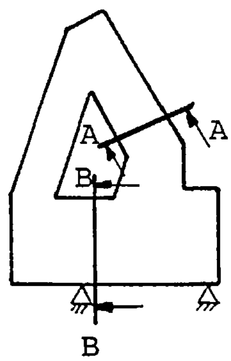

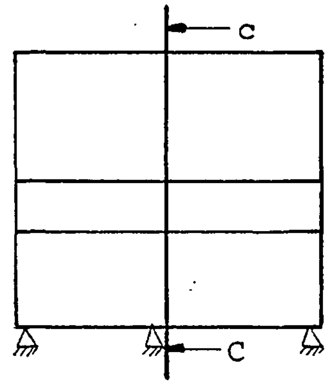

Table 3.5 Rigidity comparison of the two structures

Structure 1 (Heavy)		Structure 2 (light)	
Node number	deflection (cm)	Node number	deflection (cm)
162	$-3.5*10^{-4}$	316	$-5*10^{-4}$
196	$-5.8*10^{-4}$	323	$-4.5*10^{-4}$
210	$-4.7*10^{-4}$	282	$-5.6*10^{-4}$
224	$-3.54*10^{-4}$	275	$-6.2*10^{-4}$

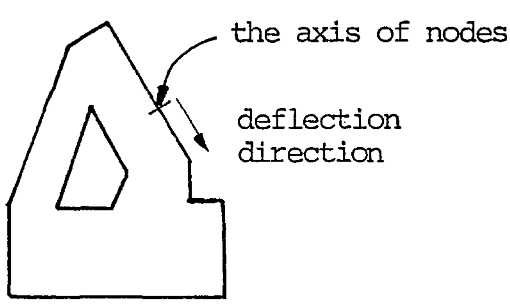

However, because of the support configuration and shape of the structure, that moment component will not substantially affect the deflections. Stress requirements were very easily fulfilled for case a). Therefore, the analysis as based on case a) will be satisfactory.

The reinforcement calculations were carried out with the FE results by using a factor of safety of 2.5. This safety factor is intended for the uncertainties in the loading and also for dynamic load effects. However, this will not compensate for stress concentration effects. Therefore, during the design, heavier reinforcement was used around the stress concentration points. It is also necessary to round the corners as much as possible to reduce stress concentrations.

A general stiffness comparison between the two structures were carried out in table 3.1. However, the most important stiffness direction is the one which is perpendicular to the cutting velocity. The stiffness in this direction affects the accuracy of the machine tool directly. Deflections along this critical direction is given in table 3.5 for the nodes which are near to the middle of the bed. These deflections are obtained from the FE analysis without taking the reinforcement into account. In order to see the effect of reinforcement equation 3.7 can be used (24).

$$I_{ucr} = bh^3/12 + (m-1)\ As\left(\frac{h}{2} - d_2\right)^2 \qquad (3.7)$$

where I_{ucr} is the second moment of area of the uncracked section, including the steel. The rest follows the same convention as in fig 3.14.

Substituting into eqn (3.7) for section A.A

$A_s = 12.27 * 2 = 24.54\ cm^2$ $m = 7.5$, $b = 150$ cm,
$h = 25$ cm $d_2 = 4$ cm

I_{ucr} is obtained as 206 840 cm^4 which is bigger by 6% than the second moment of area which does not include steel. Then for the cross section A.A deflections will be decreased by 6% because of the reinforcement. Heavier reinforcement was employed around the columns. This will further decrease the reinforcement.

In order to make a conservative assessment of accuracy values of deflection based on the unreinforced structure can be used. From the table 3.5, the maximum deflection is obtained as 0.006 mm. This deflection takes place during rough cutting. If the forces are halved for finishing cuts, the deflections come down to around 0.003 mm which leaves 0.007 mm of permissible deflections for the other parts of the structure to satisfy the 0.01 mm accuracy requirement. However, the accuracy is affected by the stability of the cutting process as well. Therefore, some safety margin should be left for the dynamic cutting process. Dynamic properties of the structure will be analysed in the following chapters.

Another important consideration for the reinforced concrete bed is the long term stability due to creep and shrinkage. To calculate the total deflection due to creep and shrinkage equation (A.11) can be used,

$$\Delta_t = K_r \, T_u \, \Delta_i$$

$$K_r = 1.7 \text{ (from equation A.12)}$$

and T_u can be taken as 2 from table A.1 assuming that the loading of the structure will be commenced after 28 days. Knowing that Δ_i is 0.006 mm, maximum creep and shrinkage deflection can be found as 0.007 mm. That is a considerable amount of deflection when the required accuracy of the machine tool is considered. However, knowing that about half of the creep and shrinkage deflection takes place in the first two months, and about 95% of the phenomena is completed in the first year, the shipping and recalibration can be arranged to eliminate the errors due to creep and shrinkage.

Thermal behaviour of the structure is also a very important factor in the overall assessment of a machine tool. Thermal behaviour of NC machine tools has been investigated by Spur (35), and many others (36), (37). The investigations show that it is very important to minimize the thermal effects at the initial design of the structure. For this purpose, all the heat generating parts of the structure such as the motors should be placed away from the structure. Also, the design of the tool should be suitable for chip removal. In this particular design, these effects were considered and an inclined bed machine tool were designed. If during the detail design, the heat generating parts of the structure are kept away from the working area thermal deformation will not represent a problem for the accuracy range we are interested in. However, to nullify these effects completely, temperature changes on some vital parts can be measured and fed back to the microprocessor which in turn sends the necessary commands for compensation. In a versatile control system on microprocessors that can be implemented in an economical way.

A final consideration on the reinforced concrete bed will be to secure its resistance agains the swarf abrasion and lubricants. There are two main alternatives practiced at the moment (29), one is to paint the surface with an epoxy paint the other is to cover the surface with a thin sheet of metal or plastic. The first method is still under development and the effectiveness of the coatings should be examined in more detail. The second method is more practical at the moment. Plastics are noise free and they have a low coefficient of friction; therefore they can be preferred to metal if they have sufficient wear resistance.

3.8 Conclusions:

In this chapter static analysis of the reinforced concrete bed was explained. Deflections and stresses were found by using finite element methods. A comparison of boundary integral equation and finite element methods for structural problems was carried out and it was seen that, except for the cases where surface to volume ratio is large, the boundary integral equation is more economical.

A detailed steel reinforcement design for the concrete bed was explained. In the design doubly reinforced sections were used with the intention of decreasing creep. Heavier reinforcement was employed at the regions where deflections were important. The resulting reinforcement was still light, the percentage areas being about half of the 'economic' percentage values given by British Standards.

The effect of creep and shrinkage on the long term accuracy of concrete was analysed and for the concrete bed designed, it was found to be satisfactory.

CHAPTER 4

DYNAMIC ANALYSIS OF THE STRUCTURE

4.1 Introduction:

Dynamic stiffness as well as static stiffness plays an important role in the accuracy of a machine tool. Machine tools can be subjected to vibration because of disturbing periodic forces or because of the nature of the cutting process. The periodic forces result from unbalanced rotating parts or errors in the accuracy of driving elements (61). The second type of vibration is energised by the cutting process. It is known as chatter and is important because it results in unacceptable undulations on the machined surface and endangers the strength and life of the parts of the machine and of the cutting tools. Dynamic analysis of a machine tool should be carried out so as to minimize those two types of vibrations.

In this chapter, after a short explanation of chatter and the existing dynamic analysis methods, the mode shapes and natural frequencies of the structure as obtained from a finite element computer program are presented. These results are utilised to obtain the frequency response curves for the structure. The curves together with the natural frequency values are used to select the support configuration for the structure. The dynamic analysis method used here is simpler and cheaper than the other frequency response techniques. It is very effective for comparison and it also helps to indicate how the dynamic stiffness may be improved.

4.2 Chatter on Machine Tools:

Chatter is caused by the interaction of the cutting process and the machine tool structure. It may result from the previous undulations (regenerative chatter), it can also be caused by the "mode coupling" effect or because of a phase shift between the change of the chip thickness and the change of the cutting force (the velocity component principle).

In case of "regenerative chatter," as seen in Fig 4.1 because of the undulation Y_o (23), the cutting force contains a variable component which excites vibration X of the vibratory system with the normal component Y. Mode coupling can act only within vibratory systems with at least two degrees of freedom. As seen in Fig 4.2, if vibration occurs with a frequency ω, the mass m vibrates simultaneously in both directions (X_1) and (X_2) with different amplitudes and with a difference in phase resulting in an elliptical movement. During the movement from B to A performed with a greater average depth of cut, the average force in this half-period is greater than the average force in the first one, ie movement from A to B.

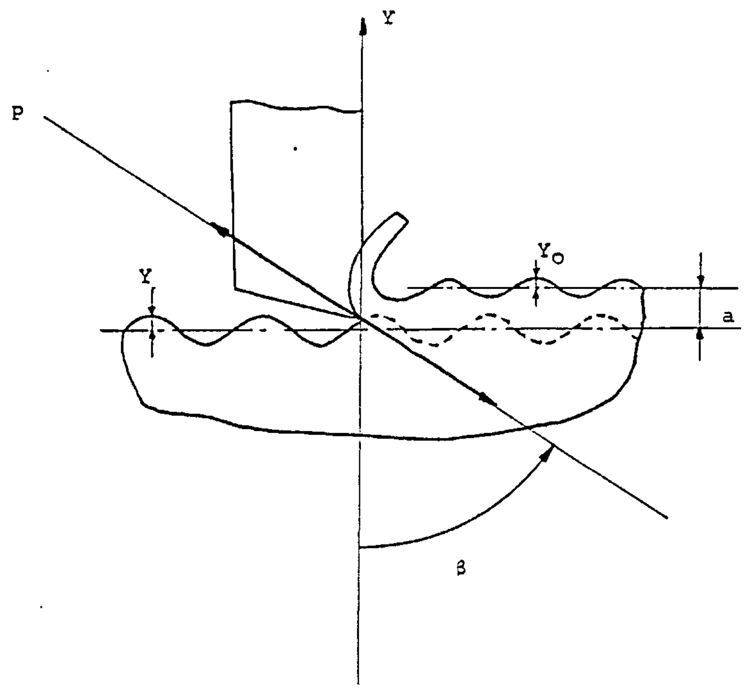

Fig 4.1 Cutting on undulated surface

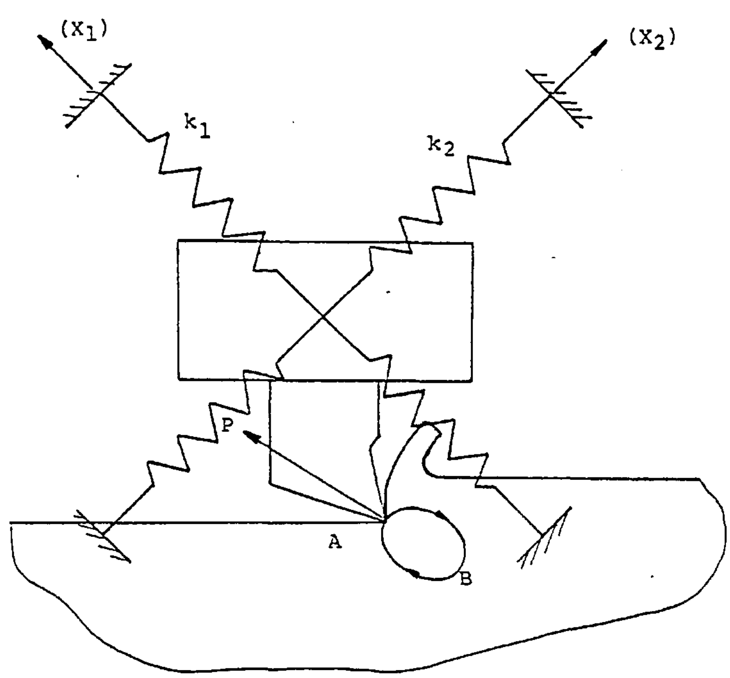

Figure 4.2 Mode coupling in a system with two degrees of freedom

Consequently, in one cycle the energy delivered to the system is greater than the energy dissipated by the system, causing self-excited vibrations to develop.

Mathematical models of chatter have been produced (61), (63), (23), but there are still some doubts about the theories. The following simplifications are usually assumed with the models:

a) The vibratory system of the machine is linear.

b) The direction of the variable component of the cutting force is constant.

c) The variable component of the cutting force depends only on vibration in the direction of the normal to the cut surface.

d) The value of the variable component of the cutting force varies proportionately and instantaneously with vibrational displacement y.

e) The frequency of the vibration and the mutual shift of undulations in subsequent overlapping cuts are not influenced by the relationship of wavelength to the length of cut; this assumption corresponds to an infinite length for every cut or, practically, to planing.

The method used by Tobias (61), Kudinov and Peters (23), does not have the assumptions d) and e). Thus, they accept a possible phase shift between the chip thickness variation and the variation of the cutting force and also they investigate the effect of interference of the undulations of subsequent cuts on stability. However, Tlusty and Polacek show that the methods with the assumptions d) and e) are more suited to machine tool design because they permit an understanding of how the limit of stability depends on the individual modes of the structure and leads to the suggestion of adequate changes of the structure. The method of Tlusty and Polacek is given in Appendix F.

In recent years, there has been a lot of effort put into both the development of mathematical models of chatter and the dynamic analysis of machine tool structures based on such models. The models were accepted without much questioning and used in practical design problems. However, more recently some results have been published showing that, the deviation between the measured and calculated (from the chatter theory) limiting depth of cut can be as high as 200% (64). It has also been pointed out that in most cases chatter is not the most important limitation. Other factors such as thermal deformations, noise, sensitivity to forced vibrations, the level of vibration when running light etc, can be more important measures of dynamic quality of machine tools than chatter. For these reasons it is thought that it is not necessary to base the dynamic analysis of machine tools on chatter. Nevertheless, the following experimental and theoretical findings about the influence of various conditions on chatter can be used as a guideline during the design and operation of a machine tool.

i) As the feedrate increases, the chatter tendency decreases.

ii) At low speed range (with HSS tools) increase in cutting speed increases the chatter tendency, however at higher speeds (with carbide tools), it causes an opposite effect.

iii) An increase in rake angle and a reduction of the relief angle to unusually small values of about 1° to 2°, decreases the tendency to chatter.

iv) Increase of stiffness of the spindle and its mounting on a lathe has a great influence on stability, but any change in the stiffness of the tool holder has a little effect because of the inherent damping of the tool holder. High stiffness for the tailstock is also very important for a low chatter tendency.

4.3 Methods of Dynamic Analysis:

One of the oldest methods of dynamic analysis is to prepare a model of the structure and to conduct experiments on the model. This method is very time consuming and not necessarily reliable. Therefore, with the advent of computers, analytical methods have been developed and used in conjunction with the experimental work. Most of the basic analytical methods are described below.

a) The Classical Beam Method:

In this method, all the machine tool elements are represented as beams. The general equation for the modes of vibration for each beam is written as in eqn (4.1)

$$y_r = C_{1r} \sin \frac{z_r}{\ell_r} x_r + C_{2r} \cos \frac{z_r}{\ell_r} x_r + C_{3r} \sin h \frac{z_r}{\ell_r} x_r + C_{4r} \cos h \frac{x_r}{\ell_r} \qquad (4.1)$$

$$r = 1,2,3, \ldots n$$

where n is the number of beams in the structure, ℓ_r is the second moment of cross-sectional area and Z_r is a frequency dependent constant.

Constant C_{ir}'s are evaluated by solving a system of equations, resulting from the application of boundary conditions on to the equation (4.1). This system of equations also gives the natural frequencies. (54).

b) Lumped-Constants Method:

In this method, the structure is divided up into a number of concentrated (lumped) masses which are joined together by elastic beams. Then, the force exerted by each mass on the structure during vibration is formulated. By using the flexibility matrix, the corresponding displacements are written resulting in a set of equations as shown below,

$$\{q\}\ g = \omega^2 \begin{bmatrix} \alpha \end{bmatrix} \begin{bmatrix} M \end{bmatrix} \{q\} \qquad (4.2)$$

Where q is the displacement matrix, α is the flexibility matrix and M is the mass matrix.

Equation (4.2) gives an eigen value problem, solution of which results in the mode shapes and natural frequencies (55).

c) Method of Receptances:

In this method, the relationship between exciting forces $F_1e^{i\omega t}$, $F_2e^{i\omega t}$, ... $F_ne^{i\omega t}$ exerted on a member and the oscillatory displacements $x_1\ e^{i\omega t}$, $x_2\ e^{i\omega t}$, ..., $x_m\ e^{i\omega t}$ measured at the points where the forces are applied is written by using the matrix algebra. Receptances of each system member are calculated from the vibration theory of an elastic body. Repeating the series of computations for many different frequencies in the frequency range of interest, the harmonic response and natural frequencies of the composite system can be derived.

The basic equation used in this method is (57),

$$\{X\} = \begin{bmatrix} \alpha \end{bmatrix} \{F\} \qquad (4.3)$$

where {X} is the displacement vector, {F} is the force vector and α is the receptance matrix.

d) Complex Modal Method:

In this method, the structure is again discretized by using a suitable method. After that the equations for damped or undamped systems can be written,

$$\begin{bmatrix} M \end{bmatrix} \{\ddot{x}(t)\} + \begin{bmatrix} k \end{bmatrix} \{x(t)\} = \{f(t)\} \qquad (4.4)$$

and

$$\begin{bmatrix} M \end{bmatrix} \{\ddot{x}(t)\} + \begin{bmatrix} c \end{bmatrix} \{\dot{x}(t)\} + \begin{bmatrix} k \end{bmatrix} \{x(t)\} = \{f(t)\} \qquad (4.5)$$

From equation (4.4) and (4.5) after some manipulations, mode shapes and natural frequencies can be obtained. Using the calculated mode shapes and natural frequencies, the frequency response for the structure can also be derived (62). For an undamped system the frequency response can be written as,

$$\{X\} = \sum_{k=1}^{n} \frac{\{\psi_k\} \{\psi_k\}^t \{F\}}{k_k\left[1 - \left(\frac{\omega}{\omega_k}\right)^2\right]} \qquad (4.6)$$

Where $\{\psi_k\}$ is the k_{th} modal vector, k_k is the k_{th} stiffness term, ω_k is the k_{th} natural frequency, {F} is a set of forces and {X} is the displacement vector.

The frequency response for equation (4.5) can also be derived by assuming proportional damping. The derived mathematical model is usually checked automatically through a computer program using experimental results. The correlation can be used as a guide for future studies.

Among all the methods considered, the last two appear to be more versatile, because they can take damping into account.

Besides the general methods of dynamic analysis, there have been attempts to lay down procedures for optimum design of machine tool structures. Yashimura (57) is one of the pioneers in this field. The principles he uses for optimum design can be stated as follows,

i) for every resonance mode identified, compute the distribution of kinetic and potential energy in the system, and also calculate the modal flexibility,

ii) focus on the particular mode where the modal flexibility is predominantly high and by consulting the energy distribution at the mode, propose a design change such that energy is more evenly distributed in the system.

iii) After repeating the second procedure a sufficient number of times, try to allocate greater latent damping at the parts of the machine at which greater potential energy is stored.

However, this requires a good knowledge on the damping distribution in the structure which is difficult to evaluate. Also, the overall method is expensive and as yet it has not been proven that the method justifies its complications.

4.4 Finite Element Method and Its Application:

The finite element method for static problems were described in chapter 3. Dynamic problems can also be used in a similar manner by using the finite element method. For a general dynamic equation of the form,

$$\frac{\partial}{\partial x}\left(k_x \frac{\partial \phi}{\partial x}\right) + \frac{\partial}{\partial y}\left(k_y \frac{\partial \phi}{\partial y}\right) + \frac{\partial}{\partial z}\left(k_z \frac{\partial \phi}{\partial z}\right)$$

$$+ \left(\bar{Q} - \mu \frac{\partial \phi}{\partial t} - \rho \frac{\partial^2 \phi}{\partial t^2}\right) = 0 \qquad (4.7)$$

the finite element discretization gives the matrix equation, (45) $\left[M \right] \{\ddot{a}\} + \left[C \right] \{\dot{a}\} + \left[K \right] \{a\} + \{f\} = 0$ (4.8)

where a is the nodal displacements represented by,

$$\phi = \Sigma N_i a_i = \left[N \right] \{a\} \qquad (4.9)$$

through the shape function N_i.

As seen here, equation (4.8) is exactly the same as equation (4.5). Therefore, FEM is not an entirely new method but it is just a method of discretizing the structure. It can represent the system very closely and therefore gives accurate results. The method can be used to obtain the natural frequencies and modal shapes in an economical manner. Therefore, the FEM provides a very attractive technique for the dynamic analysis of a structure. Consequently, it was decided to use the FE method in this investigation.

The dynamic analysis was carried out for the lighter structure. The finite element mesh used for the static analysis of this structure was given in chapter 3. The same mesh was used in the dynamic analysis. It is stated in the literature that dynamic modulus of concrete is higher than its elastic modulus and the ratio is around two (53). For this reason in the analysis, elastic modulus of concrete was taken as $4.4*10^5$ kg/cm^2 (4400 MN/m^2). Dynamic analysis was carried out for two cases; structure with three supports and structure with five supports. The natural frequencies for the first five modes are shown in table 4.1. The mode shapes are indicated in figures 4.3 and 4.4. The CPU time on the CDC 6000 computer was 900 secs.

4.5 Evaluation of the Results and Frequency Response Characteristics

The natural frequencies for the two cases as listed in table 4.1 can be analysed with regard to the forced vibrations. For three support cases, first natural frequency is 803.7 rad/sec which corresponds to approximately 7600 rpm. This is unacceptably near to 6000 rpm which is the upper range of the spindle speed. Therefore, with only three supports the structure may have unacceptable vibrations at high speeds. However, in case of five supports, first natural frequency is about two times that of the three support case. For this reason using five supports will be a much safer selection.

The modal shapes can be used to determine the main springs and masses of the structure and therefore they indicate which parts of the structure to stiffen in order to obtain a better overall dynamic stiffness. However, with modal shapes, the direction of vibrations can not be determined accurately. Frequency response gives a much clearer interpretation of the results. An exciting force can be applied at a point near to the cutting tool and the amplitude of vibrations in the direction of interest can be found. In order to obtain a good surface finish, amplitude of vibrations perpendicular to the cut surface should be small.

Table 4.1 The natural frequencies for the structure

	3 Support	5 Support
Mode No	w rad/sec (Hz)	w rad/sec (Hz)
1	803.7 (127.9	1649 (262.4)
2	1104 (175.8)	1836 (292.2)
3	1582 (251.8)	2509 (399.4)
4	2022 (321.8)	3609 (542.5)
5	2581 (410.7)	3909 (622.1)

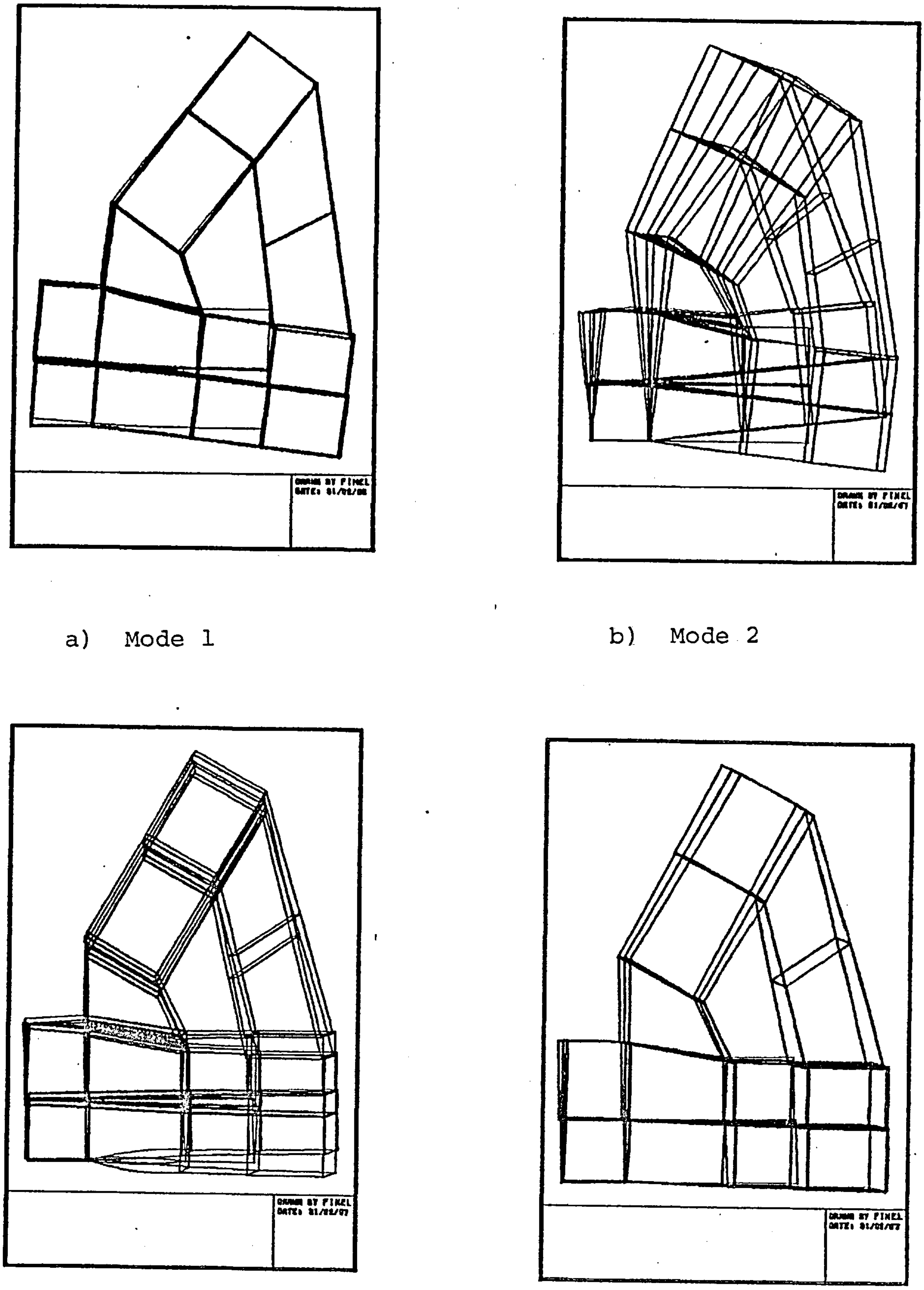

a) Mode 1

b) Mode 2

c) Mode 3

d) Mode 4

Figure 4.3 Mode shapes for three support case

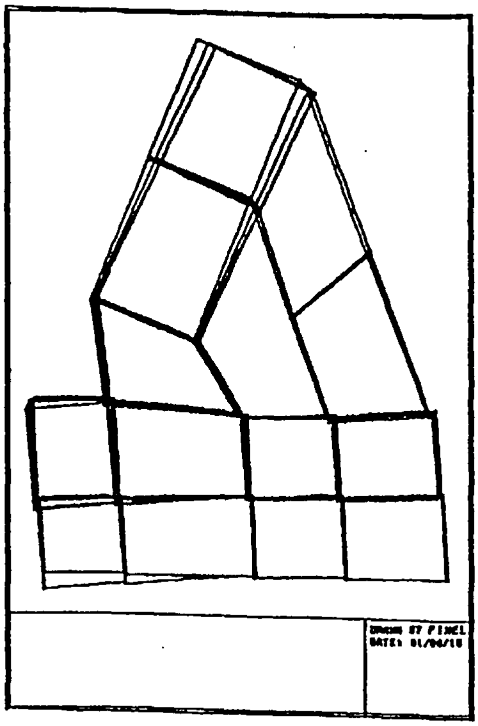

a) Mode 1

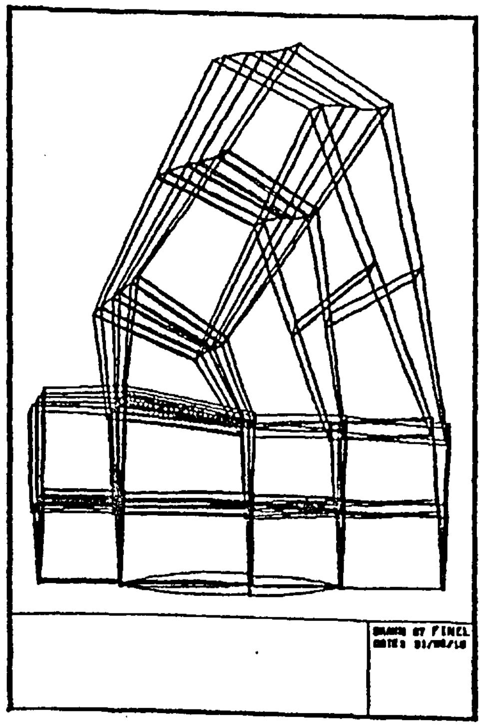

b) Mode 2

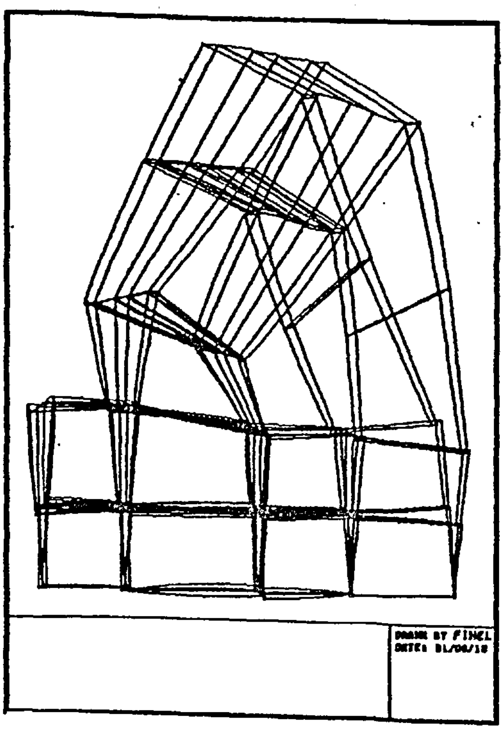

c) Mode 3

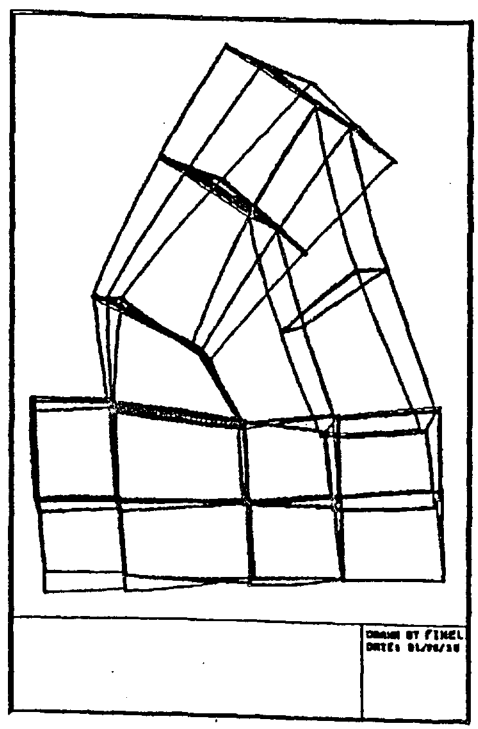

d) Mode 4

Figure 4.4 Mode shapes for five support cases

This requirement can be checked thoroughly with frequency response method. Therefore, further analysis of the results will be carried out after the frequency response curve have been obtained.

In frequency response methods, the usual procedure is to apply an exciting force at a certain frequency and then find the resulting amplitude and direction of vibrations. This procedure has to be repeated for a wide range of frequencies so that a complete picture of frequency response is obtained. This method is very time consuming and expensive. Here, the modal analysis results will be used to obtain the frequency response curves. Because of the scaling on the mode shapes used in the finite element analysis, the amplitudes obtained will not be absolute. However, they will still form a good basis for comparison.

The equations to obtain the frequency response can be derived as follows,

$$\underline{M}\,\ddot{\underline{D}} + \underline{kD} = 0 \qquad (4.10)$$

is the equation solved by the finite element program, where $\underline{D}$ is the displacement vector which can be written as,

$$\underline{D} = \sum_{i=1}^{r} \phi_i \; A_i(t) = \underline{\phi}\;\underline{A}\;(t) \qquad (4.11)$$

where A_i is the generalised coordinate of mode i and

ϕ_i is the ith mode shape

r is the number of modes considered.

Using equation (4.11) and (4.10), for forced response,

$$\underline{M}\ \underline{\phi}\ \ddot{\underline{A}} + \underline{k}\ \underline{\phi}\ \underline{A} = \underline{R} \qquad (4.12)$$

where R is the forcing vector. Multiplying each side by $\underline{\phi}^T$, the equation becomes,

$$\underline{\phi}^T\ \underline{M}\ \underline{\phi}\ \ddot{\underline{A}} + \underline{\phi}^T\ \underline{K}\ \underline{\phi}\ \underline{A} = \underline{\phi}^T\ \underline{R} \qquad (4.13)$$

In finite element solution, the following identities are used,

$$\underline{\phi}^T\ \underline{M\phi} = I \text{ and } \underline{\phi}^T\ \underline{K}\ \underline{\phi} = \left[\diagdown \omega_i^2 \diagdown\right]$$

where ω_i^2 is a diagonal matrix consisting of the natural frequencies.

Then equation (4.13) becomes,

$$\ddot{\underline{A}} + \left[\diagdown \omega_i^2 \diagdown\right] \underline{A} = \underline{\phi}^T\ \underline{R} \qquad (4.14)$$

Because eigen values and eigen vectors of the system will not change very significantly, it is possible to incorporate damping into the above analysis. Assuming proportional damping equation (4.14) becomes,

$$\ddot{\underline{A}} + \left[\diagdown 2\xi_i\omega_i \diagdown\right] \dot{A} + \left[\diagdown \omega_i^2 \diagdown\right] \underline{A} = \underline{\phi}^T\ \underline{R} \qquad (4.15)$$

ξ_i can be written as a function of the logarithmic decrement δ.

$$\delta \simeq 2\pi\xi \qquad (4.16)$$

δ for concrete is given in reference (103), as approximately 0.02 for a wide range of frequencies.

Equations (4.15) is composed of a set of linear differential equations. These equations can be solved to obtain the generalized coordinate for each mode, then by using equation 4.11, the displacement vector can be calculated.

The frequency response curves using the above method were obtained for three and five support cases and are shown in figures (4.5) and (4.6) respectively. The exciting force is applied to the middle of the slant part of the structure at a point near to the cutting area. The structure is weaker in this region because it is distant from the supports. The frequency response curves are then calculated for three points.

i) Point of application of the load
ii) Middle of one of the supports
iii) Middle point at the connection between the base and the slant part of the bed.

Three support cases was discarded because the lowest natural frequency was near to the upper end of the spindle speed. However, if that mode corresponds to a mode which does not affect the surface finish, then it may still be justifiable to choose the three support case . Frequency response curves in Fig 4.5, shows that the first mode corresponds to the vibrations in

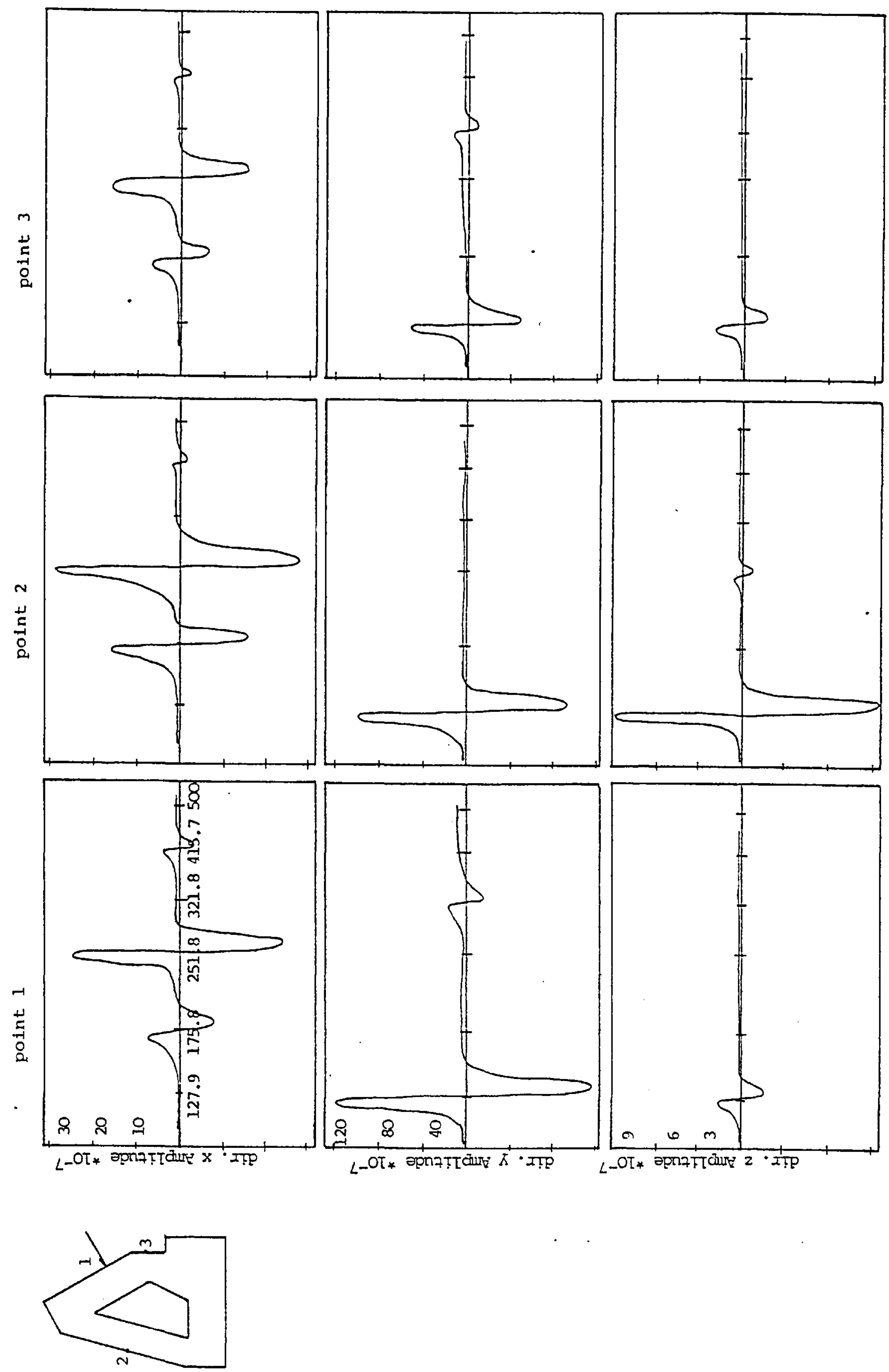

Figure 4.5 Frequency response curves for three support case

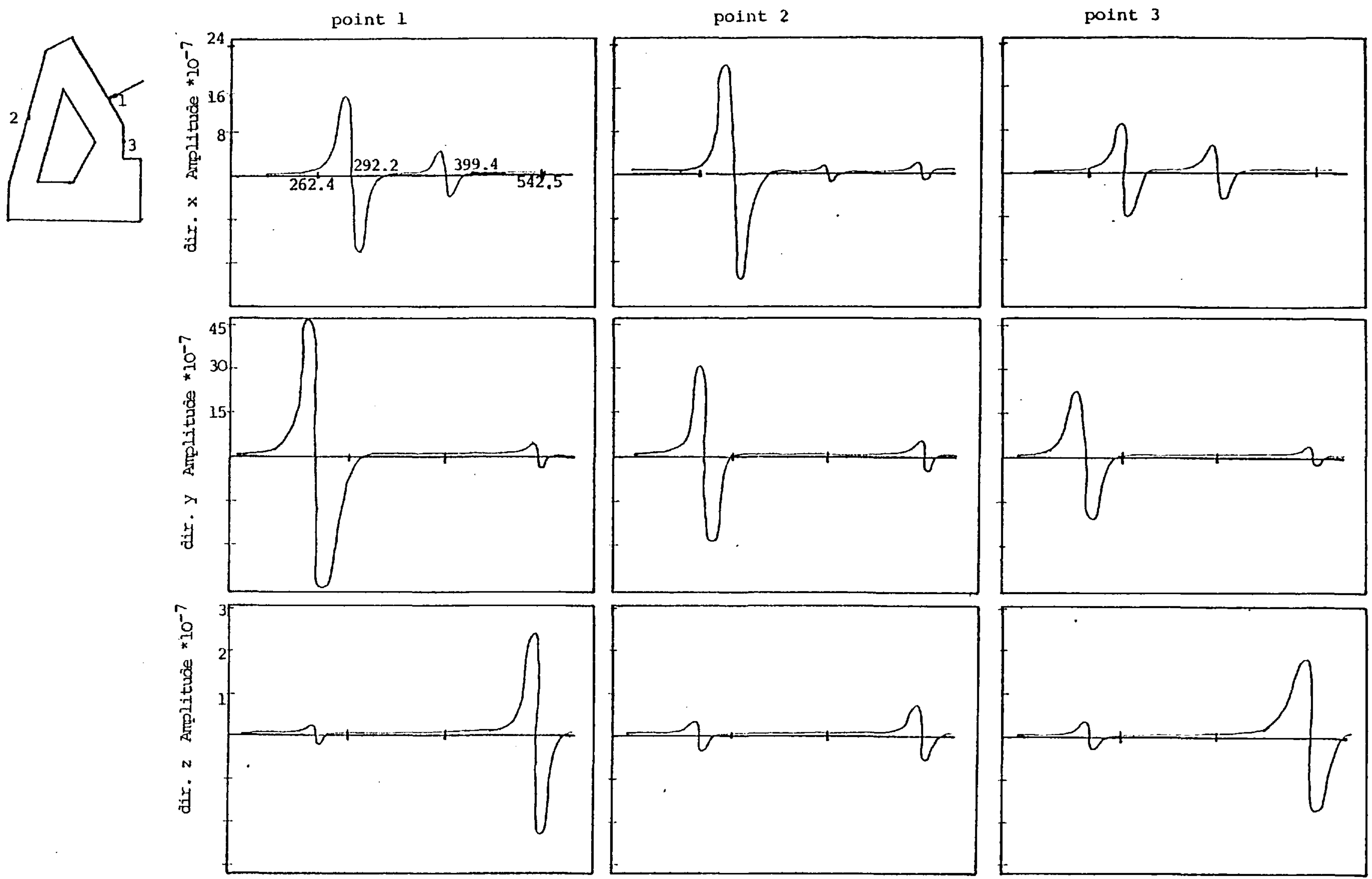

Figure 4.6 Frequency response curves for five support case

y and z directions. These directions are important for the surface finish because their components determine the amplitude of the undulations on the cut surface. Therefore, the selection of five support case was a better alternative.

Having determined the number of supports the frequency response curves for five supports can be analysed to see how the dynamic stability of the structure can be improved. As mentioned earlier, the direction of prime importance is the direction which is perpendicular to the cut surface and the vibrations along these directions are mainly affected by the vibrations along y and z directions.

From the natural frequencies obtained from modal analysis, it is seen that the first and second natural frequencies are very close to each other (262.4 and 292.2 Hz respectively). If these two modes are associated with y and z directions, when they are superimposed, the vibrations along the prime direction will increase (ie along the direction perpendicular to the cut surface). However, from the frequency response curves it is seen that only the first mode is associated with y direction. The second mode is associated with x direction which does not affect the prime direction. Therefore, closeness of the two natural frequencies will not increase the vibrations along the prime direction.

The relative dynamic stiffness of the different parts of the structure can be compared by using the frequency response curves. It is seen that in the more dominant modes such as the first or second amplitude of vibrations for the part which connects the inclined surface to the base is smaller when compared with the others. Therefore, that part need not be strengthened further. However, the graphs show that the first mode is quite critical, because the amplitude of vibrations are high when compared with the other and the vibrations are acting in y direction which closely affect the surface finish of the component. The curves show that amplitude of vibrations for the column is considerable suggesting that for this particular mode columns are not acting as good supports. Therefore, strengthening the columns is required which should decrease the amplitude of vibrations.

Another direction which is important for the surface finish of the workpiece, the z direction occurs in the fourth mode. However, this mode is much stiffer and the amplitude of vibrations less. Therefore, this mode need not be considered in more detail.

4.6 Discussion

In this chapter, several modelling and dynamic analysis methods are considered. As a modelling method, finite element is chosen, because it can represent the structure more closely and gives more accurate results than lumped constant or classical beam methods. The finite element model was used to obtain the natural frequencies and mode shapes. These results were then used to obtain the frequency response. As a result of the normalization procedure used in the finite element program, the eigen vectors were evaluated according to an unknown scale. For this reason, exact values of dynamic receptances can not be found and consequently no quantitative chatter analysis can be carried out. However, the deviations between the theoretical chatter analysis and experimental results as given in the literature were pointed out earlier in this chapter. Therefore, it is thought unnecessary to overstiffen the structures, when the chatter theory can not give accurate results. In this work a qualitative chatter analysis was carried out as explained in section 4.5. The possibility of tackling the chatter problem in an on-line manner will be explained in chapter 8.

The dynamic analysis results indicated that the structure as it is designed should be supported on five supports. If three supports were to be used, the stiffness of the structure should be increased considerably. However, this will increase the weight of the machine tool, making it harder to sell the machine tool to small workshops. Therefore, five supports are to be preferred.

The effect of different parts of the structure on the dynamic stiffnes was also considered. It was seen that further stiffening of the supports will be beneficial for the surface finish of the workpiece and for the overall performance of the machine tool. However, because concrete has very good damping properties the vibrations will die very rapidly and the absolute amplitudes will be small. Besides, the possible weakness of the structure was realised in the static analysis and the reinforcement around that region was increased (please see chapter 3). This will help to decrease the vibrations as well. Therefore, the overall structural configuration can remain unchanged. More attention to the dynamic characteristics should be given when designing individual components ie, slideways, tailstock, spindle assembly etc, because the effect of joints and these individual components are also very important in the overall dynamic stiffness to the machine tool.

CHAPTER 5

GUIDEWAYS

5.1 Introduction:

In machine tools, the cutting tool or the workpiece must be guided along straight lines with a sufficient accuracy under both static and dynamic loading. There are two main types of straight line guidance; slideways (sliding-friction ways) and antifriction (rolling-friction) ways.

The guideways have to satisfy the following basic requirements:

1. Accuracy of travel: this depends mainly upon the accuracy with which the ways are machined and is characterised by the degree to which the actual travel is strictly rectilinear.

2. Durability: this is characterised by the capacity of the ways to retain the initial accuracy of travel over a specified period of operation. It is also necessary to have means of compensating for any inaccuracy or wear that may occur.

3. Rigidity: this is characterised by elastic displacements due to contact in the ways under the action of normal loads both static and dynamic.

4. Ease of assembly and economy in manufacture is very important.

5. Guideways should have freedom from restraint, to prevent jamming.

6. Accumulation of swarf should be prevented, and the chip removal easily accomplished.

7. In a CNC machine tool, the difference between static and dynamic friction coefficients should be minimised to prevent the stick-slip phenomena.

In this chapter, different types of guideways are analysed and the selection methods for anti-friction types of ways reviewed. Several alternative designs for the particular machine tool are presented and their static and dynamic performance determined through finite element methods.

5.2 Types of Guideways:

There are basically three types of guideways (fig. 5.1),

a) Plain slideways
b) Externally pressurized slideways
c) Anti-friction guideways

5.2.1 Plain Slideways:

Many different designs of plain slideways exist, as shown in fig. 5.2. Usually, small machines and

Guideways

- Plain
- externally pressurized
  - oil
  - air
- Anti-friction
  - needle rollers
  - recirculating balls
  - recirculating rollers
  - non-recirculating balls
  - non-recirculating rollers

Figure 5.1 Types of Guideways

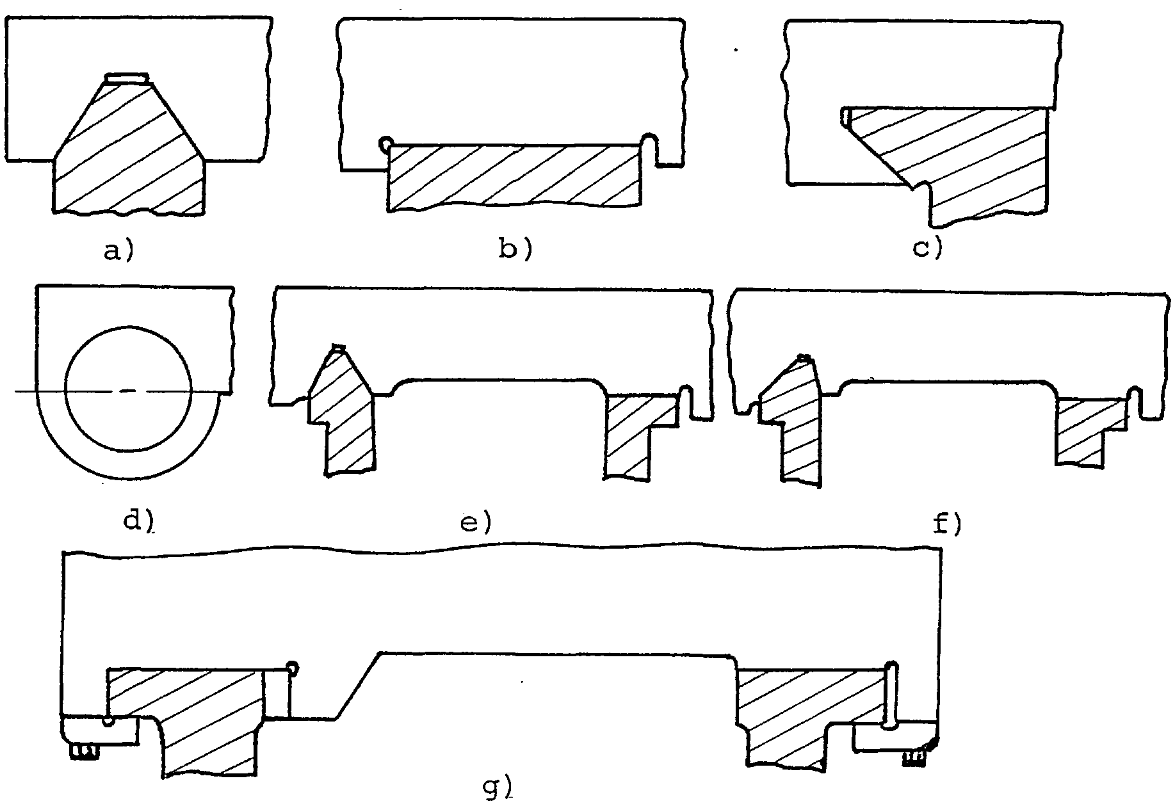

Fig 5.2 Different designs of plain slideways

horizontal beds have slideways that are kinematically correct, ie. types e and f. However, in inclined or vertical beds and in large machines more positively restrained type slideways (type g) are preferred. This type of slideways are also easier to machine, reducing the cost of the overall slideway system.

It is possible to use several combinations of materials for slideways. They can be listed as follows,

i) cast iron/cast iron
ii) steel/cast iron
iii) cast iron/plastics
iv) steel/plastics

Plastics have recently been developed as a slideway material. They are mostly used in the form of thin polymeric coatings applied by spraying or glueing on to the slideway. In order to improve friction stiffness, and wear characteristics of plastics, they are usually impregnated with another substance such as bronze or graphite.

The general requirements for a slideway system were given in section 5.1. The characteristics of plain slideways are analysed below to see how well they satisfy the requirements.

a) Wear: Wear characteristics of the most common slideway materials have been analysed by several authors (73), (77). The wear depths obtained after 36 km of sliding against a cup-ground cast-iron surface for several materials are given in reference (72). The tabulated values in table 5.1 show that plastics such as VB60, Turcite 'B', SKC3, Rulon LD have favourable wear resistance. Plastics also eliminate scoring because foreign particles embed themselves into plastics. However, abrasion would still occur, therefore the use of wipers to prevent the ingress of foreign particles, between the sliding parts, is still necessary.

There are also other factors which affect the wear rate. Lubrication usually reduces wear. Also, as hardness increase wear rate decreases. Surface finish has also an important affect. It is reported that (73), with plastics, surface finishes above 0.8 μm CLA cause a serious increase in wear rate.

b) Friction Characteristics: Static and dynamic coefficients of friction for slideway materials have been measured and reported by several authors (71), (73). Some of these values are given in table 5.2. As mentioned in section 5.1, to eliminate stick-slip phenomena static and dynamic coefficients of friction should be as near to each other as possible. Table 5.2 shows that plastics again are favourable because

Table 5.1 Wear characteristics of slideway materials

Rotating	Wear Depths (μm)			
	Testpiece		Stationary testpiece	
	clean lubricant	lubricant with abrasives	clean lubricant	lubricant with abrasives
cast iron	3	25	2	28
Ferobestos P.T.F.E	3	10	1	18
Tufnol P.T.F.E	3	5	2	10
VB 60	6	2	1	5
Turcite 'B'	8	5	2	4
Rulon LD	2	3	1	4
SKC 3	3	7	2	4
Bakelaque B21	4	18	2	6

Table 5.2 Friction characteristics of slideway materials
* Lubricant used is Shell Tonna 33

Material	Coefficient of friction			
	Trace of lubrication *		Flooded lubrication	
	Static	Dynamic	Static	Dynamic
cast iron	0.075	0.060	0.060	0.030
Ferobestos P.T.F.E	0.100	0.090	0.080	0.060
Tufnal P.T.F.E	0.080	0.075	0.075	0.070
VB 60	0.035	0.022	0.035	0.022
Turcite 'B'	0.070	0.065	0.065	0.061
Rulon LD	0.051	0.044	0.025	0.022
SKC 3	0.041	0.040	0.040	0.031
Bakelaque B21	0.056	0.041	0.052	0.033

of their low and near to constant friction coefficients. In some literature P.T.F.E. based plastics (VB60, Turcite 'B', Rulon LD) are shown to have larger dynamic friction coefficients (73).

However, there are other factors which affect the coefficient of friction. The effect of lubricant type has been studied by Burdekin and Bell (71). They report that with polar lubricants the dynamic friction coefficient of cast iron slideways is greater than the static friction coefficient, thus eliminating the stick-slip phenomena. However, polar lubricants can increase the wear rate of the slideways especially when there is external contamination. Also, they may damage the stiffness conditions seriously in cases of large specific loading and velocities (34).

c) Static and Dynamic Rigidity:

Static stiffness of slideways depends on many factors. Considering the results obtained by Hajdu (74), Levina (79), (80), and Burdekin and Bell (71), (72), the following conclusions can be made:

i) the stiffness of sliding guideways decreases progressively as oil viscosity increases.

ii) the stiffness will be decreased by increasing the sliding velocity

iii) the stiffness increases by the increased specific loading.

iv) the higher the modulus of elasticity of a material, the higher its surface rigidity.

v) the stiffness decreases with roughness of the contacting surfaces, however, it is not affected by hardness.

vi) using flat slideways instead of prismatic increases the stiffness in the case of large loads

vii) for speeds below 4m/min, it is considered that the specific surface loading should be above 0.8 kgf/cm^2 and for higher speeds above 1.2 kgf/cm^2.

Dynamic characteristics of slideways can be analysed in two directions, normal and parellel to the joint face. They have been analysed by Koenigsberger (78), and Burdekin (71). From their analysis the following conclusions can be drawn.

i) The dynamic stiffness of a joint rises with an increase in the static preload, however, that causes the damping ratio to decrease.

ii) The presence of oil or greases in the joint interface increases both the dynamic stiffness and damping ratio of the joint.

iii) When oil is present in the joint the damping ratio increases almost linearly with increase in frequency of the applied load.

iv) The more viscous the oil in the interface the greater will be the increase in dynamic stiffness and damping ratio.

v) Rough surfaces exhibit less dynamic stiffness, but a slightly better damping ratio than smooth surfaces provided flatness errors are not present.

vi) For dry surfaces in contact, the dynamic stiffness is similar to the static behaviour.

vii) Plastics offer better damping characteristics.

viii) The frictional damping of plain slideways are low above sliding speeds of 0.4 m/min. (damping ratio is around 0.02 for a wide range of slideway materials and lubricant combinations).

5.2.2 Externally Pressurized Slideways:

Externally pressurized slideways normally 'float' on a film of pressurized oil, typically 30 μm thick, between the two moving elements. (Air has been used for this purpose on occasions, but only for positioning type machines).

The friction and damping characteristics of these slideways are also superior to the plain slideways. The major disadvantages with this type of slideway are the complexities involved in the pumping and recycling arrangements for the oil.

5.2.3 Anti-friction Guideways

With anti-friction slideways, the contact condition at the interface is one of rolling by either balls, rollers or needle rollers. Their characteristics are summarised below.

a) Wear: The wear mechanism is usually one of a surface fatigue which causes flaking of the surface. The life of such guideways is normally evaluated by the designer from information supplied by the manufacturers. However, the ratings in the catalogues are given for central loads and do not take misalignments into account. Therefore, special attention should be paid to the selection procedure.

   A further common reason for failure is ingress of foreign matter through the seals. Therefore, they should be enclosed and wipers used.

b) Friction Characteristics: The coefficient of friction is very low (0.005 - 0.01) and does not change with the speed of sliding. However, excessive preloads can cause considerable increase in coefficient of friction and can impair the operating characteristics.

c) Static and Dynamic Rigidity:

Static and dynamic rigidity of anti-friction guideways have been analysed by Levina (79), (80) and also by Hajdu (74). From their analysis, the following general conclusions can be drawn.

i) Preloading increases both the dynamic and static stiffness. However, this increase is up to a certain point and then stiffness is independent of preloading. Because excessive preloading causes large increases in friction coefficient, there is an optimum preloading and it is 5-10 μm for ball guideways and 10-15 μm for roller type of guideways.

ii) Damping of rolling guideways increases proportionally to the square root of prestressing.

iii) The rigidity of the guideways changes according to the type and also according to the nature of the load, ie. centrally applied load, a moment in the vertical plane, a moment in the horizontal plane, etc.

iv) The static and dynamic stiffnesses of anti-friction guideways are independent of the speed. Therefore, at large speeds the static and dynamic stiffnesses of anti-friction guideways are usually higher than plain slideways. (For cross roller guideways with vertical loading, this speed is around 4 m/min).

v) Manufacturing errors have a very important influence on rigidity. The increase in dimensional difference of rolling elements from 1 to 4 μm would cause a 20-30% reduction in rigidity. Surface finish is similarly important.

5.3 Comparison and Selection:

A comparison of the guideway types as covered in the previous section is carried out below,

a) Wear: Externally pressurized slideways have the best wear characteristics. Plain slideways covered with Turcite 'B', SKC3, Rulon LD or VB60 are also favourable.

b) Friction Characteristics: Externally pressurized slideways and anti-friction guideways have very low coefficient of friction (around 0.005). Plain slideways covered with plastics can have a friction coefficient from 0.02 to 0.2 according to the lubrication conditions and type of plastic used.

Stick-slip phenomena does not exist for the first two types of guideways. For plain slideways, the ones covered with Turcite 'B' or Rulon LD show the best characteristics.

c) Static and Dynamic Rigidity: The static and dynamic rigidity of the slideways depend very much on the design and the kind of loading; therefore, although some guidelines are indicated in the previous section, they should be analysed for a particular design.

Damping characteristics of anti-friction guideways being in dry contact is worse than the other types. However, it can be improved by prestressing or by using squeeze film devices (75). Active control methods as described in chapter 8 can also increase damping.

Longitudinal damping is low for almost all types. This can be compensated for by using stiffer drives (91).

d) Accuracy and Sensitivity of Setting Traverses: The accuracy and sensitivity of setting traverses in plain slideways depend on sliding speed, the weight of the unit and drive stiffness whereas in anti-friction or externally pressurised type of guideways, it depends only on the drive stiffness.

In anti-friction or externally pressurized type of guideways setting accuracy of 0.1 to 0.2 μm is possible. However, in case of plain guide-ways even with no stick-slip the setting errors are around 2-5 μm. (80).

e) Cost: Definitive figures are difficult to give, as the selection of the type of guideway can affect the total design and production of the machine. Additionally the drive cost can be different for a different type of guideway because of the changes in the friction coefficient. However, it is accepted that in general plain slideways even with plastic coatings are the cheapest. Of the other two types anti-friction guideways tend to be cheaper (77).

The above considerations show that externally pressurized guideways are not suitable for the machine tool considered here. They are expensive and difficult to manufacture and also pumping and recycling create complications.

Plain slideways coated with plastics present an attractive solution. As to the kind of material, Turcite 'B' or Rulon LD appears to be the most suitable alternatives. However, anti-friction guideways being available off the shelf make the overall manufacturing of the machine tool easier. Additionally, when the cost including the drive motors are considered it may not be very much different from plain slideways. Their only disadvantage is lower damping ratio at small sliding speeds. However, prestressing or added squeeze films could cure the problem and also their dynamic stiffness in some loading cases is higher than plain slideways (80). Therefore, they will not be discarded at this point, but their static and dynamic properties for this particular machine tool will be analysed further.

5.4 Size and Stiffness Calculations

5.4.1 Plain Slideways:

Initially the configuration of the slideways needs to be determined. The discussion in section 5.2 suggests that for high loads flat slideways should be used. The ease in manufacture of this type of slideways confirms its selection. To compensate for parallelism or alignment errors, the front slideway will have a gap. Figure 5.3 shows the slideway design adopted here. The next step will be to calculate the dimensions of the slideway. The force configuration is shown in fig. 5.4. Because of the gap, all the axial forces will be taken by the rear slide; therefore $F_{yA} = 0$. Then, from the equilibrium equations,

$$F_{xA} = 1363 \text{ kg}; \quad F_{xB} = -238 \text{ kg}; \quad F_{yB} = 83.5 \text{ kg}.$$

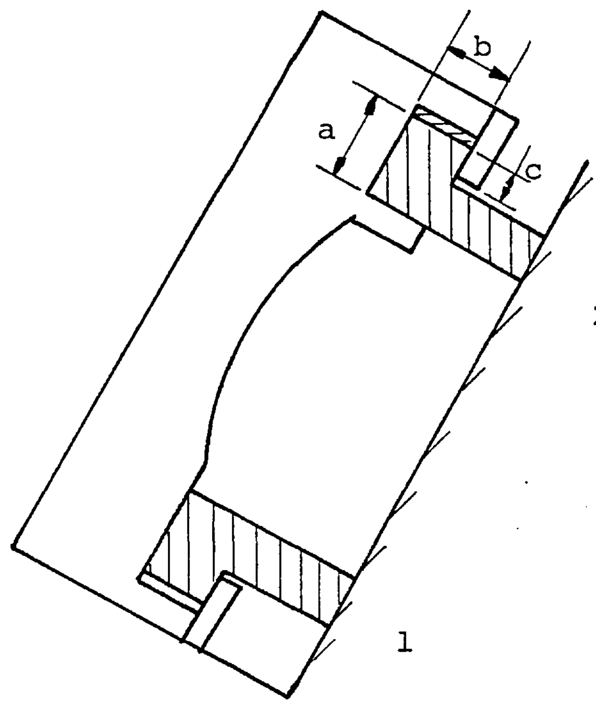

Fig 5.3 Plain Slideway Design

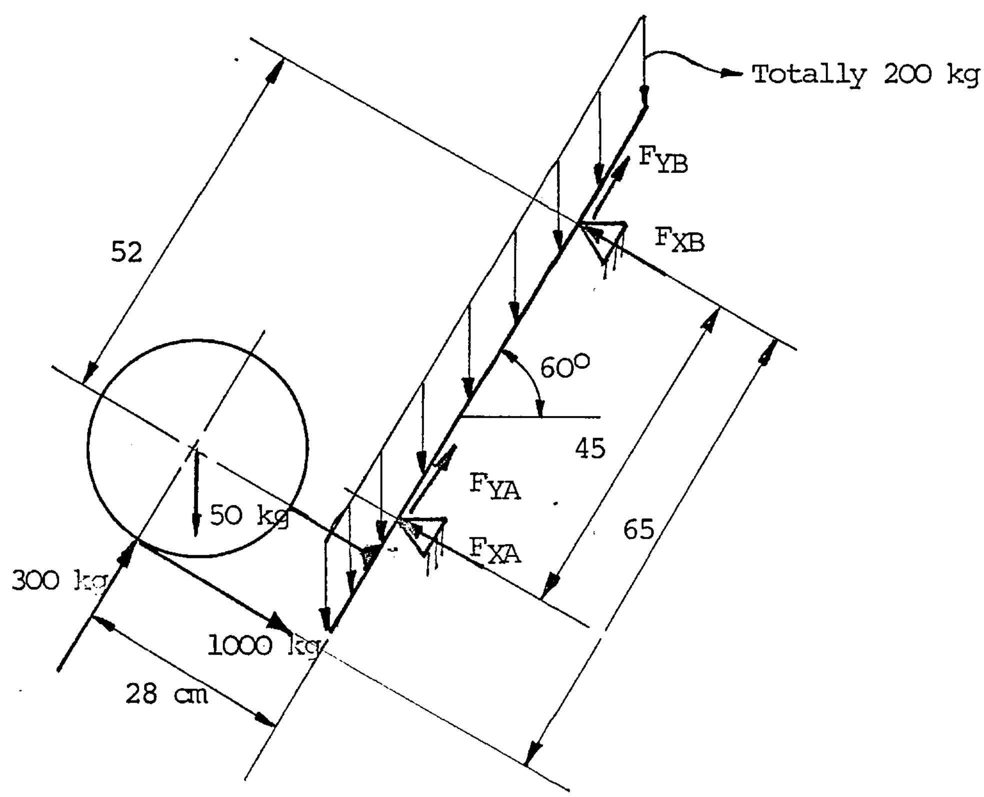

Fig 5.4 Force configuration for the slideways

Specific pressure will be chosen as 5 kg/cm^2. With most plastics specific pressures up to 10 kg/cm^2 are allowable. For slideway (1) (fig 5.4), the forces are acting onto the slideway; then a load of 1400 kg corresponds to 280 cm^2 area. For slideway (2), the forces are acting away from the slideway. A load of 240 kg and a specific pressure of 4 kg/cm^2 gives a 60 cm^2 area. For the sideload a smaller specific pressure can be chosen. Assuming 1.4 kg/cm^2 as the specific pressure, area is obtained as 60 cm^2 for the sideload. All the above specific pressures are in the range recommended by Hajdu (74). Assuming 30 cm length for the slide gives a = 9.3 cm b = c = 2 cm (fig 5.3).

The next step is to calculate the stiffness values in the various directions. The stiffness of plain slideways for pressures below 14 kg/cm^2 is given by the following equation (72).

$$S = \frac{dW}{d\lambda} = A_a \frac{p(1-m)}{mn} \qquad (5.1)$$

Where S is the stiffness,

A_a is the apparent contact area

P is the specific pressure and

m and n are constants which change according to the material combination and surface finish. In the same reference, m and n values are given for cast iron glacier DU (PTFE and lead impregnated bronze) combination.

The suggested materials were Turcite 'B' and Rulon LD. These are also PTFE based. As they are likely to have similar stiffness characteristics values for glacier DU will be taken as a base.

Then from reference (72), m = 0.5 and n = 1.866, which gives the following stiffness equation for cast iron-glacier DU combination.

$$S = A_a \quad \frac{P^{0.5}}{0.933} \qquad (5.2)$$

where A_a is in cm^2

P is in kg/cm^2 and

S is in kg/μm

This equation shows that stiffness is a function of the contact area as well as the specific pressure. Therefore, the guidelines given by Hajdu should be treated with care and it should be kept in mind that they are true only for a constant area. For a constant load, the effect of area on stiffness can be found by using the following equation,

$$S = A_a^{0.5} \quad \frac{W^{0.5}}{0.933} \qquad (5.3)$$

The equation is plotted in fig 5.5. The curves show that for a constant load, stiffness increases with area, and decreases with pressure as opposed to the image given by equation 5.2.

Therefore, guidelines on specific pressure without giving any consideration to the load can be misleading. The following procedure can be adapted for the selection of specific pressure.

1) Contact area is usually fixed by the geometry, find the allowable range.

2) Calculate the forces acting on the slideway.

3) Choose a specific pressure by using the load given and the allowable range of the contact area.

4) Check that specific pressure for changes in stiffness according to the speed. Above 4m/min the specific pressure should be higher than 1.2 m/min.

When the above procedure is repeated for the design carried out here, it will be seen that the selected specific pressures are satisfactory.

The stiffness of the sliding pair can be calculated according to equation 5.2. The results are as follows,

Slideway 1		Slideway 2	
Normal Stiffness:	670 kg/μm	Normal Stiffness:	130 kg/μm
Side Stiffness:	0	Side Stiffness:	80 kg/μm

In these calculations it is assumed that the specific pressure is applied over the area uniformly. This is an acceptable assumption if the accuracy of the slide-ways is good and if there is no sideway tilting.

Similar calculations can be carried out for the end turret slideways. The forces acting on the slide-ways can be calculated using the equilibrium equations. The following values are found (fig. 5.6),

$F_1 = 62$ kg; $F_2 = -205$ kg; $F_3 = 840$ kg

Then, the following parameters for the slideways can be obtained,

Slideway 1

A) Normal

$P = 3.5$ kg/cm^2

$A = 60$ cm^2

$S = 120$ kg/µm

B) Side Stiffness is zero

Slideway 3

A) Normal

$P = 0.8$ kg/cm^2

$A = 400$ cm^2

$S = 383$ kg/µm

B) Side

$P = 6$ kg/cm^2

$A = 140$

$S = 367$ kg/cm^2

5.4.2 Anti-friction Guideways:

As stated in section 5.2, there are many types of anti-friction guideways. Size and stiffness calculations will be carried out on the most common three types (fig 5.7). In the calculations, equivalent central load should be found by using the compatibility equation for deflections together with the equilibrium equations. That is very important, because the selection from the catalogues should be based on the central load. If approximate calculations are used, the life of the bearing can turn out to be much less than expected.

a) Point Contact Balls:

The force layout assuming four bearings are used is shown in figure 5.8. In section 5.4.1, $F_1 + F_4$ and $F_2 + F_3$ were already calculated. If two more equations are written, one being related to deflections, the other being an equilibrium of moments, the four equations can be solved for the four unknowns.

If the cross-slide is assumed to be rigid, the following equation can be written for deflections,

$$\sigma_1 + \sigma_4 = \sigma_2 + \sigma_3 \qquad (5.4)$$

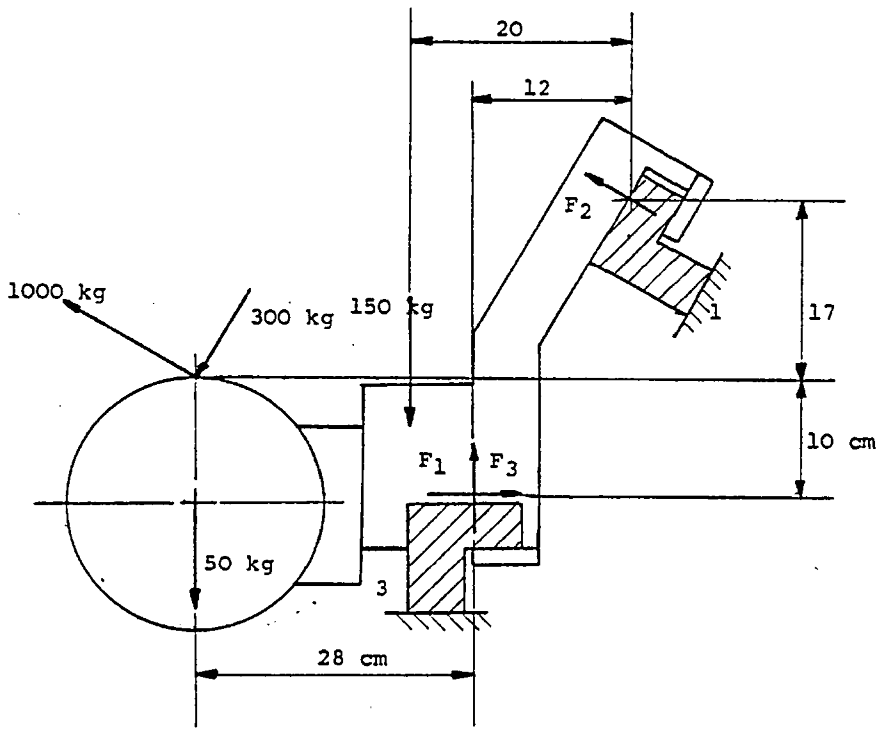

Figure 5.6 End Turret slideways

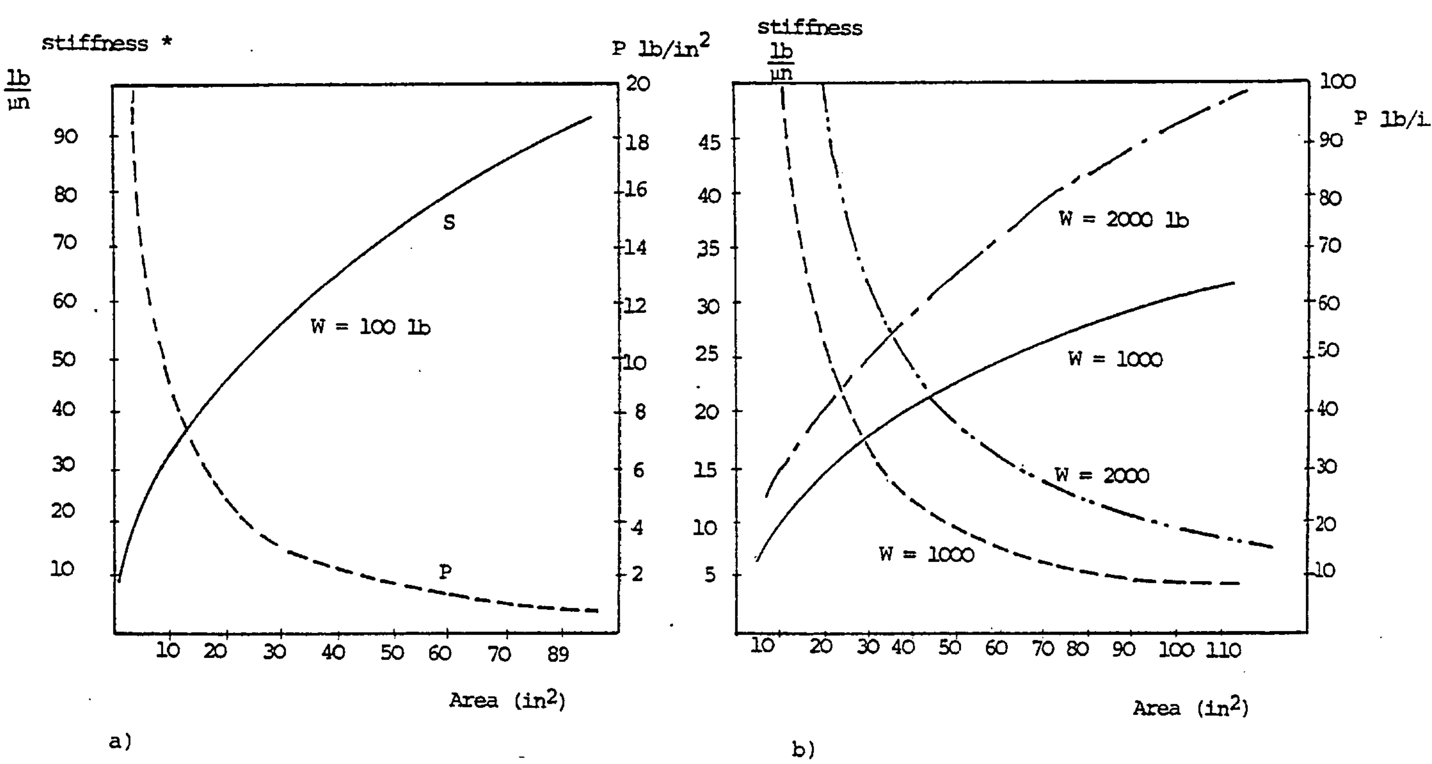

* $1\ lb/in^2 = 690\ kg/m^2$; $1\ in^2 = 6.45 * 10^{-4}\ m^2$; $1\ \frac{lb}{\mu in} = 17.9\ \frac{kg}{\mu m}$

Figure 5.5 Relation betweeen specific pressure, stiffness and area

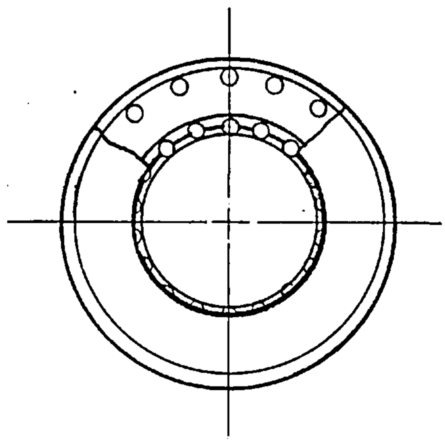

a) Point contact balls

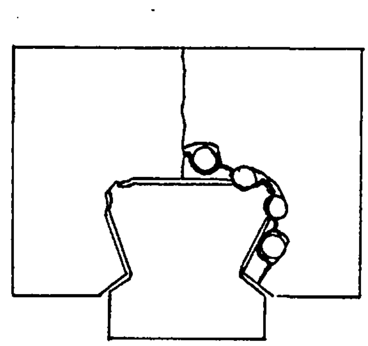

b) Line contact balls

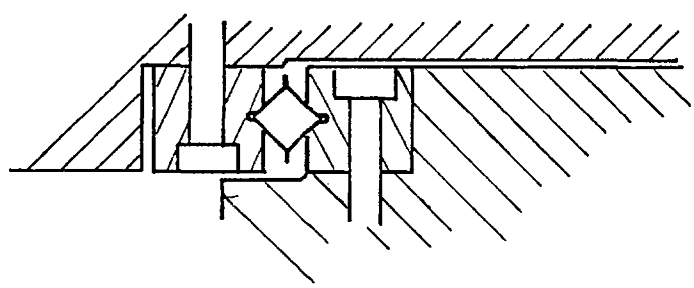

c) cross roller bearing

Fig 5.7 Three types of anti-friction guideways

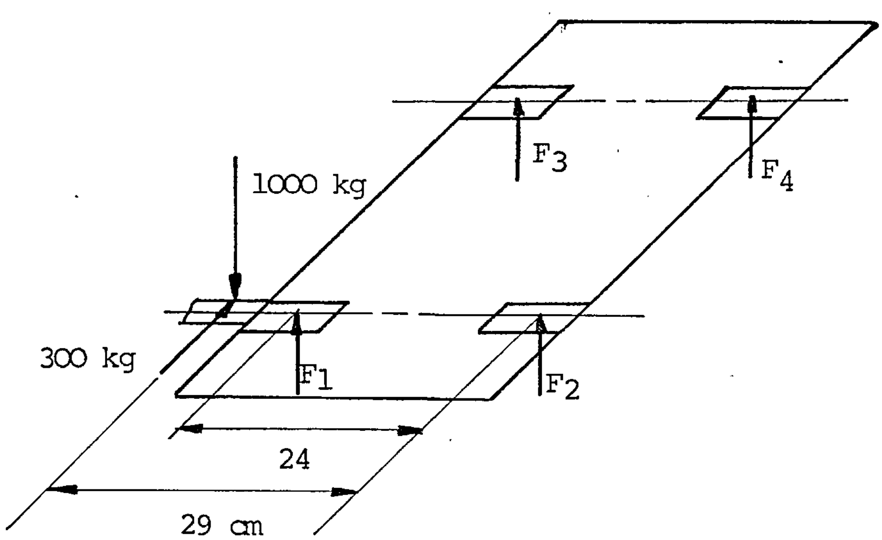

Fig 5.8 Layout of the forces for the anti-friction guideways

For a sphere in point contact with a plane surface deflection equation is;

$$\delta = KF^{2/3} \qquad (5.5)$$

where F is the load acting on the sphere and K is a constant.

Substituting (5.5) into (5.4),

$$\left(\frac{F_1}{N_1}\right)^{2/3} + \left(\frac{F_4}{N_4}\right)^{2/3} = \left(\frac{F_2}{N_2}\right)^{2/3} + \left(\frac{F_3}{N_3}\right)^{2/3} \qquad (5.6)$$

Where N_1, N_2, N_3 and N_4 are the number of balls that take the load on each bearing. For a closed type bearing, they will be equal, for an open type, they will change according to the direction of the load. It will be assumed that when the load is acting as to press the bearing on to the guideway, the number of effective balls is twice that when the load is acting in the opposite direction.

Equilibrium equations together with equation 5.6 can be solved to give the following results,

F_1 = 1380 kg; F_2 = -17 kg; F_3 = 207.5 kg; F_4 = -447.5 kg.

The guideway will be chosen among RHP linear motion products. In the selection, load rating is calculated on the basis of bearing life by using the equations given in the catalogue. The calculations are carried out and 0678-080 RHP bearing with a life of 2.6* 10^6 m is chosen. Bearing is to fit onto an 80 mm ground shaft.

Stiffness can be calculated by using the equation given by Levina ,

$$S = \frac{dP_x}{d\delta_x} = \frac{3}{2} \gamma^{2/3} P_x^{1/3} \qquad (5.7)$$

Where $\gamma = 0.38 \sqrt{d}$ for steel to steel contact d being the diameter of the ball in cm, Q_x is the load on the ball with coordinate x in kg.

Based on the catalogue, it is assumed that positive loads are taken by 32 balls, whereas negative loads are taken by 16. Equation 5.7 shows that stiffness is not effected so much by the load. Therefore, load per ball will be assumed as 20 kg,

$$S = 1.8 \text{ kg}/\mu\text{m per ball}$$

b) Line Contact Balls:

For this kind of anti-friction guideways, force calculations can be performed exactly in the same manner as described above. However, in this case the compatibility equation will be different, because for a ball in line contact the deflection equation will change. For this case, the deflection equation will be taken as a roller on a plane surface. The equation can be written as follows,

$$\delta = 0.6 \frac{Q^{0.9}}{\ell^{0.8}} \mu\text{m} \qquad (5.8)$$

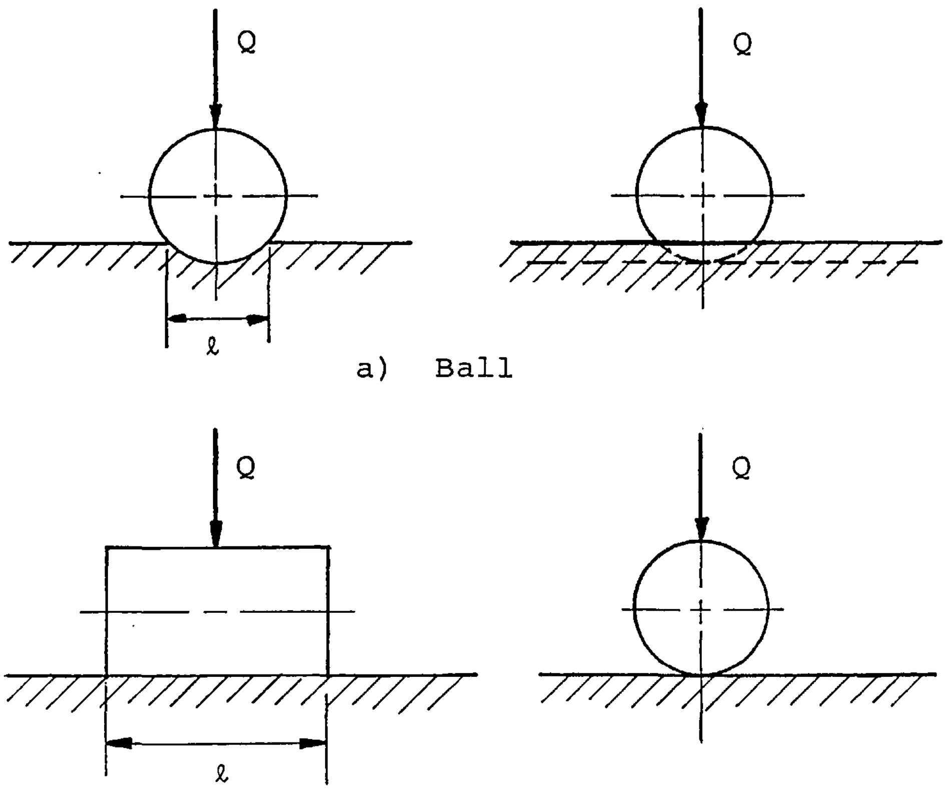

Fig 5.9 Ball and roller in line contact

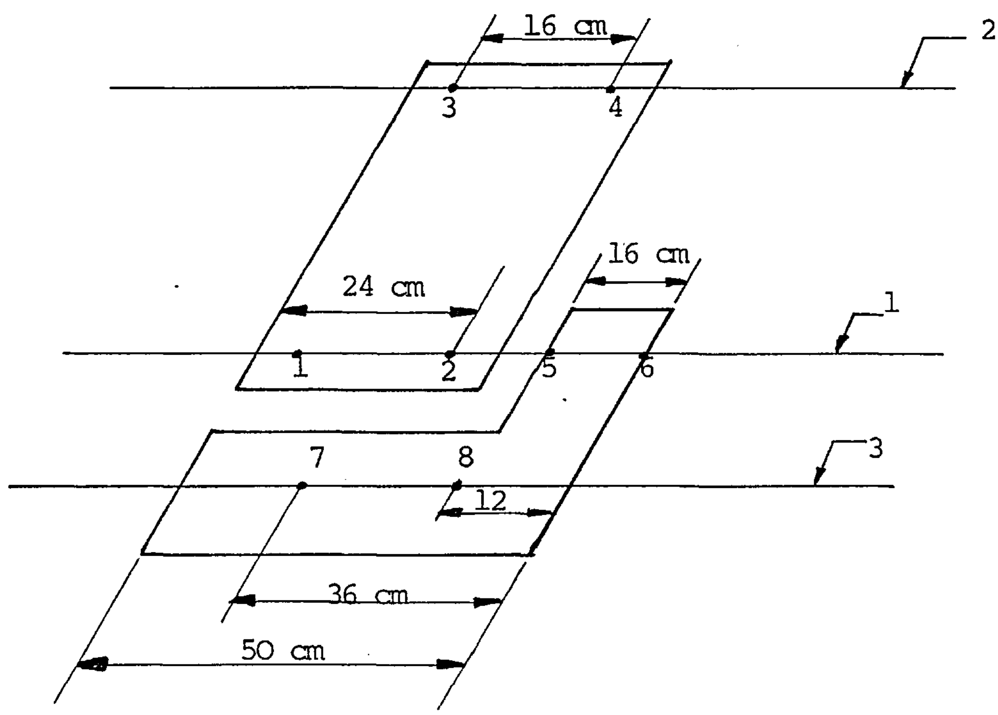

Fig 5.10 Points where the contact stiffness are designated

where Q is in kg and ℓ is in mm. Q and ℓ are shown for a ball and a roller in fig 5.9. Then the compatibility equation becomes,

$$\left(\frac{F_1}{N_1}\right)^{0.9} + \left(\frac{F_4}{N_4}\right)^{0.9} = \left(\frac{F_2}{N_2}\right)^{0.9} + \left(\frac{F_3}{N_3}\right)^{0.9} \qquad (5.9)$$

Assuming for positive loads the number of balls is twice that for negative loads, by iterating, the compatibility equation together with equilibrium equations can be solved to obtain,

F_1 = 1330 kg; F_2 = 33 kg; F_3 = 257.5 kg; F_4 = -497.5 kg

Again, the selection of the bearings will be based on a life of 2600 km. From the 'UNIMATIC' catalogue NSR 100TBA type bearings with 6 mm ball diameter chosen.

Stiffness can be obtained by using the following equation,

$$S = 1.85\ (\ell)^{0.8}\ (Q)^{0.1}\ \mu m \qquad (5.10)$$

The effect of load on the stiffness is small. Assuming Q = 40 kg and ℓ = 3 mm, stiffness is obtained as,

S = 6.4 kg/μm per ball.

For positive loads 32 balls and for negative loads 16 balls will be assumed. Based on the manufacturer's drawings side loads will be assumed to be taken by 24 balls.

c) Cross Roller:

In this case, because the deflection equation is identical, loads will be the same as calculated above. Therefore, the maximum load is 1750 kg. From 'UNIMATIC, catalog a cage length of 70 cm is chosen. Then an XR24 type crossed roller guideway with 4.2 cm pitch and 24 mm roller diameter is chosen. In the catalog, the calculations are based on the assumption that the load is taken by all the rollers. To compensate for this assumption a factor of safety of 1.2 is used and the biggest available guideway is chosen.

Taking $Q = 50$ kg and $\rho = 10$ mm, the stiffness can be calculated as,

$S = 20$ kg/μm per roller.

5.5 Stiffness Comparisons and Finite Element Analysis:

5.5.1 Stiffness of each individual type of slideway

As the above calculations suggested, stiffness of the guideways depends very much on the type of design and kind of loading. Therefore, for a thorough comparison, stiffness calculations should be carried out separately for each particular machine tool and loading configuration. Here, only the loading condition for which the calculations are performed will be analysed. This being one of the critical conditions should give good guidelines for comparison.

In order to do the analysis a finite element model was prepared. In the model the guideways are represented by beam elements and the slides are represented grids composed of beam elements. Contact stiffnesses will be simulated by beam elements with cross-sectional areas to give the relevant stiffness. The locations of these beams are shown in fig 5.10. In the previous section, general stiffnesses were calculated, now they have to be converted to the stiffnesses at these locations. Below this conversion is explained briefly.

a) Plain Slideways:

The stiffness calculations assumed that there was no sideway tilting, ie, F_1 and F_2 are positive and F_3 and F_4 are negative. If this assumption is not satisfied, on the same slideways one of the reaction forces can act as to try to lift the slide out while the other acts as to press it on to the slideway. In this case, effective areas will be considerably different which will in turn change the stiffnesses. Therefore, in order to check the validity of the stiffness modelling, the forces at each point should be calculated.

For each slide, there are four forces. With three equilibrium equations and one deflection equation, it is possible to calculate all the forces. The equilibrium equation for the first slide can be written as follows,

$$\frac{F_1}{k_1} + \frac{F_4}{k_4} = \frac{F_2}{k_2} + \frac{F_3}{k_3} \qquad (5.11)$$

k_1, k_2, k_3 and k_4 are the stiffnesses. It will be assumed that there will only be two values of stiffness according to the direction of the force. Then, by trial and error, it is found that, the equations are satisfied, when F_1 and F_3 are positive and F_2 and F_4 are negative. The actual values can be found by using the results given in section 5.4.1.

In a similar way, it was found that for the second slide F_5, F_6, F_7 are negative while F_8 is positive. The stiffness values are tabulated in table 5.3.

b) Point Contact Balls:

In section 5.4.2, it was assumed that the loads at points 1 and 3 are supported by 32 balls and the loads at points 2 and 4 by 16. Then, from the stiffness per ball calculated, the total stiffness of the bearings at each point can be calculated.

	1		2		3		4		5		6		7		8	
	Normal	Side	Normal	Side	Normal	Side	Normal	Side	Normal	Side	Normal	Side	Normal	Side	Normal	Side
Plain Slide-ways	335	0	65	0	335	40	65	40	60	0	60	0	190	112	190	112
Point contact balls	58	0	29	0	58	58	29	58	29	0	58	0	29	58	58	58
Line contact balls	205	0	102	0	205	154	102	154	102	0	205	0	102	154	205	154
Crossed Rollers	80	0	80	0	80	160	80	160	80	0	80	0	80	160	80	160

Table 5.3 Contact Stiffnesses for different types of Guideways (units are in kg/μm)

For the points on the other slide, the compatibility equation in conjunction with the equilibrium equations can be solved to find the direction of the forces. The results show that F_5 and F_7 are negative while F_6 and F_8 are positive.

c) Line Contact Balls:

In section 5.4.2, for different direction of loads, the following number of balls are assumed.

Positive loads:	32 balls
Negative loads:	16 balls
Side loads:	24 balls

For the other slide, the direction of the forces are found to be positive for F_6 and F_8 and negative for F_1 and F_3.

d) Crossed Roller:

A cross roller type of bearing with a 70 cm cage length and 4.2 cm pitch was chosen in section 5.4.2 This corresponds to 16 rollers. For vertical loading only 8 of them will be effective, because rollers contact the surface alternately. For side loads all of them will be effective. In this case, for vertical loads, the direction of the load does not affect the stiffness.

The stiffness values for each type of guideway are tabulated in table 5.3. The cross-sectional areas of the beams used to model the contact stiffnesses can be found from the equation,

$$A = \frac{S.\rho}{E} \qquad (5.12)$$

where S is the stiffness, ρ is the length of the beam and E is the Young's Modulus. The corresponding cross sectional areas are shown on the same table.

5.5.2 Finite Element Analysis and the Representation of the Structure

The purpose of the analysis can be summarised as follows,

1. To compare the rigidity of different types of slideways

2. To analyse the effect of the supports for the point contact type slideways

3. To analyse the effect of the machine bed on the overall rigidity.

The main purpose of the analysis is to compare the rigidity of different types of slideways. As seen from table 5.3, the contact stiffnesses of the slideways change according to the direction and while one type of slideway has a higher stiffness in one direction, it might not be so stiff in the other direction. Therefore, comparison of the stiffness is not straightforward. The point contact ball bearings have lower stiffnesses in all the directions. However, it will still be included in the analysis to establish the deflections along the direction perpendicular to the cut surface. Additionally, the effect of the supports used together with this type of guideway will be analysed. This is important because if the supports have a considerable effect on the overall deflection, then non-standard more rigid supports will have to be used.

Another purpose of the analysis is to investigate the effect of the structure on the deflections. If the deflections are largely due to the stiffness of the structure, rather than to the slideways, then the structure design should be reviewed and a more rigid structure built.

The finite element mesh prepared for the analysis is shown in figure 5.11. The stiffnesses indicated in table 5.3 are represented by springs along the relevant directions. The slideways and the springs are described with 3-D beam elements (fig. 5.12). The tool slides are also described as combination of beam elements. Their effect will not be considered in the analysis, so the beams comprising the tool slides are made rigid.

The second purpose of the analysis was to investigate the effect of the supports for point contact ball type slideways. For this reason the supports were analysed separately. A finite element mesh for the support was prepared. It is shown in fig. 5.14. To find the stiffness of the supports a unit load first in the direction 1 and then 2 was applied. The problem was solved both by using "plane strain" and "plane stress" assumptions.

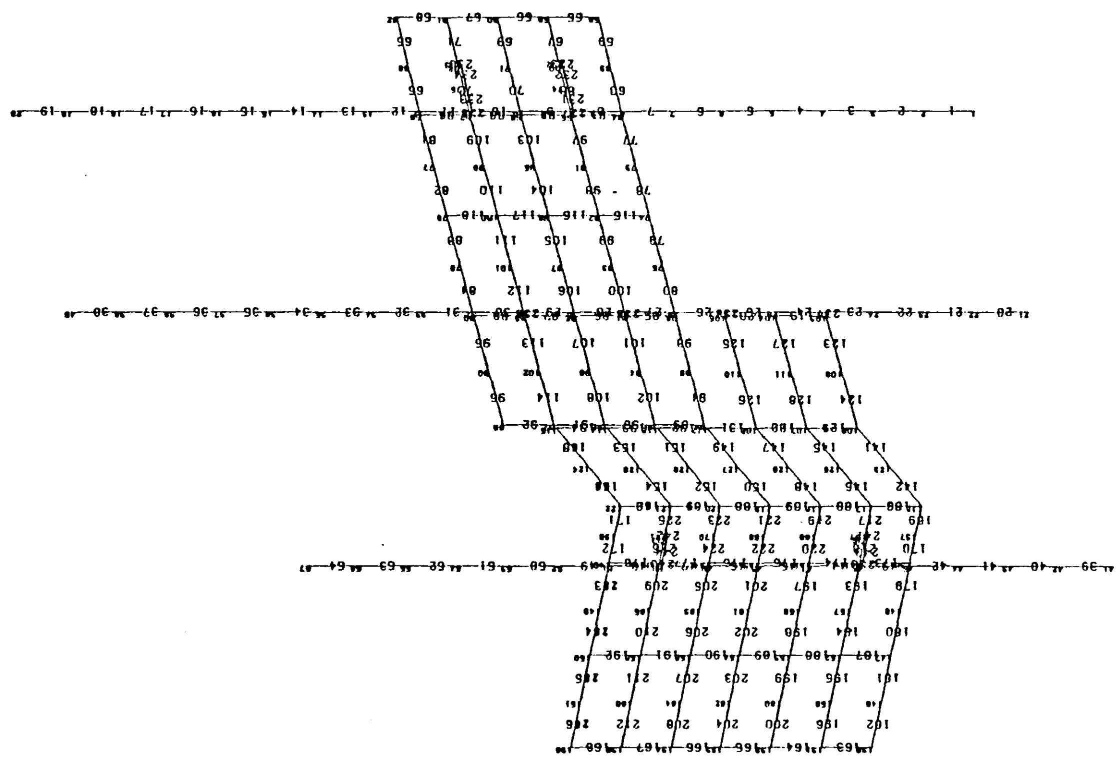

177 nodes, 245 elements, time taken 88.9 secs on CDC 6600

Fig 5.11 Finite element mesh for the slideways

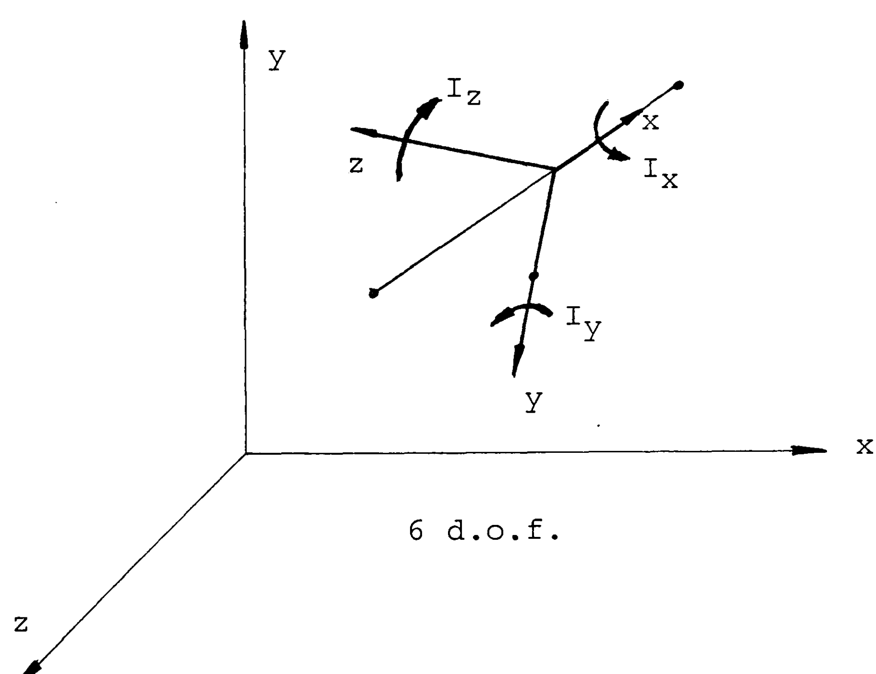

Fig 5.12 3-D Beam element used in the finite element analysis

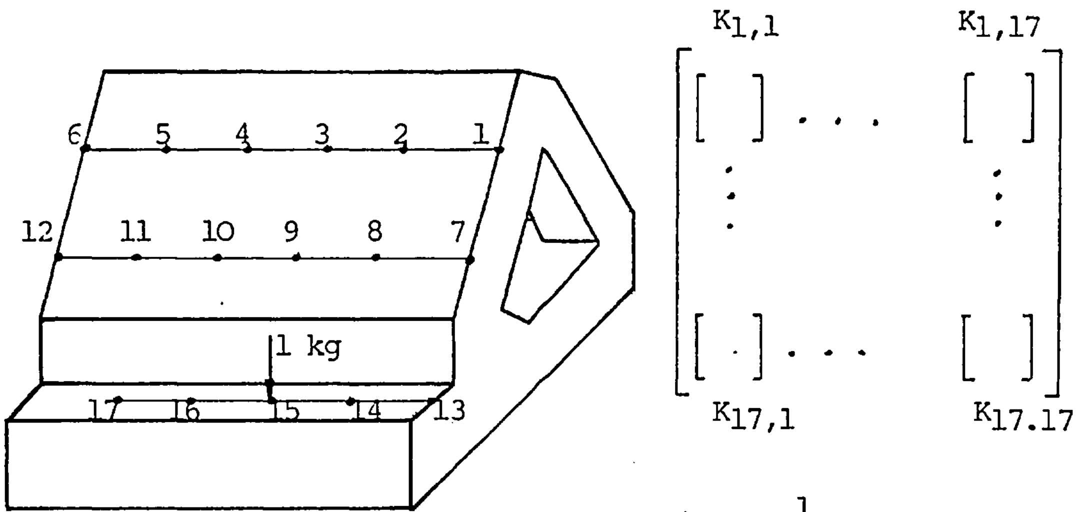

$$(K_{15,15}) = \frac{1}{(\Delta y)_{15}} \qquad (K_{15,15}) \; \frac{1}{(\Delta z)_{15}}$$

$$(K_{1,15})_z = \frac{1}{(\Delta z)_1}$$

Fig 5.13 Formation of the stiffness matrix for the structure

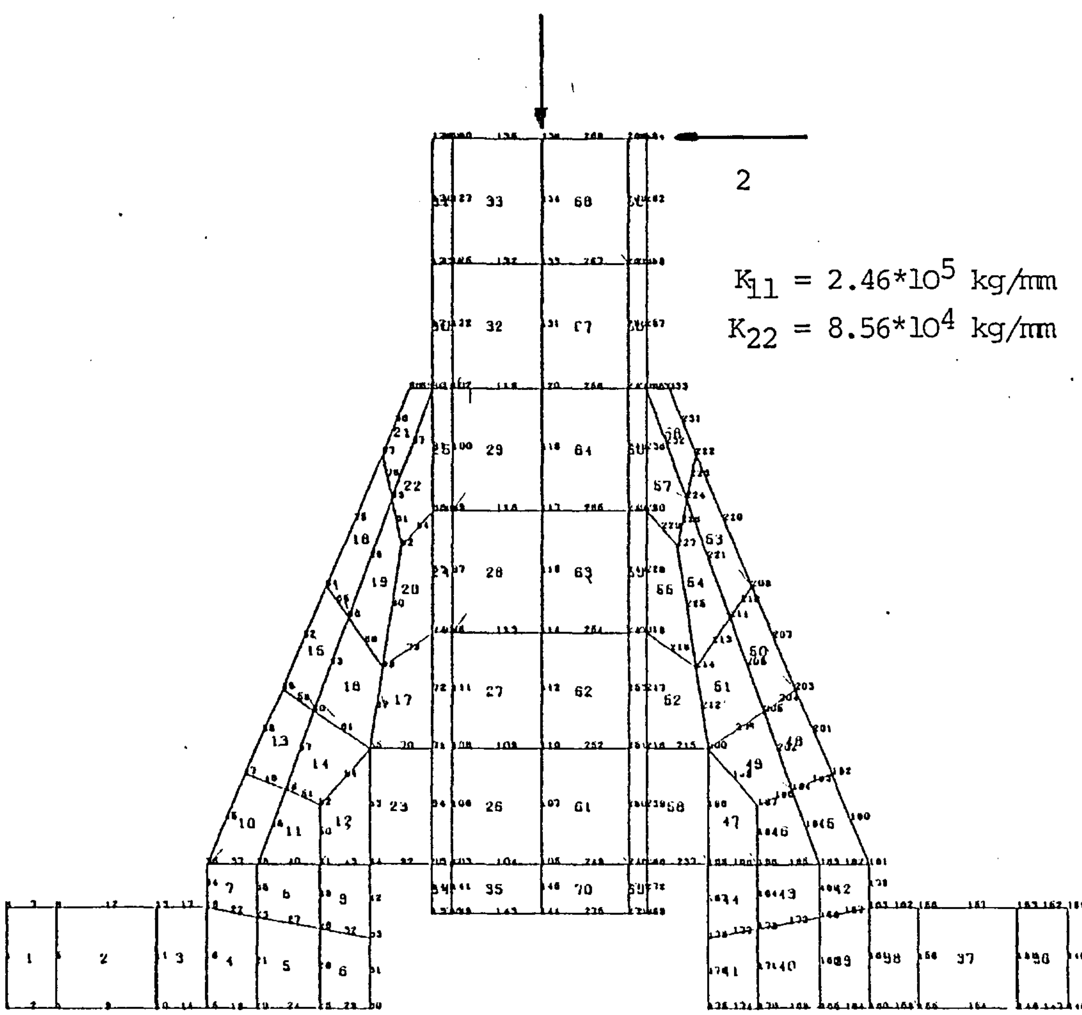

Fig 5.14 Finite element mesh for the supports

The deviation between the results was found to be around 9%. The stiffnesses were found by using the average values obtained from the two different assumptions. The calculated stiffness values are given in fig. 5.14.

Lastly, the effect of the structure on the deflections should be considered. The simplest solution would be to prepare a mesh which combines the structure and the slideway system together. However, the elements used for the structure had three degrees of freedom (3-D Brick), whereas the beams used for the slideways had 6. Therefore, the two are not compatible and they can not be combined. In this case, the only solution left was to prepare a new element which has the stiffness characteristics of the structure. For this purpose, 17 relevant points on the structure were chosen. They are shown in fig. 5.13. A unit load at each particular point was applied and the corresponding deflections were found by using the finite element program. From the deflection values, it is possible to find the direct and cross receptances for each individual point. A computer program was prepared and a 17*17 stiffness matrix was formed. The result was stored as the stiffness matrix of a new element. In the analysis this new element was used in conjunction with the mesh shown in fig. 5.11.

Based on the prepared meshes and obtained stiffness values, a thorough analysis was carried out to achieve the purposes set at the beginning of the section. The results are discussed in the next section.

5.5.3 The Results of the Analysis:

Deflections at the points indicated in fig. 5.11, as obtained from the finite element analysis are given in table 5.4. The deflections were found for seven different cases.

A. Line contact ball guideways as connected to the structure

B. Plain slideways as connected to the structure

C. Point contact ball guideways connected to the structure

D. Roller guideways as connected to the structure

E. Plain slideways not connected to the structure but connected to a rigid fixed plane

F. Point contact ball guideways without the supports connected to a fixed plane

G. Point contact ball guideways with the supports connected to a fixed plane

The first four cases are for the rigidity comparison of the slideways. Cases B and E and C and F are for

Table 5.4 Deflections for different types of slideways

		150 (μm)		151		136		90			88		
		y	z	y	z	y	z	y	z	perpendicular to cut	y	z	P
A	Line contact	-3.481	25.47	-3.481	28.01	-3.481	30.56	27.07	-8.546	6.134	28.88	-9.591	6.134
B	Plain	-8.347	-0.2589	-8.347	0.9522	-8.347	2.164	19.85	-8.725	2.369	22.12	-10.04	2.365
C	Point contact	-11.09	54.23	-11.09	56.38	-11.09	58.53	52.99	-25.44	4.46	58.77	-28.78	4.46
D	Roller	-4.986	29.48	-4.986	32.22	-4.986	34.97	38.47	-15.63	5.699	41.42	-17.33	5.697
E	Plain fixed ends	-5.617	-0.6255	-5.617	-0.1407	-5.617	0.3445	9.251	-4.288	0.9119	10.47	-4.989	0.9144
F	point contact fixed ends	-11.04	40.7	-11.04	41.74	-11.04	42.78	35.71	-21.21	-0.5134	40.49	-23.98	-0.5223
G	point contact supports and fixed	-13.56	44.94	-13.56	46.54	-13.56	48.15	40.57	-24.03	-0.5256	46.18	-27.27	-0.5265

the effect of the structure. The last two cases are to investigate the effect of the shaft supports used with the point contact ball type guideways.

The nodes where the deflections are given are the nodes which are nearest to the cutting area. The nodes 150, 151 and 136 are located on the end turret slide and the nodes 90 and 88 are located on the main turret slide. To give a better picture of the results, the deflections on nodes 88 and 136 are presented in a chart form in fig. 5.15. For node 88, the direction which affects the surface finish is not y or z, but the one which is perpendicular to the cut surface. Therefore, for 88 deflections are given in this direction. For the node 136, deflections along both y and z axis can be important according to the application and therefore, both are given.

From the results for the end turret along the z direction the type of guideways can be listed in the order of decreasing stiffness as follows. In brackets the stiffness values are given as a percentage of the stiffest one.

1. Plain slideways (100%)
2. Line contact ball type guideways (7%)
3. Crossed roller guideways (6.1%)
4. Point contact ball type guideways (3.7%)

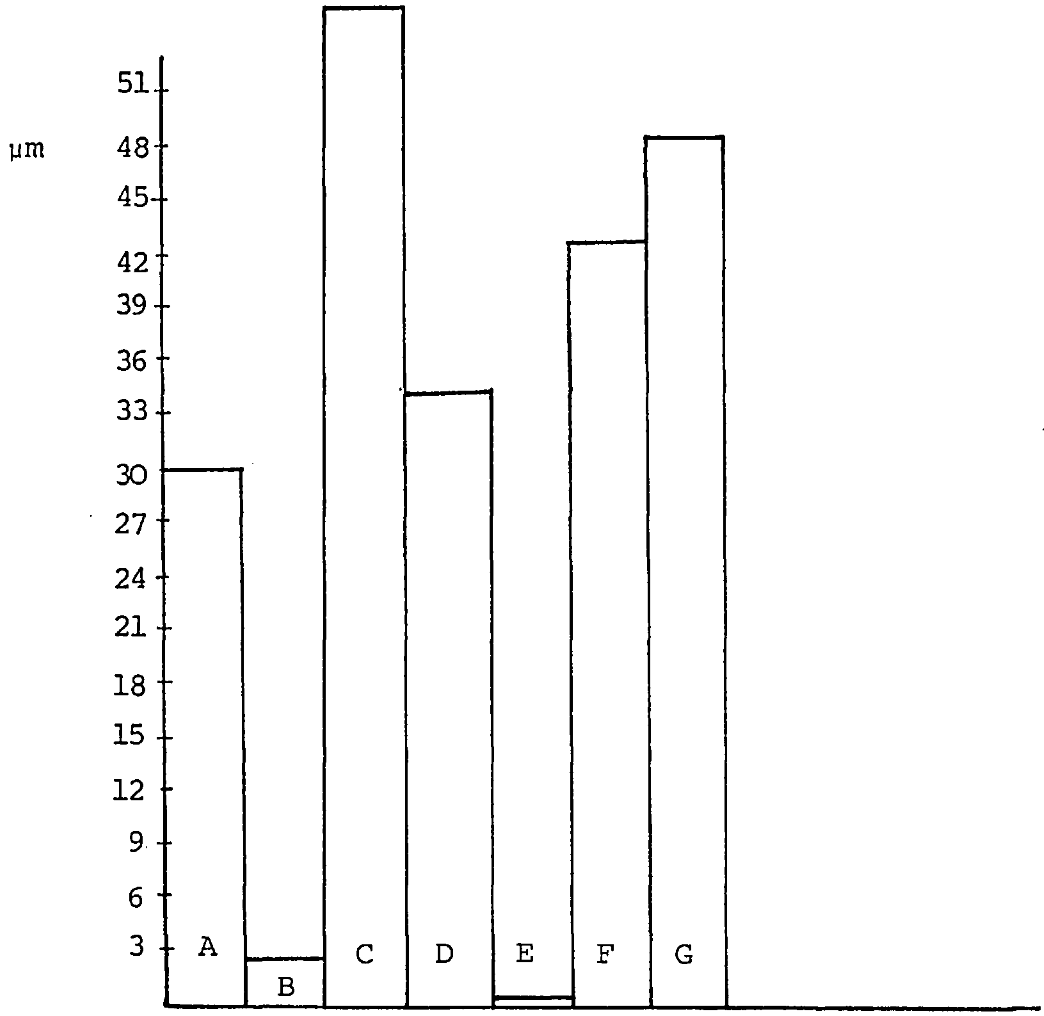

a) Node 136, deflections for z in µm

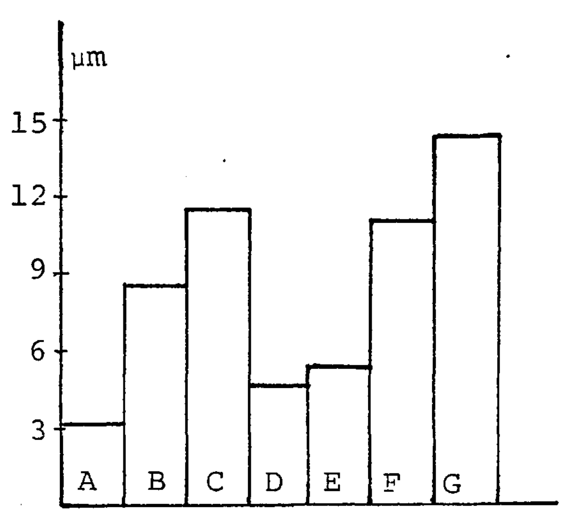

b) Node 136, deflections for y in µm

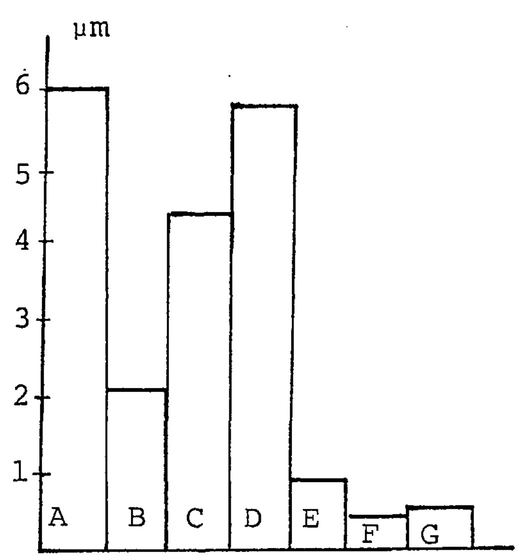

c) Node 88, deflections along the direction perpendicular to the cutting surface

Fig 5.15 Deflection comparisons for the cases given in Table 5.4

In the case of y direction, the order is,

1. Line contact (100%)
2. Crossed roller (69.8%)
3. Plain (41.7%)
4. Point contact (31.3%)

Finally, in the case of the main cutting turret,

1. Plain (100%)
2. Point (53%)
3. Crossed roller (41.5%)
4. Line contact (38.5%)

As it is seen from the results, the stiffness of the slideways can change considerably according to the direction. However, for a final selection, the main cutting turret should be dominating. The results for the main cutting turret gives plain slideways as the stiffest alternative. That is not the case, though, when the end turret and the y-direction are considered. However, deflections along that direction are small when compared with the others. Therefore, plain slideways still appears to be the best alternative.

The results show that with point contact ball type guideways, although the least rigid for the end turret, their deflection along the direction perpendicular to the cut surface is, for the main cutting turret, less than that of the other two types of anti-friction guideways. That is because the combination of deflections along y and z directions turned out to be favourable for this particular load case. This favourable combination almost certainly fortuitous may not repeat itself for other load cases.

The effect of the supports for point contact ball type guideways can be seen from cases F and G of fig. 5.15. The results show that the maximum deviation between the two cases, when the shafts are supported with the standard supports and when they are directly supported at the same points by a fixed frame, is around 10%. This sort of deviation is acceptable, therefore the standard supports can be used without any additional measures.

The effect of the structure on the static behaviour is represented by cases B and E or C and F of fig. 5.15. The results show that the deflections can be decreased by about 1.5 to 5 times by making the machine tool bed completely rigid, The most important effect of the structure appears to be along Z axis. This suggests that the recesses introduced to decrease the weight decreases the static stiffness along Z-direction considerably. Although deflections was found to be acceptable in chapter 3, it will still be advisable to use heavier reinforcement along that cross-section. The results also show that deviation in the case of main turret is bigger, suggesting that the upper plane should also be strengthened. Necessary precautions should be taken for the reinforcement of the upper plane.

The results can be extrapolated to estimate the relative dynamic rigidity of the slideways, because static rigidity and dynamic rigidity follow the same pattern. Plain slideways being statically more rigid for this particular case, will also have higher natural frequencies. As pointed out in section 5.2, their damping capacity is also higher than the anti-friction type of guideways. Therefore, plain slideways with their higher dynamic stiffness and damping capacity, are superior in their dynamic behaviour.

5.6 Discussions and Conclusions

In this chapter, the general requirements for slideways were set out and the existing types of slideways were reviewed.

The possible pitfalls during the selection of anti-friction type of guideways were pointed out. The need for the calculation of equivalent central forces through the solution of compatibility and equilibrium equations was emphasized.

From the literature, it was seen that the rigidity of the slideways changes according to the application of the load and the direction in which the deflections are important. Therefore, for a comprehensive comparison, finite element analysis was used and plastic coated plain slideways were compared with three types of anti-friction guideways. The results showed that plain slideways are in general more rigid than the other types. Only for one direction, line contact ball type guideways were more rigid.

When the high damping characteristics of the plain slideways are considered as well, they appear to be the most attractive solution. However, if the research to improve the damping capacity of the anti-friction type of guideways gives good results, they become a more attractive alternative, because they can be bought off the shelf helping the modularity and standardization. principles set forward for this machine tool. At the moment, though, plain slideways with Turcite 'B', or Rulon LD coating are the best solution.

Finite element analysis was used to investigate the effect of the structure on the deflections. The results indicated that the upper plane and the recessed parts of the structure needs further strengthening. Heavier reinforcement was suggested for these sections.

In this chapter, emphasis was given on the comparison of the existing types of guideways. The actual design of the slides and slideways was not considered in detail, because it depends on the type of turret to be used and on the motor size. This is a job of detailed design and will not be attempted here. However, in detail design, the results of the above analysis should be taken into account. Layout of the slideways should be such that deflections are minimized. For example, the forces should be arranged in such a way that they push the slide onto the slideways, instead of trying to lift it up.

CHAPTER 6

DRIVE SYSTEMS

6.1 Introduction:

As the analysis in the first chapter showed, today's modern machine tools have to meet stringent requirements and should have high performance drives for this purpose. In order to compete in the highly competitive machine tool market, the speed of the drives should be infinitely variable within a wide range and should have high maximum. They must have high accuracy and resolution. Quietness and reliability are also important factors.

In this chapter, the available drive systems which are considered suitable for this application are analysed. Mechanical and pneumatic drives are not included in this discussion. Mechanical drives usually have a maximum speed range of about 10:1 which is inadequate for this application, and the pneumatic motors can be excluded as their power rating is generally too low.

6.2 Electrical Drives:

Electrical drive systems can broadly be divided into three groups.

i) D.C. Drives

ii) A.C. Drives

iii) Stepping Motors

6.2.1 D.C. Drives

A D.C. drive system consists of a controller, amplifier and the d.c. motor. There are basically four types of d.c. motors suitable for machine tools,

a) Motors of conventional design
b) Permanent magnet motors with low inertia
c) Permanent magnet motors with high inertia
d) Brushless d.c. motor.

Their characteristics are tabulated in table 6.1. From the table, although brushless d.c. motors seem to be the most attractive, they are not yet widely available for high power applications.

There are several methods of driving d.c. motors. The most commonly used power sources are:

a) The line-frequency switched thyristor controller (SCR)
b) The continuous transistor amplifier
c) The rotary converter (Ward-Leonard set)
d) The high-frequency switched transistor controller.

Their relative merits are shown in table 6.2.

Table 6.1 Relative merits of the four principal types of D.C. motors

	Conventional Design	Low inertia 1) Printer circuit 2) Disk Rotor 3) Minertia (cylinder)	High inertia Torque motors	D.C. Brushless
speed range	100:1	500:1-5000:1	5000:1-10000:1	5000:1-10000:1
max.spindle range	3000 rpm	3000 rpm	3000 rpm	3000 rpm
Peak torque/ rated torque	3	8-10	5-10	5-10
Acceleration	700-1000 rad/sec^2	10000 rad/sec^2	5000 rad/sec^2	5000-10000 rad/sec^2
Comments:	1. There are also motors specially designed for rapid acceleration.	1. Their thermal characteristics are poor. 2. They are not robust	1. They can be directly coupled.	1. They have no mechanical wear problem due to commutation. 2. However, they are more expensive and not widely available for high power applications yet.
Relative Cost	low	medium-high	medium	high

Table 6.2 Relative Merits of the four principal types of D.C. motor drive systems

Type	Power	Bandwith	Speed range	Comments
SCR	up to 500 kW	5-30 Hz	Usually lower than trans-istor types	Low cost per watt. Not reco-mmended for low speed Higher form factor
Continuous Transistor Amplifiers	up to 1 kW	can exceed 1000 Hz	high	efficiency is usually low (60%)
Rotary Converter	Exceeds 10 kW	up to 100 Hz	low	Noisy and bulky, requires periodic servicing
PWM Transistor Controller	up to 25 kW	can exceed 1000 Hz	high	Ideal within the 0.5 to 25 kW range.

In the past, speed and position control of the d.c. motors have been achieved using the power amplifiers mentioned above together with analogue circuitry. More recently, especially with the advent of microprocessors, digital control has become more and more important (86). Employing microprocessors for the control of d.c. motors can eliminate much of the analogue circuitry resulting in an economically attractive system. Figures 6.1 a), b) and c), show how microprocessors can be used to take over the tasks of analogue circuitry. A microprocessor control system also results in flexibility which can be used to compensate for most of the system non-linearities.

6.2.2 A.C. Drives

At present d.c. commutator motors are used almost exclusively for the feed and main drives of the machine tools. These together with suitable servo-amplifiers and control devices are able to meet most requirements. The performance of these drives is, however, often limited, particularly when operating in unfavourable factory surroundings, by the loading capacity of the commutator. Therefore, considerable effort has been spent for the development of an equivalent A.C. motor drive without commutator.

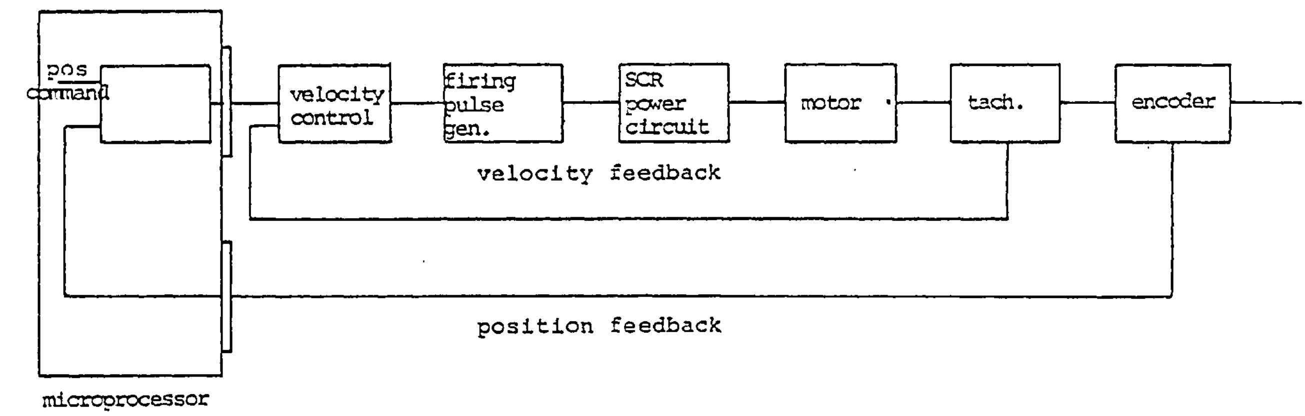

a) Microprocessor controlled conventional SCR drive with analog velocity loop.

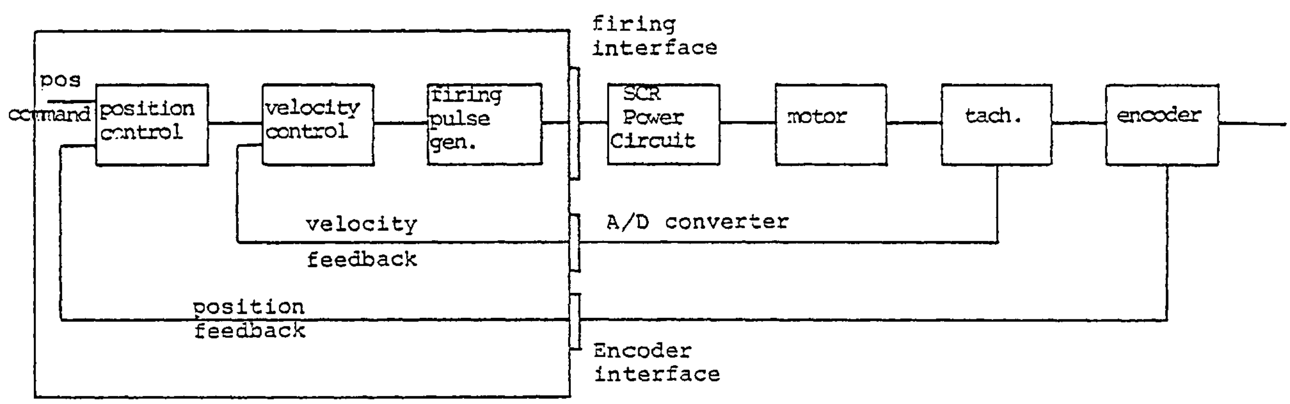

b) Microprocessor controlled SCR Drive with digitised tachometer

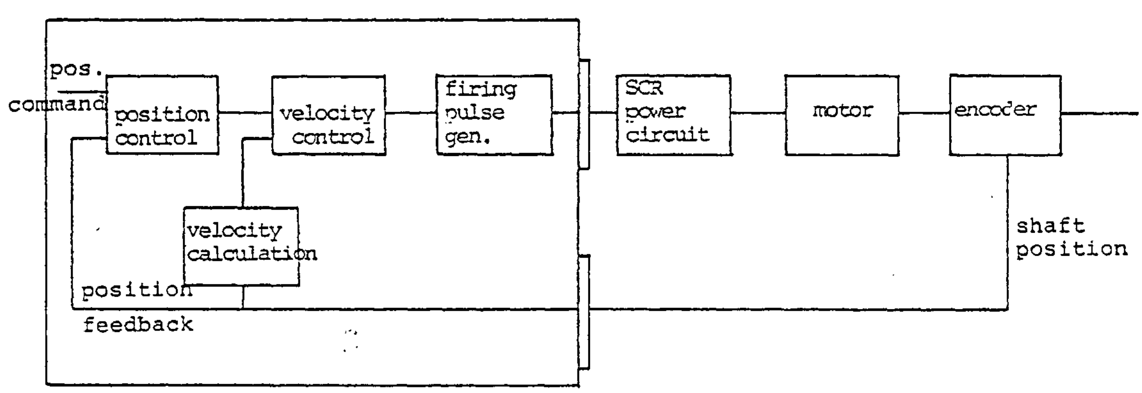

c) Microprocessor controlled SCR Drive with encoder feedback and derived velocity

Figure 6.1 Alternatives of microprocessor control with SCR Drives

However, wide application of the robust and effectively maintenance-free A.C. drives for machine tools has been held back by the high control costs. More recently, with the rapid development of semi-conductor and microprocessor building blocks, it became possible to realise cheap and effective drives of this kind (92), (93). Both synchronous and asynchorous drive motors may be used. With synchronous motors, continuous speed change can only be achieved by changing the frequency of the rotating magnetic field ie. a change in supply frequency is necessary. The asynchronous motors offer the additional possibility of slip control by setting of the stator voltage or by feeding an additional voltage into the rotor winding via slip rings.

Another A.C. drive involves eddy-current coupling. This form of drive quite popular especially in high power ranges (above 3 kw). It comprises a ferromagnetic drum driven at constant speed by an induction motor and a field member rotating relative to the drum, connected to the output shaft. Variable speed is obtained, by varying the slip power dissipated in the drum, by controlling the excitation of the field system. However, the speed is usually limited by the heat-dissipation capacity of the coupling, and it is usually around 20:1.

The idea of having robust and maintenance free A.C. motors on machine tools is attractive, however, A.C.

motors and controls with the performance levels required are not yet widely available at a competitive price.

6.2.3 Stepping Motors

A stepping motor is an electro-magnetic device which converts digital input, in the form of a train of voltage pulses, into an equal number of discrete angular steps. There are three main types of stepping motors;

a) Permanent Magnet
b) Variable Reluctance
c) Hybrid

Permanent magnet type motors are usually available with basic step angles of 120° and 90°. The motors are fairly efficient, have good damping characteristics and provide a certain amount of holding torque. However, the torque to inertia ratio is quite unfavourable.

Torque to inertia ratio is much better with variable reluctance motors. They are obtainable with a basic step angle of 15° and can operate at fast stepping rates at light loads. However, they have no holding torque and they are prone to resonances and oscillation due to the lack of inherent damping.

Hybrid motors are a combination of the two types of motors described above. They can have much smaller stepping angles (1.8^{o}) and a high resolution. They can also provide a holding torque and are capable of high stepping rates. However, their torque to inertia ratio is not very favourable and resonances may still occur at certain speeds.

Although stepping motors have been in existence for approximately half a century only in recent years has it been possible to produce these motors with output torques which are sufficiently high for use in machine tools. However, at higher torques the dynamic performance of stepping motors becomes poor. Therefore, a proper control technique is very important for a good performance.

The most straight forward technique is the open-loop control. However, because of their non-adaptive nature, open-loop systems impose severe constraints on system designers. The system must be well defined. Parameters such as system inertia, friction and supply voltage must change little. In a machine tool environment, it is very hard to secure these. Therefore, in high accuracy machine tools open-loop control will not be satisfactory.

As demands on motor performance increase, closed-loop control becomes a better technique to employ. Closed-loop operation allows minimizing motor performance by allowing higher frequency operation resulting in increased efficiency. It also gives freedom from hunting, high acceleration capability, high velocity with usable torque, multi-velocity capability, tolerance to impulse loading and simple deceleration scheme.

Motor driver circuits also play an important role in motor performance. The simplest form of stepping motor drive consists of an oscillator, logic and amplifier. These control motor speed, mode of operation and power input to the motor respectively. Motor dynamics can be drastically improved by using proper circuitry for a given motor.

Further improvement can be obtained using a micro-processor based controller as they allow the implementation of quite sophisticated control algorithms in an economical way.

6.3 Hydraulic Drives:

The basic fluid power controllers are the pumps, control valves and the actuators, ie. cylinders and motors.

There are three main types of pumps; gear, vane and axial piston. Gear pumps are used mainly for low pressure applications and they are fixed displacement type. Vane and axial displacement pumps are available as variable displacement units as well. Vane pumps cover the low to medium-high pressure, capacity and speed ranges. Pulsations are low in amplitude and they are generally quiet. Axial piston pumps are used for high pressure applications. They usually have a high efficiency. However, they are noisier than vane pumps.

The speed range that can be obtained from a hydraulic system depends very much on the selection of right hydraulic components and the right control system. It is reported in the literature (98), that with hydraulic feed drives 1000:1 speed ratio is quite common. For spindle drives, that ratio appears to be around 50:1 (99), (87).

With hydraulic drives torque to inertia ratio, therefore the response rate, is very favourable. That was the basic reason for their widespread application to machine tool feed drives. However, with the advances in d.c. motor technology it became possible to produce d.c. motors with high torque to inertia ratios. Then hydraulics being associated with drawbacks such as low efficiencies, noise, high maintenance requirements and low damping, started to disappear from the machine tool market.

However, with the advances in hydraulic technology and also with the introduction of microprocessors,it may now be possible to have high performance, quieter hydraulic systems (95), (97). For this reason, hydraulics and their control have been analysed further as described in Chapter 7.

6.4 Spindle Drive Selection:

Before attempting to select the most suitable spindle speed drive for a machine tool, requirements must be determined in detail.

In turning and milling machines, for a constant metal removal rate, a constant power output is necessary. However, at low speeds, output is limited by the stiffness of the mechanical system. Therefore, a constant power ratio of 3:1 to 5:1 is acceptable (figure 6.2).

A fast response rate is also a major requirement. Today, there are turrets with 2 secs indexing times. To fully utilize such turrets, 3-4 secs acceleration times are necessary. However, this can be limited by the dynamic stiffness of the structure.

Keeping the above discussion in mind, the requirements for the spindle drive of the machine tool considered in this work can be written as follows:

1. 15-20 hp is required
2. A stepless speed range of at least 100:1
3. Maximum speed of about 5000-6000 rpm (for ceramic tools)
4. Constant power range of at least 3:1
5. Four quadrant operation
6. Maximum error in speed 1-2% over the whole speed range
7. 3-10 sec adjustable acceleration time
8. Good control and disturbance behaviour

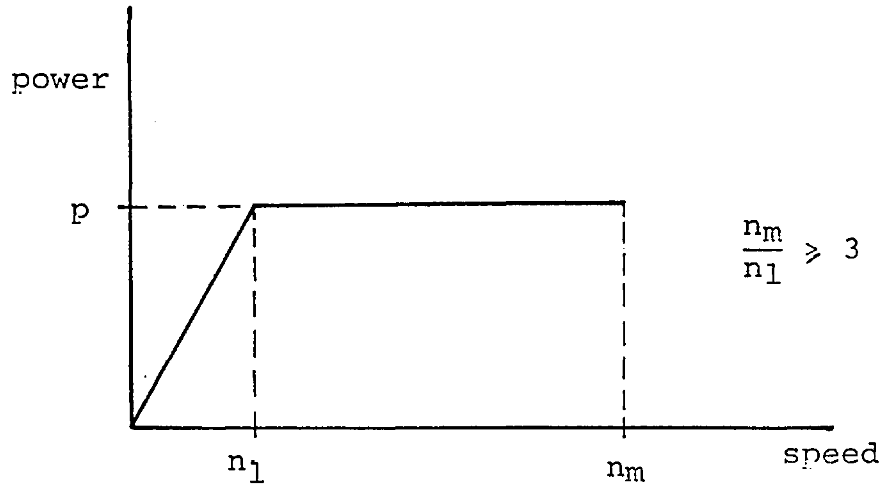

Fig 6.2 Constant power requirement for turning and milling machines

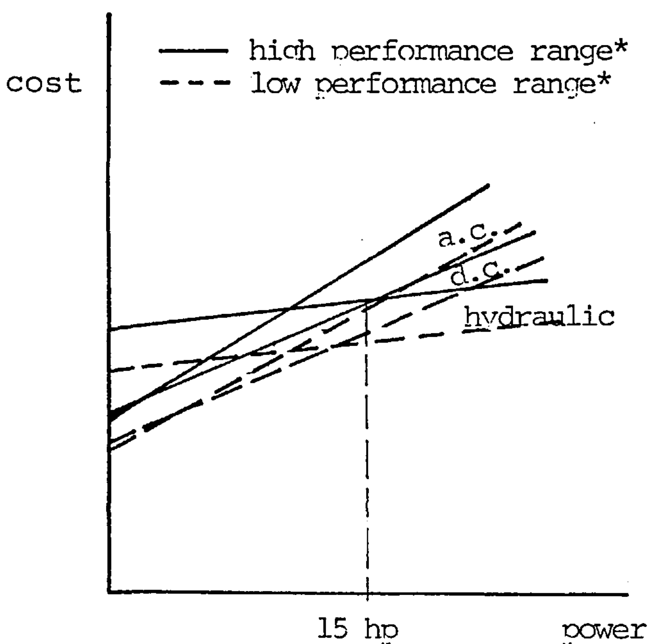

Fig 6.3 Approximate power versus cost curves for infinitely variable drives

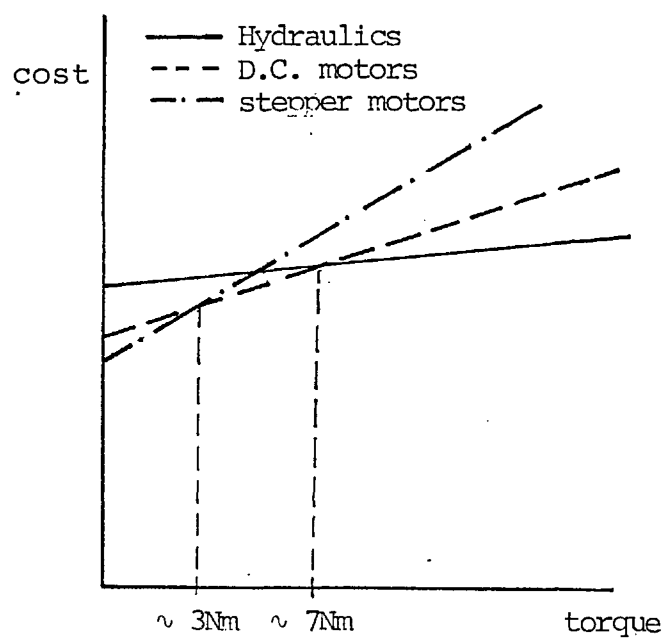

Fig 6.4 Torque versus cost comparison for servo drives (control system is not included in the comparison)

* High performance range drives are required to satisfy the requirements stated for the spindle drive

9. An overloading capacity of 1.1 to 2
10. Acceptable noise levels.

The requirements are similar for the milling head drive. However, in this case the weight of the driving motor also becomes a major consideration, because it is non-stationary.

Fig. 6.3 gives a cost versus power comparison of the alternative drives. The graphs are obtained after extrapolating manufacturers data and they should only be used as a guideline. The following generalizations can be derived from the figure:

1. High performance A.C. drives could only be found up to about 15 hp.

2. A.C. drives are at present more expensive than d.c. drives

3. For low performance drives, break even point between d.c. and hydraulic drives is around 7-10 hp where as for high performance drives this goes up to 15-20 hp.

Therefore, 15-20 hp range is a critical range and requires a careful consideration of all the possible drives. After reviewing available data it was seen that both d.c. and a.c. drives are available which satisfy all the above mentioned requirements. A 15 hp A.C. motor drive would cost approximately £3700 and a 20 hp D.C. drive approximately

£3000. A comprehensive literature survey and a search into the hydraulics manufacturer's data showed that although almost all the requirements can be satisfied with the hydraulic systems, speed range and good disturbance behaviour still are questionable and they depend heavily on the control system. It was not possible to locate a proven hydraulic unit which satisfied all the requirements. In appendix I, the possible hydraulic systems which may satisfy the requirements are analysed. Together with their control their cost is around £2500-3000.

A comparison between A.C. and D.C. drives shows that D.C. drives are considerably cheaper than A.C. Their availability for higher powers is also an advantage. Therefore, d.c. drives are a more logical choice. However, a decision between d.c. drives and hydraulics is more difficult to reach. Hydraulic drives are cheaper, but there are doubts about their performance. Therefore, it was decided to carry out more extensive research into hydraulic drives and this is covered in chapter 7. A firm decision could then be made in the light of this investigation.

6.5 Feed Drive Selection:

Feed drive requirements as obtained from a small scale market survey can be stated as follows:

1. Four-quadrant operation

2. Continuous motor shaft torque corresponding to a linear force of 400 kg, necessary for machining

3. A stepless speed range of about 1000:1
4. High acceleration rates (5000 rad/sec^2)
5. A fast traverse speed of about 10m/min
6. Good control and disturbance behaviour
7. High resolution (about 2.5 μm)
8. An overload capacity of around 1.5
9. Acceptable noise levels

In figure 6.4, a cost versus torque comparison is carried out for servo drives, a.c. drives are not included here, because no commercial a.c. servo drives are as yet available. However, there are reports on experimental a.c. servos (92), and it is believed that in a few years time, they will become one of the major alternatives.

From fig 6.4 the following conclusions can be derived:

1. The maximum capacity stepping motor which could be found has a continuous torque rating of 7 Nm.

2. The break even point between hydraulics and d.c. motors in case of servo drives is around 7 Nm.

In the selection of servo drives, hydraulics will not be considered as an alternative, because hydraulic drives will be analysed in more detail in chapter 7 and a final decision will be reached at the end of that chapter.

When stepping motors are considered, as an alternative to d.c. drives, it is seen that motors are superior for open loop systems. However, for the more demanding requirements closed loop control is necessary and especially at about 7 Nm and above d.c. drives are cheaper and easier to control. High speeds can be a problem with stepping motors where the system loses syncronism. Therefore, for closed loop control and for torque outputs around 5-7 Nm d.c. drives are the obvious choice.

However, selecting the right motor and amplifier is not so straightforward. An increase of the slide speed can for example, be achieved by changing the motor speed, or the gear ratio, or the spindle screw pitch. If the motor speed is increased, the torque of the motor will decrease. As a result the next larger motor must be used. In this case, the increased moment of inertia of the larger motor requires in turn more energy and influences the resulting temperature rise. This and similar interactions in the change of variable and the behaviour of the overall system, make extensive interactive calculations necessary in order to find a suitable drive system for the machine (100).

The computer is an ideal tool for such applications. In the next section, an algorithm for servo drive selection is presented, which is suitable for computer applications.

6.5.1 D.C. Servo Drive Selection:

There is no known formal procedure for the optimum selection of a PM servomotor. One reason is that optimum is difficult to define. Here, optimum will be defined as the most economical choice which satisfies specifications.

Before attempting a selection a thorough analysis of the machine loading is required. Frictional loads and inertial loads have to be estimated and a loading cycle determined. For the best temperature behaviour, RMS value of this cycle should be equal or less than the continuous torque of the motor (fig. 6.5). A motor can then be selected based on the speed and torque requirements. The selected motor should be checked for its accelerator capability. For acceleration, peak torque of the motor is utilized, however, it is usually available only up to a certain speed, then it is limited to a lower value due to the commutator (fig. 6.6). Acceleration time should be calculated based on these two torque values; the following equation can be derived

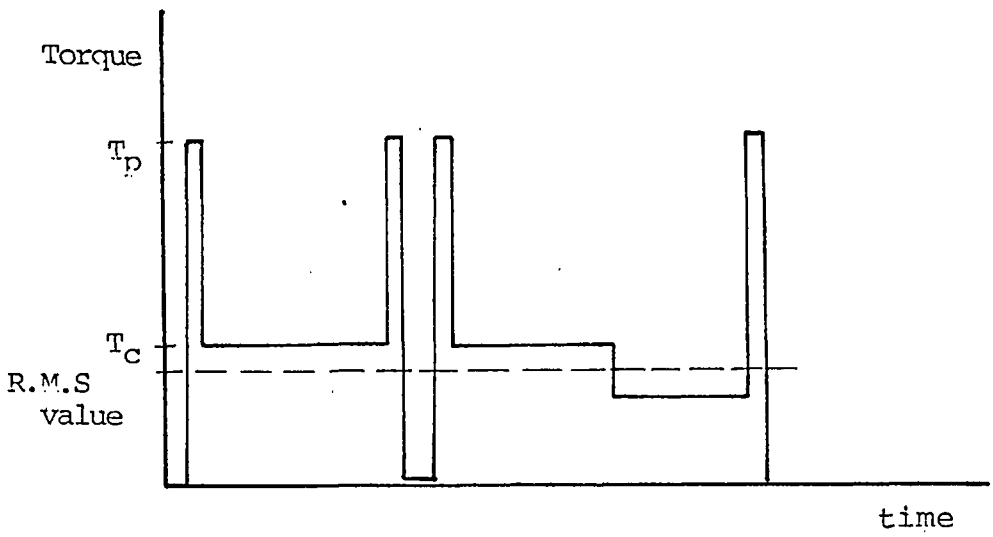

For the best temperature behaviour. $T_{rms} \leqslant T_{continuous}$

Fig 6.5 Torque cycle for a servo system

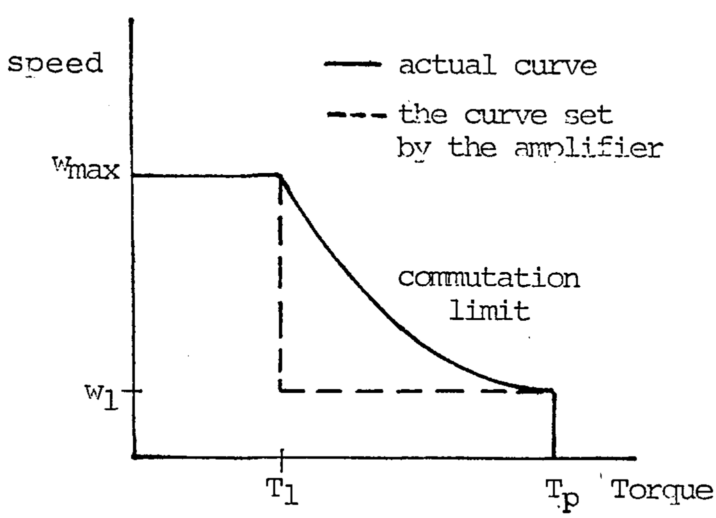

Fig 6.6 Acceleration region
for a d.c. motor

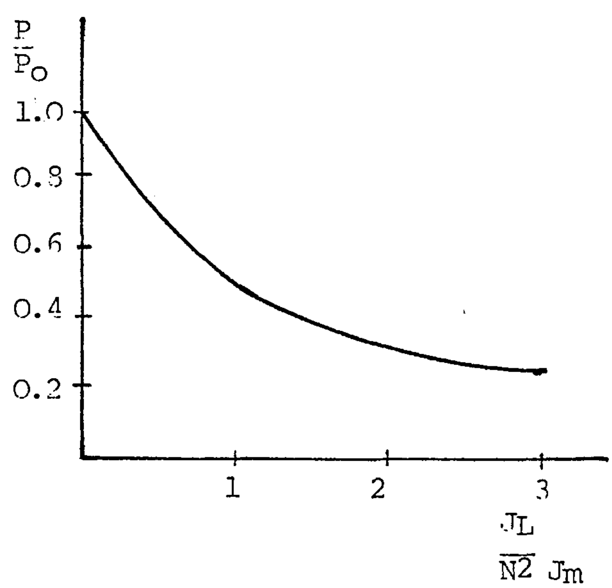

Fig 6.7 Effect of the load inertia
on the poles of the system
Po is the pole of the
motor without the load.

$$t_a = \frac{\omega_1 J}{T_{max} - T_L'} + \frac{(\omega_{max} - \omega_1) J}{T_1 - T_L'} \qquad (6.1)$$

where

$$J = Jm + \frac{J_L}{N^2}$$

J_m and J_L being the motor and load inertia and N the gear ratio, T_L' is the retarding torque. In the absence of a retarding torque, the maximum acceleration capability of a motor is achieved when the load inertia is matched to the motor inertia. However, this is only true if the same motor is used for both the matched and unmatched cases. If a larger motor is specified for the unmatched case, it may be possible to obtain a higher acceleration (102). Therefore, here inertia matching will not be taken as a criterion. The gear ratio will be selected according to the other considerations, for example, the design of the machine or the resolution, and a motor satisfying the required acceleration time will be chosen; that is, the achievement of a required acceleration is taken as the criterion.

In servo drive selection, it is also important to check the response time. For the motor, the determining factors are the electrical and mechanical time constants. Electrical time constant for a d.c. servomotor is the ratio of armature inductance to armature resistance it should be less than $\frac{1}{5}$ of the time allowed for speed changes (101),

$$\zeta_e < \frac{t_a}{5} \qquad (6.2)$$

Mechanical time constant is the time for an unloaded motor to reach 63.2% of its final velocity after applying a D.C. armature voltage. It is given as

$$\zeta_m = \frac{R\ J}{K_T\ K_E} \qquad (6.3)$$

where K_E is the voltage constant of the motor in V/rads^{-1}. For a motor the bandwidth or the break frequency is approximately the reciprocal of the time constant,

$$f_b = \frac{1}{2\pi\zeta_m}\ \text{Hz} \qquad (6.4)$$

Usually, if there is a sampling data system, the sampling rate is required to be at least two times the system bandwidth (86). This requirement relates the break frequency of the motor and load system to the sampling frequency. Then, for the amplifier, the bandwidth needs to be above the sampling frequency.

Mechanical time constant is also important as a factor that determines the dynamic behaviour of the motor and load combination. The most dominant pole can be written as,

$$p = -\frac{1}{\zeta_m} \qquad (6.5)$$

Substituting equation 6.3,

$$p = -\frac{K_T \quad K_E}{J_m \; R\left(1 + \frac{J_L}{N^2 J_m}\right)} \qquad (6.6)$$

As seen from the equation, as $\frac{J_L}{N^2 J_m}$ gets bigger, the pole comes closer to the imaginary axis, decreasing the stability of the system. The graph of $^{p}/_{p_o}$ versus $^{J_L}/_{N^2 J_m}$ can be drawn as shown in figure 6.7. From the figure it is seen that as $^{J_L}/_{N^2 J_m}$ goes above 1.5, the effect of the load becomes dominant. Then, the following relation for the ratio of the two inertias can be written,

$$\frac{J_L}{N^2 \; J_m} < 1.5$$

After the motor type is determined a suitable amplifier should be selected, based on the power and the maximum current and voltage ratings. The maximum voltage required by a motor can be written as,

$$V_{max} = RI_a + K_E \;\; \omega \qquad (6.7)$$

I_a is the armature current and can be calculated as,

$$\left(J_m + \frac{J_L}{N^2}\right) N \frac{d\omega}{dt} + T_L' = K_T \; I_a \qquad (6.8)$$

R is the armature resistance, K_e and K_T are the speed and torque coefficients of the motor respectively.

Two flow charts for motor and amplifier selection are given in figures 6.8 and 6.9 respectively. However,

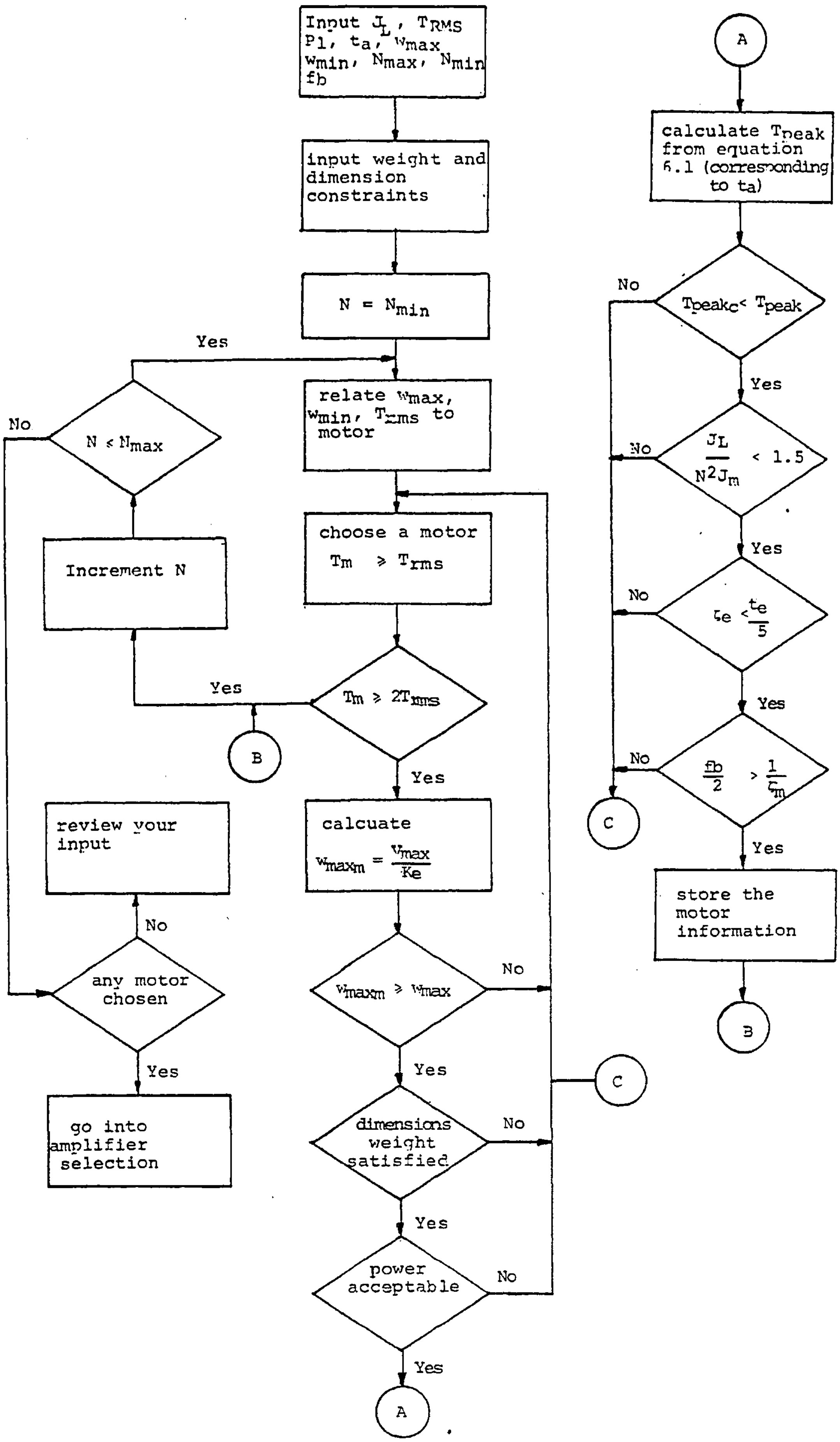

Figure 6.8 Flow chart for Servo motor selection

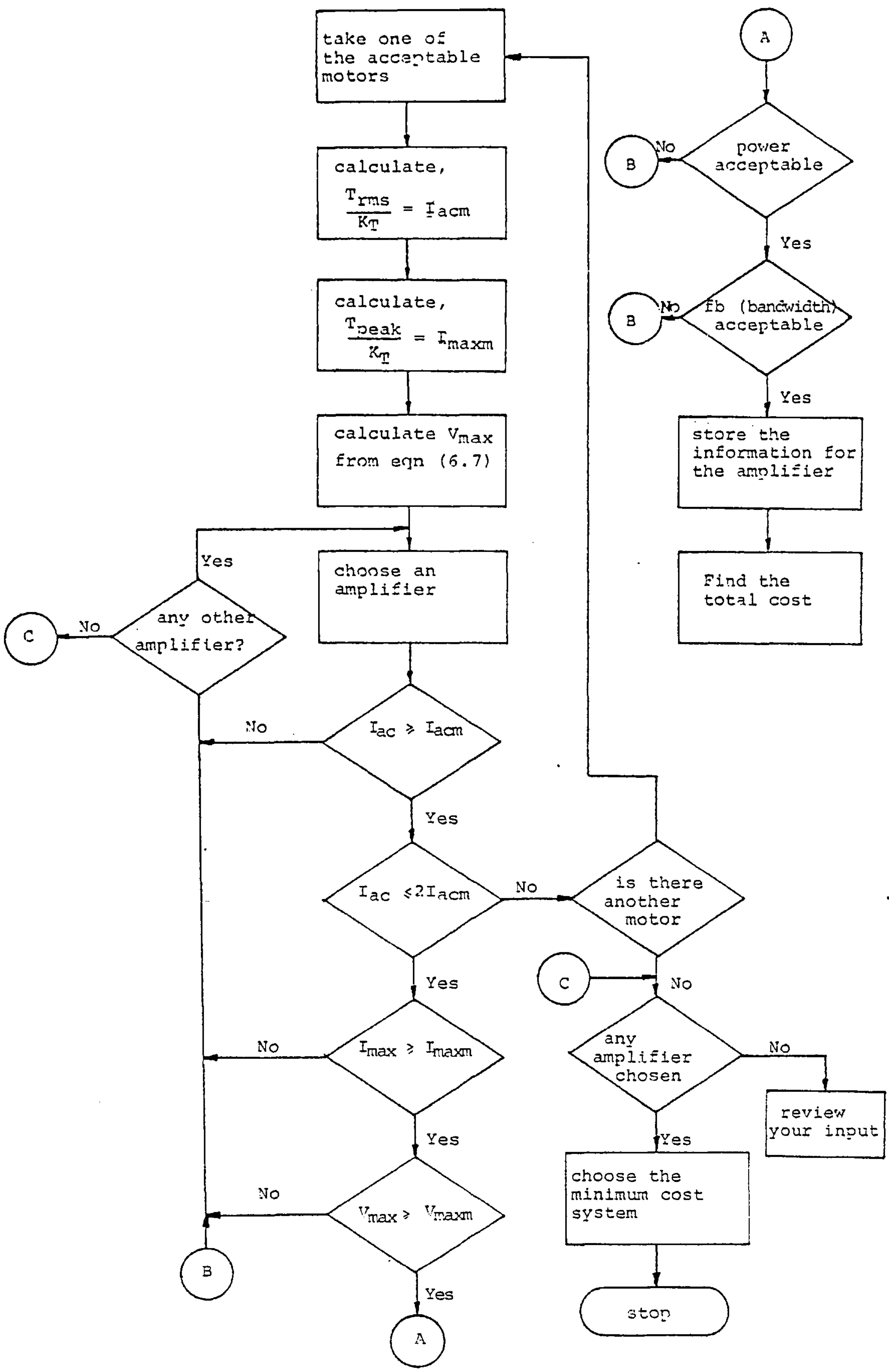

Figure 6.9 A flow chart for the amplifier selection

for a complete servo drive selection, it is also necessary to choose the type of feedback device and the type of controller.

Feedback devices can be classified broadly into two groups; linear and rotary. They are also classified according to the form of output as analogue and digital. Linear devices give the position free from mechanical errors, so they make more accurate positioning possible. However, they are more expensive than the rotary ones. When it comes to the form of output, digital transducers (linear and rotary encoders) are more expensive than analogue ones (inductosyns and resolvers), however, digital transducers are more suited for microprocessor application. Analog transducers need some interfacing equipment which takes the price of the overall system very near to that of digital devices.

Determining the control type for a servo drive system is even more involved. A block diagram approach for the overall system should be carried out and the stability and response should be analysed based on the model. In fig. 6.10 a general block diagram for a position control system is given. It is assumed that for velocity and displacement measurements a tachometer and a linear transducer are being used respectively. For different feedback devices the feedback parameter will change. Based on this model, it is possible to analyse the system stability and response with respect to the system parameters.

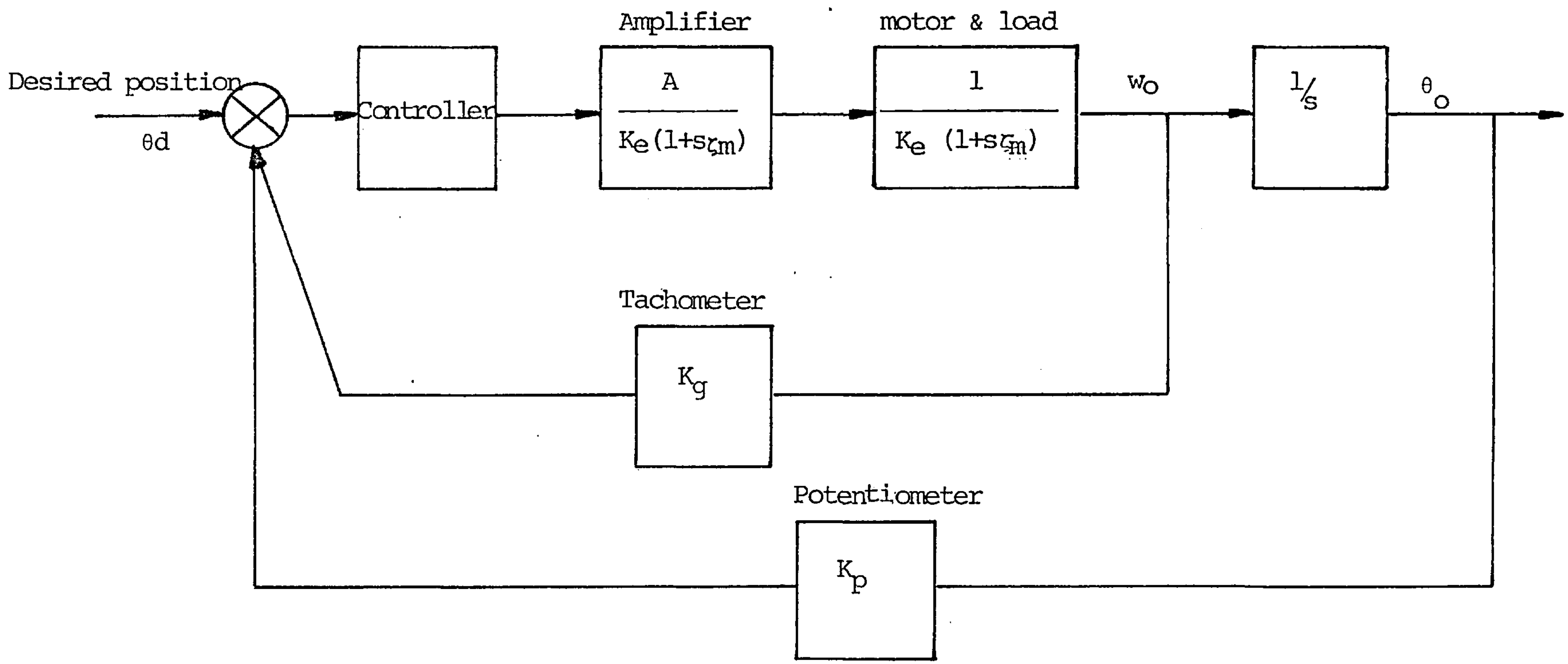

Figure 6.10 - Position Control System

Above, a general method for servo drive selection and analysis is described. A machine tool designer should follow the same steps for a good servo system, however first it is necessary to determine the parameters required for servo drive selection. In fig. 6.11, the steps a machine tool designer should follow are given in a summary form.

The above suggested servo drive selection method is applied to an example in appendix H.

6.6 Discussion:

In this chapter, the alternative feed and spindle drives for machine tools have been analysed. Hydraulic drives although promising were found to have some possible disadvantages, in their performance and their maintenance requirements. Therefore, they have been analysed further as described in Chapter 7. However, it is very important to note the rapid advance in a.c. drives. It is felt by most of the machine tool manufacturers that once they are widely on the market they may well supersede d.c. drives (82).

Also in this chapter, a detailed servo drive selection routine for d.c. systems has been given. If a data bank for the servo motors and their drives is formed, the routine can be computerized and used for optimum selection of servo drives.

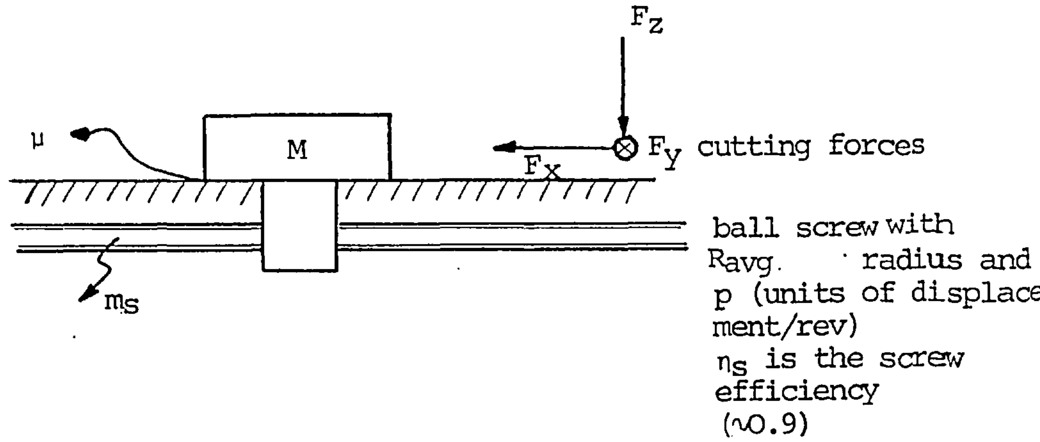

1. Choose a suitable ball screw
2. Calculate $J_L = \frac{1}{2}\, m_s\, R^2{}_{ave} + \dfrac{Mp^2}{(2\pi)^2}$ (load inertia)
3. Calculate T_L (continuous torque) and determine the speed at which that T_L is required (ω_L)

   $$F_a = (M*g + F_z + F_y).\mu + F_x$$

   $$T_L = \frac{F_a.\ P}{2\pi.\eta_s}$$

4. Determine the power required.
5. Find the acceleration requirements (t_a, n_{max}). Determine the value of the retarding torque.
6. Determine RMS value of the torque from a torque cycle curve.
7. Check if there is any weight or dimension constraint.
8. Check the bandwidth requirement (fb). For example, if adaptive control of feedrate is being employed, high bandwidths might be necessary.
9. Determine the acceptable gear ratios (N_{min}, N_{max})
10. Determine the minimum and maximum rotational speeds (ω_{min} and ω_{max})
11. Go to fig. 6.8 and 6.9.
12. Check the feedback device required.
13. Do an overall control analysis (fig 6.10)

Fig 6.11 Steps to follow for a Machine Tool Servo Drive Engineer

CHAPTER 7

HYDRAULIC SYSTEMS AND THEIR CONTROL

7.1 Introduction:

The analysis of drive systems in the previous chapter indicated that hydraulic systems may provide a feasible alternative for machine tools. However, in order to reach a firm conclusion on the technical viability of hydraulic drives, a detailed analysis of a practical hydraulic system is necessary with particular emphasis being given to the control of such a system using a microcomputer . The objective is to obtain a controllable hydraulic system, which can meet the performance specifications of the machine tool, at a low capital cost.

Speed control systems for hydrostatic systems are well established (108). However, the use of digital electronics in hydraulic control systems is relatively new and in particular the use of microprocessor technology has not been extensively tried in this application. Microcomputers through their ability to perform complex computations quickly, make the implementation of sophisticated control algorithms possible. They have also triggered the development of digital electro-hydraulic servo valves (111). These valves use stepper motors to control the spool motion in the valve which in turn controls the fluid flow.

Possible hydraulic systems, together with appropriate microcomputer controllers are presented in this chapter and their application to machine tools is discussed. A description of an experimental rig for testing rotary hydraulic drive systems with microcomputer control is given along with a theoretical analysis. Particular emphasis is given to the analysis of speed control under varying operating conditions.

7.2 Possible Hydraulic Circuits

The positive displacement hydraulic drives can be divided into four main groups:

1. Valve controlled drive
2. Pump displacement controlled drive
3. Motor displacement controlled drive
4. Pump and motor controlled drive

1. Valve Controlled Drive:

A valve placed between a hydraulic pump and a hydraulic motor acts as a dissipative element and modulates fluid flow to the motor and the pressure drop across it, and hence the output power. In its simplest form a four-way valve is supplied with fluid at constant pressure by a fixed displacement pump and a relief valve as shown in fig. 7.1.a. For such a system, the maximum ideal efficiency disregarding relief valve and the efficiencies of pump and motor, is 66 per cent, because the maximum available output

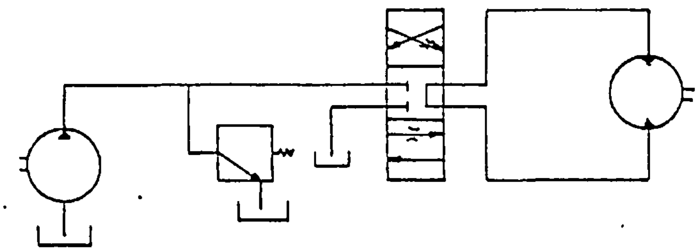

a) Fixed displacement pump with a four way servo valve

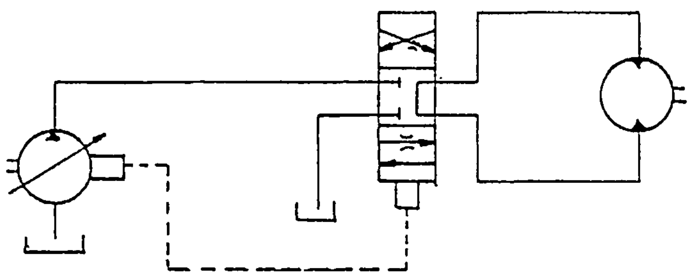

b) Pressure flow compensated pump with a four way servo valve

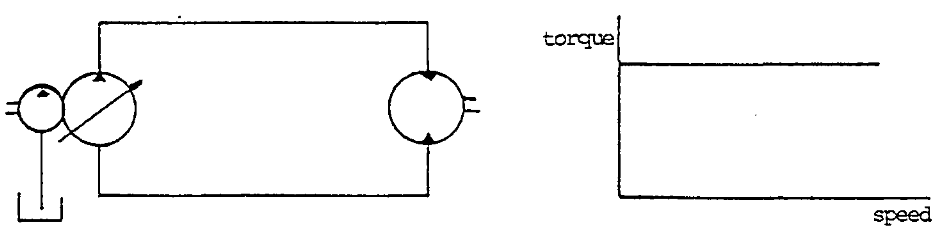

c) Pump controlled circuit

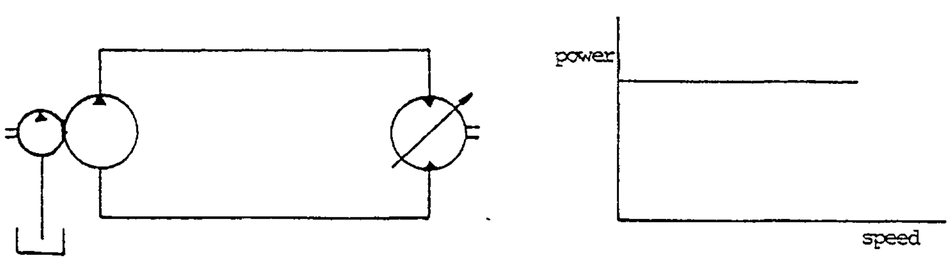

d) Motor controlled circuit

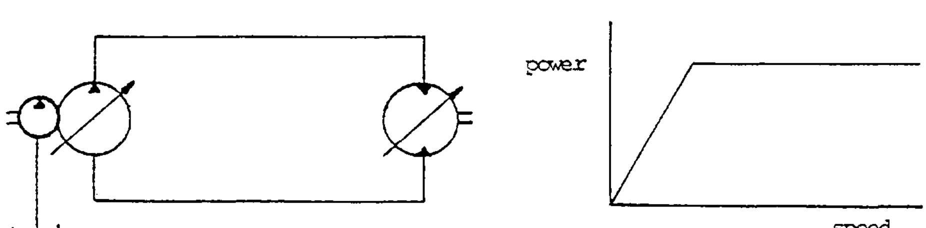

e) Pump and motor controlled circuit

Fig 7.1 The possible hydraulic circuits and their output characteristics for constant pressure power corresponds to a pressure drop across the motor of two thirds of the supply pressure. This low efficiency is very much detrimental to the overall circuit, because it increases the temperature rise considerably. However, efficiency can be improved by using a pressure-flow compensated pump as shown in figure 7.1.b.

2. Pump Displacement Controlled Drive:

A variable displacement hydraulic pump can be used to control the flow to a hydraulic motor, and the motor can be reversed by changing the direction of pump delivery or by a reversing valve between pump and motor (fig. 7.1.c). The maximum motor speed will depend on the ratio of maximum pump displacement to motor displacement, and the minimum smooth running speed of the hydraulic motor will depend on the combined inertia of the motor and load. In such systems efficiency is higher than valve controlled systems and if the maximum system pressure is limited, the ideal maximum torque is constant throughout the speed range.

3. Motor Displacement Controlled Drive:

If the displacement per revolution of a hydraulic motor is varied, then for a constant flow, the speed of the motor must vary inversely with motor displacement (fig. 7.1.d). If system pressure is limited then the output horsepower is ideally constant throughout the speed range. The available speed range will depend on the ratio of maximum to minimum motor displacement and will be limited, in a real system, by considerations of efficiency, to a typical value of 6:1 or 8:1 (104). The motor can not be reversed without stopping the pump.

4. Pump and Motor Controlled Drive:

This system is a combination of the two types previously described. The first part of the speed range is obtained by increasing pump displacement at maximum motor displacement and thereafter speed is increased by reducing motor displacement. The available speed range is then equal to the speed range under pump control multiplied by the speed range under motor control. The circuit and its output characteristics are shown in fig. 7.1.e.

From the above discussion, it is seen that because of its output characteristics and higher speed range combined pump and motor controlled drives are the best suited for the application of machine tool spindle drives. However, their control will be more complicated and also they will be more costly than a pump controlled drive. Therefore, it was decided initially, to perform the microprocessor control experiments on a pump controlled drive. The methods developed could then be extended to pump and motor controlled drives if the purely pump controlled system proved unsatisfactory. If the feed drives are to be hydraulic as well, then the simplest and the most economical solution is to use one pressure-flow compensated pump with a separate servo valve for each axis. There are basically two types of servo valves, the expensive and highly accurate valves for robot or machine tool applications, and less accurate but cheaper ones for agricultural and similar industrial use. The price ratio between these two types can be around ten. Therefore, if it were possible to use the latter type of valves overcoming their shortcomings with microprocessor control then substantial savings could be achieved. For this reason, two types of the less sophisticated valves were subjected to an experimental investigation and their possible use in microprocessor controlled hydraulic circuits analysed.

One problem with the design of hydraulic systems is the complexity of and variation in possible layouts. If the systems' performance can be modelled theoretically, then various circuit designs can be analysed and their performance assessed without the need for elaborate and extensive experimentation. In this chapter, theoretical analysis of hydraulic systems are presented and their accuracy compared with the subsequent experimentation.

7.3 Theoretical Analysis:

In order to design a hydraulic system, there are three major areas that must be considered.

a) Efficiency and temperature calculations (static simulation)

b) Dynamic simulation of the hydraulics

c) Control system simulation.

In the following sections, these subjects will be analysed in detail.

7.3.1 Static Simulation:

The efficiency of a hydraulic system depends mainly on the efficiencies of the pumps and motors used in the system. Circuit efficiency can be found by estimating the pressure drops in the circuit and once the pump and the motor efficiency is known, the overall efficiency can easily be calculated. The detailed efficiency curves are usually given in the pump and motor catalogues. However, they are usually given for only two or three specific test conditions (pressure values), so it is necessary to find a method of calculating the efficiency for any oil temperature, viscosity and at any flow rate or pressure drop. The following equations can be used for this purpose (105), the volumetric efficiency of a pump

$$\eta_{up} = 1 - C_s \frac{\Delta P}{\mu N * r} \qquad (7\text{-}1)$$

and of a motor,

$$\eta_{um} = \frac{1}{1 + C_s \frac{\Delta p}{\mu N}} \qquad (7\text{-}2)$$

the mechanical efficiency of a pump,

$$\eta_{mp} = \frac{1}{1+C_d \frac{\mu N^* r}{\Delta p} + C_f + \frac{T_c}{\Delta p D p}} \qquad (7-3)$$

and of a motor,

$$\eta_{mm} = 1 - C_d \frac{\mu N}{\Delta p} - C_f - \frac{T_c}{\Delta p . D_m} \qquad (7-4)$$

where,

C_s = the slip coefficient of the pump or the motor

C_d = the drag coefficient of the pump or the motor

C_f = torque coefficient of the pump or the motor

ΔP = pressure rise across the pump or the motor

μ = viscosity of the oil

N = the speed of the pump or the motor

T_c = break away torque of the pump or the motor

r = the fractional displacement for variable displacement pumps (r is between 1 and 0)

Using the above equations and the manufacturers efficiency values, it is possible to evaluate the constants C_s, C_d, C_f and T_c for a particular motor or pump. It is then possible to calculate the efficiency values for any arbitrary set of parameters.

The steady state temperature difference can also be found theoretically by using the following equation (114),

$$\Delta T = EL/\Sigma k.A \qquad (7-5)$$

where,

k is the overall heat transfer coefficient

A is the heat dissipating area

and EL is the total energy loss in the system, it can be written as,

$$EL = Q.P. (1-\eta)/\eta_p$$

where,

Q is the flow rate,

P is the pump gauge pressure

η and η_p are the system and pump efficiencies respectively.

For more complex systems however, temperature can be different at different points of the circuit. In such cases, a more detailed heat transfer analysis is necessary. A computer program using more detailed energy equations for each component of the circuit was written and is described in appendix K.

7.3.2 Dynamic Simulation:

There are several methods of dynamic simulation. One of them is the state variable approach using one or two port elements (115). This method is very general and can be applied to any dynamic system. For hydraulic systems, it is possible to carry out a simpler analysis. However, even in this analysis, when the external leakage of the motor and the pump is considered or when the friction torque of the motor is taken into account, the resulting equations become non-linear and difficult to solve (105), (115). Therefore, in the analysis adopted here, some simplifying assumptions were made leading to a more manageable solution. The assumptions can be stated as follows:

1. The total leakage of the pump or the motor is assumed to be proportional to the pressure drop across them. It is also assumed that cavitation does not exist so that the pump and motor displace only the liquid working fluid.

2. The coefficients related to the performance of the pump and the motor as mentioned in section 7.4.1, are assumed to be constant throughout the operating pressures and flow rates.

In the analysis, the objective is to find the transfer function between the input (swash plate angle or the spool displacement) and the output (actuator speed). The details of the analysis is left to appendix J. The transfer functions obtained for the two types of circuits are shown in figure 7.2.

7.3.3 Control System Simulation:

Once the model for the hydraulic circuit is ready, the model for the overall microprocessor control circuit becomes easier to prepare. A block diagram approach is shown in fig. 7.3. In this diagram, proportional

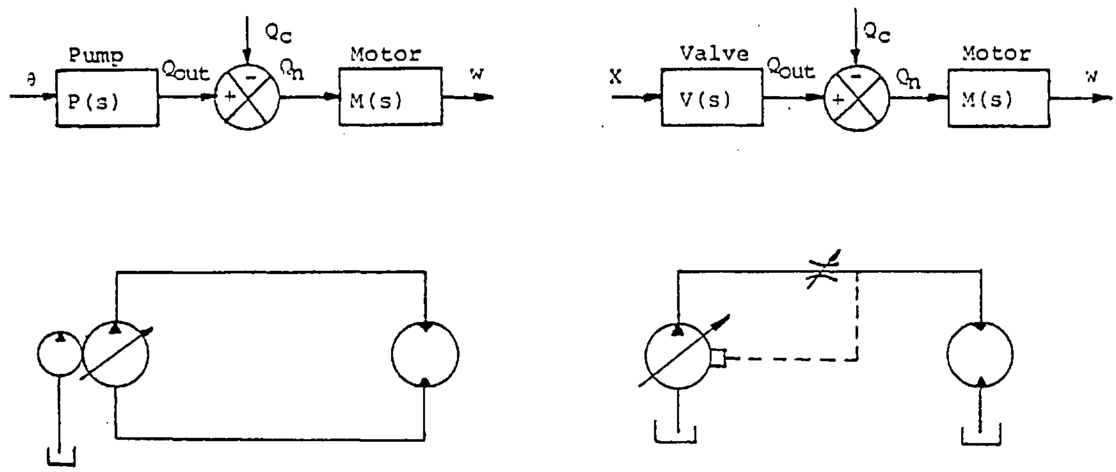

$$W = \frac{K\theta - T_L\,(\xi_4\, s + \xi_5)}{\xi_1\, s^2 + \xi_2\, s + \xi_3}$$

$$W = \frac{e^{-\zeta s}\, C'_d\, K_s \frac{\sqrt{2\Delta P v}}{\rho}\, X - T_L(\eta_4 s + \eta_5)}{\eta_1\, s^2 + \eta_2\, s + \eta_3}$$

a) Closed circuit

b) Valve control

Fig 7.2 Transfer functions and block diagrams for two kinds of hydraulic circuits

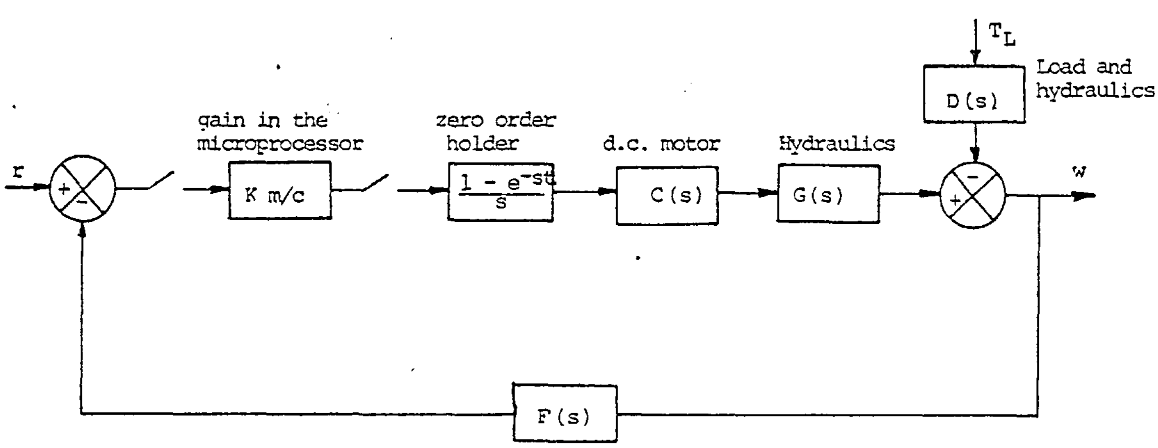

feedback gain
(tachometer or resolver)

Figure 7.3 Block diagram for the overall microprocessor control system control was assumed, however it can be extended for more complicated control schemes.

From the block diagram, the overall transfer function can easily be evaluated. Because it is a discrete system, z-transform instead of s-transform should be used. Then the equation can be written as,

$$T(z) = \frac{G'(z).M(z).Km/c}{1 + Km/c.F(z).G'(z).M(z)} \qquad (7.6)$$

where G'(z) is the z transform of,

$$G'(s) = G(s)* \frac{1-e^{-sT}}{s}$$

For an open loop system with a value,

$$M(s) = \frac{k_1 \cdot p}{2\pi . s} \qquad (7.7)$$

where,

p is the pitch of the screw that converts the rotary motion into linear, and k_1 is the gain of the motor in rpm/voltage. Equation (7-6) gives an equation in the following form,

$$T_z = \frac{Km/c\ (A_1z^3+A_2z^2+A_3z+A_4)}{-z^n(B_1z^3+B_2z^2+B_3z+B_4)+Km/c.K''(A_1z^3+A_2z^2+A_3z+A_4)} \qquad (7-8)$$

where n is a parameter that relates the response time of the pump to the sampling time.

A computer program for a valve controlled system was prepared. In the program, the coefficients A_1 to A_4

and B_1 to B_4 are calculated. Then, using the Routh-Hurwitz criteria the stability of the system is checked and also the open loop and closed loop poles are evaluated. The programming procedure is very much straightforward, so no flow chart will be given.

7.4 Experimentation:

Theoretical analysis outlined in the previous section can be used to design a hydraulic circuit without the need of extensive experimentation. However, the validity of the theoretical analysis should be proven first, and therefore it is necessary to perform some experiments. Furthermore, as explained earlier the possibility of using unsophisticated values in machine tool hydraulics should be thoroughly investigated.

The experiments performed can be divided into two main sections.

1. An investigation into the use of cheaper valves, for hydraulic systems in machine tools.

2. Microprocessor control of a hydraulic spindle drive.

The selection of the optimum components for the machine tool's spindle drive is carried out in appendix I. However, because of time and cost constraints it was not possible to use these ideal components in the experiments.

The combination of theoretical and experimental analysis should allow extrapolation of the results to these components.

7.4.1 Experiments with the Servo Valves

Two valves with a typical price range of around £100 were investigated, the results are given below.

A. Digital servo valve

The first valve to be tested was a two way experimental servo valve with stepping motor control. Such valves have a lot of advantages because stepping motors or d.c. motors used in these valves can give high torques so they can eliminate the necessity for a pilot pressure system which is unavoidable for valves with solenoid actuators. Also, with good design and good selection of the actuator system, they can improve the accuracy and the response of the overall drive.

The diagram of the circuit, used to test the valve is shown in fig. 7.4. Efficiency and temperature evaluations for the overall system were carried out and thespeed range which can be controlled with the valve was determined.

Static characteristics of the valve are shown in fig. 7.5. The screw thread which connects the spool to the stepping motor has 20 threads/in, and a gearbox with a ratio of 20:1 is employed. Therefore, 40 revolutions on the motor is necessary to move the spool 2.54 mm which is the

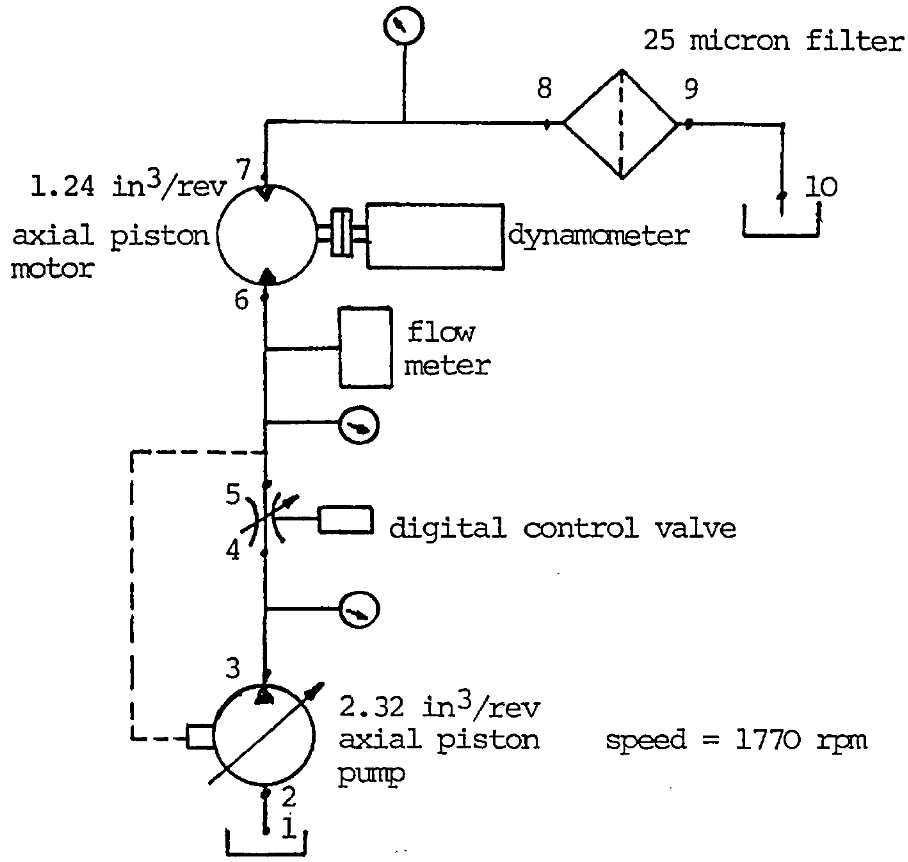

Figure 7.4 The experimental set-up for the digital servo valve

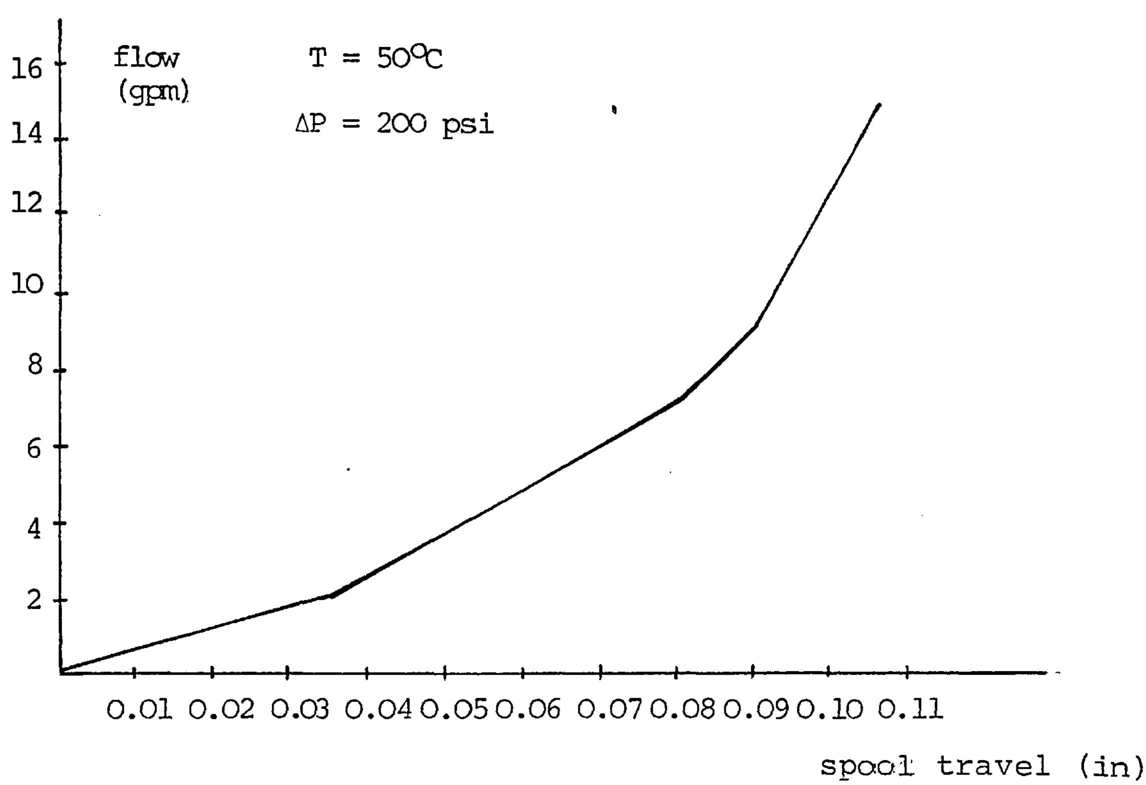

Fig 7.5 Characteristics of the digital servo valve

required movement for the full flow. The experiments showed that the torque required at the motor is about $4*10^{-2}$ Nm. Assuming 1000 rpm speed at the motor, the response time can be calculated to be 2.4 secs. The response time can be improved by having a higher speed at the motor.

In the experiments, the flow rate in the circuit and the pressure values at the points indicated in fig. 7.4, as well as the power at the dynamometer, the power input to the electric motor, leakage of the pump and the motor and the noise level of the system were measured. The electric motor efficiency was measured and found to be 0.85. Using the measured results, it is straightforward to calculate the efficiencies at the pump, motor and the overall system. The measurements and the results are tabulated in table 7.1a and 7.1b respectively.

The temperature characteristics of the circuit were determined by measuring the temperature at several locations on the hydraulic circuit. Figure 7.6 shows the temperature versus time curves for several pressure and flow values. As it is seen, at a pressure of 700 psi and a flow rate of 10 gpm temperature tends to stabilize around 70^{o}C. However, at higher pressures the temperature might exceed 70^{o}C, so a heat exchanger will be necessary.

Finally, the hydraulic circuit was tested to find the minimum operational speed of the hydraulic motor. The minimum stable speed was obtained around 100 rpm. Maximum

Table 7.1.a Measured Parameters on the Hydraulic Circuit

No	Flow rate (gpm)	p1 pump (psi)	p2 motor (psi)	power at dyno (kW)	power input to e.m. (kW)	speed motor (rpm)	noise at motor (dBA)	noise at pump (dBA)
1	2.5	200	120	-	2.16	600	97	162
2	2.8	300	200	0.15	3.14	617	98	103
3	2.8	650	450	0.48	2.99	617	97	102
4	2.8	750	600	0.75	3.48	617	99	104
5	5.0	250	150	-	2.99	1160	100	104
6	5.1	400	300	0.50	3.59	1160	99	103
7	5.3	775	600	1.34	4.92	1160	101	105
8	5.4	1100	950	2.18	6.35	1180	101	106
9	7.5	370	240	-	3.60	1523	110	107
10	7.65	400	250	-	4.20	1600	106	107
11	7.7	700	550	1.43	5.40	1600	106	109
12	7.9	1050	900	2.92	7.31	1610	109	110
13	10.0	450	300	-	5.76	2150	108	111
14	10.5	700	540	2.07	7.43	2150	111	111
15	12.6	425	240	-	6.11	2530	108	111
16	16.0	400	240	-	6.71	3180	110	112

1 psi = 6900 N/m^2 (Pa)

1 gpm = $7.585*10^{-5}$ m^3/sec

Table 7.1.b Calculated efficiencies for the Hydraulic Circuit

No	Flow rate (gpm)	pressure pump (psi)	η pump %	η motor %	η circuit %	η total %
1	2.5	200	14.2%	-	60%	-
2	2.8	300	21.9%	52.3%	65%	7.5%
3	2.8	650	37%	73.0%	69%	19.0%
4	2.8	750	37%	85.7%	79.6%	25.3%
5	5.0	250	25.4%	-	59.8%	-
6	5.1	400	34.9%	62.8%	74.8%	16.4%
7	5.3	775	57.2%	80.7%	77.4%	32%
8	5.4	1100	57.2%	81.7%	86.3%	40.4%
9	7.5	370	42.8%	-	65%	-
10	7.65	400	40.7%	-	67.5%	-
11	7.7	700	61.4%	65.0%	78.5%	31.2%
12	7.9	1050	69.8%	79.0%	86%	47%
13	10.0	450	48.0%	-	66.6%	-
14	10.5	700	60.7%	70.1%	77.1%	32.8%
15	12.6	425	53.7%	-	56.5%	-
16	16.0	400	58.6%	-	60.0%	-

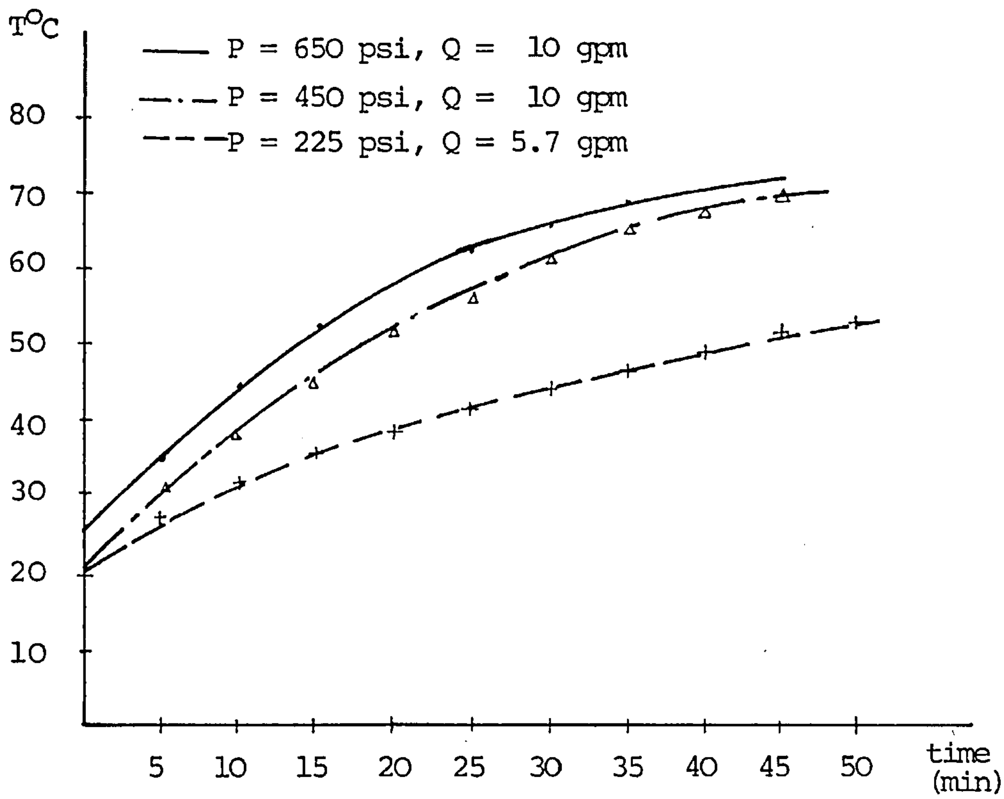

Fig 7.6 Temperature behaviour of the hydraulic circuit

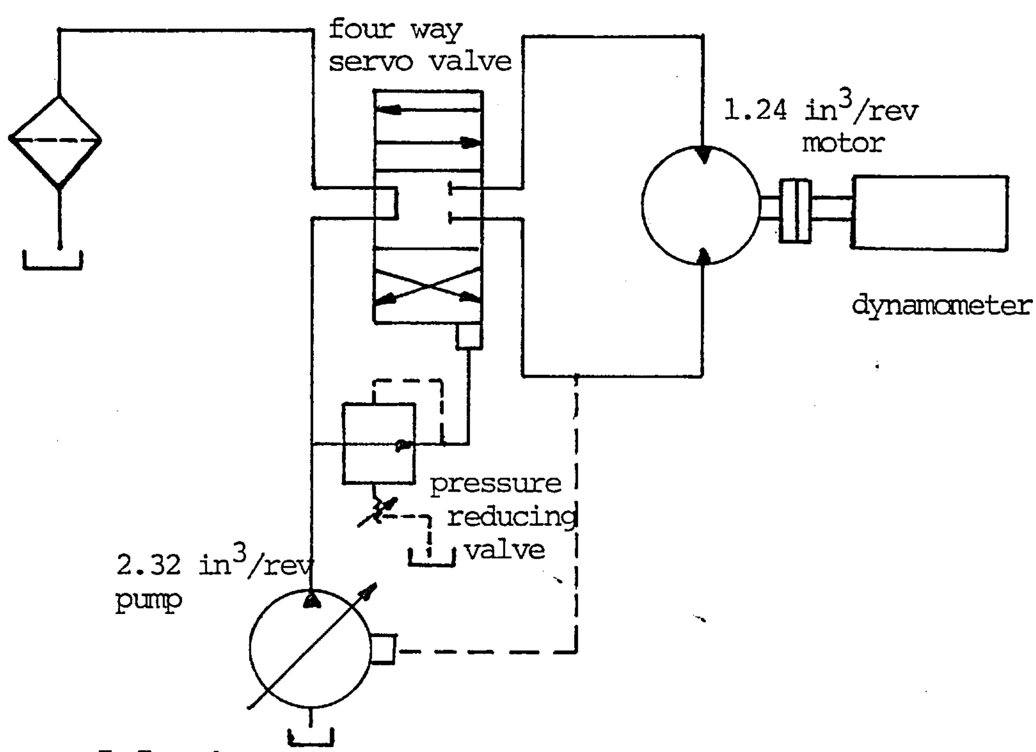

Figure 7.7 The experimental set up for the four-way servo valve

speed of the motor was 3000 rpm which gave an overall speed range of 30:1.

B. The four way servo valve:

The four way valve tested has a pilot stage which is operated by a linear force motor. In the catalogue, it is specified that the valve can give 10 gpm at 1000 psi pressure drop. Although the flow capacity is less than that required for the machine tool application, it was thought that this valve could be used to obtain information about this type of valves.

The main problem with the valve was the large amount of hysteresis. The effect of a dither voltage was investigated in an attempt to reduce hysteresis to a level which could be compensated for in a microprocessor controlled hydraulic system.

As a first step an electronic control unit to obtain a dither voltage at different waveforms and frequencies was constructed. The pilot pressure required for the valve is around 200 psi. An experimental set-up with the relevant pressure reducing valve was constructed. It is shown in figure 7.7.

In the experiments the voltage level was taken to 12 Volts and back to zero again in steps of one volt and the speed recorded at each step. This procedure was repeated for several waveforms, amplitudes and frequencies of dither. The results obtained are shown in figures 7.8, a, b, c and d. The hysteresis for each case is tabulated in table 7.2. In the experiments, it was observed that temperature was also an important factor in the level of hysteresis. For this reason, experiments at different temperatures were also performed. Two sets of experiments with sinusoidal dither voltage were carried out at 25°C. The results are tabulated in the first two columns of table 7.2. It is seen that as the oil temperature gets higher, hysteresis becomes more important. However, in general the results are in the range of 3 to 4%, which would make compensation possible.

7.4.2 Microprocessor Controlled Hydraulic Circuit:

As a check in the validity of the theoretical analysis and to gain experience with microprocessor control, it was necessary to build an experimental set up. For this purpose, the a.c. induction motor of a Colchester lathe was replaced by a hydraulic system. Only the spindle drive was hydraulic, so a closed loop circuit as shown in fig. 7.1 a) was adopted. It comprises of a fixed displacement 40 cc per rev axial piston motor and a 20 cc per rev variable swash plate piston pump. The latter is driven by a 4.5 kW induction motor.

The task was to prepare a microprocessor control with fast settling time and speed stability under varying loading and

Table 7.2 Hysteresis on the four way servo valve

V	sinosoidal ± 1.2V 50 Hz 25°C	sinosoidal ± 42V 50 Hz 55°C	sinosoidal ± 3V 50 Hz 60°C	triangular ± 1.2V 50 Hz 40°C	square ± 1.2V 50 Hz 50°C	No dither 50°C
1	21%	21%	40%	15%	21%	12.6%
2	8%	2.3%	3.1%	1.4%	2.6%	4.2%
3	1.1%	7.5%	4.9%	2.1%	10%	10%
4	0.7%	6.2%	2.9%	8.7%	2.8%	0%
5	0%	4%	1.1%	8.3%	3.1%	7.4 %
6	0.96%	6.4%	4.1%	7.9%	2.3%	4.2%
7	0.6%	3.4%	2.3%	5.5%	2.5%	2.2%
8	0.5%	2.5%	2.7%	2.9%	2.9%	2.4%
9	0.3%	1.4%	3.8%	2.6%	2.2%	0.6%
10	0%	1.4%	2.6%	0.8%	2.3%	0.3%
11	0.2%	1.8%	2%	0.9%	0.2%	0.4%

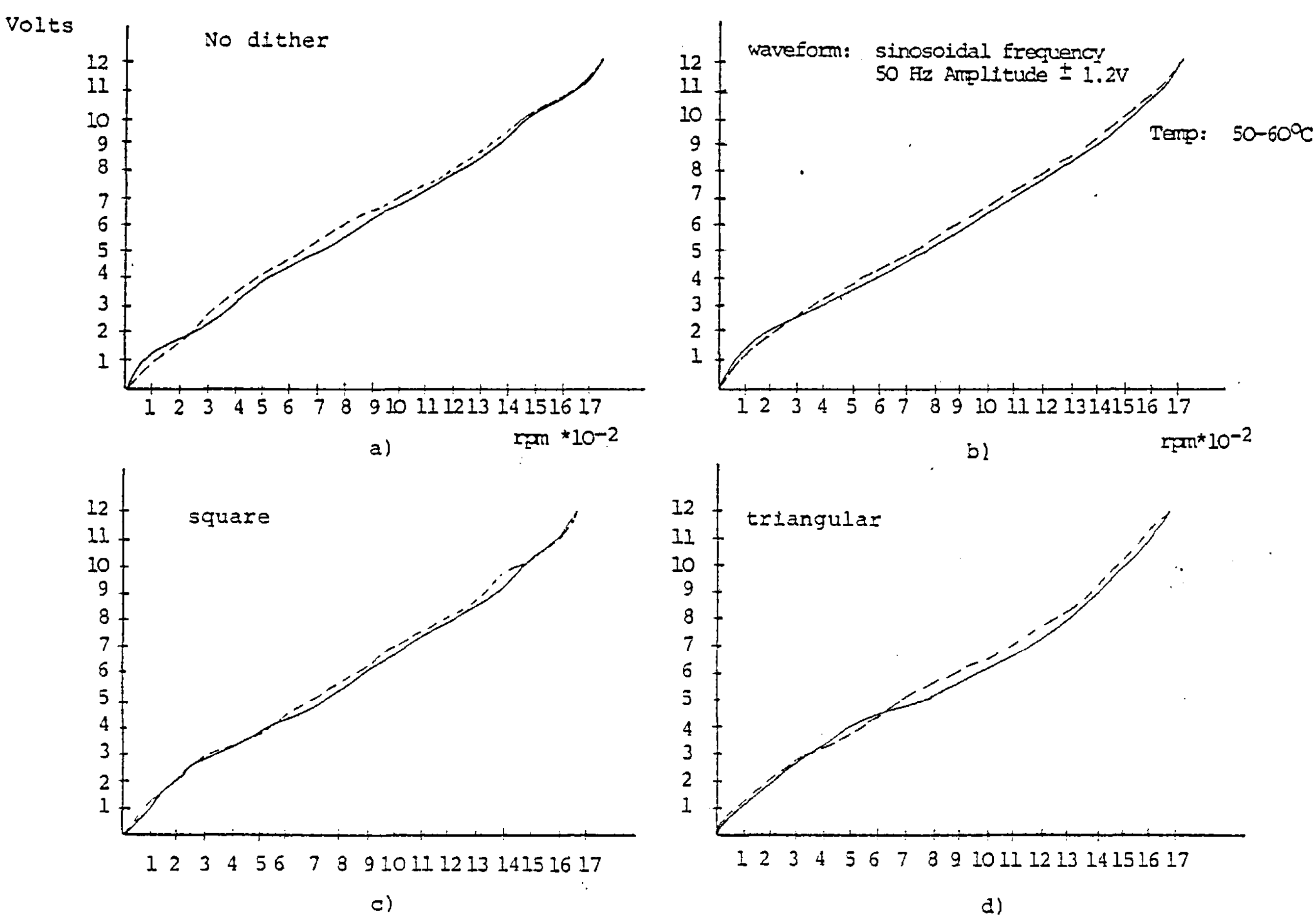

Figure 7.8 Speed versus voltage graphs for the servo valve

temperature conditions. This controller was part of a distributed processing system which controls the X and Y axis of the lathe (19). A schematic layout of the spindle controller is given in figure 7.9. An optical encoder with a resolution of 1000 pulses per revolution was fitted to the spindle. This feeds pulses to the controller where they are used to assess the current speed. If a speed correction is required due to a change in demand or in load torque then a d.c. motor is actuated. This motor is connected via a reduction gear-box to the swash plate of the hydraulic pump. The demand speed is fed to the controller via the IEEE-488 bus.

The controller is based on a Motorola. 6802 MPU which incorporates a 128*8 bit random access memory (RAM). The controller card also requires a 2k byte Erasable Programmable Read Only Memory (EPROM), an interface adaptor (GPIB) for the IEEE-488 bus, four quad transceivers interfacing to the IEEE bus, a programmable timer chip consisting of three independent timers and a peripheral Interface Adaptor (PIA).

In the controller a sample data scheme is used, driven under interrupts with a sampling period of approximately 10 msecs. Optical encoder pulses arriving during this period are counted by the timer module and hence given a value proportional to the spindle speed. This value is compared with the currently demanded speed and an error is found.

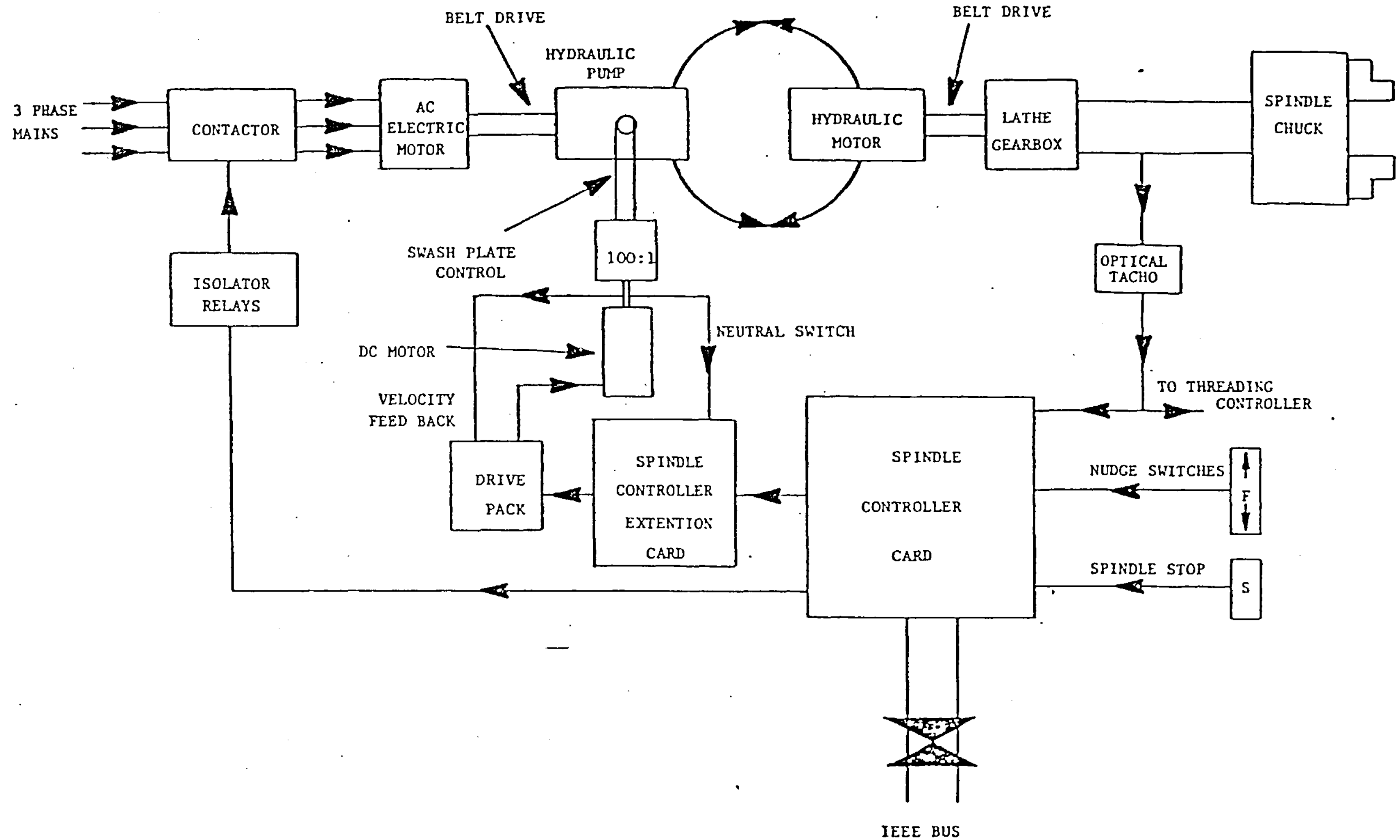

Figure 7.9 Spindle Controller

The error is then output to DAC; the DAC accepts the offset binary number and outputs a voltage to the d.c. motor drive in the range -4 to +4 volts, which in turn adjusts the speed of the swash plate actuator motor.

The speed range of the system is dependent on the size of the pump and the motor used. The present experimental system has a range of approximately $\pm$ 1400 revs/min. The minimum stable speed obtained using a simple proportional control was 30 revs/min, representing a dynamic speed range of about 45:1. The transient response of the system was measured and it was found that settling time to within 5% of demand was approximately 0.9 secs. The response to a step input is shown in figure 7.10. The closed loop steady state accuracy was measured over the full speed range and was found to be accurate to within 1% for speeds above 200 revs/min. Below 200 revs/min the error gradually increased to about 4%. This increase results mainly from the resolution of the optical encoder being too coarse at low speeds. If greater accuracy were required a finer pitch encoder would be used.

7.5 Analysis of the Results and Theoretical Comparison:

In the previous section, the experiments performed were described and the results were presented. In this section, the results will be analysed and the theory checked against the experimental results.

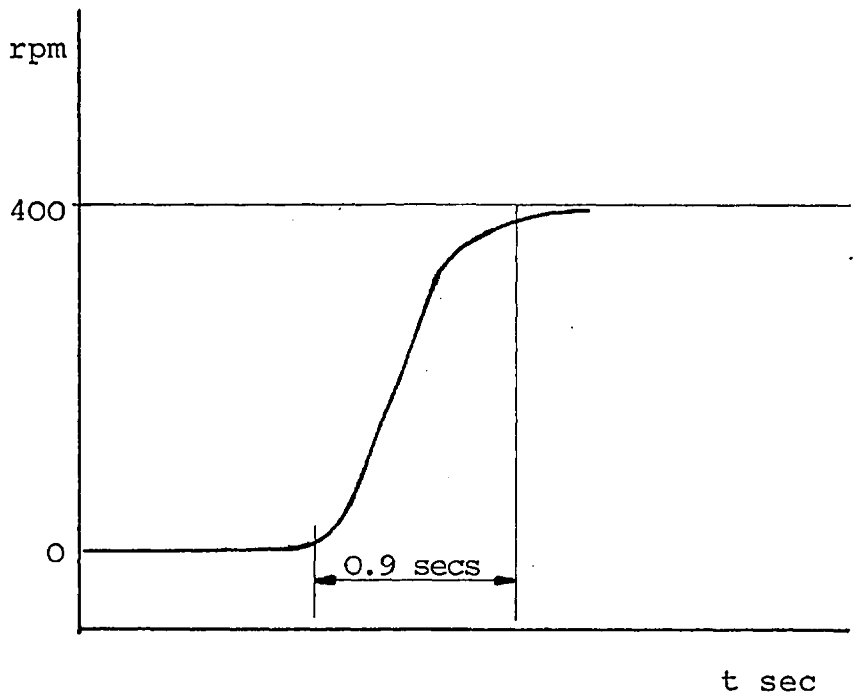

Figure 7.10 Experimental step response

7.5.1 Digital Servo Valve

The results given in table 7.1b, show surprisingly low pump efficiencies and in turn low overall efficiencies. To check the validity of these results, the first step was to perform an error analysis. The following errors in the readings are assumed:

w_1	(load measurement on the dynomometer)	= 0.0625 lb
w_2	(speed measurement)	= 5 rpm
w_3	(input power measurement)	= 5 W
w_4	(pressure measurement)	= 25 psi
w_5	(flow rate measurement)	= 0.1 gpm
w_6	(efficiency of electric motor)	= 0.05

Then by using the equation,

$$W_r = \left[\left(\frac{\partial R}{\partial X_1} w_1\right) + \left(\frac{\partial R}{\partial X_2} w_2\right)^2 + --- + \left(\frac{\partial R}{\partial X_n} wn\right)^2 \right]^{\frac{1}{2}} \qquad (7.9)$$

where $R = f\ (x_1,\ x_2,\ ---,\ x_n)$

For the total efficiency,

$$R = \frac{X_1 * X_2 / 5000}{X_3 * 24 * X_6 / 746}$$

and for the pump efficiency,

$$R = \frac{X_5 * X_5 / 1430}{X_3 * 24 * X_6 / 746}$$

Using the above relationships, the error in the total efficiency for case 6 of Table 7.1 is,

$\eta_t = (16.4 \pm 1.1)\%$

whereas the error for the efficiency of the pump is,

$\eta_p = (34.9 \pm 3.3)\%$

The errors due to the measurements are too small to account for the low efficiencies of the pump. There must be a systematic error. In order to check this, theoretical efficiencies of the pump and the motor as given in section 7.3.1 were calculated and they were plotted together with the experimental values. Parameters in the equations are calculated from the catalogue and found to be, $T_c = 0$, $C_s = 1.67*10^{-10}$, $C_d = 2.6*10^6$, $C_f = 0.01325$ for the pump and $T_c = 0$ $C_s = 1.23*10^{-9}$, $C_d = 1.82*10^6$, $C_f = 0.0893$ for the motor. The graphs shown in figures 7.11a and b indicate that although the experimental and theoretical results are in good correlation for the motor, they deviate greatly for the pump. This discrepancy strongly suggests the existence of the cavitation in the pump. Otherwise only a serious pump malfunction could result in such low efficiencies. However, the pump was checked and there was no evidence of a malfunction in the pump. An attempt was made to eliminate the cavitation by changing the reservoir height, but it was found that with the existing design of the reservoir, eliminating cavitation effects will be very

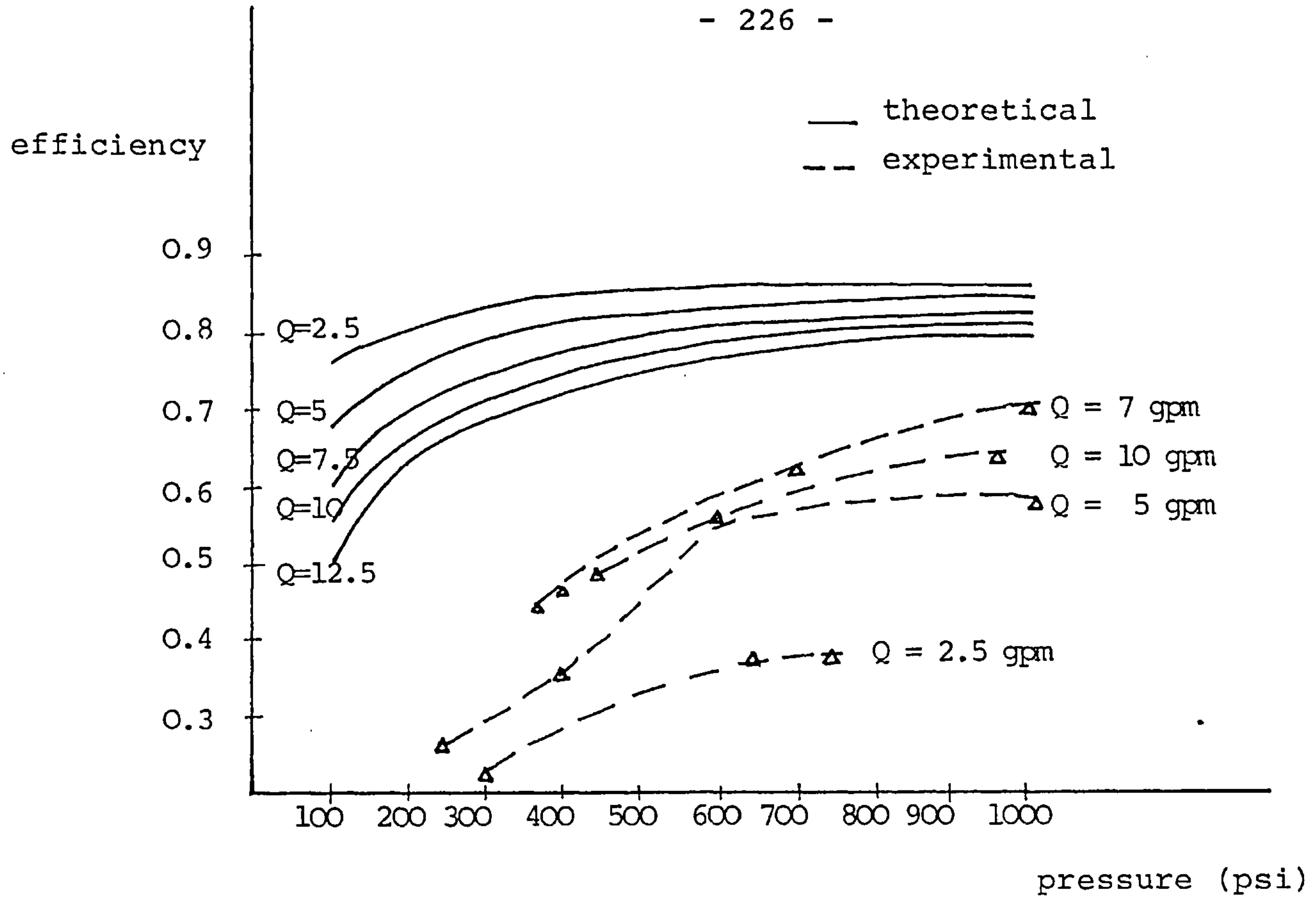

a) Efficiency curves for the pump

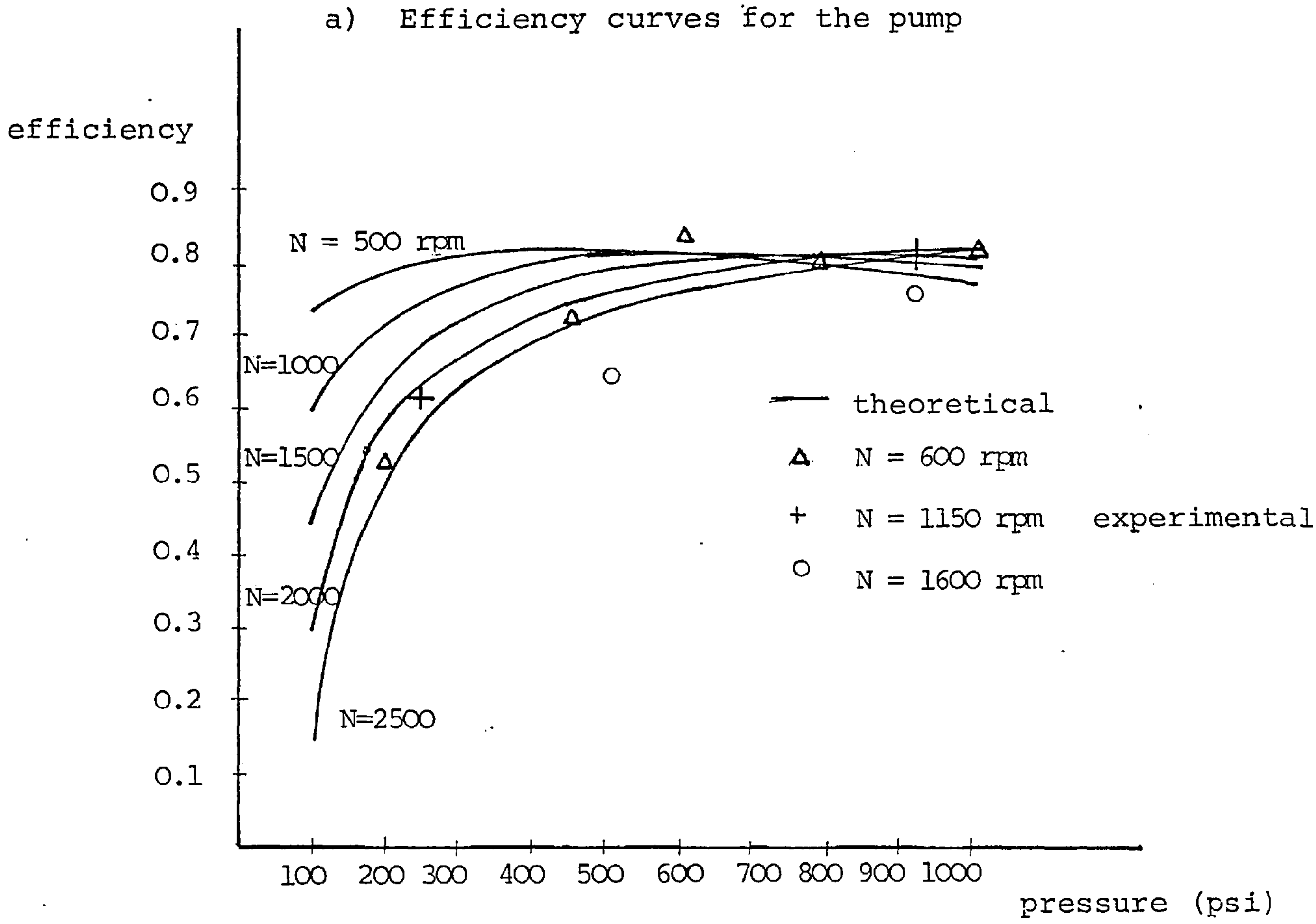

b) efficiency curves for the motor

Figure 7.11 Efficiency curves for the pump and the motor difficult. Therefore, a new power pack was proposed and designed for future experimentation.

Another aspect of the experiments was the excessive noise levels. It is well known that axial pumps are noisier than vane pumps. In reference (104) noise level for an axial pump is given by the following equation,

$$L_p = (97 + 10 \log HP\ (1-0.5\eta_p) - 20 \log r - 11)\ dB \quad (7\text{-}10)$$

where

HP is the fluid horse power
η_p is the pump efficiency
and r is the distance you are measuring the noise from (in metres).

Assuming r = 1m, the noise levels for cases 6 and 7 of table 7.1 are obtained as 87dB and 89dB respectively, which are 16dB lower than the measured values. This again suggests the existence of cavitation. For an operation without cavitation, assuming r = 1.2 m, HP = 10 hp, η_p = 0.9, the noise level obtained is 92dB. That is still excessive, therefore in the final system, the following precautions should be taken:

1. Instead of axial pumps, vane pumps should be preferred.

2. Bends in the piping should be minimized.

3. A good reservoir design should be employed and cavitation should completely be eliminated.

4. Proper attention should be given to the mounting and the guards.

Finally, the temperature behaviour of the circuit can be analysed and compared with the theoretical results. At 650 psi pressure and 10 gpm flow rate with the efficiency values as obtained for case 14, the temperature rise can be calculated from equations 7.5. The heat transfer coefficient and the heat dissipating area are estimated to be 17 J sec^{-1} c^{-1} m^{-2} (114) and 1.8 m^2 respectively. The resulting temperature is 48.8°C giving 68.8°C for an ambient temperature of 20°C which correlates well with the experimental result (70°C). The same problem was also solved by using the computer program prepared (appendix K). The area values and parameters were given as follows (node numbering is shown in fig. 7.4), $A_{1,2}$ = 0.09 m^2 $A_{3,4}$ = 0.12 m^2 $A_{5,6}$ = 0.09 m^2

$A_{7,8}$ = 0.09 m^2 $A_{9,10}$ = 0.09 m^2 $A_{10,11}$ = 1.4 m^2

Flow rate = $7.95*10^{-4}$ m^3/s (10.5 gpm) P = $4.83*10^6$Pa (700 psi)

Δ_p = $1.38*10^5$Pa (20 psi)

$\Delta_{p4,5}$ = $1.38*10^6$Pa (200 psi) η_p = 0.65 η_m = 0.60

T_{env} = 20°C Specific gravity = 0.85

Specific heat = 2000 J kg^{-1} C^{-1}

Heat transfer coefficient = 17 J sec^{-1} C^{-1} m^{-2}

The results obtained for each node are listed below,

T(1) = 67.14°C T(2) = 66.75°C T(3) = 66.91 T(4) = 67.87°C

T(5) = 67.95°C T(6) = 67.83°C T(7) = 68.62 T(8) = 68.5°C

T(9) = 69.20°C T(10) = 68.95°C

These are all close to the experimental value of 70°.

The above calculations suggest that for higher pressure and flow rate temperature values will be higher, necessitating the use of a heat exchanger. However, in a well designed system, the pump and the motor will be more efficient, therefore, temperature should be calculated according to these higher efficiencies. From the theory, assuming 90% efficiency for the pump and the motor the final temperature at an output power of 15 hp can be calculated to be approximately 70°C which is allowable.

7.5.2 The Four Way Servo Valve:

Open loop hysteresis of the valve can be decreased to about 2-3%, if an optimum wave form corresponding to each voltage level is employed. One possibility is shown in table 7.2. It is as follows,

Below 2 Volts: No dither

Between 2-3.5 Volts: Triangular dither

After 3.5 Volts: Square dither

Also, from the results it is seen that $\pm$ 1.2 V gives better hysteresis values than $\pm$ 3 V which is the suggested figure in the catalogue.

If an open loop hysteresis of 2-3% is obtained a closed loop microprocessor control circuit will be able to decrease the hysteresis level even further, and then the accuracy level of the system will be satisfactory for machine tool use. The minimum stable motor speed with this valve was around 50 rpm. The maximum speed was limited to 1500 rpm due to the size of the valve giving a speed ratio of around 30:1.

7.5.3 Microprocessor Controlled Hydraulic Circuit:

The circuit gave a 50:1 speed range with the existing pump and the motor. If the size of the pump was increased so that the motor could be taken to its maximum speed, the speed range would be approximately 100:1. The accuracy of speed control (actual speed within 1% of demand) was acceptable and the response time was short (0.9 secs).

As seen from the above results, the overall behaviour of the microprocessor controlled hydraulic circuit is very competitive. However, the investigation proved that establishing a stable system on an experimental circuit is a major task, and a good theoretical analysis would be very useful. In order to check the validity of the theoretical analysis presented in section 5.3 and appendix J, the experimental circuit was simulated. Most of the coefficients of the hydraulic system were calculated from the catalogues and the others were estimated. Using these values, the coefficients of the transfer function as shown in figure 7.2a, were found to be,

$K = 223;\quad \xi_1 = 3.066*10^{-4} \quad \xi_2 = 1.67*10^{-2}$

$\xi_3 = 4.48*10^{-1} \quad \xi_4 = 4.04*10^{-4} \quad \xi_5 = 1.91*10^{-2}$

$Km/c = 1.175*10^{-3} \quad M(s) = 7.74*10^{-2}/s \quad F(s) = 73.46$

When a z-transform analysis of the system is performed, the overall transfer function is obtained as follows,

$$T(z) = \frac{84.5*10^{-6}z^2 + 2.73*10^{-5}\, z + 5.45*10^{-6}}{z^3 - z^2\,(2.5) + z\,(2.103) - 0.6} \qquad (7.11)$$

A step response analysis of the system can be performed by using a state variable approach. The above equation can be put into state variable form as follows,

$$\begin{bmatrix} x_1\ (k+1) \\ x_2\ (k+1) \\ x_3\ (k+1) \end{bmatrix} = \begin{bmatrix} 2.5 & -2.103 & 0.6 \\ 1 & 0 & 0 \\ 0 & 1 & 0 \end{bmatrix} \begin{bmatrix} x_1(k) \\ x_2(k) \\ x_3(k) \end{bmatrix} + \begin{bmatrix} 1 \\ 0 \\ 0 \end{bmatrix} r(k)$$

7-12)

$$W(k) = \begin{bmatrix} 8.45*10^{-6} & 2.73*10^{-5} & 4.45*10^{-6} \end{bmatrix} \begin{bmatrix} x_1(k) \\ x_2(k) \\ x_3(k) \end{bmatrix}$$

Using the above equations a computer program was written and the step response for the system was obtained. The theoretical step response was compared with the experimental in fig. 7.12. The comparison shows that there is a good correlation with the experimental findings.

Once the model of the system is established, the analysis can be extended to find out the effects of changes in the system parameters. The root locus for the system is shown in fig. 7.13. It shows that when the gain of the system is sufficiently large the system may become unstable indicating that careful adjustment of the gain is necessary. The effect of load change on the spindle speed can also be analysed by using the model. This analysis was carried out and the results are shown in fig. 7.14. As seen from the figure, disturbance behaviour of the system is extremely good. The speed recovers its set value in one second without any overshoot.

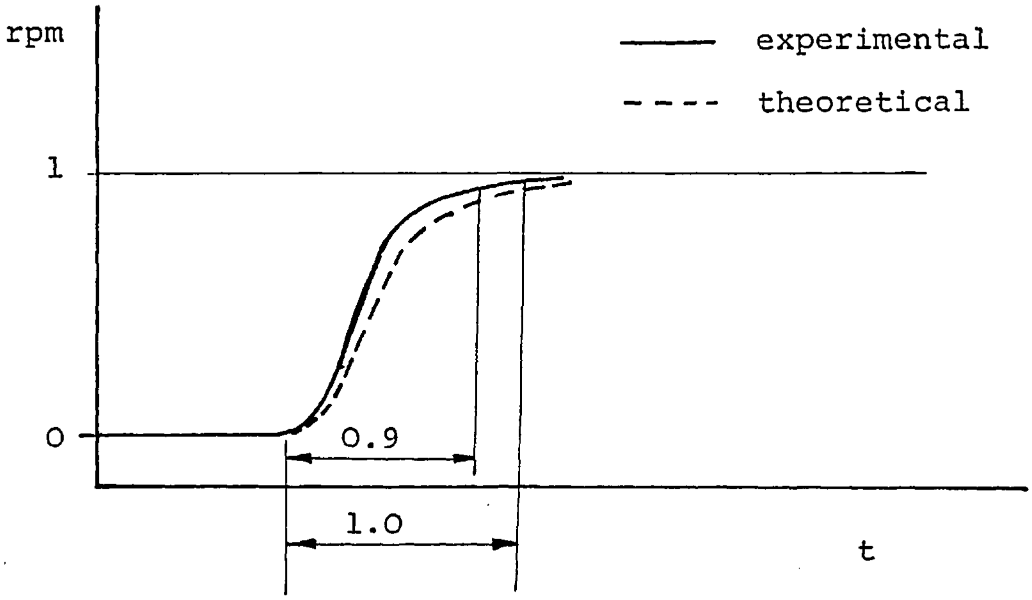

Figure 7.12 Comparison of the theoretical and experimental step response

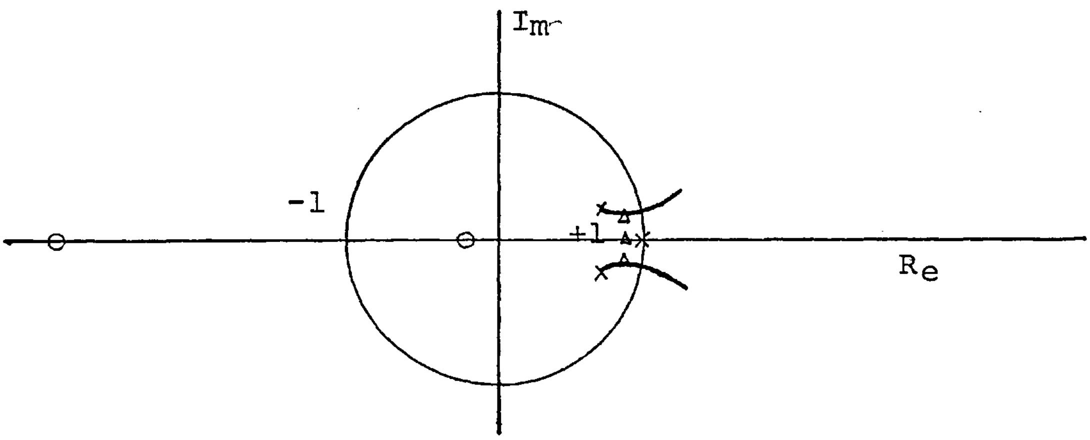

Figure 7.13 Root locus for the system

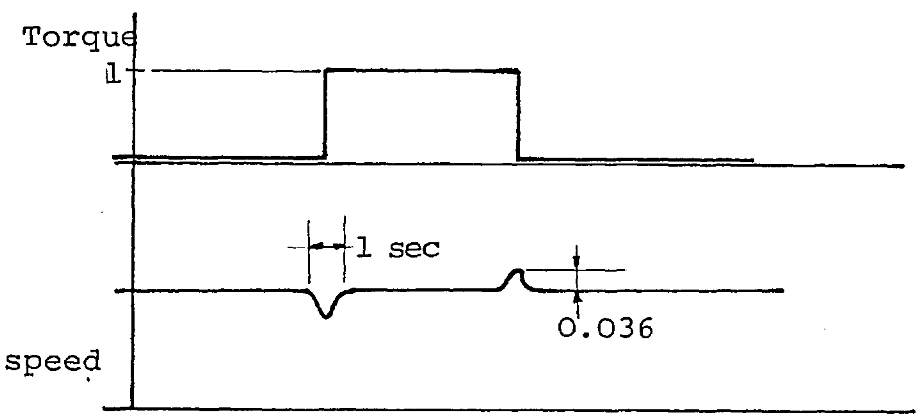

Figure 7.14 The effect of load change on spindle-speed

7.6 Conclusions:

In this chapter, experimental and theoretical analysis of hydraulic systems were described. Theoretical analysis was carried out in three main fields.

1. Efficiency and temperature calculations
2. Hydraulic system simulation
3. Control system simulation.

Results of the theoretical analysis were compared with the experimental results and it was found that the results were in correlation, validating the theoretical analysis. Therefore, the developed methods form a sound base for hydraulic systems design.

Experiments conducted were divided into two main sections.

1. Experiments with cheaper hydraulic valves
2. Experiments with microprocessor control of a closed loop hydraulic circuit.

In the first stage, two valves with a price of around £100 are tested. Their behaviour was satisfactory, however, the speed range obtained (around 30:1) was not good enough to employ the valves in a hydraulic circuit for a machine tool spindle.

On the second stage, experiments on a closed loop system were performed. For this purpose a feedback control microprocessor circuit was prepared. The results showed that microprocessor controllability of the system was excellent. Response time of 0.9 sec, an accuracy level of 1% and a good disturbance behaviour were the characteristics of the circuit. It was seen that a speed range of 100:1 was obtainable.

Although, the performance characteristics of the system are suitable, high noise levels associated with the circuit makes the use of the system in a commercial environment impossible. For quieter systems vane pumps should be used and mounting of pumps and motors should be considered with great care. Keeping this in mind and using the experimental and theoretical experience obtained, analysis of some possible designs are carried out in appendix I, and a variable pump with a variable motor was chosen as the best alternatives. The selected circuit is shown in fig. 7.15. The system has a constant power range of 3.5:1. For lower speed range pump and valve control will be used. When the speed range of the pump is combined with the speed range of the motor, a range of 100:1 can be easily achieved. The motor and pump efficiencies are 90%. At 1500 psi assuming an 86% circuit efficiency, the overall efficiency is obtained as 70% which is reasonable. The cost for such a circuit together with its control system will be around £2500. That is somewhat cheaper than an electrical d.c. drive with similar characteristics (£3000 for a d.c. drive circuit and the motor). However, there is a big resistance in the market against the hydraulics. Improperly designed hydraulic circuits have caused many maintenance problems in the past. Therefore, the market is very reluctant to accept hydraulics. It has been shown in this chapter that the performance and cost effectiveness of hydraulic drives is very attractive. However, the advantages over electrical drives are likely to be insufficient to overcome the market resistance.

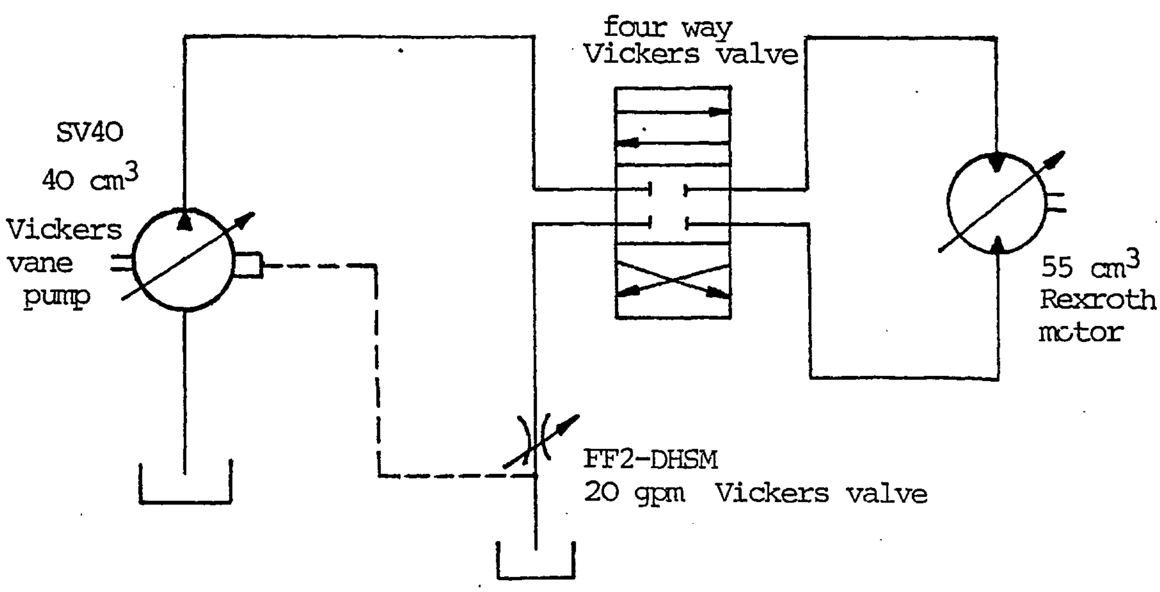

Fig 7.15 Variable displacement pump and variable displacement motor

CHAPTER 8

ADAPTIVE CONTROL

8.1 Introduction:

Adaptive Control (AC) is a systems concept conceived about 25 years ago. It is applicable to different processes or operations in many industries and as a result, its precise meaning varies. However, adaptive control of machine tools is more recent, dating back to the early 1960's. Development of an AC system for machining is particularly difficult because of the wide number of parameters and the unpredictable process variations.

There is no general agreement on a single definition for automatic adaptive control of machine tools. The exact meaning depends on the system being discussed and the systems vary from simple to sophisticated designs.

Adaptive control can broadly be classified into three groups,

i) Technological AC
ii) Geometrical AC
iii) Manual AC

Technological AC can in turn be divided into two groups. One Adaptive Control for Optimization (ACO), the other is Adaptive Control for Constraint (ACC). In ACO, the performance is optimised according to a prescribed performance index which is usually an economic function such as minimum machining cost or maximum production rate. In ACC machining conditions such as spindle speed and/or feedrate are maximized within the prescribed limits of machine and tool constraints such as maximum torque, force or horsepower.

The aim in geometrical AC systems is to control the shapes, dimensions and also the accuracy of parts being machined. It may be said to be the desired final goal of the automated machining process in that the drawing of the workpiece to be machined is the input information and the final machined component is the output.

The main difficulty in all these types of AC is the development of in-process measuring instruments which need to be reliable, robust and economical. The third group of AC emerges from this difficulty. In manual AC systems, operator is the sensor as well as the interface between the machine. In this method, operator measures the relevant dimensions after each cut and feeds them into a programmable calculator. The calculator then calculates the cutting parameters according to an optimisation criteria. Up till now, manual adaptive control has been limited to grinding machines (117).

Adaptive Control has been entirely dependent upon the skill of machine tool operators throughout the nineteenth century and for more than half of the twentieth. The advent of NC and CNC machines reduced the skill requirements of machine operators and certainly in the unmanned factories of the future, there will be no operators watching the process. Therefore, it is necessary to have a means of determining the right cutting parameters. In today's CNC machines, this is being done off-line. However, the programs to calculate the cutting parameters, must be conservative and should anticipate the worst machining conditions in selecting feeds and speeds to protect the machine, cutting tool and workpiece. Increasing combinations of work and tool materials, and the variations in the materials and cutting conditions make the selection of optimum feeds and speeds practically impossible. Therefore, the concept of adaptive control is likely to prove the best approach for determining optimum feeds and speeds in machining. Proven benefits include increased productivity and cutter life, reduced costs and scrap rates, improved product quality, greater machine and better protection of the machine, tool and workpiece from damage. Improved and simplified programming and reduced dependence on operator skill are other advantages that have been cited (118), (124).

However, at the moment there are many limitations to AC systems. High cost and complexity as well as lack of reliability have been the primary reasons for the slow acceptance of AC. As lower cost, more reliable and easily retrofittable sensors become available, AC systems will be more widespread. At the moment, they are mainly limited to the machining of complex parts and to large NC-CNC machines.

When one considers the advantages of AC and the possible unmanned operation of the machine tools in future, it becomes obvious that some form of AC system is necessary on the machine tool designed in this work. With that in mind, this chapter will review the sensors for AC together with the existing AC systems. Then some suggestions will be made as how to eliminate some of the problems in the existing systems, and some AC algorithms will be presented.

8.2 Sensors of Adaptive Control

Considerable research and development work is being devoted to the subjects of sensors for AC. Major problems being encountered are high cost and unreliability. Some important parameters such as tool wear and surface quality cannot be measured practically and accurately during cutting under production conditions with the current state of sensor technology. What is needed are sensors that are reliable, economical and suitable for use in a machine tool environment. They should also be easy to retrofit, recalibrate, and replace, and should not alter any of the machining parameters. Response speed should be compatible with the AC system, and output signals should be linear over a wide range of input values and stable over temperature variations encountered in production.

The most important parameters in an AC system are the surface roughness and the tool wear. Therefore, this section will concentrate on these two. Other cutting parameters such as forces, torque, power, temperature, vibrations and noise will be covered under the tool wear sensors.

Surface roughness can be used independently as a measure of quality of surface finish or it can be used as an indirect measurement of tool wear (126). There are four main methods of measuring the surface roughness.

i) One method developed in Germany uses microscopic measurements of a projected small light slit on surfaces being turned, using a photodiode array,

ii) Another suggested method involves measuring the intensity of reflected laser light. The relationship between the intensity of the reflected light and surface finish is affected by many parameters including the type of surface and material reflectivity. Evaluation of the distribution of the reflected light intensity seems to provide more information about the surface than peak values of the intensity (118).

iii) Another laser method, developed in Japan (118), employs a laser beam focussed, on the objective surface, in a thin a beam as possible. The spot of the beam on the surface moves around due to the movement of the surface. The movement, corresponding to the roughness, is detected by being magnified on a screen through a microscope. Then an image sensor scans the screen and converts the image into roughness.

iv) Finally, a method has been developed by Braunschweig Technical University in West Germany as a part of an experimental ACO system for cylindrical plunge grinding. A tracing stylus follows a peripheral line on the rotating workpiece, and is excited by the surface. The vibrations generated produce an electrical signal correlating to center line average and height to peak to valley.

The second important cutting parameter is the tool wear. It is measured either by direct or indirect methods. Indirect measurement methods are more suitable for on-line applications. Direct measurement methods are mostly used in off-line applications where the time in between cuts is employed.

A. Indirect Sensing of Tool Wear:

Since tool wear and life are critical parameters in the economic evaluation of any machining operation, a number of sensing methods have been developed for both direct and indirect on-line sensing of tool wear. Several indirect methods are being used in production applications of AC, but direct methods are still confined to R & D laboratories. The main indirect methods of sensing tool wear include the correlation of cutting forces, temperature and vibrations.

i) Cutting Forces:

The works of Takeyama (123), (125) and Micheletti (120), (121) showed that there is a distinct relationship between the cutting forces and the wear land. However, there are still some problems:

a) How to separate the effects of crater wear and flank wear?

b) Is the relationship valid for varied work materials and cutting conditions?

c) How to separate the force increases due to the accidental variations of other parameters (such as machining stock and hardness)?

The results given in the literature shows that radial force and the feed force while increases linearly with flank wear, they decrease with crater wear. To eliminate the effect of crater wear, a method suggested by Takeyama (125) is the use of specially machined cutting tools which have a large rake angle. He claims that this design will also minimize the variation of cutting force due to cutting speed. Micheletti states that in modern carbide tipes with normal values of the feed, and with alloy steel, the distance of the crater wear from the cutting zone is sufficient to ensure that its effect will not be seen (fig 8.1)

However, with stainless steel at very high cutting speed and with low feed value, he states it is possible to have the cutting force decrease with time due to the effect of crater wear.

Takeyama also shows that,

$$\frac{1}{d} \frac{\Delta F}{\Delta V_B} = \text{const.} = k_1 \qquad (8.1)$$

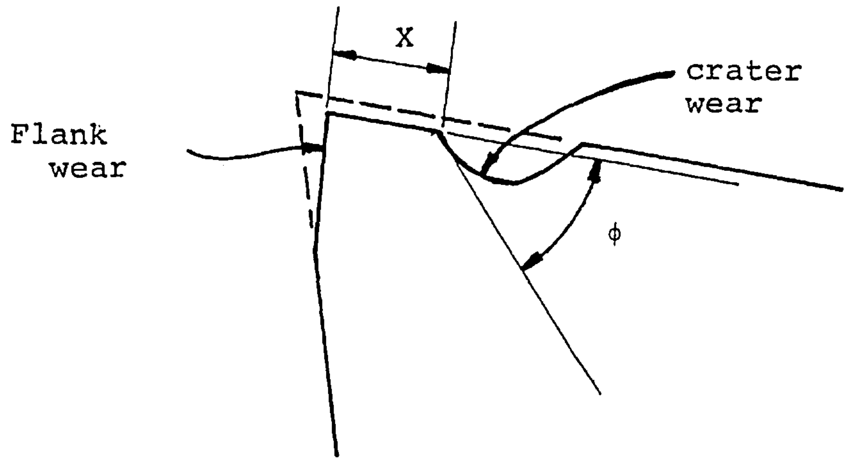

Figure 8.1 Crater wear and flank wear

where d is the depth of cut, F is the radial force and V_B is the flank wear, k_1 being closely related to the mechanical properties of the work material. However, $^{\Delta F}/_{\Delta t}$ changes with speed and feed. Takeyama states that feed effect can be avoided if the specific cutting force is taken as F instead of the total force. For the speed effect the cutting tool should be specially shaped as explained above.

In order to prevent accidental variations of other parameters from being interpreted as variations due to cutting edge wear, Micheletti suggests that forces should be measured with great accuracy. Also continuous recording is necessary for accurate control of random phenomena.

Another method of using cutting forces as a measure of tool wear has been proposed by Uehara (124). This method is based on an experimental investigation which showed that the pattern of the curve which relates the feed force and the feed per revolution is strongly influenced by the tool wear. From his experiments, Uehara claims that, it is possible to detect both the flank wear and crater wear through examining the form of the feed force versus feed rate oscillogram. It is also possible to determine the values of flank wear and crater wear quantitatively, through measuring the peak height and the flat part of the oscillogram.

ii) Temperature:

It is well known that cutting temperature is a function of cutting conditions and tool wear. For modest cutting conditions, a tool life ratio of 17:1 can be prescribed for a temperature rise from 450°C to 540°C (123), (127). Even though the correlation between temperature and tool wear is not very clear, it has still been used as a parameter in some AC systems (118).

There are basically three methods of measuring the cutting temperature: tool-workpiece thermocouple, remote or imbedded thermocouple, infrared system. Tool-workpiece thermocouple is difficult to be employed on the shop floor, because the calibration is very sensitive to the composition of the tool and workpiece materials. With the remote or imbedded thermocouple, response rate is very slow also preparation of the imbedded thermocouple causes difficulties. The infrared system, because it is non contacting has a high sensitivity and short response time, is attractive for AC applications. However, these sensors are complicated and expensive and focusing is very difficult.

iii) Vibrations:

Several authors (131), (132) have investigated the correlation between the vibrations of a machine tool (particularly lathes) and tool wear. Martin and Mutel use an accelerometer to record the vertical vibrations of a lathe tool (131). In the range of values studied, it has been shown that the power of the acceleration signal determined by spectral analysis is a linear function of the cutting speed and of the tool wear, the signal increasing in the ratio of 1:10 between the new tool and the worn tool. However, a similar analysis reported by Taglia and Portunato (132), contradicts with these results.

There are other methods of tool wear sensing mentioned in the literature. These are noise analysis, workpiece dimensional change, distance between tool post and the workpiece and the energy input to the system (126). Most of these methods suffer from the high cost and complication of the measuring instrument. Unreliability of the results due to the disturbances caused by the cutting process is another factor to hamper these methods.

B. Direct Sensing Methods:

In these methods the sensor measures tool geometry detecting the volumetric loss of the tool (land wear, crater wear or both together). These methods are very difficult (and some times impossible) to use on-line especially when there is a continuous contact between the tool and the workpiece as in turning.

The methods can be analysed in four groups:

i) Optical (light reflection, fibre optics, TV camera) sensors

ii) Electrical resistance sensors

iii) Radio active sensors

iv) Pneumatic sensors

v) Touch trigger probes.

i) Optical Sensors

Optical methods analyse the image of the illuminated wear zone when the cutting tool is not continuously in contact with the workpiece. A method which has recently been developed involves a line array of detectors charged by a low-power light source. As the tool tip passes through the line of detectors and the light source some of the detectors are occluded creating an analogue of the shape of the tool. With this method measurement can be made on fly, therefore it does not increase the idle time. However, the positioning of the sensor is important and it might not be suitable for all the works.

ii) Electrical Resistance Sensors:

The system depends upon measuring the reduction in electrical resistance through the tool-work junction which occurs as the tool wear and its contact area with the work increases. The method was successfully used to predict the wear land within $\pm$ 0.05 mm of the off-line measurements (126). However, it was found that, resistance also changed with cutting speed, feed and cutting forces.

iii) The Radioactive Sensor:

In this method, the cutting tool is activated with neutron or with charged particles. The abraded radioactive wear particles are transported by a continuous flow of oil to the measuring head where the activity is detected, and then recorded with appropriate set-up. The intensity of radioactivity in the chips is correlated to the volume of the tool material that adhered to the chips and hence to the tool wear. The radiation problems and the need to collect the chips do not allow applications for continuous sensing on the shop floor.

iv) Pneumatic Sensors:

In Technical University Aachen, a sensor has been developed for the on-line measurement of wheel wear in grinding. Using the electrically transformed signal of air pressure Δp in the nozzle, the gap between the nozzle and the grinding wheel is kept constant. Wheel wear results in an enlargement of the gap. This will activate the control system of a stepping motor in order to close the gap. By way of counting the number of steps of the feed motion, it is possible to calculate the amount of radial wheel wear.

v) Touch Trigger Probes:

They are mostly used for automatic tool setting purposes. However, with the appropriate programming, they can also be used to detect the tool wear. The new tool is moved to the probe for calibration, then between cuts it can again be moved to the probe. The discrepancy between the two movements as sensed by the servo system of the machine tool gives the tool wear. Typical resolution for such a probe is 1 μm.

In this section, the existing roughness and tool wear sensing methods have been described. A summary of the tool wear sensor methods for turning and milling processes can be seen in table 8.1.

Some of these methods are being used practically on existing ACC and/or ACO systems. The following two sections analyses these ACC and ACO systems.

Table 8.1 The existing tool wear methods for milling and turning

	Method	Pictorial Description	Limitations
Direct Methods	Optical Sensor	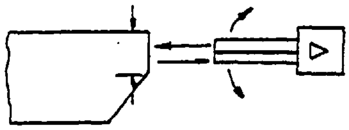	Sophisticated instrumentation not suitable for turning
Direct Methods	TV camera	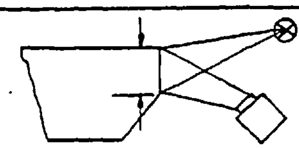	Sophisticated instrumentation not suitable for turning
Direct Methods	Electrical res.	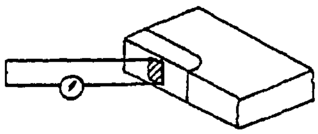	cutting conditions dependent special tool required
Indirect Methods	cutting forces	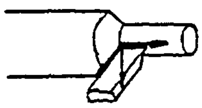	Very high accuracy in measurement is necessary. Not applicable to all the materials
Indirect Methods	cutting temperature	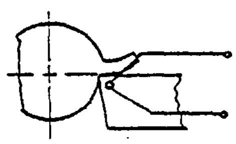	Special tool required. Relation is not very clear. Response time might be small.
Indirect Methods	vibrations	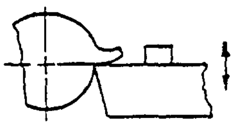	Special tooling is required. Dynamics of the tool should be compensated for; two contradicting work
Indirect Methods	workpiece dimensions change ultra-sonic method	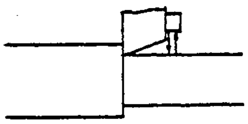	Sophisticated instrumentation Errors occur due to the deflections or vibrations or irregularities of the machined surface
Indirect Methods	two feelers to measure the retreat of the cutting edge	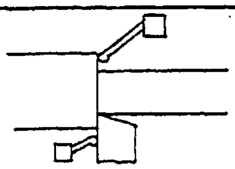	Thermal expansions cause problems, deflection or vibration of the tool or the workpiece cause problems irregularities of the machined surface cause problems.
Indirect Methods	Optical or laser beam sensor to measure the retreat of the cutting edge	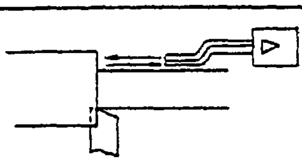	Sophisticated instrumentation Errors occur due to the deflections or vibration or irregularities of the machined surface

8.3 ACC Systems:

An adaptive control example subjected to several constraints is presented in fig 8.2 (125). In the example shown feedrate and cutting speed are taken as the parameters and the constraints are

1 Maximum force

2 Maximum power

3 Surface roughness

4 Maximum and minimum feedrate and cutting speed.

They define a certain region in which the combinations of feedrate and cutting speed are acceptable. The task in case of ACC systems is usually to follow one or two constraint lines by adjusting the feedrate and cutting speed. However, there are also other algorithms adopted in the ACC systems. These are shown in table 8.2. (133), (134), (135). As seen in the table most of the systems developed are aimed for maximum power utilization. Usually, a cutting speed is selected according to tool life criteria and the feed rate is increased until the maximum power is obtained.

8.4 ACO Systems:

ACO systems are more difficult to implement than ACC systems. Although sophisticated and costly ACO systems have been developed, most of them are of the laboratory type used essentially for research. Major difficulties with such systems have been in the development of

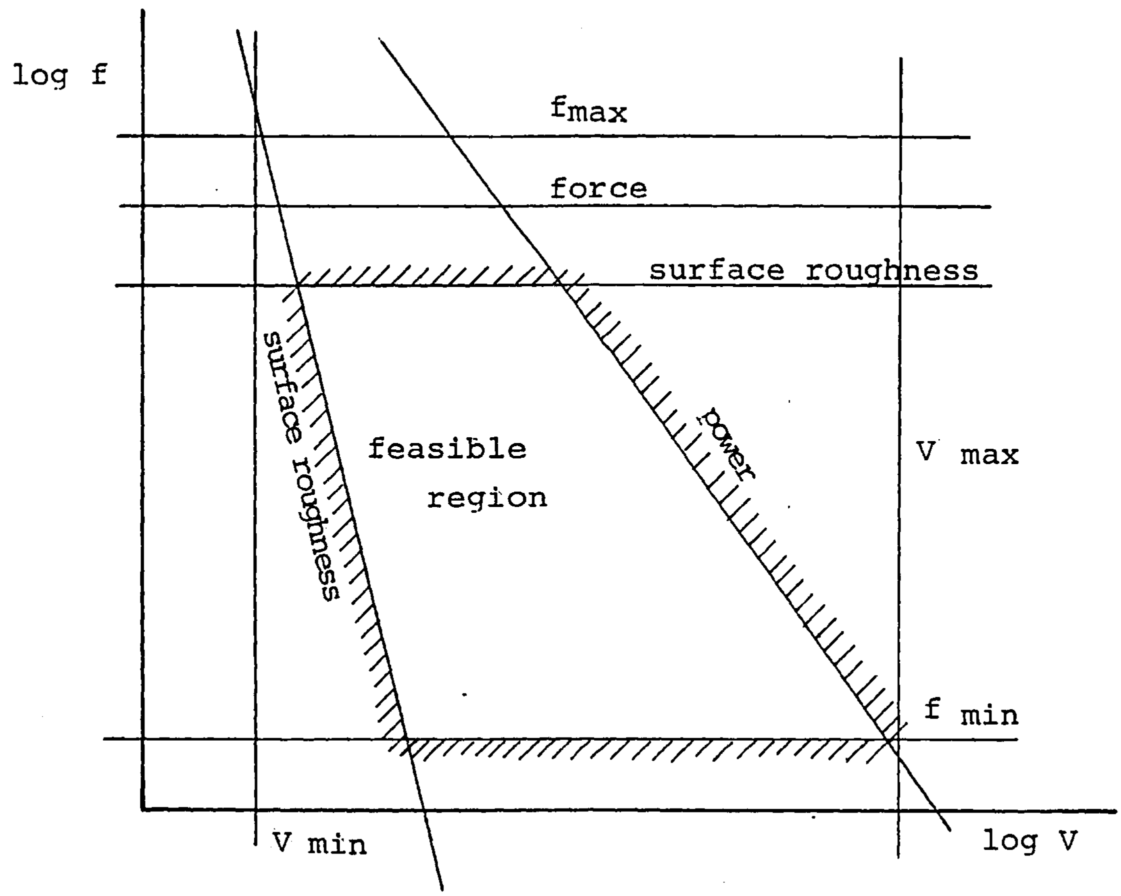

Fig 8.2 Basic parameters of adaptive control

Table 8.2 ACC Systems for Milling and Turning

place	system	Measured Quantity	Correcting Variable	Aim
ABC Pittler (Germany)	Turning	Motor load	Feedrate	Maximum Utilisation
Allen-Bradley	Milling	"	"	"
Bendix (USA)	Turning	Spindle Torque Vibration	Speed, Feedrate	Maximum Material Removal Rate
Bendix Dyna-path System 4 (USA)	Turning	Torque Motor Current Motor Temperature	Feed	Maximum Utilisation
Boeing (USA)	Turning	gap	Feedrate	Maximum Utilisation
Cincinatti Milacron (USA)	Milling	motor power	Feedrate	Maximum Utilisation
General Elec. (USA)	Turning	Motor Current Load	Speed or Feedrate	Maximum Utilisation
Dyna System (USA)	Turning	Torque	Speed Feedrate	Maximum Utilisation
Gildemeister (W Germany)	Turning	Force	Feedrate	Maximum Utilisation
Makino (Japan)	Milling	Torque	Speed Feedrate	Maximum Utilisation
Milwaukeematic 800	Milling	Power deflections	Speed Feedrate	Maximum metal removal rate
Siemens Sinumerit (W Germany)	Milling or Turning	Torque	Depth of cut feedrate	Maximum Utilisation
Sapcons (USSR)	Turning	Geometry	Tool path	Improved Accuracy
Staveley (UK)	Turning	Torque	Feedrate	Maximum Utilisation
Macotesh	Milling	Force power	Feedrate	Maximum metal removal rate, minimum deflections
Vulfson (USSR)	Turning	Force	Feedrate	Maximum Utilisation
Westinghouse	Milling	Power Vibrations	Feedrate spindle speed	Metal removal rate.

comprehensive indexes of performance and of sensors to measure the necessary parameters. However, there are two systems which are particularly important for their contribution to this field. These are Bendix system and a system developed by Takeyama (125), (134).

i) Bendix System

The sensed qualities are tool-tip temperature, spindle torque and tool vibration. They are used to evaluate the variables in the performance index. Performance index is given as follows

$$H = \frac{MRR}{\dfrac{k_1+(k_1\zeta+k_2B)}{V_B^*}\ TWR} \qquad (8.1)$$

Where V_B^* - Maximum allowable tool wear

MRR - Metal removal rate

TWR - Tool wear rate

k_1 - direct labour plus overhead rate

k_2 - cost per grind plus initial tool cost divided by maximum number of regrinds

ζ - tool change downtime

B - is a constant

If B is O, the criterion is production rate only if B = 1, the criterion is cost only. Intermediate values of B correspond to criteria which are comprimises between cost and production rate.

Equation 8.1 is maximised by changing subject to certain constraints, the feedrate and the cutting speed. This system was tested on a milling machine. The degree of cost reduction ranged from 5 to 38 per cent for the constant-depth cuts, and was on the order of 50 per cent for the variable depth cuts. However, it was pointed out that these results were obtained over a limited range of cutting conditions and much work was to be done. Also, the report gives no details on the evaluation of the tool wear rate which decreases the credibility of the method.

ii) Takeyama's Method:

Takeyama uses the rate of change of tool force as a measure of tool wear rate. Using the results of his experiments, he writes the performance index as follows,

$$H = \frac{1000\ MRR}{k_1 + \dfrac{k_1 \zeta + k_2}{d k_2 H_B (V_B^* - V_{BO})} \dfrac{\Delta F}{\Delta t}} \tag{8.2}$$

Where,

H_B - Brinell hardness of Material cut,

V_{BO} - initial flank wear 10.05 mm approximately)

V_B^* - tool life criterion

d - depth of cut

$\frac{\Delta F}{\Delta t}$ - rate of change of tool force

k_2 - is defined as follows,

$$\frac{1}{d}\frac{dF}{dV_B} = k_2 H_B$$

In this system only tool force is measured. Constraints are force, power and surface roughness. The variables are feedrate and cutting speed.

Although the method seems promising it has not been tested fully on a machine tool, probably because of the need for a special tool design as mentioned in section 8.2.

8.5 Proposals for a Feasible AC System

Before working on any proposal for a feasible AC system, the shortcomings of the existing ones should be analysed. They can be gathered into two groups:

1. The difficulty of developing reliable, economic and robust tool wear sensors which can be used in the harsh conditions of the manufacturing environment.

2. Uncertainties occur in some of the constants used to evaluate the surface roughness, tool force etc. from the cutting conditions. Such constants appear in performance index or tool wear evaluations.

In the following sections, firstly the problems associated with the tool wear evaluation will be discussed and methods to eliminate some of the shortcomings of the existing methods will be given. Secondly, two proposed adaptive control routines, one ACO and the other ACC will be described.

8.5.1 Tool Wear Evaluation:

In the evaluation of tool wear, on line methods are to be preferred, because they make use of the cutting time and therefore does not increase the floor to floor time. A reference to table 8.1 show that all the on-line methods except force measurement and vibration measurement require sophisticated and expensive instrumentation and they are not suitable for machine tool environment. There are two contradicting reports on tool wear evaluation with vibration measurement hence more work is needed in this field. Therefore, it appears that force measurement is the only feasible method of wear evaluation presently available. However, there are two major problems with this method,

1. Tool force dependent on cutting conditions

2. Effects of crater wear and flank wear can not be separated.

To tackle the first problem, equations given in reference (121) should be remembered.

$$F_r = F_{ir} + C_1 t \qquad (8.3)$$

where F_r is the radial force, F_i is the initial force, t is the cutting time and C_1 is a constant.

From equation 8.3, it is seen that F_{ir} is the cutting force at t=O. If the relation for F_{ir} is known and it can be calculated theoretically, the C_1 can be evaluated. In the literature (48), it is given that

$$F_{ir} = C\ f^{\alpha}.d^{\beta}.V^{\gamma} \qquad (8.4)$$

Where

f, d and V are the cutting conditions, and C, α, β and γ are constants related to the tool shape and workpiece and tool material combination. These constants are tabulated in handbooks for a wide range of tool and workpiece combinations. However, they all have uncertainties and using them will impair the adaptive control system. Therefore, either all of the constants should be determined in an on-line manner by some trial cuts, or the values of α, β and γ are taken as they are given in the books and only the value of C calculated in an on-line manner at t=O. With these methods whenever cutting conditions changes, the initial force value corresponding to the new cutting conditions can be calculated by using eqn. (8.4)

Then, if

$$P = F-F_c = F_i+C_1 t-F_c = c_1 t \quad (8.5)$$

is calculated, the result directly gives the slope of the relation between the radial force and the cutting time, independent of cutting conditions.

Parameters of F_c can be calculated for each individual blank, minimizing the effect of hardness variations in one batch.

The second problem is more complicated. There are basically three solutions. The first one relies on the observations of Micheletti (120). He states that for modern carbide tips with normal values of the feed and with alloy steel the effect of crater wear on tool forces is negligible. Therefore, if it is reasonable to limit the adaptive control to that range of materials and cutting conditions, nothing else need to be done. The second solution can be to analyse the feed force, feedrate relationship as mentioned in section 8.2. However, this solution requires sophisticated instrumentation to process the data and would be difficult to employ in an on-line manner. Another solution can be found by the evaluation of all three force components at the same time. Observations have shown that the effect of flank wear and crater wear on the ratio of forces is different (121). This difference can be used to separate the two wear types. However, for quantitative results, more experimentation on this method and on the ways of force measurement methods should be carried out.

8.5.2 Proposal for an ACO system:

In any ACO system, the main difficulty is developing a comprehensive performance index. The performance index should be sophisticated enough to take as many effects into consideration as possible, yet at the same time should be simple enough not to take too long on evaluation time on the microprocessor.

In most of the ACO systems the performance index is either the minimum cost or the maximum production rate. Maximum production rate is used, if the operation is a "bottleneck" in a production sequence. However, usually this is not the case, therefore minimum cost per component is a more commonly employed performance index. Whilst minimum cost per component will correspond to maximum profit per component, it does not necessarily give maximum profit overall (per year, for example). This is due to the fact that profit is affected by the time per component as well as the cost per component since idle time must be taken into account. Here maximum profit will be adopted as the criteria.

The performance index can be written as (129).

$$P = \frac{P_s - C_u}{T_u} \qquad (8.6)$$

where

P = profit per time

P_s = selling price

C_u = total cost

T_u = floor to floor time

Selling price is determined by the company according to the laws of supply and demand.

Total cost can be written as,

$$C_u = N^* \{C_o\ (tm+t_q) + (t_m/_T)(C_o t_c + C_t)\} \quad (8.7)$$

where

N = number of passes

C_o = operating cost (labour + overhead) per unit time

t_m = machining time

t_q = quick return time

T = tool life

C_t = tool cost per cutting edge

and floor to floor time can be written as,

$$T_u = t_m + t_c . tm/_T + t_h \quad (8.8)$$

where

t_c = tool changing time

t_h = handling time

Machining time for a multiple pass,

$$t_m = \frac{\pi(D-\Sigma 2d\ell)L}{12.f.\nu} \qquad (8.9)$$

where

D = diameter of the workpiece

d_ℓ = depth of cut in the previous pass

L = length of the pass

f = feed rate

ν = cutting speed

and the number of passes,

$$N = \frac{a-\Sigma d\ell}{dn} \qquad (8.10)$$

where

a = total depth of cut

d_n = depth of cut in the present pass

All the above parameters can be readily evaluated, except the tool life. For the tool life Takeyoma derives the following relation,

$$\frac{1}{T} = \frac{dF/dt}{d\ k_2\ H_B(V_B{}^*-V_{BO})} \qquad (8.11)$$

where the parameters are as defined for equation 8.2.

Once the performance index is defined the next step is the determination of the constraints.

1. Dimensional Accuracy;

This is a constraint which is of importance in finishing cuts. Therefore, it should only be used in final cut.

One of the factors that causes the inaccuracies in the workpiece is the deflection of the tool and workpiece and machine tool components under the action of the cutting forces. Given the tolerance of the workpiece it is possible to calculate the allowable deflection. Then, according to the way the workpiece is mounted on the lathe, the maximum permissible force can be calculated. Here, as an example, the case of a workpiece between centres will be analysed. Assuming that the deflections of the machine tool components are negligible and taking the workpiece between centres as equivalent to a beam with one end rigidly fixed and the other hinged, the following equation can be used to determine the permissible max. cutting force,

$$\Delta Y max = \frac{F}{EI} \quad \frac{7\ell^3}{768} \qquad (8.12)$$

where E and I is the Young's modulus, and area moment of inertia respectively, and ℓ is the length of the workpiece.

If the allowable Δy is taken as $\frac{1}{3}$ of the tolerance, the constraint equation is derived as,

$$F < \frac{1}{3} \Delta T_o \text{ (EI) } \frac{768}{7\ell^3} \quad (8.13)$$

where ΔT_o is the tolerance requirement for the workpiece.

In order to increase the final accuracy, besides limiting the force, compensation techniques for tool wear and temperature changes should be employed and vibrations should be controlled. Surface roughness is also an important parameter. However, the measurement methods require sophisticated instrumentation and therefore expensive. Consequently, controlling surface roughness in an off-line manner is a better solution. Takeyama (125), gives the equation for surface roughness as,

$$\frac{f^2}{8R} < R_{mmax} \qquad (8.14)$$

$$fV^{\gamma} > S$$

where γ and S are constants and R_{mmax} is the maximum roughness permissible. R is the tool radius. γ is approximately 2 and S ranges from 1200 to 1400 for high carbon to low carbon steels.

2. Vibrations:

Vibrations of the cutting tool, usually known as chatter is very detrimental to the cutting tool and also to the surface finish. Therefore, their amplitude should be measured. The cutting conditions can be changed to keep the amplitude of vibrations below a certain limit determined by the surface finish requirements.

3. Power:

At a certain cutting speed the maximum cutting force is limited to the power available at the spindle. This is a constraint which is of concern in rough cutting procedures.

4. Time Limit:

If there is an order to be fulfilled by a fixed deadline, then time is also a constraint. Assume that n_p pieces/min is required. Then the constraint equation can be written as follows:

$$\frac{1}{n_p} > \frac{a - \Sigma d\ell}{d_n} \cdot \frac{\pi(D - \Sigma 2 d\ell_i).L}{12.f.\nu.} \qquad (8.15)$$

5. Feed rate and cutting speed:

These are limited by the capacity of the drive systems.

Together with the performance index given in eqn. (8.6) and the above constraints an ACO system for both rough cutting and finish cutting procedures can be developed. Among the cutting parameters, changing depth of cut in parallel to an ACO routine can cause difficulties. Therefore, only feedrate and spindle speed will be adapted as the ACO variables.

The ACO system explained here is summarised in Table 8.3.

8.5.3 Proposals for ACC systems:

AC systems are a step towards manless operation. Therefore, any ACC system should try to satisfy at least the minimum requirements for completely automatic operation. These requirements can be stated as follows:

1. Tool life monitoring and tool failure detection.
2. Dimensional accuracy control.

Tool life monitoring and tool failure detection can be achieved, through force measurement. Tool life monitoring can be performed by using eqn. (8.11), whereas tool failure is indicated by a sudden change in the cutting force.

Dimensional accuracy control is only necessary for finishing cuts and it has been covered in the earlier section.

System	Rough Cut					Finish Cut				
	Performance Index	Constraints	Measured Variables	Control Variables	Comments	Performance Index	Constraints	Measured Variables	Control Variables	Comments
1. ACO	Maximum profit eqn. (8.6)	1. Vibrations 2. Power 3. Time limit 4. Speed and Feed range	1. Force 2. Vibrations	1. Cutting speed 2. Feed	Independent of cutting conditions however limited to carbide tools	Maximum profit eqn. (8.6)	1. Vibrations 2. Force	1. Force 2. Vibrations 3. Temperature at important points	1. Cutting speed 2. Feed	Compensation for tool wear and temperature changes should be carried out. Surface roughness checked.
2. ACC	constant tool wear rate eqn. (8.11)	1. Vibrations 2. Power 3. Time limit 4. Speed and feed range	1. Force 2. Vibrations	1. Cutting speed 2. Feed	Tool life is monitored through eqn. 8.11. Tool breakage is detected by a sudden jump in tool force. Limited to carbide tools.	-	1. Vibrations 2. Force	1. Force 2. Vibrations 3. Temperature at important points.	1. Cutting speed 2. Feed	Same as above.

Table 8.3 Proposed Adaptive Control Systems

The ACC systems proposed for roughing and finishing cuts are summarised in table 8.3.

In all the above proposed systems, vibrations are measured and the cutting conditions changed to keep the vibration amplitude below a certain level. Most of the time this will decrease the metal removal rate quite considerably. Therefore, an alternative method of suppressing the vibrations should be found. In the following section, active structural control is analysed as a remedy to decrease the vibration amplitudes.

8.6 Active Chatter Control:

The proposed solutions to the chatter problem have largely been concerned with redesign of the machine structure and with the use of tuned vibration absorbers to reduce chatter amplitude. These are all passive methods, so their application is related to specific machine tools and to very specific conditions of chatter.

Adaptive control has also been used to control machine tool chatter (133). However, in this method cutting parameters are changed to decrease chatter, resulting in lower metal cutting rates. The purpose of active control is to increase the metal removal rates without reducing the relative stability of the controlled machine tool system.

Active control of chatter has been analysed by Nachigal and Comstock (137), (138). In order to prevent chatter, they measured and controlled the movement of the tool. However, this necessitates a special tool holder with a "floating" tool and a hydraulic force application unit, and is therefore, not very practical.

Here, a new approach to chatter control developed in this work will be described. As pointed out in chapter 4, there are some parts of machine tools which are especially prone to vibrations. Tailstock and spindle assembly are the most important areas. Chatter is usually a limiting factor for centre turning of long workpieces, and this is mostly caused due to the weakness of the tailstock. If the stiffness of the tailstock can be changed in an on-line manner to minimize the deflections and the amplitude of vibrations, the effects of chatter can be eliminated. This can be achieved by applying active force control on the tailstock. Employing a state variable control system, it should be possible to add stiffness and damping to the tailstock, therefore prevent chatter. This method also can compensate for the low damping of antifriction guideways enabling the manufacturers to use standard antifriction guideways even for heavy machine tools.

The control strategy will be illustrated on a tool holder model given in reference (75). Bell measured the frequency response of a tool holder on anti-friction guideways and developed a model for the system. It is shown in fig. 8.3.

The dynamic equation of the system can be written as follows,

$$M\ddot{X} + C\dot{X} + 4k_R X = 0 \qquad (8.16)$$

If a controlling force U is applied, the above equation can be written in state variable form as,

$$\underline{\dot{X}} = \underline{A}\,\underline{X} + \underline{B}\,\underline{U} \qquad (8.17)$$

where $\underline{\dot{X}} = \begin{vmatrix} \dot{X}_1 \\ \dot{X}_2 \end{vmatrix}$

$$A = \begin{vmatrix} 0 & 1 \\ \frac{-4k_r}{M} & 0 \end{vmatrix}$$

$$B = \begin{vmatrix} 0 \\ \frac{1}{M} \end{vmatrix}$$

In the above equations, $X_1 = X$ and $X_2 = \dot{X}$.

According to the optimum control theory, assuming a performance index of the form,

$$P.I. = \int_0^{\infty} \underline{X}^T\,\underline{Q}\,\underline{X} + \underline{U}^T\,\underline{P}\,\underline{U} \quad dt \qquad (8.18)$$

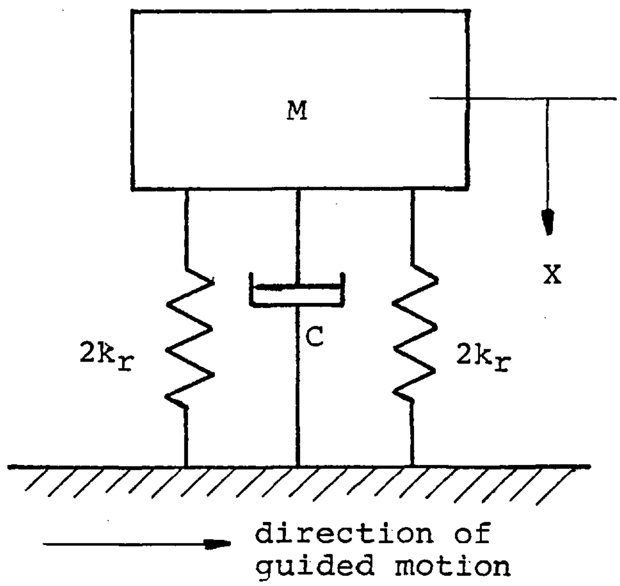

$M = 434$ kg
$4\,k_r = 8.82{*}10^8$ N/m
$C = 3.88{*}10^4 \; \frac{N}{m}$ sec

Fig 8.3 The lumped element representation of the tailstock and the guideway system it is possible to find an optimum control vector,

$$\underline{U}^{o}\ (X) = -\underline{K}^{T}\ \underline{X} \qquad (8.19)$$

where K^T is found by solving Kalman's equation,

$$\left\{\underline{I} + \underline{D}\ \underline{K}^{T}\ \underline{\phi}\ (s)\ \underline{B}\ \underline{D}^{-1}\right\}^{2} = \underline{I} + \left\{\underline{\gamma}^{T}\ \phi\ (s)\ \underline{B}\ \underline{D}^{-1}\right\}^{2} \qquad (8.20)$$

where

$Q = \gamma\gamma^{T}$

$P = DD^{T}$

$\phi(s) = sI-A$

Kalman's equation assumes that the plant and the performance criteria are time invariant (115). Therefore, it will be assumed that stiffness and damping characteristics will not change with time. Q and P matrices in eqn (8.18) are a measure of the system performance. Q for a second order system can be determined by building a first order idealized model, then P is a measure of the effect of the control. For p = 0 idealised model is achieved, however that requires theoretically an infinite control force. For this particular problem, assuming a settling time for 1 msec, the following P and Q matrices can be chosen,

$$P = 0.1$$

$$Q = \begin{vmatrix} 3*10^{15} & 0 \\ 0 & 3*10^{9} \end{vmatrix}$$

For this system eqn (8.20) becomes,

$$\left| 1 + \frac{1}{\eta} \; \frac{1}{M} \; (k_1 + k_2 s) \right|^2 = 1 + \left| \frac{1}{\eta} \; \frac{1}{M} \begin{bmatrix} \gamma_1 \\ \gamma_2 s \end{bmatrix} \; \frac{1}{p} \right|^2 \qquad (8.21)$$

where

$$\eta = s^2 + \frac{sc}{M} + \frac{4k_R}{M}$$

$$\gamma_1 = \sqrt{1*10^{15}} \quad \text{and} \quad \gamma_2 = \sqrt{1*10^{9}}$$

and k_1 and k_2 are the elements of matrix $\underline{K}$.

Noting,

$$\left| m(s) \right|^2 = m(-s) \; m(s)$$

Equation 8.20 gives,

$$k_1 = -k \mp \sqrt{k^2 + \frac{\gamma_1{}^2}{p^2}} \qquad (8.22a)$$

$$k_2 = C \mp \sqrt{C^2 + k_1 \, m + \frac{\gamma_2{}^2}{p^2}} \qquad (8.22b)$$

where $k = 4k_R$

Substituting the variables into the equations 8.22a and 8.22b, and taking the positive values,

$k_1 = 1.56*10^8$ N/m $\qquad k_2 = 6.46*10^5$ N/m/s

Then the equation of the controlled system can be written as,

$$434\,\ddot{X} + 6.82\,*10^5\,\dot{X} + 1.04 * 10^9\,X = 0 \qquad (8.23)$$

The dynamic stiffness of the model and the controlled system is shown in fig. 8.4. In the same figure, the dynamic stiffness of the original system as taken from reference (75) is shown. From the figure, it is seen that the model closely approximates the original system. What is more significant is the high damping and high dynamic stiffness imposed on the system through a force control.

This theoretical consideration shows that by using active force control it is possible to increase the dynamic stiffness of the cross slide. The method can be very useful for chatter control. However, in the analysis, no time lag in the force application loop has been assumed. Therefore, before any experimental study, a more detailed analysis including the response time of the actuator system should be performed. (139).

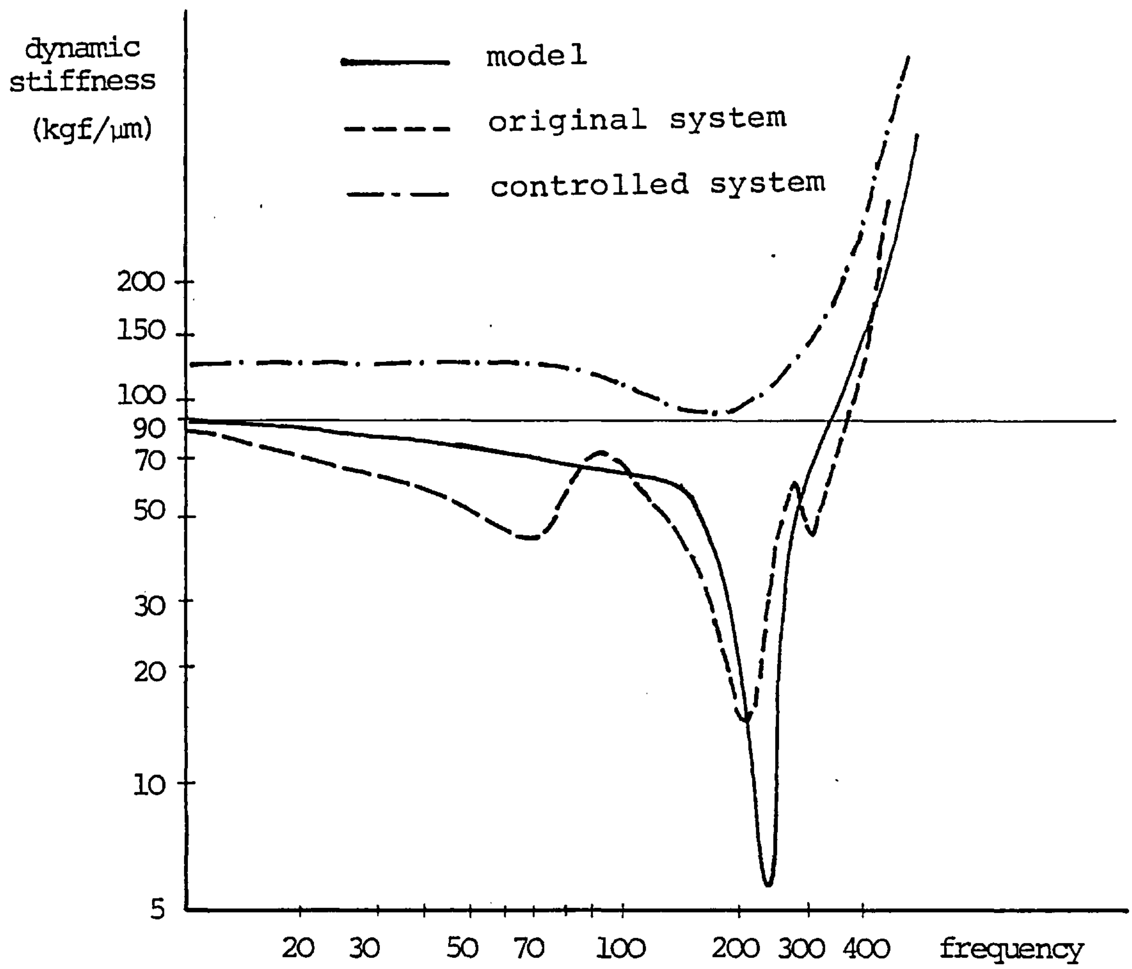

Figure 8.4 Dynamic stiffness for the controlled system

8.7 Discussion and Conclusions

In this chapter, existing tool wear sensors together with their limitations have been reviewed. Also, existing adaptive control systems have been discussed. Two AC methods, one ACO and the other ACC have been proposed. Both of them are superior to the existing methods, because they are independent of the cutting conditions. However, these methods are still limited to carbide tools. Also, in order to prove the feasibility of the methods, experimentation is necessary. Unfortunately, because of the lack of a proper CNC lathe, comprehensive AC experiments could not be performed. However, a simple force monitoring AC system was prepared and experimented with (please see appendix L). In this system, the tangential component of the cutting force was measured and the feedrate was changed to keep the force constant. Such a system is useful to sense the air gap in forgings and to increase the productivity. Such systems also exists in the literature (135).

Accuracy improvement is also a very important application of AC systems. The variables like temperature change or deflections of the workpiece should be evaluated and compensated for. Tool wear should also be measured and path of the tool should be changed accordingly. Although, the proposed AC systems can monitor the tool life and detect the tool failure, they can not estimate the actual value of tool wear properly. In eqn. (8.11), it is assumed that,

$$\frac{1}{d} \frac{dF}{dV_B} = k_2 H_B \qquad (8.23)$$

where k_2 and H_B are prone to variations. Therefore, to improve the system it is necessary to have an off-line tool wear sensor. Any of the off-line methods described in section 8.2 can be used for this purpose. The measurement can be used to correct the on-line tool wear method. Although the method will result in a more reliable AC system off-line measurement methods are usually expensive and increase costs. Therefore, conflicting with the requirement of providing a low cost system. Consequently, it would be advantageous to perform a wide range of experiments with the on-line tool wear evaluation method employed and use the results to estimate the tool wear. For example, from the experimental results, if a certain increase in cutting force (ΔF) is found to correspond to a certain tool wear, ($VB \pm \Delta VB$), the result can be used to compensate for the tool wear with an uncertainty of $\pm \Delta VB$. Although the method is cruder than off-line measurement, the system will have a lower cost because force measurement is usually easier. They can be found by measuring the current on the motor or through strain gauge dynamometers used in the machine tool.

In the light of the above discussion, the following conclusions can be made,

1. In the machine tool proposed here, compensation techniques and tool wear monitoring should certainly be applied. With a versatile control system as described in chapter 1, it should be possible to implement these economically.

2. In the second stage the suggested ACC system and then the ACO system should be implemented. However, more experiments and research into the tool wear evaluation is necessary to make these systems fully reliable.

3. Chatter can be controlled without decreasing the metal removal rate. However, more research is necessary on to the active chatter control as suggested in section 8.6.

CHAPTER 9

CONCLUSIONS AND FUTURE WORK

9.1 Conclusions

The objective of the project as set in chapter 1, was to analyse the state of the art of machine tool design, investigate the existing design techniques and procedures and their use in assessing the design of the machine tool structures and components. While carrying this out, a design methodology was to be developed and it was to be applied to produce an optimum outline design for a machine tool which would be versatile enough to make full use of a new multi-microprocessor control system. The overall design was to be low cost and to be suitable for both small workshops and bigger industrial plants.

The initial design concept was based on these ideas. As seen in figure 1.7, the resulting machine tool is very versatile. This versatility is achieved with minimum setting times, by providing turning and milling capabilities in such a manner that they can be performed independently. The versatility is also important for a cost effective design. Such a machine tool by adopting a modular approach can specify a wide range of requirements with minor changes in the components (fig. 1.7). This encourages the use of the same components on different machines, increasing the batch size.

After setting up the general configuration of the machine tool, a thorough survey of existing machine tool materials was carried out and concrete was selected for its high damping capability and low cost. It was found that the problem of its long term stability can be overcome if precautions are taken in both the design of the mix and the reinforcement configuration.

The finite element method was used for the static and dynamic analysis of the structure. Additionally, the boundary integral equation method was applied and assessed and a comparison was made between the two methods. It was found that except where surface to volume ratio is high, the boundary integral equation method is more economical than the finite element method. The results of the finite element analysis were used for the reinforcement calculations.

A structure below 2 tons was achieved so that the structure would not be too heavy for small workshops. High accuracy and high performance were still maintained by using heavier reinforcement around the regions where the stiffness can be important. In order to decrease creep and shrinkage doubly reinforced cross-sections were used. A cost comparison was also carried out. The cost for the concrete bed was quoted as £800-1000. A typical fabricated steel bed for a machine tool of similar size would cost around £1800 showing that reinforced concrete bed can be cheaper by 50%.

The dynamic analysis was based on the mode shapes and the natural frequencies. Frequency response curves were derived from these results and the effect of different parts of the structure on the overall dynamic stiffness was analysed. This method gave a more economical approach to the problem than frequency response methods. The results showed that the main modes were associated with the supports and the inclined plane; strengthening them would make the structure dynamically stiffer. However, it was considered that high damping of concrete and the heavier reinforcement used around these regions would result in a satisfactory dynamic stiffness. The analysis was also used to determine the support configuration. Three support configuration gave natural frequencies near to the higher range of the spindle speed, therefore five support configuration which raised the lowest frequency by about 100% was chosen.

Existing types of slideways were fully analysed. It was seen that the rigidity of the slideways changes according to the direction and application point of the load and the direction in which the deflections are important. Therefore, for a comprehensive comparison, finite element analysis was used and plastic coated plain slideways were compared with three types of anti-friction guideways. Out of the three directions analysed, plain slideways gave better results in two directions, perpendicular to cut direction and z-direction (see fig. 3.15), in the first 2 times in the latter 10 times stiffer than the next stiffest slideway. In the third direction (y-direction) line contact ball type guideways were 100% stiffer than the plain slideways. These results when taken with the superior dynamic properties of plain slideways indicate that the plain slideway system provide the optimum combination of characteristics. The effect of the structure on the static behaviour was also analysed using finite element methods. It was seen that the overall deflections were decreased by about 1.5 to 5 times by making the machine tool completely rigid. The sections need to be strengthened appeared to be the recesses at the base and the supports. This analysis further justified the use of heavier reinforcement around these sections.

A thorough analysis of the spindle and the feed drive systems was carried out. Hydraulic systems appeared to have excellent characteristics, such as high response rate, good disturbance behaviour. Consequently, they were analysed in more detail. Some experiments were carried out with low cost servo valves in order to assess the feasibility of using such valves to produce a very economical system. However, it was found that the speed range (30:1) was insufficient for machine tool applications.

Because hydraulic system design is usually complicated and requires extensive experimentation; a theoretical method for the design of microprocessor controlled hydraulic systems was established and it was validated by comparison with experimental results obtained from a closed loop hydraulic circuit driving the spindle of a prototype lathe. The performance of the closed loop hydraulic circuit was found to be satisfactory. A theoretical analysis carried out for open loop systems also showed that it is possible to build hydraulic circuits with suitable performance and with a lower cost than electrical systems. However, the level of advantage is probably insufficient to overcome the market resistance which exists at present and electrical systems using DC motors would appear to be the best alternative. Finally, to aid the design of each systems an algorithm for the selection of servo motors and the amplifier was prepared.

It was established that adaptive control should be a feature of this new machine tool. Existing tool wear sensors were analysed and tool wear sensing through force measurement was found to be the most promising method. A method which uses force measurement and which makes tool wear monitoring independent of cutting conditions was proposed. It was shown that active control techniques present a possible method which can be used both to prevent chatter and to increase damping in guideways.

9.2 Recapitulation:

A good theoretical approach to machine tool design is invaluable because it decreases the time spent for prototype testing which is usually expensive and time consuming. It also helps in obtaining the right design the first time decreasing the overall cost of a project.

In this project a systematic approach to machine tool design was established. The result is a sound theoretical method which needs a general finite element program and some additional small algorithms and computer programs. The approach is especially useful, because it is independent of any specialised program packages; this allows even the small establishments to use the method.

The method was applied for the outline design of a machine tool proposed in the first chapter. The machine tool was to employ a multi-processor control system, should have a high performance with a lower cost than the same range of machine tools. The principles set to achieve this was a versatile and modular design for the machine tool, a reinforced concrete bed and the employment of compensation techniques to improve the accuracy. The systematic approach adopted in this project made a sound analysis of the design possible.

9.3 Future Work:

Research and development in machine tools can be analysed in three broad categories. They are summarised in fig. 9.1. In this work, the problems associated with machine tool hardware and adaptive control have been investigated. Therefore, only the future work in these two subjects will be considered.

There is a considerable research being conducted to increase the damping capacity of anti-friction type of guideways. This is especially important to eliminate vibrations during cutting. In chapter 8 the idea of using active control to compensate for chatter was discussed. If this idea can be realised, the anti-friction guideways can be used without any problems. With anti-friction guideways and with active control of chatter the cutting times can be decreased increasing productivity. Anti-friction

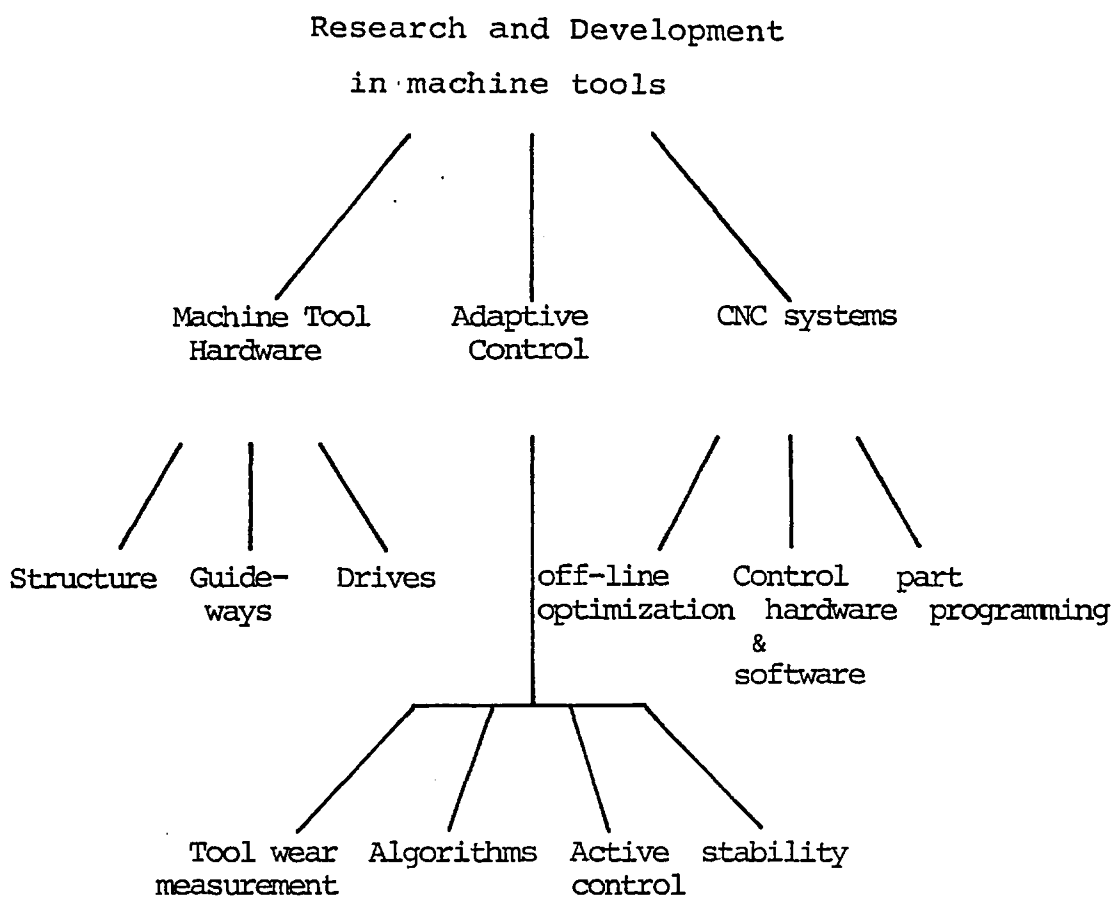

Figure 9.1 Research and Development in Machine Tools

guideways also help in obtaining a more modular machine tool. Therefore, both experimental and theoretical research should be conducted in active control.

Active control can also be used to produce some lightweight, structurally simple machines. For example, two shafts can be mounted on two steel side panels. With a tool slide mounted on them, normally it is impossible to do any reasonable cutting. However, if these shafts are supported by actuators whose force output is controlled via an active control algorithm that compensates for the vibrations and deflections, the picture will be different. Such a method has been used in civil engineering applications to control the deflections of a bridge (68). However, with machine tools, it is more complicated because of the higher frequency of vibrations (200-300 Hz). With the rapid advance of microprocessor technology though, it might be possible to achieve a "flexible machine tool" with active control. Then the benefits will be substantial.

A further area where research is necessary is the adaptive control of machine tools. In chapter 8, the existing methods were discussed and new algorithms proposed. These algorithms need to be tested by extensive experimental research. A great deal of effort is also required to find a suitable transducer to measure the tool wear in an on-line manner.

Compensation techniques, although simple in theory are likely to give rise to complications in practical applications. Consequently, research is required into techniques of measuring forces, deflections, vibrations and temperature on machine tools, so that such measurements may be used to estimate the tool tip errors. Compensation could then be employed to improve the accuracy.

Appendix A

A.1 Elastic Properties of Concrete:

Concrete is not a truly elastic material. When the stress/strain relationship for concrete is analysed it is seen that although the curve starts roughly as a straight line at the origin, as the stresses increase, and long before failure, the strains increase non-linearly. Therefore, when one talks about the modulus of elasticity of concrete it is really the "instantaneous elastic modulus" which is usually defined according to the initial tangent to the stress-strain curve. Elastic modulus is approximately proportional to the product of compressive strength and the density of concrete in question (24).

A.2 Creep and Shrinkage of Concrete:

The instantaneous stress/strain curve for concrete is a straight line and if the stressing force is then instantaneously removed the specimen will recover almost to its original length with no permanent set. However, if the stressing force is applied slowly, or if the stress is allowed to persist, additional and permanent strains will develop over a period of years, the rate of development of these additional strains reducing with time. It is these strains additional to the instantaneous elastic strain which are known as <u>creep</u>. While creep is dependent on the externally applied stresses, shrinkage is the type of volume change that occurs during the hardening process completely independent of the externally applied stresses.

There are many factors which affect the creep and shrinkage:

i) Influence of Stress:

Within the range of working stresses, creep is proportional to the applied stress. At higher stress-strength ratios, (0.4 to 0.6) creep increases at an increasing rate.

ii) Influence of Age at loading:

Age of concrete at loading is a factor in creep in so far as age influences the degree of hydration during the curing operation. Under conditions such as that the degree of hydration remains substantially constant, the age at loading ceases to influence creep. Besides, the influence of loading age on creep does not change greatly after about 28 days.

iii) Influence of Aggregate:

The volumetric content of aggregate is of considerable influence on the magnitude of shrinkage and creep developed by concrete. Experiments show that as the volumetric content or modulus of elasticity of aggregates increases, the creep and shrinkage decreases (26).

iv) Influence of Cement:

Although it is still controversial, it is believed that the finer the cement is the higher the shrinkage and creep becomes. Also shrinkage increases with cement content.

v) Influence of Strength:

Creep is inversely proportional to the strength of concrete. Creep, therefore, increases with an increase in the water-cement ratio of the mix.

vi) Influence of size:

As volume to surface ratio increases shrinkage and creep decreases. Theyalso decrease with an increase in size of the specimen, but when specimen thickness exceeds about a meter no further effect is apparent.

vii) Influence at Ambient Humidity:

As relative humidity where concrete is stored increases, creep and shrinkage decreases.

viii) Influence of Reinforcement:

A good reinforcement design is important to decrease the effects of shrinkage and creep. The following rules can be set for a good reinforcement design.

a) The reinforcement should be symmetrical.

b) Compression steel should be used where shrinkage and creep effects are undesirable.

c) Reinforcement should be moderate, as reinforcement increases so does the curvature due to shrinkage.

d) Reinforcement should not be very close to the surface. The farther the reinforcing steel from the neutral axis, the higher is the shrinkage curvature.

There are several methods to estimate creep and shrinkage of concrete. A set of equations obtained after long theoretical and experimental studies are given in reference (24). They are summarised in the following section.

A.3 Equations for creep and shrinkage estimation

Loading age of 7 days for moist-cured concrete,

$$C_t = \frac{t^{0.60}}{10 + t^{0.60}} C_u \qquad (A.1)$$

$$(E_{sh})_t = \frac{t}{35 + t} (E_{sh})_u \qquad (A.2)$$

Loading age of 1.3 days for steam-cured concrete,

$$C_t = \frac{t^{0.60}}{10 + t^{0.60}} C_u \qquad (A.3)$$

$$(E_{sh})_t = \frac{t}{55 + t} (E_{sh})_u \qquad (A.4)$$

where,

C_t = creep coefficient (ratio of creep strain to initial strain)

C_u = ultimate creep coefficient (2.35 is the average)

t = time in days

$(E_{sh})_t$ = shrinkage strain

$(E_{sh})_u$ = ultimate shrinkage strain (780×10^{-6} cm/cm is the average)

After C_t is calculated, creep per unit stress can be calculated as follows

$$\delta_t = \frac{C_t}{E_{ci}} \qquad (A.5)$$

where E_{ci} is the instantaneous elastic modulus.

For several other conditions, the following correction factors should be applied to equations A.1 to A.4.

1. Loading ages later than 7 days for moist-cured concrete and later than 1-3 days for steam-cured concrete.
   Creep (C.F) = $1.25\ t^{-0.118}$ for moist-cured
   Creep (C.F) = $1.13\ t^{-0.095}$ for steam-cured

2. Ambient relative humidity greater than 40 percent,
   Creep (C.F.) = $1.27 - 0.0067H$ when $H > 40\%$

Shrinkage (C.F.) = 1.40 - 0.010H when 40% < H < 80%

Shrinkage (C.F.) = 3.00 - 0.030H when 80% < H < 100%

3. For thickness values between 15 and 35 cm.

   Creep (C.F.) = 1.10 - 0.00669T

   Shrinkage (C.F.) = 1.17 - 0.0114T

4. Percentage fines,

   Creep (C.F.) = 0.88 + 0.0024F (A.6)

   Shrinkage (C.F.) = 0.30 + 0.0140F for F < 50% (A.7)

   = 0.90 + 0.0020F for F > 50% (A.8)

   where F is the percentage of fine aggregate by weight.

5. Creep (C.F.) = 1.0 (A.9)

   Shrinkage (C.F) = 0.75 - 0.044B (A.10)

   where B is the number of bags of cement per cubic meter of concrete.

Of course, the calculations for creep and shrinkage are different when concrete is reinforced and it is used as a structural member ie, restrained. The following equations can be used to find the combined effect of creep and shrinkage (24),

$$\Delta_t = \Delta_{sh} + \Delta_{cp} = k_r \, T_u \, \Delta_i \qquad \text{(A.11)}$$

where

Δ_t is the creep plus shrinkage deflection

Δ_i is the initial deflection computed by an appropriate method

Table A.1 Multiplier T_u for creep and shrinkage

Concrete strength of 28 days	Average relative humidity; age when loaded								
	100%			70%			50%		
	< 7d	14d	> 28d	< 7d	14d	>28d	< 7d	14d	>28d
17 to 27 (N/mm^2	2.0	1.5	1.0	3.0	2.0	1.5	4.0	3.0	2.0
727 N/mm^2	1.5	1.0	0.7	2.5	1.8	1.2	3.5	2.5	1.5

For the period:	1 month or less	3 months	1 year	5 years or more
use:	25%	50%	75%	100%

of table values

T_u is the combined creep plus shrinkage coefficient (its values are given in table (A.1) and k_r is the given reduction factor which can be estimated as follows,

$$k_r = 1/(1 + 0.70\, A_{sc}/A_{st}) \qquad (A.12)$$

where A_{sc} and A_{st} is the areas of compression steel and tension steel respectively.

A.4 Thermal Properties of Concrete

Thermal properties of concrete affect its performance over long periods under varying conditions and are also of vital importance in planning concrete constructions. The basic properties involved are: thermal conductivity, thermal diffusivity, specific heat, and the coefficient of thermal expansion.

a) Thermal Conductivity:

This measures the ability of the material to conduct heat and is defined as the ratio of the flux of heat to temperature gradient. The following factors affect the thermal conductivity (26),

i) Conductivity increases with the density of concrete

ii) The lower the water content of the mix at the time of placing of the concrete the higher the conductivity of the hardened concrete.

iii) The thermal conductivity of aggregates greatly differs. Therefore, the selection and the volume of aggregate affect the conductivity of concrete as well.

b) Thermal diffusivity and Specific Heat:
Diffusivity represents the rate at which temperature changes within a mass can take place and is thus an index of the facility with which concrete can undergo temperature changes. Diffusivity, δ is related to thermal conductivity K by the equation

$$\delta = \frac{K}{cw} \qquad (A.13)$$

where c is the specific heat and w is the unit weight of concrete. The range of typical values of diffusivity of ordinary concrete is between 0.002 and 0.006 m^2/hr depending on the type of aggregate used

c) Coefficient of Thermal Expansion:
It is a measure of the volume change of concrete as a function of temperature changes. The following factors affect the coefficient of thermal expansion;

i) The type and the volume of aggregate is an important factor. Not to have any differential movement between the aggregate and the surrounding paste, the coefficient of aggregate and the and the cement paste should be as near as possible.

ii) As the water content or the humidity increases the coefficient of thermal expansion increases as well.

APPENDIX B

Weight Calculation and Number of Supports.

The final dimensions of the bed of the machine tool is shown in figure B.1. If the unit weight of the concrete is taken as 2.4 kg/cm^3 (which can be estimated from the concrete mixture as chosen in chapter 2), the weight of the structure can be found to be 2862 kg. Once the dimensions of the structure is known, centre of gravity can be calculated quite easily; it is shown in figure B.1.

The next step is the determination of the number of supports. The most desirable configuration is usually three point support case, because the resulting structure is statically determinate and it is going to be independent of the inaccuracies of the foundation.

In figure B.2, the estimated weight of the several parts of the structure has been shown. For the support configuration shown in the figure, the reaction forces are found to be as follows,

R_A = 3116.4 kg

R_{B1} = 1511.35 kg

R_{B2} = 404.25 kg

That particular support configuration has been found after several trials and seems to be satisfactory.

The final support configuration will be determined after the static analysis and dynamic analysis of the structure.

Although the above structure seems to be satisfactory, it may be found that it is too heavy for some machine shops. Therefore, an alternative structure has been designed with a weight of just under 2 tons. The structure has been shown in figure B.3. The reaction forces on the supports for the new design are given below,

R_A = 2181 kg

R_{B1} = 1400 kg

R_{B2} = 502 kg

The calculations have been repeated for several locations of the slide and they have been found to be satisfactory.

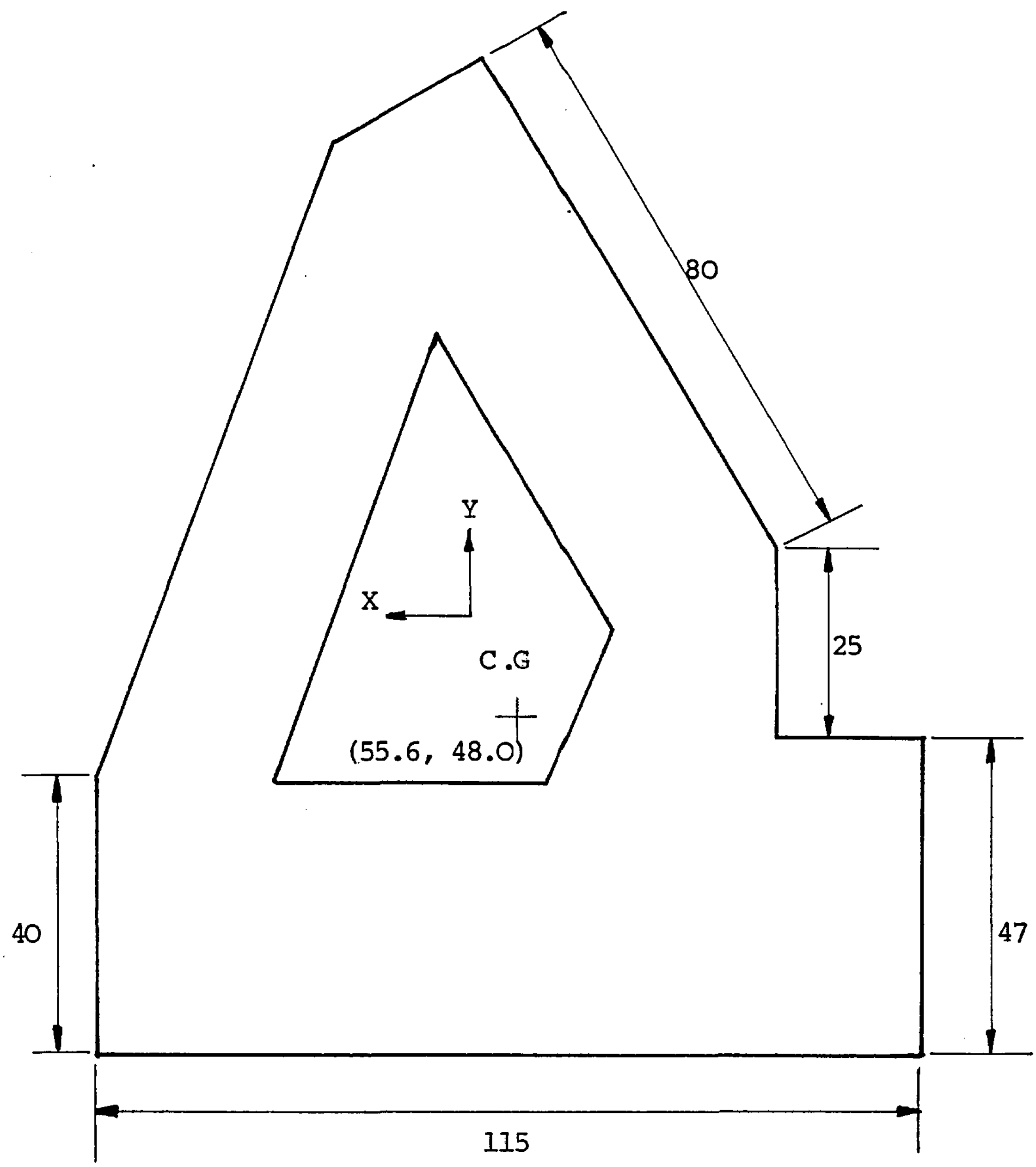

W_T = 2862 kg

Figure B.1 Overall weight and centre of gravity of the structure (units are in cm)

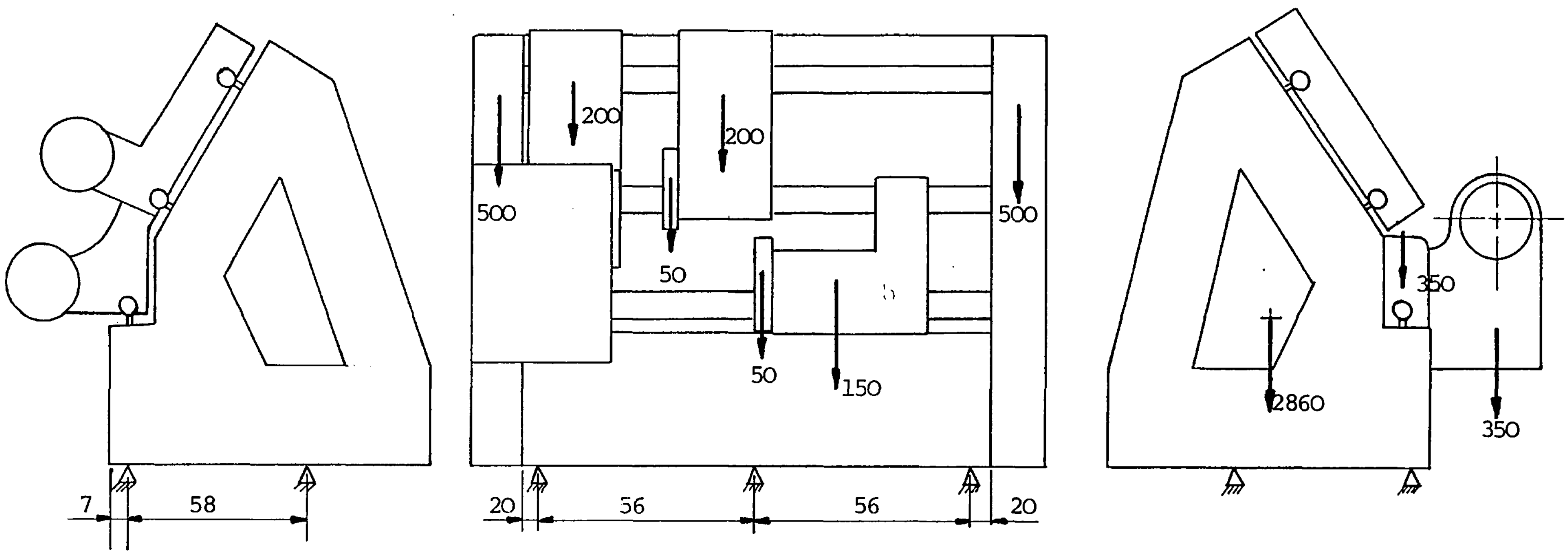

Note: Weights are in kg, lengths are in cm.

Figure B.2 The structure and the dead weights

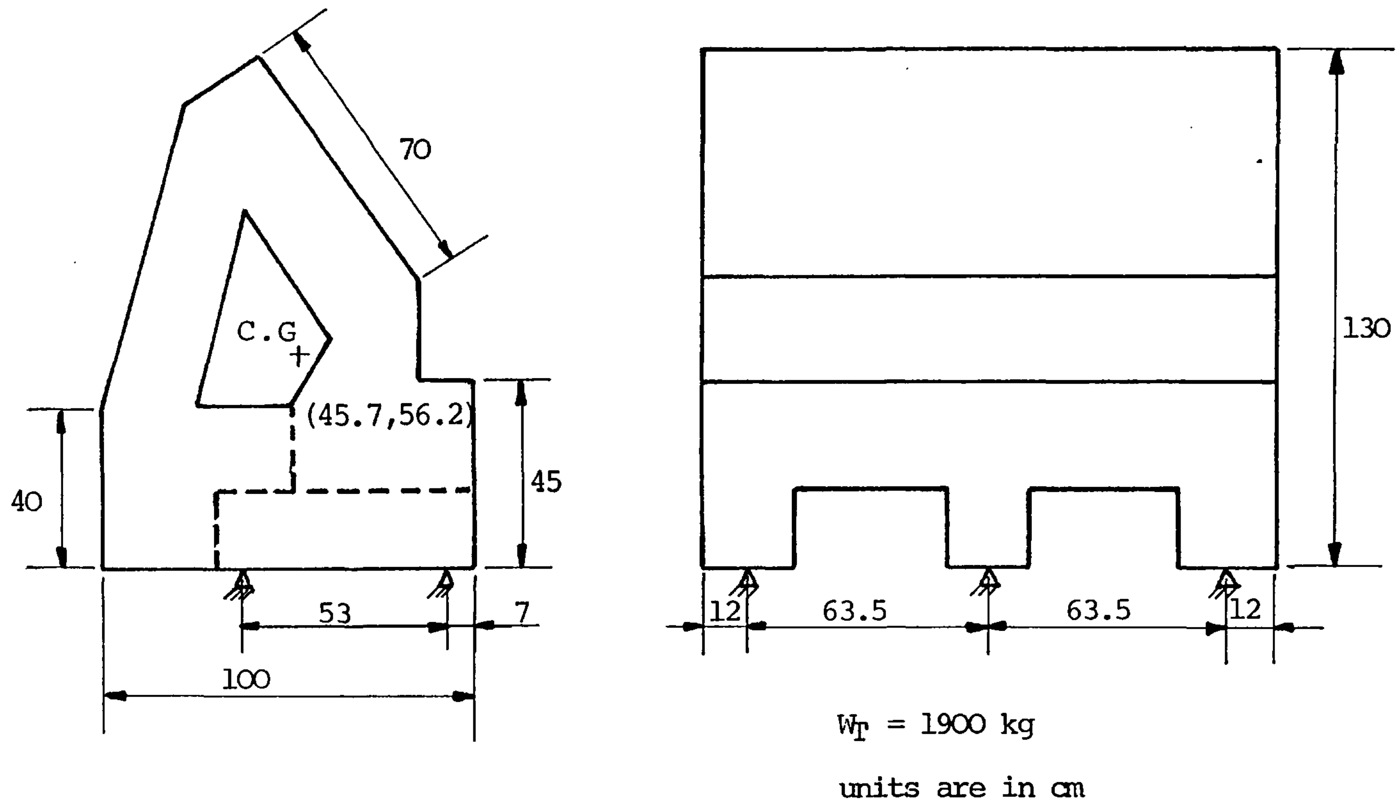

Figure B.3 The lighter structure

APPENDIX C

FORCES ACTING ON THE STRUCTURE

C.1 Introduction

The calculation of forces acting on the structure is a vital preliminary step in the static analysis. The forces which act on the various parts of a machine tool structure arise from:

1) the masses of the structural components
2) the masses of the fixtures and clamping devices
3) the mass of the workpiece
4) friction between moving parts
5) the cutting action.

For this particular application, because the friction is to be minimised, friction forces will not be taken into account. Also, the mass of the workpiece will be taken as negligible when compared with the cutting forces. Cutting forces are calculated according to the 15 hp requirement for turning and 2 hp for milling.

C.2 Dead Weights

The dead weights of several structural components have been estimated as follows,

a) Milling Head : 300 kg
b) Turning Slide : 250 kg
c) Tailstock : 200 kg

d) Headstock : 400 kg

e) Side panels : 500 kg (each)

C.3 Cutting Forces:

a) Turning

The three components of forces developed during a turning operation is shown in figure C.1 a) There is no fixed relation between the force components, P_x, P_y and P_z. A statistically established relationship between the forces has been given in reference (49). Using the relationship, $P_z \simeq 3 P_y$ and $P_y \simeq P_x$.

In the machinability tables (47) the following cutting conditions are given for cutting steel with HSS round nose cutting tools for a tool life of one hour,

d (depth of cut) = $2.54*10^{-2}$ m

f (feed rate) = $1*10^{-4}$ m/rev

v (cutting speed) = 70 m/min

In the same reference, the corresponding power for the cutting conditions is given as 10 kW, which is near to the power range the machine is to be designed at. The corresponding cutting force, then can be calculated by using equation C.1.

$$N = \frac{P_z . V}{6120} \quad (kW) \qquad (C,1)$$

therefore

$$P_z \simeq 845 \text{ kg.}$$

To be safe, P_z will be taken as 1000 kg. Then, from the above analysis, the following forces are assumed for static calculations.

P_z = 1000 kg

P_y = 350 kg

P_x = 300 kg

b) Milling

The cutting forces developed during the face milling operation are shown in figure C.1. The forces can be calculated either by estimating an average cutting speed and using equation (C.1), or by using the force equations as given below (48),

$$F_t = 81150 \; w.d^{0.80}.f^{0.69} \quad a)$$
$$F_f = 9960 \; w.d^{0.655}.f^{0.670} \quad b) \qquad (C.2)$$
$$HP = 0.5 \; nNw.d^{0.87}.f^{0.81} \quad c)$$

Where,

n = number of teeth,

N = the cutter speed in rpm,

w = width of cut (in)

d = depth of cut (in)

f = feed per tooth (in)

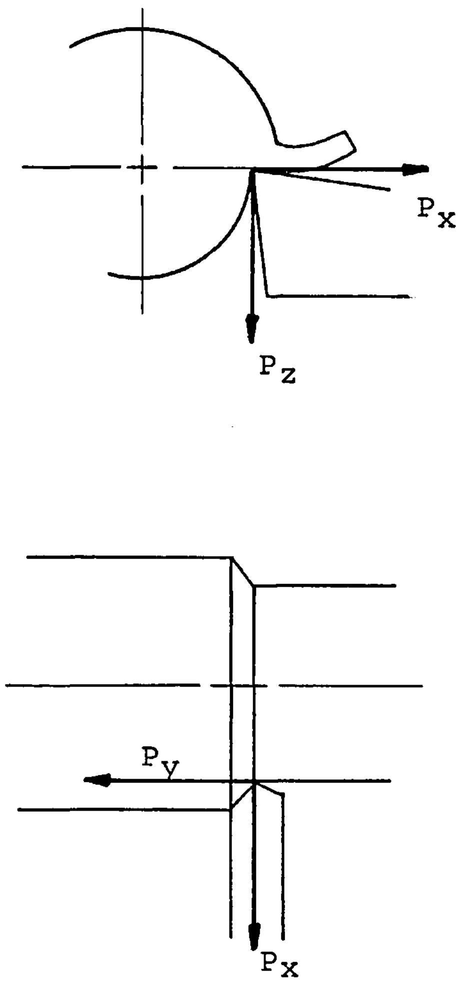

a) Turning

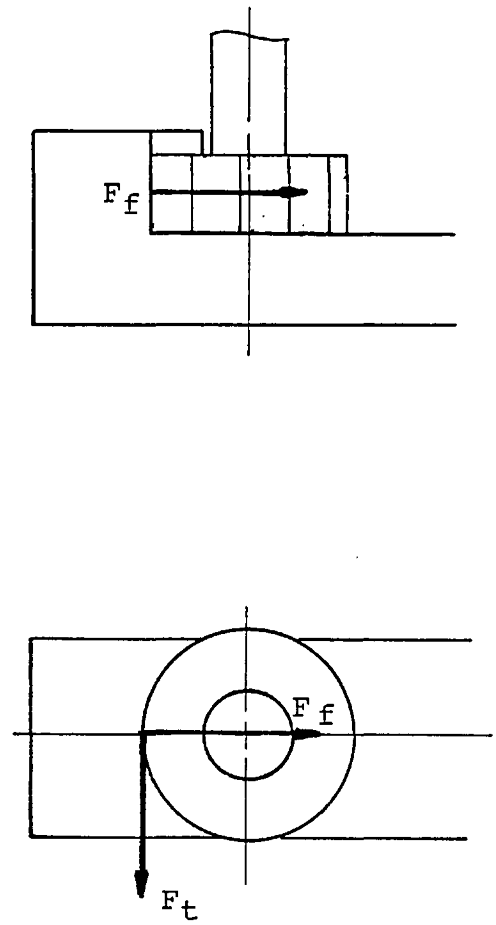

b) milling

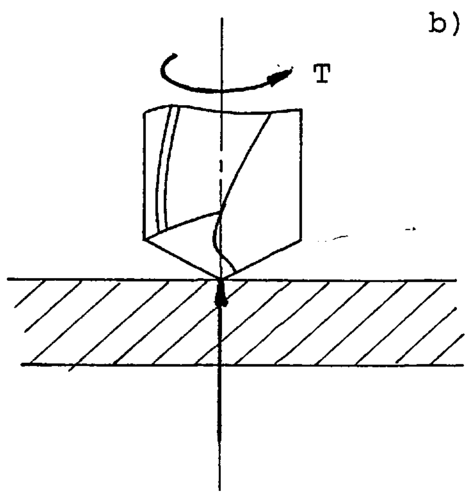

c) drilling

Figure C.1 Cutting forces in turning, milling and drilling

From reference (45), the following suggested values are taken,

$N = 800$ rpm; $n = 4$; $w = 1$ in ; $d = 0.15$ in

Then from equations (C.2),

$f = 0.002$ in per tooth

$F_t \approx 245$ lb $= 111$ kg

$F_A \approx 45$ lb $= 20$ kg

are found. These force values are smaller than the ones estimated for turning. Therefore, the governing forces for the stress calculations will be taken as the ones caused by turning. However, for the detailed analysis of the milling slide the forces due to milling and also drilling operations have to be calculated.

c) Drilling

In reference (48), the following values of thrust and torque for drilling steel are given, corresponding to a power of two horsepower.

Diameter of the drills = $\frac{3}{4}$"; $N = 300$ rpm;

$f = 0.012$ in/rev ; F (thrust) $= 600$ kg; Torque ≈ 534 kg-cm

For drilling by the end turret, a drill size of $1\frac{1}{2}$" (3.8 cm) will be taken. It is unlikely that drillings larger than this will be performed in one step. Then, in the same reference, the following cutting conditions and resistance values are given.

N = 150 rpm; f = 0.015 in/rev; F = 1360 kg;
Torque = 1990 kg-cm and the corresponding power is 5 hp.

C.4 Determination of Forces Transferred on to the Structure:

The forces acting on the structure will change according to the position of the cutting tool. Therefore, a few cases should be analysed and the design of the structure should be done according to the most critical condition (fig C.2)

There are two kinds of turning operations; one is between centres and the other is chucking. When the workpiece is turned between centres, some of the force is carried by the tailstock, so less force is transferred to the headstock. Taking these different aspects into account, three cases have been determined to be analysed. Simultaneous cutting is not included in the analysis, because then the forces on each turret will decrease by half and distribution will be more homogeneous. This case apparently is not as critical as others. End drilling is also omitted in the analysis. Although the forces involved in drilling are high, because of the large torque arms on the end slide (figure C.4), the effect of these forces will be low.

Below the calculations for case a) are given in detail, for cases b) and c) only the results are going to be indicated.

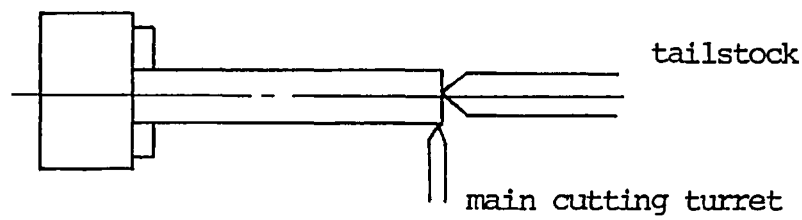

a)

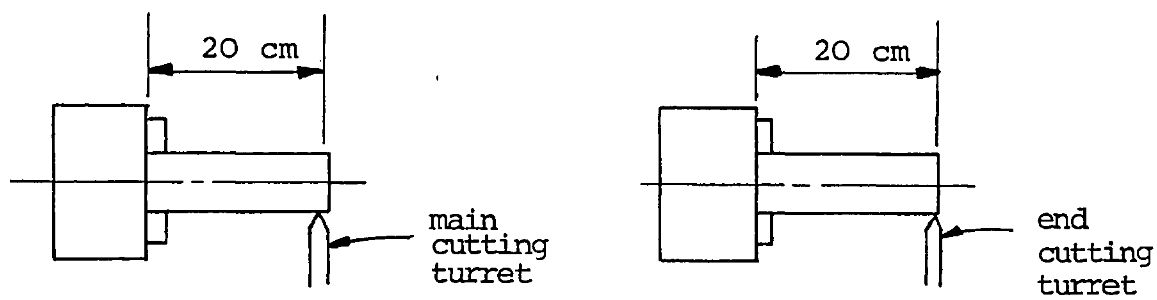

b) c)

Fig C.2 The cases to be analysed for turning operations

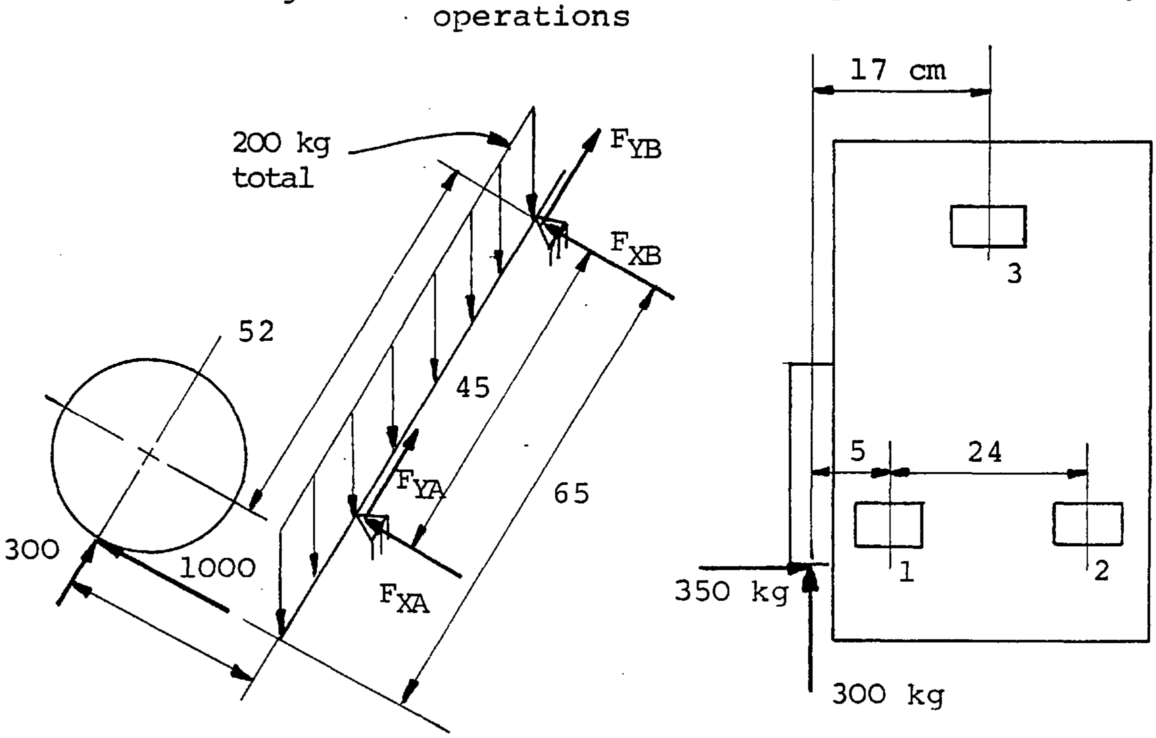

Fig C.3 The forces acting on the turning slide

a) Forces acting on the slideways;

First the forces acting on the slideways due to the main cutting turret will be calculated. The force configuration is shown in figure A.6. The force 1000 kg is considered to be acting upwards, because this is the most critical condition. In the figure, three point contact between the slideways and the slide is assumed. By using the equilibrium equations and assuming $F_{yA} = F_{yB}$, the forces are found as follows,

$F_{1x} = -1488.5$ kg $\quad F_{yA} = F_{yB} = -83.5$ kg

$F_{2x} = -36.5$ kg

$F_{3x} = 650$ kg

Secondly, the forces acting on the shaft through the end turret should be calculated. The forces acting on the end turret is shown in figure C.4. The problem is an indeterminate one, to solve the problem first $F_{1'x}$ then $F_{2'x}$ is assumed to be zero, then the average force values are found. The results are as follows,

$F_{1'y} = 1150$ kg $\quad F_{A'x} = F_{B'x} = -350$ kg

$F'_{2y} = 1950$ kg

$F'_{3y} = -250$ kg

b) Forces due to the headstock:

The spindle unit will be connected to the structure through a steel base as shown in figure C.5. For the first case, there will not be any cutting forces acting on the headstock,

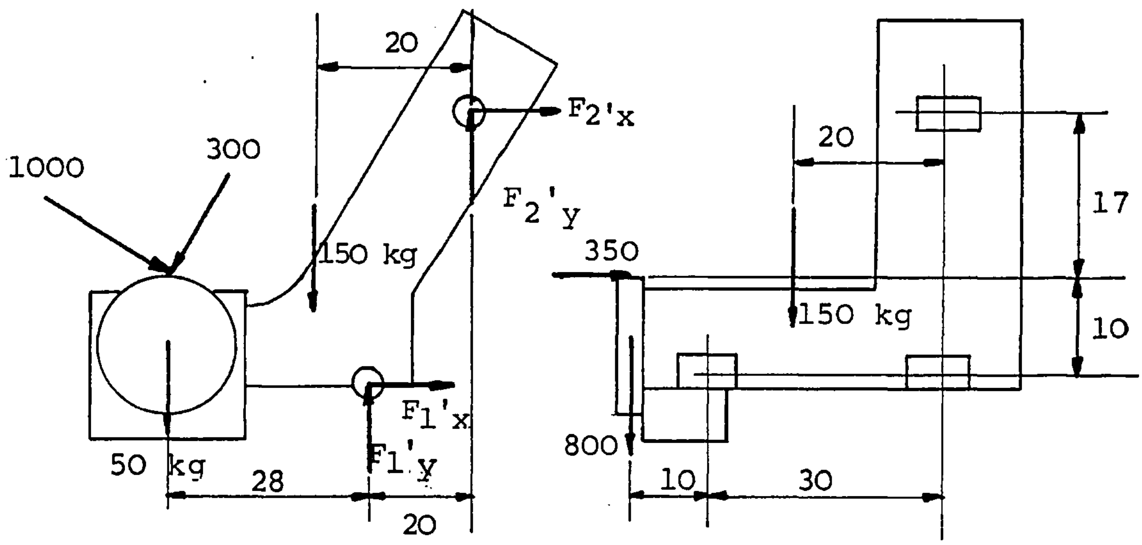

Figure C.4 The forces on the end turret

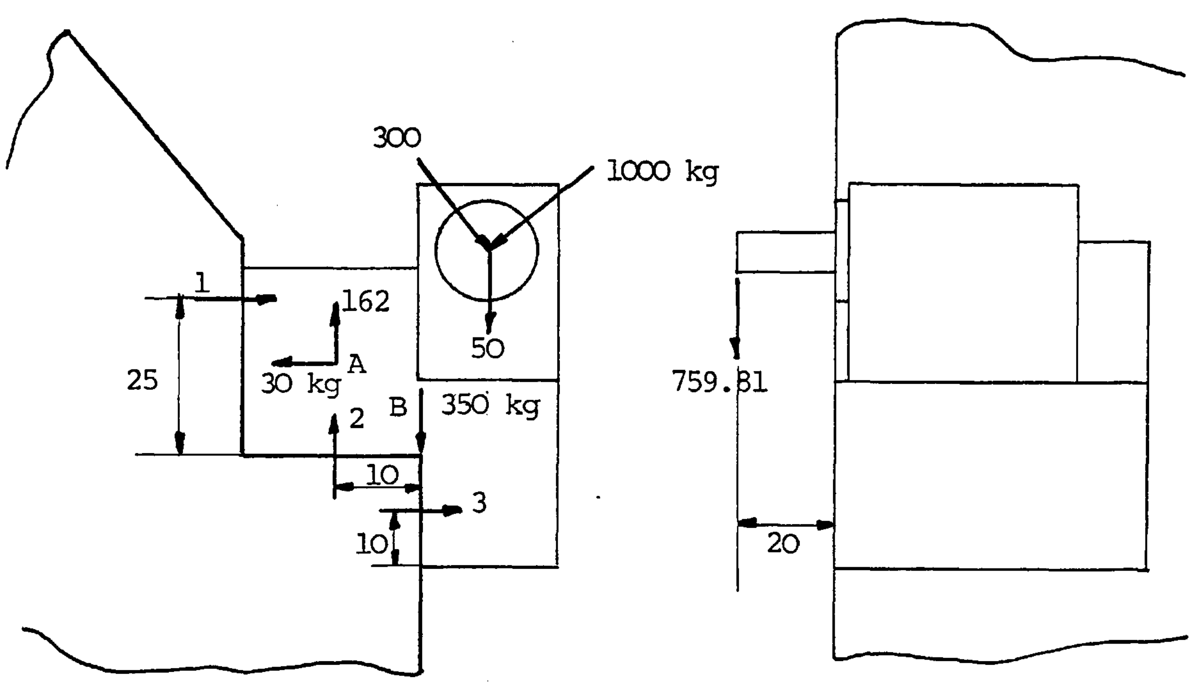

Figure C.5 The connection of headstock to the structure because it is assumed that the cutting forces are supported completely by the tailstock. The forces at point A are the forces transferred through the shaft of the tailstock. The weight of the spindle unit and the weight of the base are assumed to be 50 kg and 350 kg respectively. By using the equilibrium equations, the forces are found to be,

$F_1 = -108.6$ kg; $F_2 = 238$ kg; $F_3 = 138.6$ kg

c) The forces due to the side panels:

In case round slide ways are used on the machine tool, it is necessary to have steel side panels to support the shafts at the ends. The forces acting on the side panels due to the shafts have been given in part d).

If four supports are assumed for the side panels, the problem becomes an indeterminate one; in that case the best solution seems to be the finite element model. In the finite element model the side panels are approximated as beams as shown in figure C.6.

From the results of the finite element analysis, the moments at the supports C, D and E are found as follows,

$M = 9270$ kg-cm	Support C
$M = -785.7$ kg-cm	Support D
$M = -122$ kg-cm	Support E

By using the moment values as above, and the displacement values, the support forces are found as follows,

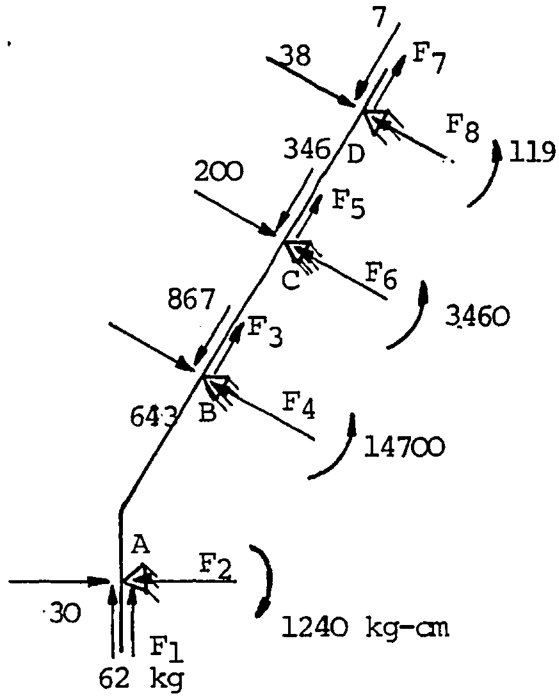

$A = 62\ cm^2$
$I = 4880\ cm^4$
$E = 2.1*10^6\ kg/cm^2$
$\mu = 0.3$

Figure C.6 Beam approximation for the side panels

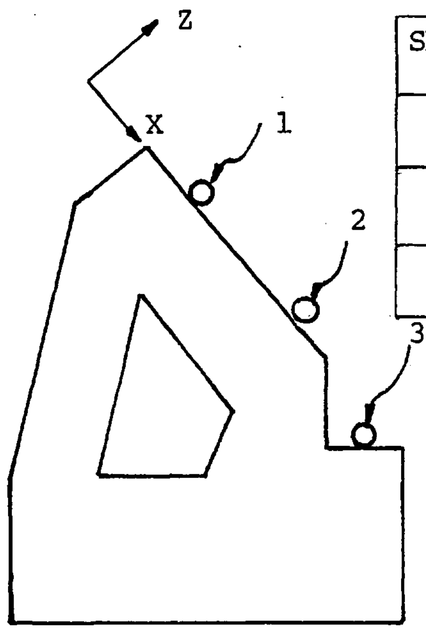

Shaft No	Support No	Max. deflection (mm)
1	4	0.0032
2	5	0.0026
3	4	0.0036

Figure C.7 Shafts and number of supports

F_1 = 100 kg ; F_2 = 172.8 kg

F_3 = 960.5 kg ; F_4 = 1060 kg

F_5 = 320 kg ; F_6 = −455 kg

F_7 = 7 kg ; F_8 = 60 kg

d) The forces transmitted through the shaft supports:

As slideways, if shafts are used, very probably some intermediate supports will be necessary. Therefore, for the purposes of stress analysis on the bed, the forces acting through the supports should be calculated. In case, a continuously supported slideway is used, still the results of the intermittent support slideway can be used, because it gives a safer analysis.

The minimum number of supports for each individual shaft has been determined by using deflection analysis. For the loading case finishing cuts were taken as the criteria. Deflections corresponding to different numbers of support were calculated by using the finite element program. The number of supports was chosen according to the allowable deflection set by the accuracy limit. Maximum deflections are shown in fig. C.7. The reaction forces corresponding to these supports can be found by using the three moment equation (47), or by using finite element methods. The results of the two methods are compared in table (C.1) for shaft number 2 (figure C.7).

Table C.1 Comparison of the results obtained from FE and three moment equation

Support	Three moment Equation (kg-cm) Mx	Finite Element Method (kg-cm) Mx
2	1129.8	1197
3	3850	3620
4	2879	2638

As seen from the table, the two results are in coincidence, so the finite element results can be used with confidence. The calculated reaction forces in direction x and z are given together with the rest of the forces in table (C.2).

To summarise the above analysis, the points where the forces are applied onto the bed are shown in figure C.8. There are three sets of forces applied at these points. The first set of forces corresponding to case a) (figure C.2) has been determined as shown above. The forces for cases b) and c) have been determined in the same way, and they are given in table C.2.

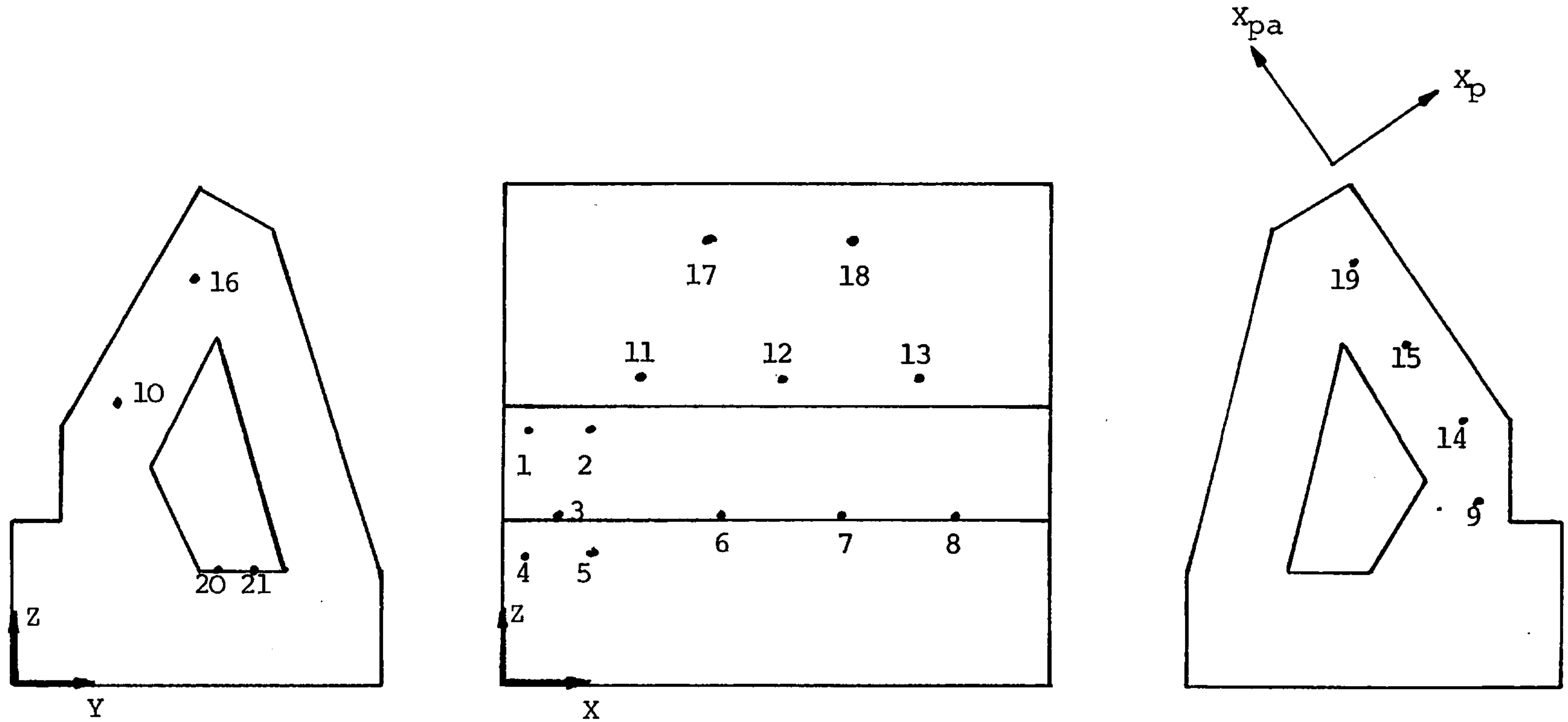

Figure C.8 The points of application of the forces

Table C.2 The forces acting on the structure

	case a (kg)	case b (kg)	case c (kg)
F_{1y}	50	210	210
F_{2y}	50	210	210
F_{3z}	-250	-998	-998
F_{4y}	-70	160	160
F_{5y}	-70	160	160
F_{6z}	-1300	55	-964
F_{6y}	200		-283.4
F_{7z}	-1350	-260	-1032
F_{7y}	250		-304
F_{8z}	300	+240	265
F_{8y}	-45		65
F_{9z}	100	32	-40
F_{9x}	150		
F_{9y}	-173		-10
F^*_{10p}	-130	-130	-275
F_{11p}	-9	-9	-150
F_{11pa}	-95	-95	60
F_{12p}	650	650	520
F_{12pa}	-95	-95	-304
F_{13p}	650	650	600
F_{13pa}	-200	-200	-283
F_{14pa}	960.5	960	50
F_{14p}	1060	1060	-100
F_{14x}	50	-150	
F_{15p}	-455	-455	-100
F_{15pa}	320	320	
F_{16p}	-130	-130	-250
F_{16pa}	-130	-130	
F_{17p}	-50	-50	-100
F_{17pa}	-100	-100	
F_{18p}	-650	-650	-50
F_{18pa}	-70	-70	
F_{19p}	71	60	-150
F_{19pa}	7	7	
F_{20z}	-75	-75	-75
F_{21z}	-75	-75	-75
F_{10pa}	-130	-130	

* For cases a and b, F_p is perpendicular to the inclined surface and F_{pa} is parallel, for case c they are in the z and y directions respectively.

APPENDIX D

REINFORCEMENT CALCULATIONS

Once some critical sections are determined, the average stress values for these sections can be found by using the finite element values. The reinforcement can then be calculated using the method in chapter 3. Area of the compression steel will be taken as equal to the area of the tensile steel because this will improve the creep characteristics as mentioned in chapter 2.

As seen in chapter 3, there are two alternative structures. To aid the comparison, the reinforcement calculations will be carried out for both. The critical sections for the two different structures are indicated in fig. D.1. As an example of the method used, the calculations for the section A.A of the first structure will be given in detail. The remaining results will be presented without detailed calculations.

In table D.1, the relevant stress values for the nodes of section A.A as found from the finite element analysis are given. The normal stresses to that section can be calculated easily by using the equation

$$S_n = \sigma_{xx}\, \ell^2 + \sigma_{yy}\, m^2 + \sigma_{zz}\, n^2 + 2\, \zeta_{xy}\, \ell\, m + 2\zeta_{xz}\, \ell m + 2\zeta_{yz} mn$$

knowing $\ell = 0$, $m = -0.5$ and $n = -0.866$, the equation becomes,

$$S_n = \sigma_{yy}\, 0.25 + \sigma_{zz}\, 0.75 + \zeta_{23}\, 0.866$$

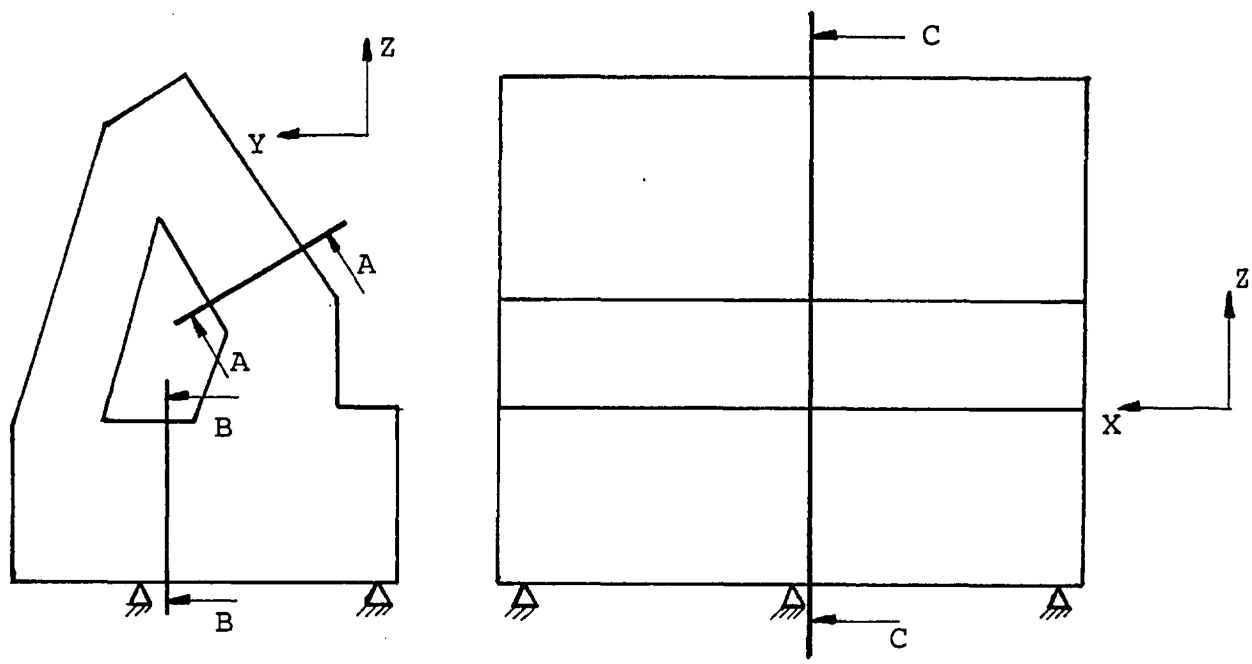

a) stiffer structure

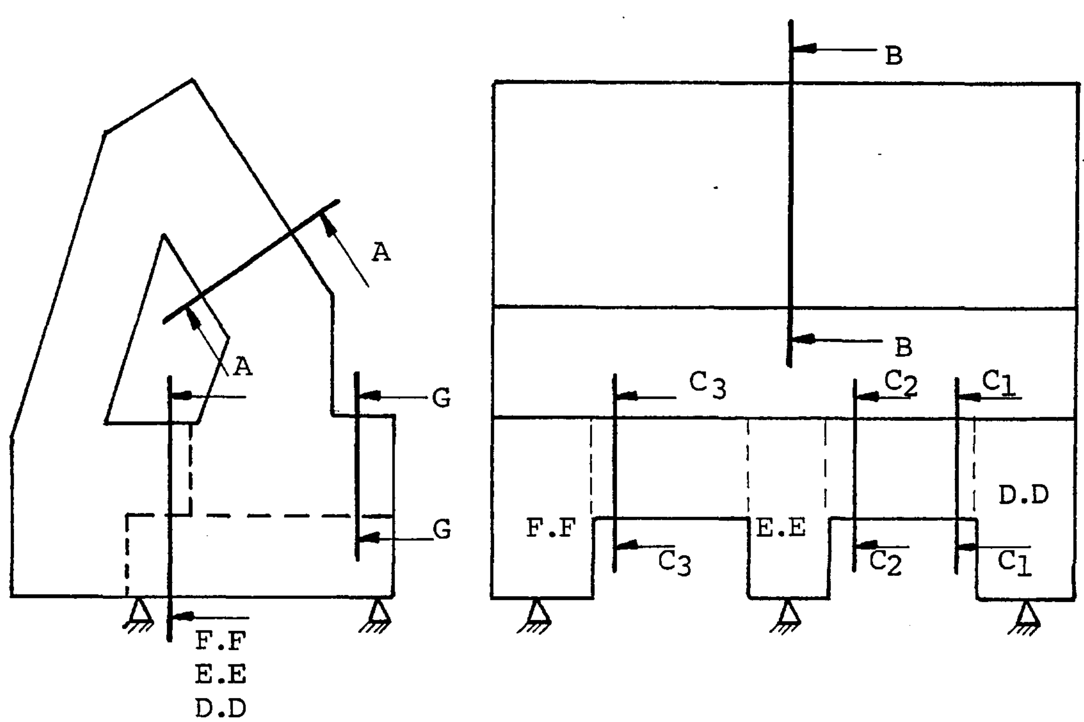

b) Lighter structure

Figure D.1 Critical sections for reinforcement calculations

The normal stresses are tabulated in table D.2. By using the average stress values given on the same table the stress distribution for the section can be shown as in fig D.2 .

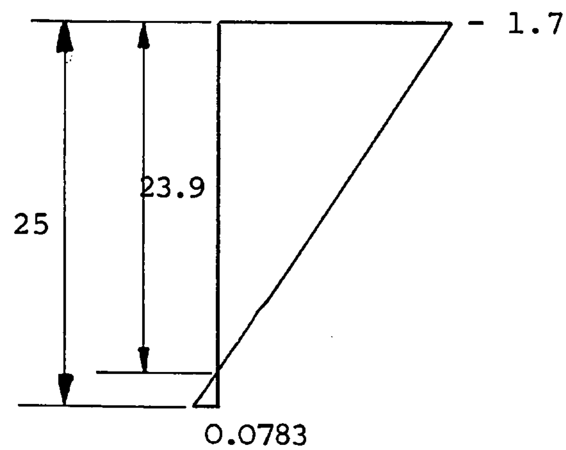

Figure D.2 Stress distribution on Section A.A

In the analysis, as a safety factor, it will be assumed that stress can be alternating. Therefore, regardless of its sign the bigger stress value will be taken as a base in the calculations.

Then,

$$F_t = A * \sigma = 23.9 * \frac{152}{2} * 1.7 = 3087.9 \text{ kg}$$

Taking the factor of safety as 2.5 and the allowable steel stress as 1270 kg/cm^2, the steel area can be found as,

$$A_{st} = \frac{F_t * F.S.}{f_{st}} = \frac{3078.9 * 2.5}{1270} = 6.06 \text{ cm}^2$$

The same section should be checked also along the column connections because these are the points where the stresses tend to concentrate. A similar analysis as above gives a steel area of 0.6 cm^2 at the columns.

In the same way as above, the steel areas required for other sections can be calculated. The results are summarised in table D.3. On the same table, the required number of bars and their diameters are also given. Fig D.3 gives the reinforcement details in a simple form.

The calculations for the lighter structure can be carried out in the same way. The critical sections for which the steel areas are calculated have been shown in fig D.1 b. The results for this structure have been tabulated in table D.4. For the calculations of lateral tie bars (stirrups), although some calculations have been made, they were not found to be critical, so some "rule of thumbs" given in the literature (25) have been used. The minimum recommended diameter for the lateral ties is 0.25 in, and the spacing should not be more than 16 bar diameters, 48 tie diameters or the least dimension of the column.

Nodes	S_{22}	S_{33}	S_{23}	Nodes	S_{22}	S_{33}	S_{23}	Nodes	S_{22}	S_{33}	S_{23}
110	-1.3765	-6.409	-0.0568	108	-0.0936	-1.737	-0.65865	109	-0.4204	-2.887	-0.0873
114	-0.8638	-4.006	-0.781	113	-0.0607	-0.5757	-0.323				
124	-0.101	-2.4135	-0.9167	122	-0.266	-0.1352	0.306	123	-0.1697	-1.365	-0.278
176	-0.2533	-1.73	-0.7453	175	0.0835	0.2	0.057				
186	-0.858	-1.2975	-0.438	184	-0.2453	0.7822	-0.247	185	0.523	-0.1348	-0.3
190	-0.2335	-0.3969	-0.5579	189	0.145	0.6834	0.0709				
200	-0.05965	0.1868	-0.505	198	-0.3673	0.8384	0.1308	199	-0.1845	0.2161	-0.0836
204	-0.0965	-0.2438	-0.4791	203	0.1995	0.672	0.1418				
214	-0.57715	-0.973	-0.286	212	-0.1225	0.7795	-0.0863	213	-0.3128	-0.0065	-0.1515
218	-0.2404	-1.025	-0.2491	217	-0.077	0.4394	-0.0196				
228	0.09286	-1.0996	-0.264	226	-0.1334	0.2784	0.0199	227	-0.1159	-0.4431	-0.123
230	-0.0748	-1.296	-0.1689	229	0.005	0.2562	-0.0386				
237	-0.1691	-1.6179	0.1144	235	-0.11	-0.0018	-0.0235	236	-0.1646	-0.7307	0.0593

Table D.1 Stress values on the cross section A.A (in kg/cm^2)

Table D.2 Stress values normal to the cross section A.A

Node	S	Node	S	Node	S
110	-5.2 *	108	-1.896	109	-2.346
114	-3.897	113	-0.727		
124	-2.629	122	0.097	123	1.307
176	-2.006	175	0.22		
186	-1.567	184	0.311	185	-0.492
190	-0.839	189	0.61		
200	-0.312	198	0.65	199	0.042
204	-0.6218	203	0.677		
214	-1.1217	212	0.479	213	-0.214
218	-1.0446	217	0.293		
228	-1.03	226	0.1927	227	-0.468
230	-1.137	229	0.16		
237	-1.157	235	0.049	236	0.038
av.	-1.7		0.0783		-0.76

* units are in kg/cm^2

Table D.3 Steel areas required at several sections of the first structure

	A (cm^2)	details of the bars (area)
section A.A	6.06	7ϕ42 (7.9)
section A.A at column	0.6	
section B.B	1.8	7ϕ6 (2.8)
section C.C upper plane	0.75	3ϕ6 (0.84)
section C.C at column	0.2	2ϕ6 (0.96)
section C.C lower plane	1.58	6ϕ6 (1.68)
Column	0.6	4ϕ8 bars with 7ϕ6 stirrups

Table D.4 Steel areas required at several sections of the second structure

	A	details of the bars (area)
section A.A	8.313	10ϕ12 (11.31)
section B.B	1.2	2ϕ12+3ϕ10 (4.6)
section C.C (max)	0.91	3ϕ12 (3.39)
section D.D	0.19	4ϕ10 (3.14)
section E.E	1.6	4ϕ10 (3.14)
section F.F	0.19	4ϕ10 (3.14)
section G.G	0.4	2ϕ10 (1.6)
column	0.6	4ϕ12 bars with 7ϕ6 stirrups

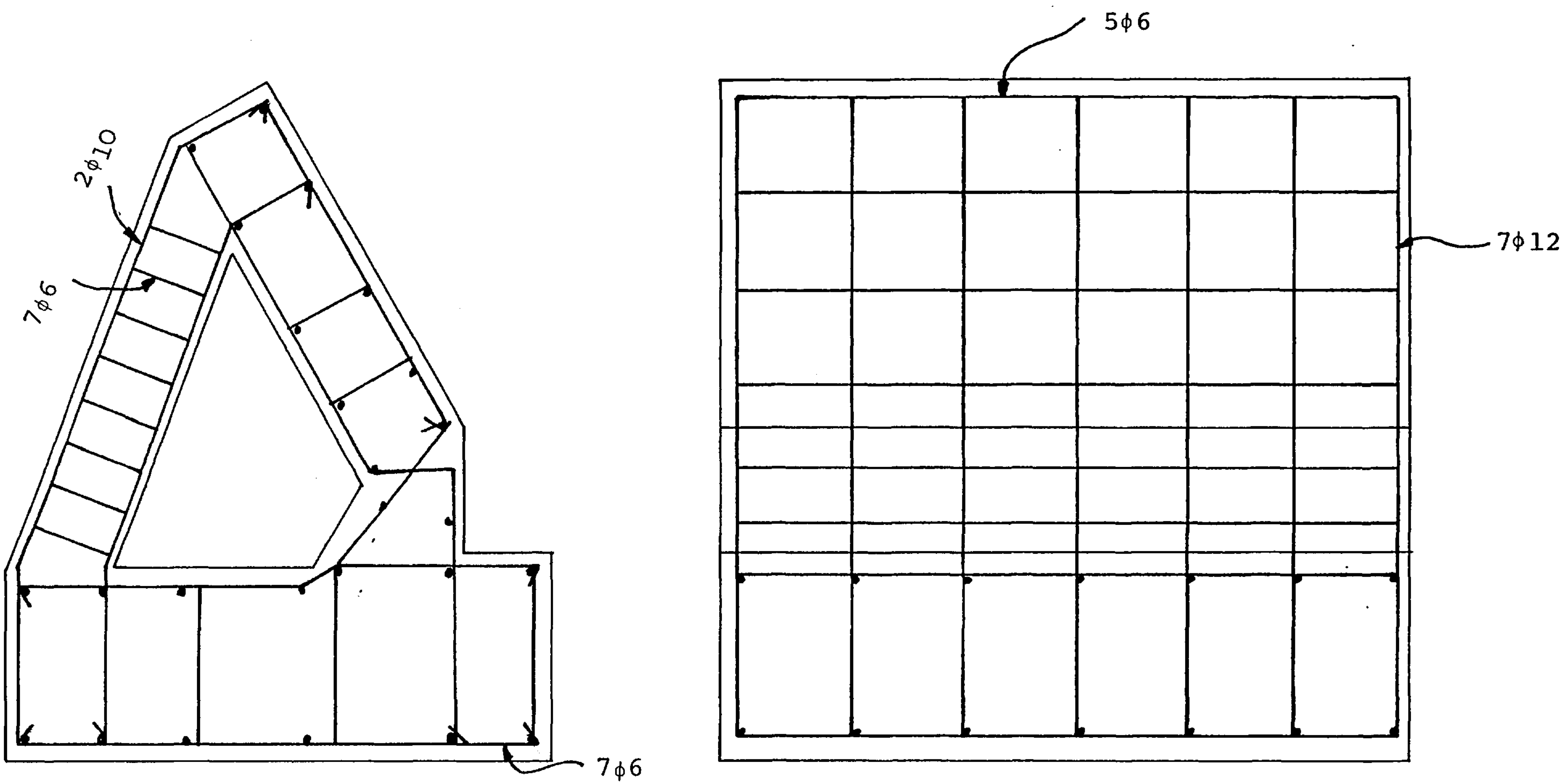

Figure D.3 Reinforcement for the first structure
units are in mm

APPENDIX E

INSERT AND ATTACHMENT CALCULATIONS

Separate plates will be cast on to the structure to provide connection points for the other parts of the machine tool. For the calculations, the maximum force values acting on one of the supports of the slideways will be taken as basis. The same plate size and anchorage dimensions will be used all over the structure.

The parameters for one of the plates are shown in figure E.1. The compressive strength of the concrete will be taken as 1000 psi (7 MN/m^2) because of the fatigue considerations for concrete.

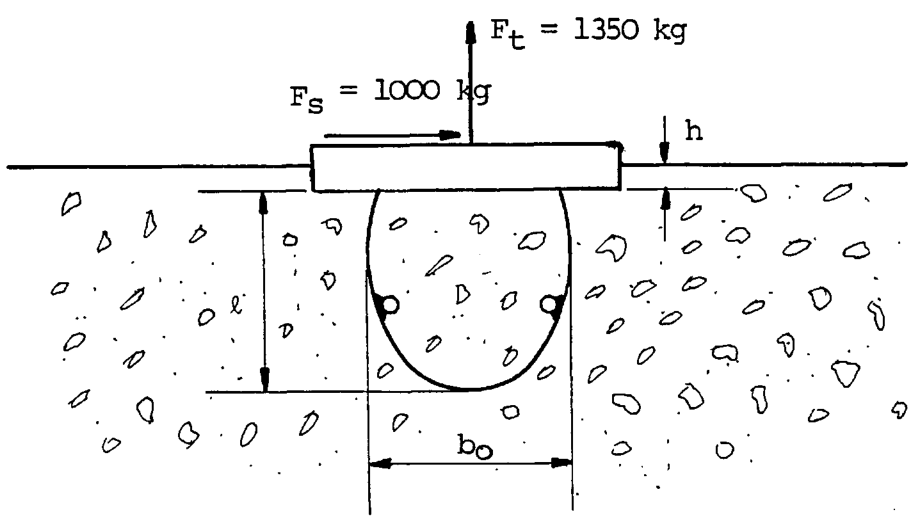

Figure E.1 Dimensions of an attachment for the concrete bed

a) Dimensions of the anchorage:

A formula for the calculation of ℓ and b_o is given in reference (49),

$$F_t = 0.53 \ A_c \ \sqrt{f'c} \qquad (E.1)$$

Where f'c is the compressive strength of the concrete and $A_c = (\ell + b_o) * \ell * \pi$

Then, from equation (E.1)

$$A_c = \frac{1350}{0.53\sqrt{70}} = 304.4 \ \ cm^2$$

If 8 cm is taken for b_o and ℓ, A_c is obtained as 400 cm^2 which is reasonable.

To find the diameter of the bars, the bearing strength of concrete should be checked together with the yield stress of steel. Using these criteria, the result is found as 0.85 cm.

To recapitulate,

ℓ = 8 cm; b_o = 8 cm; d = 1 cm

are taken for anchorage bar dimensions.

b) Dimensions for the Plate:

Bearing strength of concrete assuming no contribution from the anchorage bars, will be taken as the basis for

for this analysis. Assuming $h = 1$ cm, the analysis gives the required length of the steel plate as 7 cm. The width of the plate are mainly governed by the dimensions of the supports to be mounted onto it, but it should not be less than 7 cm either.

APPENDIX F

BASIC THEORY OF SELF-EXCITED VIBRATION IN METAL CUTTING

The following theory has been developed by Tlusty and Polacek and uses the assumptions given in section 4.2.

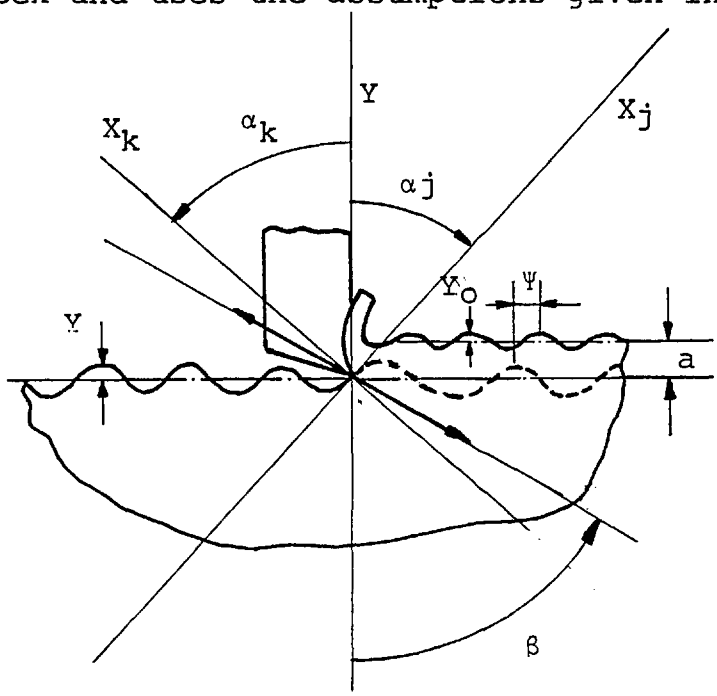

Fig F.1 Basic diagram for the process of self excited vibration

From fig F.1, the force P can be written as,

$$P = -b.r. (Y-Y_o) \quad (F.1)$$

where b is chip width and r is a coefficient depending on all other cutting conditions except b.

Y represents the vibration amplitude in an n degrees of freedom system, and it can be represented as follows,

$$Y = P.\phi(\omega) \quad (F.2)$$

where $\phi(\omega)$ is the receptance of the system represented as $\phi(\omega) = G(\omega) + jH(\omega) = \sum_{i=1}^{i=n} (U_i\, G_i + jU_i\, H_i)$ (F.3)

where $U_i = \cos\alpha \quad \cos(\alpha_i - \beta)$

From equations (F.1) and (F.2)

$$\frac{Y}{\phi} = b.r. \quad (Y_o - Y)$$

From which follows the equation,

$$\frac{Y_o}{Y} = \frac{1/br + \phi}{\phi} \qquad \text{(F.4)}$$

Equation (F.4) describes the closed-loop system of self-excited vibrations. The condition for the limit of stability can be expressed as:

$$|q| = \left|\frac{Y_o}{Y}\right| = \left|\frac{1/br + \phi}{\phi}\right| = 1 \qquad \text{(F.5)}$$

which signifies that the amplitude Y of vibrations in a cut will equal to the amplitude Y_o of vibrations in the preceding cut.

Using equation (F.3) together with equation (F.5) and simplifying, one obtains the condition,

$$\frac{1}{2br} = -G \qquad \text{(F.6)}$$

Equation (F.6) is the simplest form of the condition for the limit of stability. From the equation it is easy to see that, the limiting width of cut b_{lim} is obtained when the real part of the receptance is equalled to its minimum value. Therefore,

$$\frac{1}{2b_{lim}r} = - G_{min} \qquad (F.7)$$

Equation (F.7) signifies that the value of the minimum chip width b_{lim} for which the limit of stability is obtained, or the maximum chip width b_{lim} for which in the given case cutting can be stable, is dependent on the value of the minimum of the real receptance G of the vibratory system.

APPENDIX H EXAMPLE FOR SERVO MOTOR SELECTION

In figure 6.10, a method for machine tool servo design selection is given. The method will be applied to the machine tool designed in outline in this work.

1. The first step is the selection of a suitable ball screw. This depends on the coefficient of friction between the slideways and cross-slide. For antifriction type of slideways it is around 0.01 and for plain slideways coated with Turcite, 0.2 is a reasonable figure.

The forces acting on the cross-slide are shown in fig. H.1. Assuming only half of these forces act for finishing cuts, the following axial force values can be determined for a friction coefficient of 0.2.

Rapid traverse: $F_{a_1} = 500$ N
Rough cutting: $F_{a_2} = 6600$ N
Finish cutting: $F_{a_3} = 3300$ N

For a better resolution, if a pitch of 5 mm/rev is assumed, a maximum speed of 10 m/min gives a speed of 2000 rpm. The cutting conditions given in appendix C for rough cutting corresponds to 100 rpm. Then for finish cutting 200 rpm is a reasonable speed. Assuming that the machine will mainly be used for rough cutting operations, the speed and time ratio for the three phases can be written as follows,

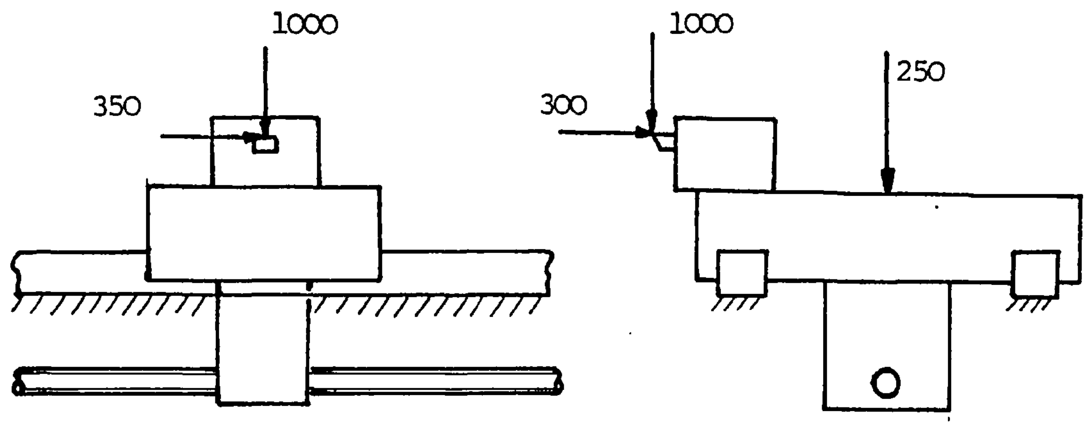

Fig H.1 The forces acting on the cross slide (in kg)

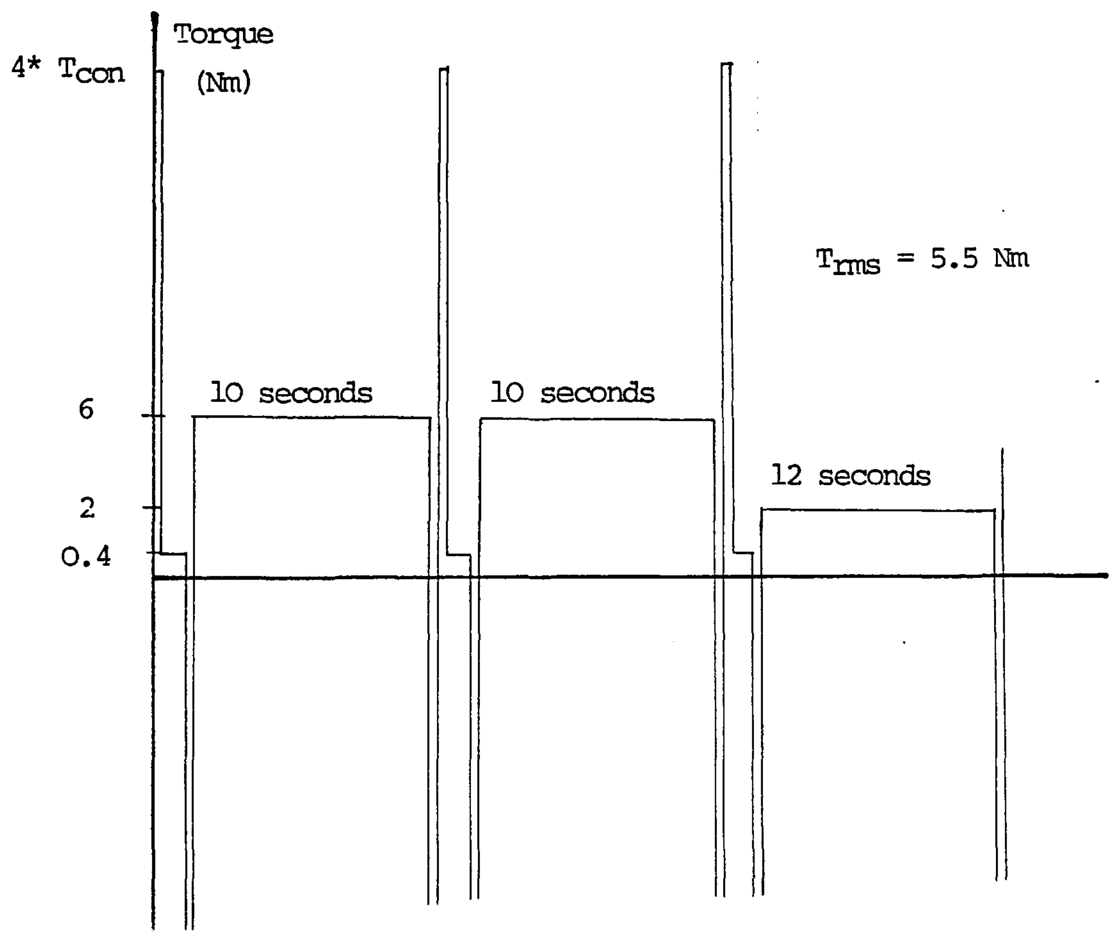

Figure H.2 A typical duty cycle

Rapid traverse: $n_1 = 2000$ rpm $q_1 = 20\%$

Rough cutting: $n_2 = 100$ rpm $q_2 = 60\%$

Finish cutting: $n_3 = 200$ rpm $q_3 = 20\%$

For the ball screw selection a "Warner Electric" catalogue will be used. Then the average speed and average load can be calculated by using the following equations:

$$n_m = n_1 \frac{q_1}{100} + n_2 \frac{q_2}{100} + n_3 \frac{q_3}{100} \quad \text{(H-1)}$$

$$F_{am} = \sqrt[3]{F_{a_1}^3 \frac{q_1}{100} \frac{n_1}{n_m} + F_{a_2}^3 \frac{q_2}{100} \frac{n_2}{n_m} + F_{a_3}^3 \frac{q_3}{100} \frac{n_3}{n_m}} \quad \text{(H-2)}$$

$n_m = 500$ rpm

and

$F_{am} = 3350$ N

Assuming a life of 20000 hours, $L = 60.Lh.n_m f_n$ (H-3)
where f_n is the utilisation factor (screw operat. time/ machine life). $f_n = 0.8$ will be chosen for this case, then $L = 4.8*10^8$ revs.

Then the required load capacity can be found by using the equation,

$$C = F_{am} \sqrt[3]{\frac{L}{10^6}} \quad \text{(H-4)}$$

$C = 26230$ N

After checking the critical speed and the load carrying capacity, a 50 mm ball screw with 5 turns is chosen. The pitch of the ball screw is 5 mm as decided earlier. Stiffness calculations carried out on this ball screw according to the equations given in the catalogue gave 8 μm at the maximum load which is satisfactory.

2. The ball screw mass is approximately, 13 kg. Then.

$$J_L = \frac{1}{2}\ 13\ (0.025)^2 + \frac{250\,(0.005)^2}{(2\pi)^2}$$

$$J_L = 0.0043 \text{ kg m}^2$$

3. $F_a = (250 + 1000 + 300) * 0.2 + 350$

$$F_a = 660 \text{ kg} = 6600 \text{ N}$$

$$T_L = \frac{6600 * 0.005}{2\pi\ 0.9} = 5.83 \text{ Nm}$$

So take T_L = 6 Nm

For antifriction slideways, the requirement will be 3.2 Nm.

4. This torque is required at 100 rpm, which corresponds to a power of only 65 W. The power required for rapid traverse can also be calculated. The torque due to friction is 0.4 Nm, the corresponding power at 2000 rpm is around 100 W.

5. Next step is to determine the acceleration and time for acceleration. In the machine tool proposed here,

adaptive control of feedrate might be used. In such cases, it is necessary to decelerate as rapidly as possible when the tool touches the workpiece. Tool life considerations indicate that full deceleration should be completed in one revolution of the workpiece (130). If the spindle speed is 1000 rpm, the deceleration time should be 60 msec. In the deceleration, cutting force will also be helping. Therefore, for acceleration a time period somewhat greater than 60 msec should be suitable. Then 80 msec will be chosen as the acceleration time. Maximum speed will be 2000 rpm (209 rad/sec). Retarding torque is just the friction torque which is estimated as 0.4 Nm.

6. A typical duty cycle is shown in figure H.2. T_{ems} is found as 5.5 Nm. To be safe 6 Nm will be taken.

7. It will be assumed that there is no weight and dimension constraints.

8. If an adaptive control with a sampling time of 10 msec is employed, for the amplifier a bandwidth more than 100 hz is desirable and for the motor and load system, it must be less than 50 hz.

9. $N_{min} = 1$ $N_{max} = 3$, At this point inertias for a few gear ratio should be given. The ones in between can be interpolated.

10. $\omega_{min} = 0.5$ rpm $\omega_{max} = 2000$ rpm

11. Now, the flow chart in figure 6.6 can be followed.

i) $N = 1$

ii) The selection will be performed by using a GEC d.c. servometer catalogue, an MT52K8-87 motor with 7.5 Nm rating is tentatively chosen.

iii) That torque is required at 100 rpm which is within the capability of the motor.

iv) $V_{max} = RI_a + K_e\omega$

$$I_a = \frac{T}{K_T}$$

Then $V_{max} = 0.406 * \dfrac{0.4}{0.845} + 0.83 * 209 = 173$ V.

V_{max} of this motor is 130 V, which is not suitable. Then, MT52K8-62 motor is chosen, V_{max} requirement for this motor is 125 V, which is within the capacity of the motor.

v) From the motor catalogues, it is seen that peak torque is available up to 450 rpm. Then the maximum available torque is 9 Nm. From equation 6.1,

$$t_a = \frac{41.9*(0.013+0.0043)}{59-0.4} + \frac{162.3*(0.013+0.0043)}{9-0.4}$$

$t_a = 0.34$ secs = 340 msecs.

The acceleration time is not satisfactory.

At this point a review of the other available catalogues showed that a motor which satisfied all the criteria can not be found.

Therefore, it is necessary to change the pitch of the ball screw. If a ball screw, with a pitch of 10 mm is chosen, the continuous torque requirement becomes 12 Nm. However, maximum speed requirement goes down to 1000 rpm. For this value of the pitch, a smaller size ball screw may be satisfactory. However, to provide a safety margin, calculations will still be based on the inertia of the 50 mm screw.

In this case, a motor with a 13.5 Nm continuous torque rating is chosen (MT52V8-87). $J_m = 0.026$ and the peak torque is 115 Nm which is available up to 400 rpm. For speedshigher than 400 rpm, 40 Nm is the available torque. Then from equation 6.1, for 80 msec acceleration time the peak torque requirement is calculated to be 40 Nm which is within the capacity of the motor.

vi) At this step the ratio of the inertias should be checked,

$$\frac{J_L}{J_m} = \frac{0.0043}{0.026} = 0.16 < 1.5$$

Therefore, this condition is satisfied.

vii) Electrical time constant of the motor is 4 msec. That is smaller than fifth of the acceleration time.

viii) The bandwidth of the motor and load system is,

$$f_b = \frac{K_E\ K_T}{2\pi\ RJ} = \frac{0.83 * 0.823}{2\pi * 0.406 * (0.026+0.0043)}$$

$$f_b = 8.8 \text{ Hz}$$

which is much smaller than 50 Hz

ix) A motor is chosen, the next step is the amplifier selection.

$$I_a = \frac{T}{K_T} = \frac{12}{0.823} = 14.6 \text{ A}$$

For the maximum current,

$$I_{max} = \frac{T_p}{K_T} = \frac{40}{0.823} = 49 \text{ A}$$

The maximum voltage is,

$$V = RI_a + K_E\ \omega = 0.406*49 + 0.83 * \frac{1000*2\pi}{60}$$

$$V \simeq 105 \text{ V}$$

Then a GEC make, GEMDRIVE-AXIS 30 amplifier can be chosen with I_a = 30A, I_{peak} = 90 A, V_{max} = 200 V. The power rate and bandwidth requirements of the amplifier are also suitable.

After the motor and amplifier is selected, then a feedback device and a control system should be selected to satisfy the resolution and response requirements. However, they constitute basically a control problem, will not be included here.

APPENDIX I

HYDRAULIC CIRCUIT DESIGN

In this appendix the design will be carried out for both the closed and open circuits assuming that only the main drive will be hydraulic. The requirements for the hydraulic system can be listed as follows;

the power of the motor:	15 hp = 11.185 kW
maximum speed:	3000 rpm (higher speeds can be obtained through a belt drive)
maximum pressure:	2000 psi = 136 bar
estimated output load inertia:	0.50 lb-ft-sec^2 = 0.68 kgm^2
required response rate:	1 sec to 1000 rpm
the constant hp range:	1:3

The type of circuit which can be used for the main drive of a machine tool is shown in figure I.1. The overload relief valves are to protect the circuit from sudden surges of pressure. In this circuit, a variable displacement axial piston pump together with its internal charging unit is used.

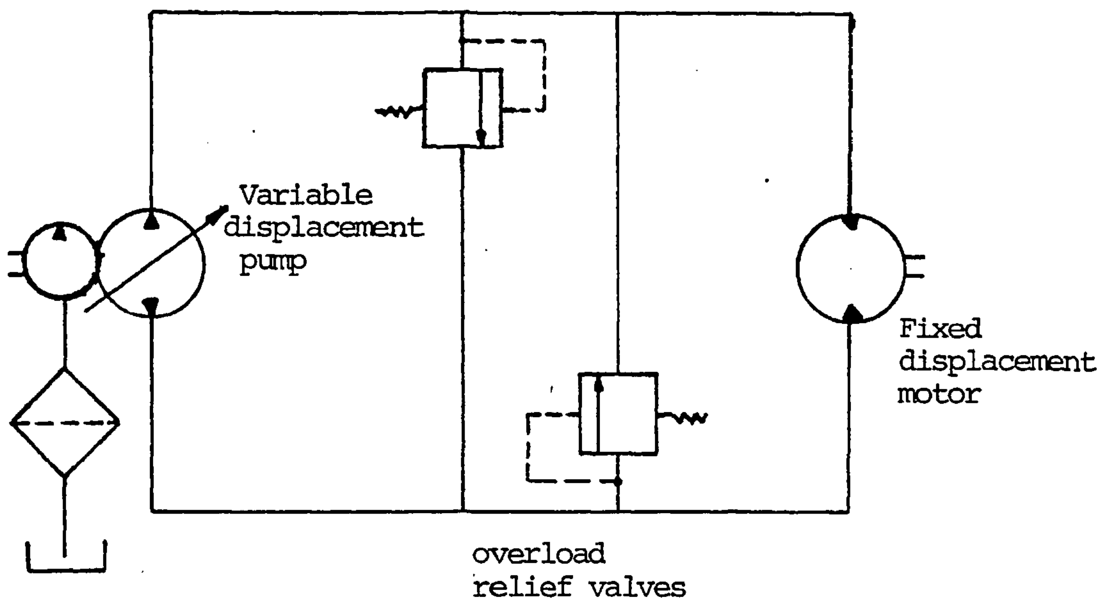

Figure I.1 A closed circuit hydraulic system

The pump horsepower is given by the equation,

$$hp = \frac{\eta_p \, D_p . N_1 \, P}{277.4 * 1430} \qquad (I.1)$$

where

η_p is the pump efficiency

D_p is the pump displacement in^3/rev

N_1 is the pump speed rpm

P is the pump pressure psi

Assuming, $\eta_p = 0.9$, equation (I.1) becomes,

$$hp = \frac{D_p . P . N_1}{4.41 * 10^5} \qquad (I.2)$$

Equation (I-2) can be plotted as shown in figure I.2. Then, a vertical line is erected for each pump under consideration, to a height not exceeding the rated pressure for the particular pump. Its intersection with the constant horsepower line indicates the pressure developed by the pump to give the required horsepower. Because a constant power range of 3:1 is required, the vertical lines should be drawn from $D_p/3$.

Similarly, for the motor,

$$hp = \frac{\eta_m \, D_m \, N_2 \, nP}{277.4*1430} \qquad \text{(I-3)}$$

where

D_m is the motor displacement,

N_2 is the spindle speed at which matching is to be made

n gear ratio between the motor and the spindle.

Assuming $\eta_m = 0.85$ and $n=1$,

$$hp = \frac{D_m. \; P. \; N_2}{4.66*10^5} \qquad \text{(I-4)}$$

Equation (I-4) is now plotted for a constant hp of 15 as shown in fig. I.3. Again, vertical lines are erected at the values of D_m for the motors under consideration, with the same restriction on pressure as before.

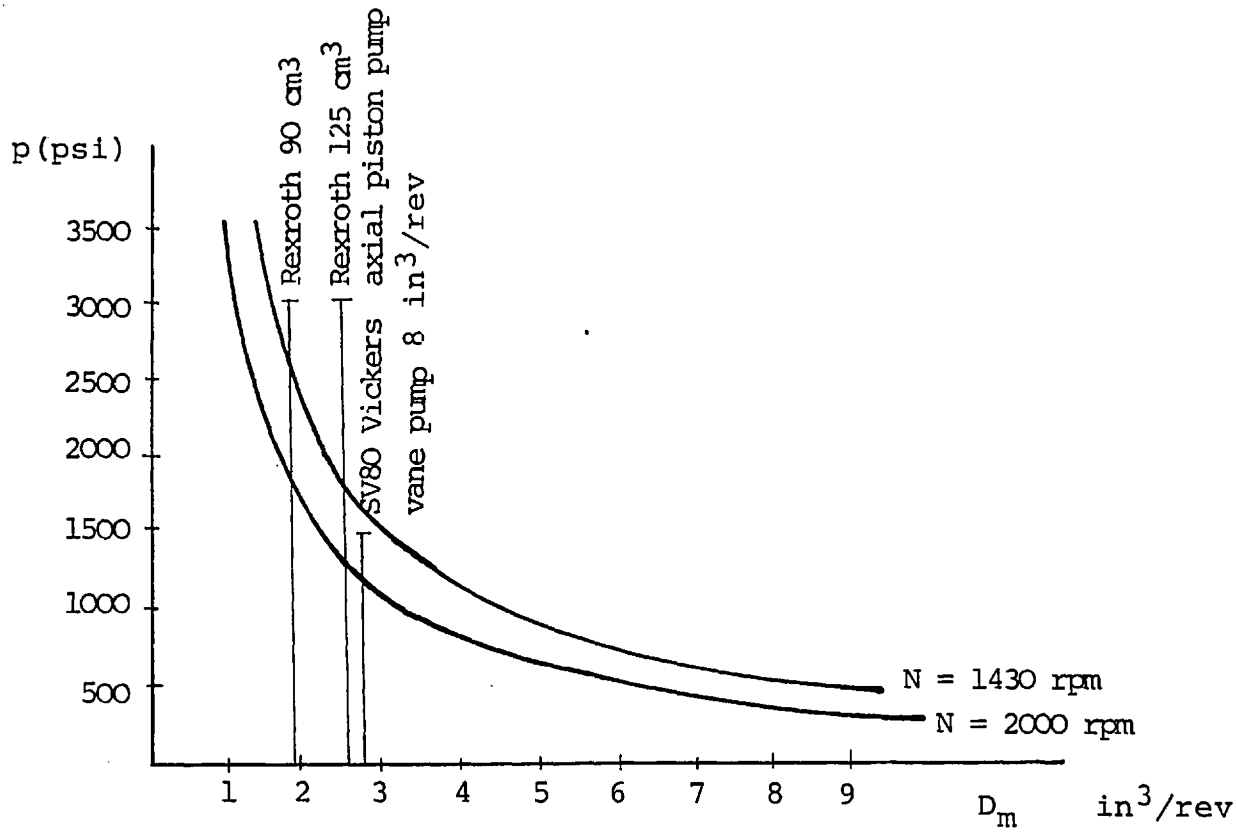

Figure I.2 Graphs for pump selection

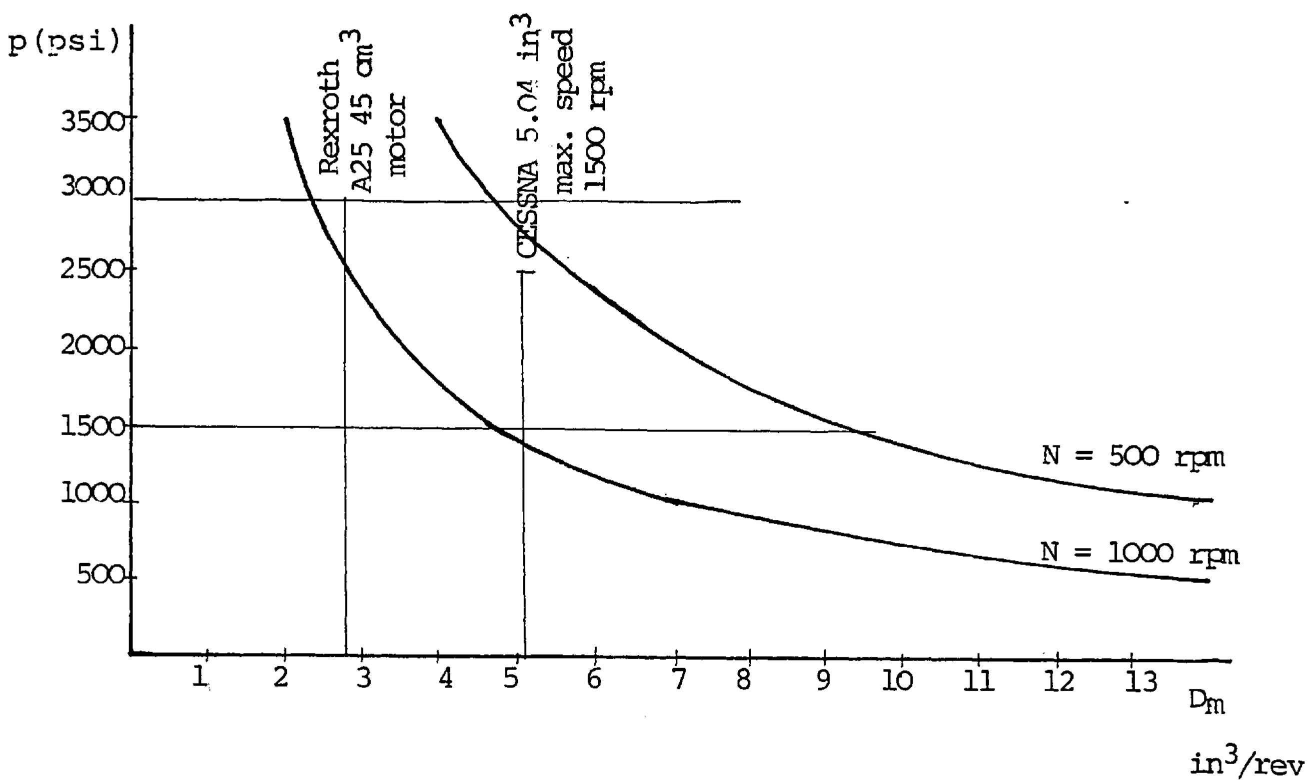

Figure I.3 Graphs for fixed displacement motor selection

Horizontal lines are drawn at the pressures corresponding to the required horsepower for the various pumps under consideration. Vertical and horizontal lines intersecting on or near to, the constant horsepower line now show a suitable choice of units.

Results show that Rexroth 90 cm^3 axial displacement pump and Rexroth 45 cm^3 axial displacement motor are suitable. The pressure and speed characteristics of the motor for a constant hp of 15 is shown in figure I.4. The graph shows that 3:1 constant hp requirement is satisfied. The total speed range will be around 100:1.

The surge pressure for the motor is 5000 psi. So, the response time and overload capacity of the system will be acceptable.

For the open circuit, the selection of the pump and the motor can be performed in the same way as described above. However, this time pressure drop across the valve should be taken into account, while drawing the lines for the motor. If a pressure-flow compensated pump which keeps a constant pressure drop of 200 psi across the valve is used, the vertical lines for the motor should be taken to a height 200 psi less than the supply pressure of a prospective pump, provided it can be run at this pressure. From figures I.2 and I.3, it is seen that a Rexroth 80 cm^3 pressure flow compensated pump together with a 45 cm^3 Rexroth motor are suitable. With this pump and motor,

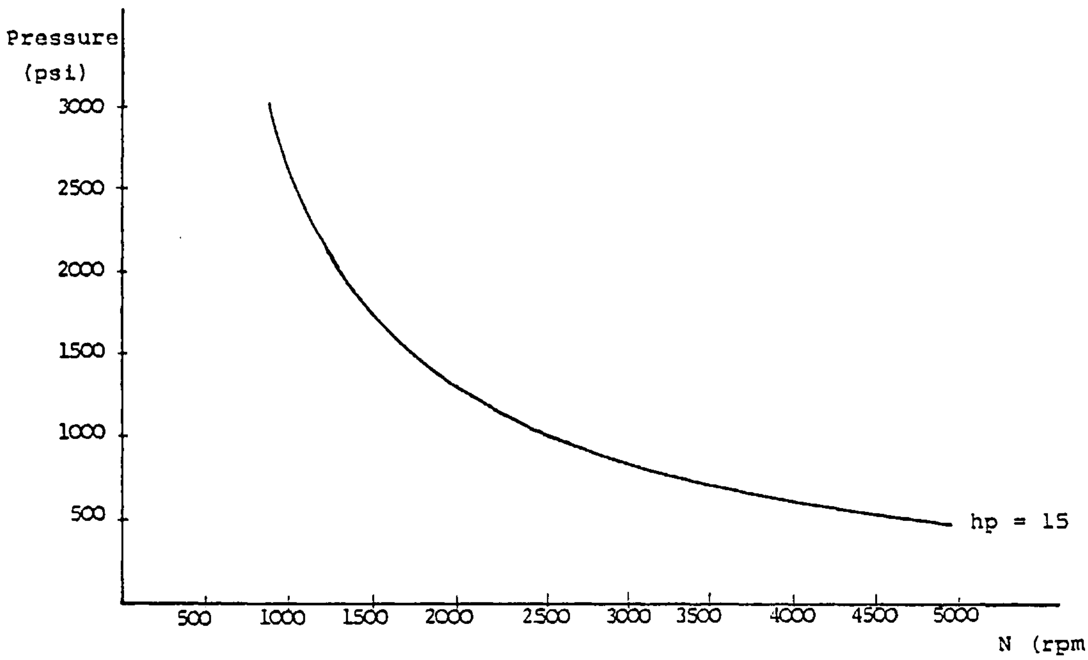

Figure I.4 Pressure and speed characteristics of a fixed displacement motor, variable displacement pump system

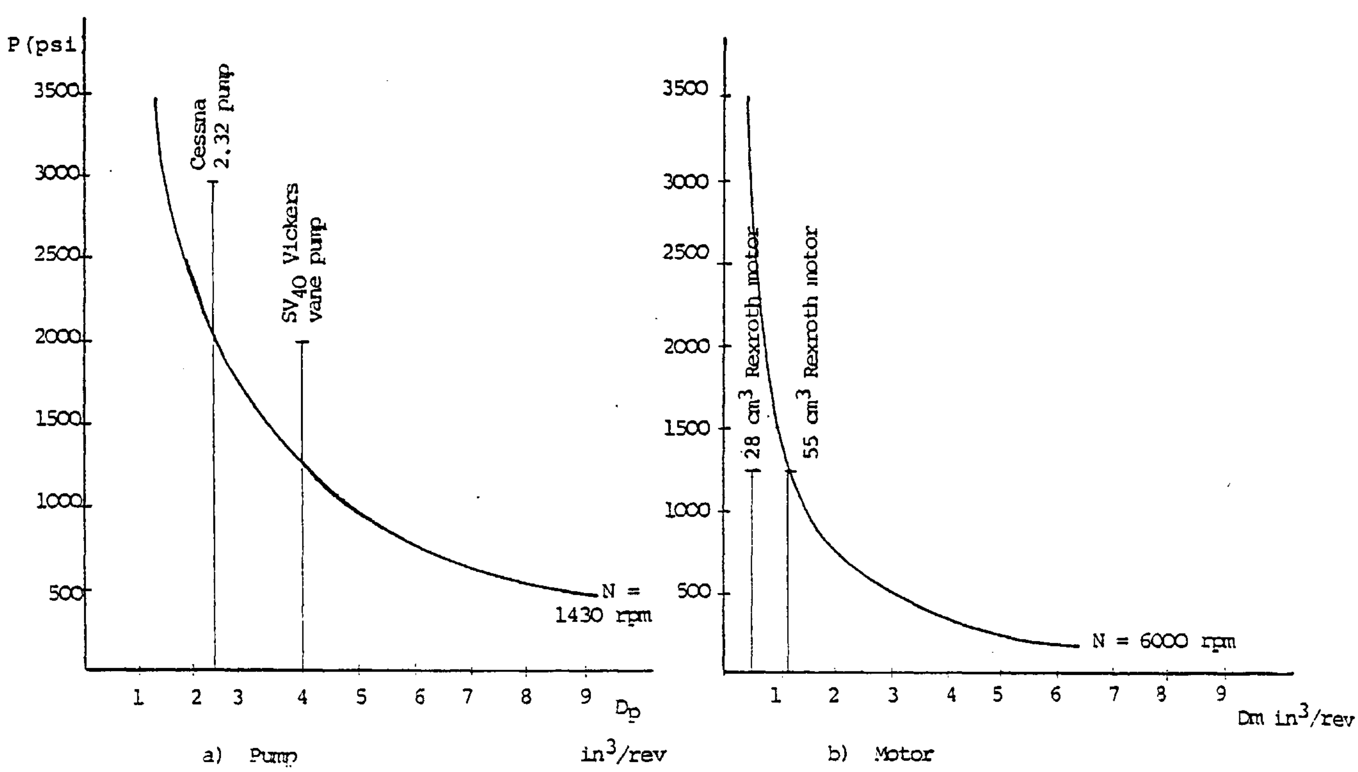

Figure I.5 Graphs for variable displacement motor selection maximum flow requirement is 30 gpm. Therefore, a Vickers flow control valve with a capacity of 30 gpm can be chosen.

The component determination for the two kinds of hydraulic circuits show that, with fixed displacement motors, although it was possible to have 3:1 constant power range, the motors and pumps selected were highly overrated. This necessitates the use of bigger reservoir, bigger diameter pipes, increasing the overall cost of the system. Therefore, another design, this time using a variable displacement motor will be carried out and the two solutions will be compared.

By using the same method, figure I.5 gives SV40 Vickers vane pump and 55 cm^3 Rexroth motor as the most suitable pair. Displacement of the motor can be changed in the range of 3.5:1 giving an acceptable constant power range. Because the maximum speed of the motor is 5000 rpm, the required flow rate in the system is 18 gpm. Then a Vickers $3/_8$" 20 gpm rated flow control valve can be chosen for the task.

A cost comparison between an open loop variable displacement motor circuit and an open loop fixed displacement motor circuit showed that the cost for the two systems are about the same range (£2000).

APPENDIX J

HYDRAULIC SYSTEM SIMULATION

The equations to simulate a hydraulic system will be derived in the appendix. The governing assumptions are given in section 7.3.2. Only three types of hydraulic elements will be considered; pump, orifice valve and motor. Cylinders can be analysed in a similar way. In the analysis compressibility effects will be taken into account.

i) Pump

Pump flow can be written as,

$$Q_{out} = Q_i - Q_\ell \qquad \text{(J-1)}$$

where

$$Q_i = k\theta \qquad \text{(J-2)}$$

θ is the swash plate angle and,

$$K = N^* \frac{D_p}{\theta_{max}}$$

θ max is the maximum swash plate position, N is the speed of the motor and D_p is volume displacement of the pump. The leakage flow rate can be written as,

$$Q_\ell = K_L (\Delta P)_p \qquad \text{(J-3)}$$

where,

$$K_L = C_S \frac{2\pi D_p}{\mu}$$

C_S is the slip coefficient of the pump and μ is the viscosity of the oil

ii) The circuit:

Compressibility effects in the circuit can be written as,

$$Q_c = \frac{V}{\beta} \frac{dP}{dt} \qquad (J-4)$$

where

V is the volume of the oil, and

β is the Bulk's modulus.

iii) Orifice Valve;

The flow through an orifice valve can be written as follows,

$$Q = \delta(t-\zeta)(C'_d . K_s . X \sqrt{\frac{2(\Delta P)}{\rho}} \qquad (J-5)$$

where

$\delta(t-\zeta)$ is the time delay which may be caused by a pressure flow compensated pump

C'_d is the discharge coefficient

X is the spool displacement

K_S is the orifice width and

ρ is the density of oil

iv) Motor:

The rotational speed of the motor can be written as,

$$D_m \cdot \omega = Q_n - Q_{pm} \qquad (J-6)$$

where

Q_n is the flow into the motor,

Q_{pm} is the motor leakage written as,

$$Q_{Lm} = C_S \frac{2\pi D_m}{\mu} (\Delta P)_m \qquad (J-7)$$

The pressure difference across a hydraulic motor can be found by using the torque relation,

$$T_m = D_m (\Delta P)_m - C_d \cdot D_m \cdot \mu \cdot \omega - C_f (\Delta P)_m D_m \qquad (J-8)$$

where,

$$T_m = (J \frac{d}{dt} + B_V) \omega + T_L \qquad (J-9)$$

where J is the load inertia, B_V is the viscous coefficient at the load and T_L is the external torque.

Using the above equations,

$$Q_n = D_m \omega + C_S \frac{2\pi}{\mu} \frac{1}{(1-C_f)} (J \frac{d\omega}{dt} + B_V \omega + T_L + C_d \cdot \mu \cdot D_m \cdot \omega)$$

$$(J-10)$$

The equations of different units can be connected together in the form of a block diagram according to the connections as shown in fig. 7.2. Then the transfer functions can be obtained as, for a closed loop system,

$$W = \frac{k\theta - T_L(\xi_4 S + \xi_5)}{\xi_1 S^2 + \xi_2 S + \xi_3} \qquad \text{(J-11)}$$

where

$$\xi_1 = \frac{V}{\beta D_m} \frac{1}{(1-C_f)} J$$

$$\xi_2 = \left(JC_s \frac{2\pi}{\mu} + K_L \frac{J}{D_m} + \frac{V}{\beta D_m} B_V + \frac{V}{\beta} C_d \cdot \mu\right) \frac{1}{(1-C_f)}$$

$$\xi_3 = \frac{D_m}{(1-C_f)} \left[(1-C_f) + C_S \frac{2\pi}{\mu D_m} \left(B_V + \frac{C_d \cdot \mu}{(1-C_f)}\right) + \right.$$

$$\left. + K_L \frac{B_V}{D_m} + \frac{C_d \ \mu \ K_L}{D_m}\right]$$

$$\xi_4 = \frac{V}{\beta \ Dm} \frac{1}{(1-C_f)}$$

$$\xi_5 = \left(\frac{K_L}{Dm} + \frac{2\pi}{\mu} C_S\right) \frac{1}{(1-C_f)}$$

and for an open loop system with valve control,

$$W = \frac{e^{-\zeta s} C'_d K_S \sqrt{\frac{2(\Delta P)}{\rho}} X - T_L (\eta_4 5 + \eta_5)}{\eta_1 s^2 + \eta_2 S + \eta_3} \qquad \text{(J-12)}$$

$$\eta_1 = \frac{JV}{\beta D_m (1-C_f)}$$

$$n_2 = \frac{V}{\beta D_m (1-C_f)} (B_v + C_d . D_m . \mu) + C_5 \frac{2\pi D_m}{\mu} J$$

$$n_3 = C_S \frac{2\pi D_m}{\mu} (B_v + C_d D_m \mu) + D_m$$

$$n_4 = \frac{V}{\beta D_m (1-C_f)}$$

$$n_5 = C_S \frac{2\pi D_m}{\mu}$$

Where C_S, C_d and C_f are the constants related to the motor.

APPENDIX K

TEMPERATURE DISTRIBUTION PROGRAM

This program calculates the final temperatures at several points in a hydraulic circuit. For complicated systems, that is very useful.

The theory used to prepare the program employs the general energy equation for the kinds of components such as pumps, motors, pipes or mixing devices (114). For example in case of a pump and motor the equation is,

$$Q - W = h_{out} - h_{in} \qquad (K-1)$$

where as in case of a pipe or a mixing device the equations can be written as follows,

$$Q = h_{out} - h_{in} \qquad (K-2)$$

$$\Sigma\, h_{in} = \Sigma\, h_{out} \qquad (K-3)$$

respectively

where

Q is the transferred heat

W is the work and

h is the specific enthalpy.

Then all these can be written in terms of the temperature and system variables by using some simple thermodynamic relations (114). Then, for a certain set of system variables the temperature values at several points in the circuit can be calculated.

One of the most important items in the input data of the computer program is the generation of the connection matrix. This matrix tells the computer program the connection between the components of a hydraulic circuit.

Only the upper triangle of the matrix is given as the input. Elements of the matrix consist of the following numbers:

0 - indicates no connection between the ports
1 - indicates a pipe between the ports
2 - indicates a pump between the ports
3 - indicates a motor between the ports
4 - indicates a valve between the ports
5 - indicates a mixing device between the ports.

The sign - or + gives the direction of the flow. For example, if the flow is from port 7 to 1, then the matrix element (1-7) must be a negative number. The flow chart is given in figure K.1.

The results of an example problem are given in section 7.5.1.

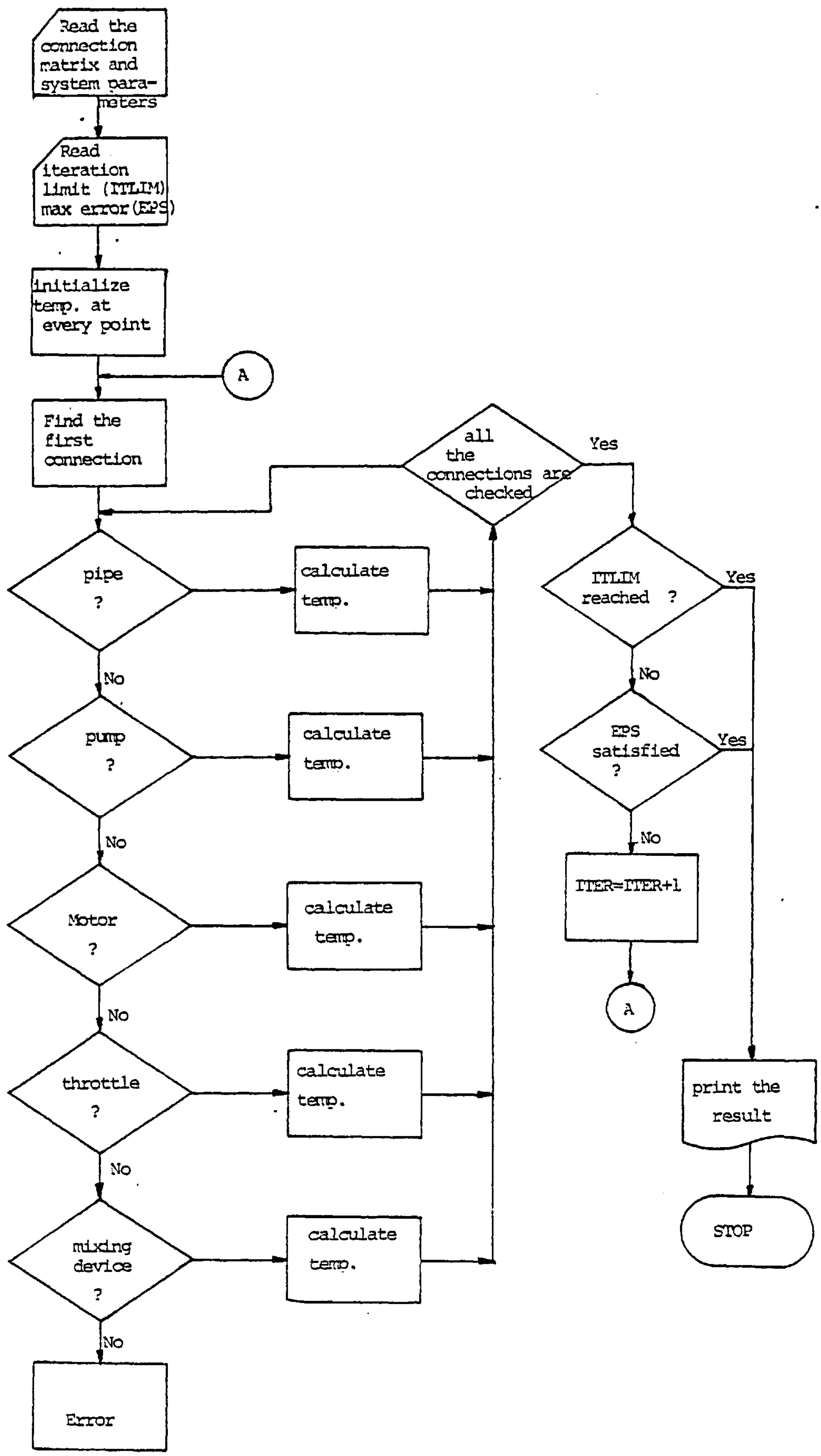

Figure K.1 Flow chart for the temperature distribution program

APPENDIX L

A FORCE MONITORING SYSTEM

The estimation of appropriate feedrates becomes very important especially when cutting forged blanks. The force sensing adaptive control routines are mainly used for such applications (135).

In order to implement such an AC system on the controller described in chapter 1, it was necessary to build a dynomometer first. To this aim a special tool holder was built and two semiconductor strain gauges were placed as shown in fig L.1. These gauges together with two dummy ones were connected into a Wheatstone bridge. The Wheatstone bridge arrangement helped to nullify the temperature change effects. Then, the AC algorithm was written and stored in the feedrate controller (19). Experimentation showed that the constant tool force cutting could successfully be performed (fig. L.2).

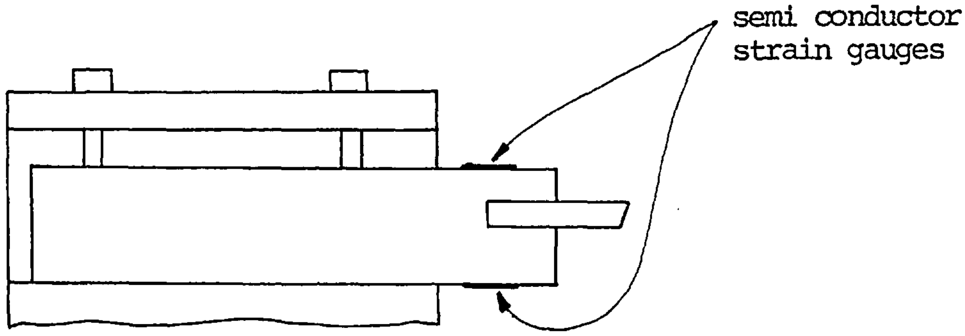

Fig L.1 The arrangement on the tool holder to measure the main cutting force

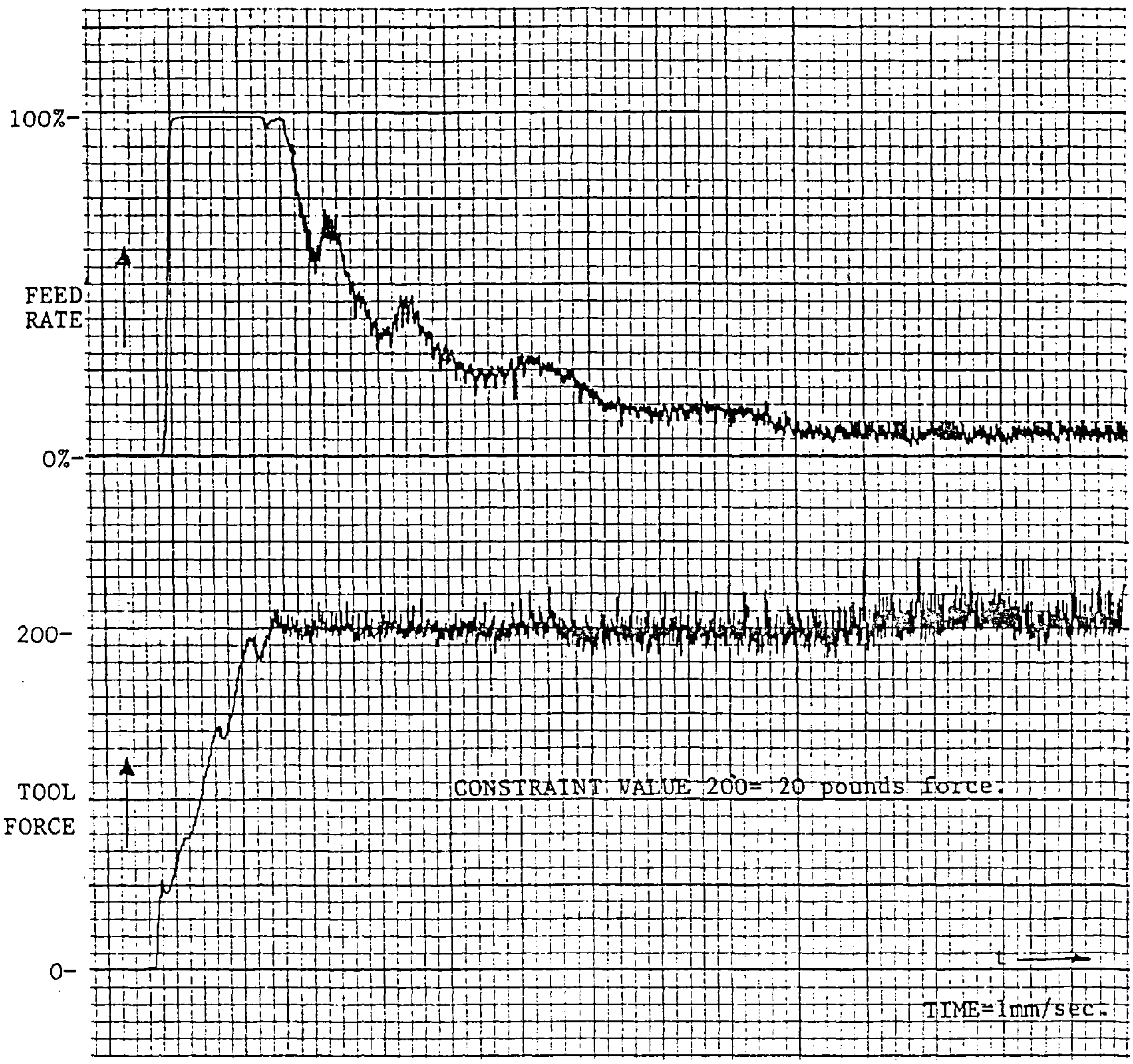

Fig L.2 Tool force constraint cutting (extract from reference (19))

REFERENCES

1. PRESSMAN, R. S. and WILLIAMS, J. E. (1977) Numerical control and computer aided manufacturing. London, John Wiley and Sons Inc.

2. KOENIGSBERGER, F. (1964) Design principals of metal cutting machine tools. New York, The Macmillan Company.

3. ACHERKAN, N. and PUSH, V. (1973) Machine tool design. Moscow, MIR publishers.

4. SIMON, W. (1973) The numerical control of machine tools, Surrey, Edward Arnold Publishers.

5. BAKEL, J. F. (1975) Factors to consider in the design of machines equipped with automatic controls. IMTDR conf. proc., pp. 89-94.

6. DAVIES, B. J. (1975) The role of design in the introduction of a new machine tool. IMTDR conf. proc., pp. 1-12.

7. MERCHANT, M E. (1975) Long-range trends in the automation of machine tools and manufacturing. IMTDR pp. 13-19.

8. DAVIS, J. B. and JACKSON, W. J. (1970) The machine tool designer and the customer, IMTDR conf. proc., pp. 217-232.

9. UMBACH, R. and HAFERKORN, W. (1969) Some examples and problems in implementation of modern design features on large size machine tools. IMTDR conf. proc., pp. 5-34.

10. STOCKMANN, P. (1969) N/c development influences conventional turning machines. IMTDR conf. proc., pp. 35-55.

11. THORNEYCROFT, M. and SCHOLEY, D. (1975) Multi-axis NC turning IMTDR conf. proc., pp. 681-685.

12. WICK, C. (1980) Increasing productivity with NC lathes. Manufacturing Engineering, March, pp. 54-64.

13. SPARKES, C. A. (1971) Machine tools - the total concept IMTDR conf. proc., pp. 41-45.

14. GRINDROD, D and FARNWORTH, G. (1971) The modula range of NC machine tools. IMTDR conf. proc., pp. 31-37.

15. MOSS I. F. (1973) An analysis of market requirements for NC turning. IMTDR conf. proc., pp. 19-23.

16. TAYLOR, A. J. (1973) The user's view of the machine tool industry. IMTDR conf. proc., pp. 53-56.

17. FELTEN, K. (1978) Safety aspects in design of NC turning machines IMTDR conf. proc., pp. 61-63.

18. (1979) Machine Tools: Cutting Edge of Technology Machine Design, January 25, pp. 18-47.

19. DALLZELL, D. (1981) Intelligent machine tool and the microprocessor, Ph.D. thesis, Imperial College.

20. SHAH, R. (1980) N.C. Guide, Zurich, NCA Verlag.

21. ROUNDSEPP, E. (1979) Creativity, Machine Design, 12 April, pp. 86-89.

22. ROHS, H. G. (1973) Low cost or high performance NC turning machines. IMTDR conf. proc., pp

23. KOENIGSBERGER, F. and TLUSTY, J. (1970) Machine Tool Structures, New York, Pergamon Press Ltd.

24. Branson, D. E. (1977), Deformation of Concrete Structures, New York, McGraw Inc.

25. FABER, J. and MEAD, F. (1961) Reinforced Concrete. London, E & F.N. Span Ltd

26. BRESLER, B. (1974), Reinforced concrete engineering London, John Wiley & Sons Inc.

27. MORGAN, G. H., McKEOWN P. A. and RENKER, H. J. 1979 Materials for machine tool structures. IMTDR conf. proc., pp. 429-434.

28. McKEOWN P. A. and MORGAN, G. H. (1979) Epoxy granite: a structural material for precision machines. precision engineering, pp. 227-229.

29. HUNT, L. and STANSFIELD, F. M. (1980) Using concrete for machine tool structures. Chartered Mechanical Eng. July pp. 61-67.

30. COLE, G. D. and SPOONER, D. C. (1965) The damping capacity of concrete. Proc. of Int. conf. on the structure of concrete, paper E1 pp. 217-225.

31. STEPHEN, A. C., TAYLOR, S. (1968) Computer Analysis of machine tool structures by the finite element method. IMTDR conf. proc. pp.

32. WECK, M. and HEIMANN, A. (1976) Analysis of variants of machine tool structures by means of the finite element method. IMTDR conf. proc., pp. 553-559.

33. COWLEY, A. (1972) Co-operative work in computer aided design in the CIRP. Annals of the CIRP, pp 257-266.

34. CORLEY, W. and HANSON, J. (1978) Design of reinforced concrete for fatigue. ASCE proceedings, Jrn. of the Structural division, June, pp. 921-932.

35. SPUR, G. and HAAS, P. (1974) Thermal behaviour of NC machine tools IMTDR conf. proc. pp. 267-273.

36. SATA, T. TAKEUCHI, W, and SATO, N. (1975) Analysis of thermal deformation of machine tool structure and its application.

37. HEMINGRAY, C. P. (1973) Some aspects of the accuracy evaluation of machine tools. IMTDR conf. proc. pp. 281-285.

38. TIMOSHENCO, S. P., YOUNG, D. H. (1965) Theory of structures, New York, McGraw Hill

39. TAYLOR, S. and TOBIAS, S. A. (1966) Lumped-constants method for the prediction of vibration characteristics of machine tool structures. IMTDR conf. proc. pp. 37-50.

40. MALTBEEK, J. C. (1966) Classical beam method for the prediction of vibration characteristics of machine tool structures. IMTDR conf. proc. pp. 23-35.

41. TAN, C. L. and FENNER, R. T. (1978) Three dimensional stress analysis by the boundary integral equation method. Jrn of Stain Analysis, 4, pp. 213-219.

42. DANSON, D., COLLINGTON, D. and ADEY, R. (1981) Boundary element systems for engineering analysis and design Software Engineering Conf. proc. pp. 862-877.

43. TAN, C. L. (1980) Boundary Integral Equation seminar notes.

44. ZIENKIEWICZ, O. C. (1977) The finite element method. London, McGraw-Hill Ltd.

45. FENNER, R. T. (1976) Finite Element Methods for Engineers, London, Macmillan Press Ltd.

46. TOURRET, R. (1958), Performance of metal-cutting tools. London, Butterworths Scientific Publications.

47. (1958) Kent's Mechanical Engineering handbook, New York, John Wiley & Sons, inc.

48. BOSTON, O. N. (1958) Metal processing, London. John Wiley & Sons Inc.

49. KACZMAREK, J. (1976) Principles of machinery by cutting, abrasion and erosion. Stevenage, England, Peter Peregrinus Ltd.

50. SHIGLEY, J. E. (1972) Mechanical Engineering design London, McGraw-Hill Ltd.

51. HITCHINGS, D. (1980) Finel Users Manual, Imperial College.

52. (1969) Mechanical Fasteners for Concrete, Detroit, American Concrete Institute.

53. BAKER, A. L. L. (1970) Limit State Design of reinforced concrete. London, Cement and concrete Assoc.

54. MALTBAEK, J. C. (1966) Classical beam method for the prediction of vibration characteristics of machine tool structures. IMTDR conf. proc. pp. 23-35.

55. TAYLOR, S. and TOBIAS, S. A. (1966) Lumped constants method for the prediction of the vibration characteristics of machine tool structures IMTDR conf. proc. pp. 37-50.

56. YOSHIMURA, M. and HOSHI, T. (1972) Computer approach to dynamically optimum design of machine tool structures. IMTDR conf. proc. pp. 439-446.

57. YOSHIMURA, M. (1975) Analysis and optimisation of structural dynamics of machine tools by a synthesis of dynamic rigidity program system. IMTDR conf. proc. pp. 209-214.

58. TLUSTY, J. and ISMAIL, F. (1979) Dynamic structural identification tasks and methods. ANNALS of CIRP pp. 251-255.

59. INAMURA, T., STAT, T. (1979) Stiffness and damping identification of the elements of a machine tool structure Annals of CIRP pp. 235-239.

60. STAUFERT, G. and TSCHUOI, J. P. (1979) Estimation of the dynamic behaviour of the working machine tools by cepstral averaging, Annals of CIRP, pp. 229-234.

61. TOBIAS, S. A. (1965) Machine Tool Vibration. London. Blackie & Son Ltd.

62. PETERS, J. and MERGEAY, M. (1976) Dynamic Analysis of machine tools using complex modal method. Annals of CIRP, pp. 257-261.

63. SHANKER, A. and PANDEY, P. C. (1976) An analysis of chatter vibration while turning slender work-pieces between centres. Annals of CIRP, pp. 273-276.

64. LAMBARD, J. and BEESON, H. D. (1976) Dynamic performance tests for machine tools some findings from the industrial experiences of CERMO and MTIRA. Annals of CIRP, pp 281-286.

65. MURTHY, J. R. and REDDY, G. R. (1979) Optimisation of functional properties of machine tool structures. A finite element analysis. IMTDR conf. proc. pp. 435-442.

66. ABDEL-ROHMAN, M. and LEIPHOLZ, H. (1979) A general approach to active structural control. Proc. of ASCE, of the Eng. Mech. Div, 6. pp. 1007-1023.

67. JANN-NAN, Y. (1975) Application of optimum control theory to civil engineering structures. Proc. of ASCE, J. of the Eng. Mech. Div. pp. 819-837.

68. ABDEL-ROHMAND, M. and LEIPHOLZ, H. (1979) Automatic active control of structures. Proc. of Int. IUTAM Symp. on Structural Control, pp 29-55

69. BELL R. and DOLBEY M.P. (1971)
The contact stiffness of joints at low apparent interface pressures, Annals of CIRP, pp. 67-79.

70. YAYRA Z. and POLACEK M. (1967)
The influence of different types of guideways on the static and dynamic behaviour of feed drives, IMTDR conf. proc., pp. 1127, 1138.

71. BELL R. and BURDEKIN M. (1966)
Dynamic Behaviour of plain slideways, Proc. Instn. Mech. Engrs, 8 pp. 169-184.

72. BACK N., BURDEKIN M. and COWLEY A. (1972)
Review of the Research on fixed and sliding joints proc. IMTDR conf. pp. 87-98.

73. HEMINGRAY C. P. (1972)
The friction and wear of plastics with special reference to machine tool slideways, proc. IMTDR conf. pp. 99-106.

74. HAJDU G. (1973) The influence of the characteristics of machine tool guideways concerning the dynamic behaviour of machine tool slides, proc. IMTDR conf.

75. HALLOWES J. G. M. and BELL R. (1972)
The dynamic stiffness of anti-friction roller guideways, proc. IMTDR conf. pp. 107-112.

76. DE FRAINE J. (1971) The choice of ball slideways for machine tools, proc. IMTDR conf. pp. 193-198.

77. BURDEKIN M. and COWLEY A. (1971) Wear of slideways Tribology 2 pp. 15-20.

78. THORNLEY R. H. and KOENIGSBERGER F. (1971) Dynamic characteristics of machined joints loaded and excited normal to the joint face. CIRP Annals, pp. 459-469.

79. LEVINA E. M. (1965) Calculation of contact deformation in slideways, Machines and Tooling, 1 pp. 8-16.

80. LEVINA E. M. (1965) Main operating characteristics of anti-friction slideways, Machines and Tooling, 7 pp. 11-18.

81. ALANKUS O. B. (1979) A survey of infinitely variable speed drive systems, internal report, Imperial College, London.

82. BAILEY S. J. (1981) Variable speed motor drives' 81: designers exhibit energy concern. Control Eng. 1, pp. 61-67.

83. DERKSEN J. (1976) Spindle drives for machine tools Siemens Review, 1 pp. 20-24.

84. REIHS R. (1971) Thyristor-controlled main drives for machine tools, Siemens Review, 3 pp. 119-122.

85. (1981) Fundamental approach to machine design pushes up d.c. electric motor performance <u>Engineering, 7</u>, pp. 550-551.

86. BOLLINGER J. G., BRUSSEL N. Y., DINSDALE J. (1980) Digital controls and feed drives, state of the and new developments <u>Annals of the CIRP</u>, pp. 497-506.

87. FIRTH O. and CUNNINGHAM S. U. (1968) Hydrostatic drives in machine tools, <u>Fluid Power Int. Conf. proc</u>.

88. KNIGHTS D. E. (1980) Electrical and electronic variable speed drives. <u>Engineers' Digest, 3</u>, pp. 33-40.

89. AVRAMOVIC D., and FORT P. (1976) Characteristics of electro-hydraulic feed drives under dynamic load conditions. <u>IMTDR conf. proc</u>.

90. SETO K. (1979) New NC device for feedback controlled feed drives. <u>Int. J. Machine Tool Design Res</u>, pp. 53-67.

91. SCHMUTZ R. H. (1980) State variable feedback control of hydraulic feed drives. <u>Annals of the CIRP</u>, pp. 299-302.

92. (1980) Microprocessor controlled A.C. servo drive system for machine tool feed slides, <u>Engineers' Digest, 3</u>, pp. 15,18.

93. (1976) MACH 76 exhibition review, Metal working production, 9 pp. 135-140

94. PAWLETKO J. P. (1976) Advances in step motor controls. Proceedings of the Int. Conf. on stepping motors and systems, pp. 68-80.

95. BEERCHECK R. C. (1981) Controlling Hydraulics with electronics, Machine Design, January 22, pp. 57-60.

96. IBIARY Y. E. (1978) Coming: smart hydraulic valves, Machine Design, November 23, pp. 99-102.

97. KLEIN E. A. and NORRIS G. A. (1977) Hydrostatics tackle tough new job, Machine Design, August 25, pp. 83-87.

98. TOWN H. C. (1971) Hydraulic rotary drives and controls for machine tools, Fluid Power International, 10, pp. 19-22.

99. SELLORS G. (1972) Hydraulics for machine tools, Fluid Power International, 6, pp. 47-50.

100. ACKERMANN U. and BOBEL K. H. (1976) Rechnerunterstutzte Auswahl von elektrischen Vorschubantrieben, Ind. Fertigung, 3, pp. 129-136.

101. (1977) DC Motors, speed controls and servo systems; a handbook by Electro-Craft Corporation, Pergamon Press, Oxford.

102. BOLTON H. R., DAWSON C. and ASHEN R. A. (1981) Investigations into certain categories of long travel rotary actuators, proc. of Int. conf. on small electrical motors.

103. COLE G. D. and SPOONER D. C. (1965) The damping capacity of concrete. proc. of Int. conf. on the structure of concrete, pp. 217-225.

104. KORN J. (1969) Hydrostatic Transmission systems, International Textbook Company, London.

105. BLACKBURN J. F. (1960) Fluid Power Control, John Wiley and Sons. Inc. New York.

106. ESPOSITO A. (1980) Fluid Power with applications, Prentice-Hall, Inc., New Jersey.

107. McCLOY D. and MARTIN H. R. (1980) Control of fluid power: Analysis and design, Ellis Horwood Ltd, London.

108. GREEN W. L. (1971) The Control of Speed, Fluid Power Int., 3 pp. 47-49.

109. AVRAMOVIC D. and FORT P. (1976) Characteristics of Electro-hydraulic feed drives under dynamic load conditions. IMTDR conf. proc.

110. BEERCHECK R. C. (1981)
Controlling Hydraulics with Electronics,
Machine Design, January 22, pp. 57-60.

111. IBIAZY Y. E. (1978) Coming: smart hydraulic
values, Machine Design, November 23,
pp. 99-104.

112. KINSEY D. (1972) Constant pressure operation
of hydraulic motors, Fluid power Int, 9
pp. 49-51.

113. SCULTHORPE H. J. (1977)
Pump controls that serve energy, Machine Design,
April 21, pp. 255-259.

114. PARKER J. D. and McQUISTON F. C. (1964)
Thermal Analysis of Hydraulic Systems,
Hydraulics and Pneumatics, 8, 10, pp. 57-61 and
pp. 112-115 (parts 1 & 2).

115. ERCAN Y. (1979) System Dynamics and optimum
control lecture notes, Middle East Technical
University, Turkey.

116. KUO C. B. (1980) Digital Control Systems,
Holt, Rinehart and Winston, Inc., New York.

117. SHAW M. C. and AVERY J. (1978)
Experience with manual adaptive control,
Annals of CIRP, 27, pp. 425-428.

118. WICK C. (1977) Automatic adaptive control of machine tools, Manuf. Eng., 9, pp. 38-45.

119. MITSUI K. and SATO H. (1978) Frequency characteristics of cutting process identified by an in-process measurement of surface roughness. Annals of CIRP. pp. 67-71.

120. IPPOLITO R. and MICHELETTI G. F. (1968) Tool wear and cutting forces in steel turning. Annals of CIRP, pp. 353-360.

121. IPPOLITO R. and MICHELETTI G. F. (1975) Experimental analysis of the correlation between cutting forces variation with time and cutting data, IMTDR conf. proc.

122. MICHELETTI G. F. (1973) Analyse der Zusammenhange zwischen schnittkraft und verschleiß bei der adaptiven steuerung, Werkstatt und Betrieb, pp. 637-641.

123. TAKEYAMA H. and DOI Y. (1966) Sensors of tool life for optimisation of machining, IMTDR conf. proc. pp.

124. UEHARA K. (1979) Automatic tool wear monitoring in NC turning, Annals of CIRP, 28 pp. 39-42.

125. TAKEYAMA H. and SEKIGUCHI H. (1970) One approach for optimising control in metal cutting, Annals of CIRP, pp. 345-351.

126. MICHELETTI G., KOENIG W. and VICTOR H. (1976) In process tool wear sensors for cutting operations, Annals of CIRP, pp. 483-495.

127. BOOTHROYD G. and EAGLE M. (1966) Effect of tool flank wear on the temperatures generated during metal cutting, IMTDR conf. proc.

128. HINDS K. (1977) Control of tool wear during metal cutting using a computer and on-line measurements, Int. J. Prod. Res., 3 pp. 291-301.

129. WU S. M. and ERMER D. S. (1966) Maximum profit as the criterion in the determination of the optimum cutting conditions. Trans. ASME journ. Eng. for Industry, 10, pp. 435-439.

130. BRUNSHTEIN G. V. and KUSHNIR E. F. (1974) Calculation of in-feed rates for lathes with adaptive control, Machines and tooling, 8, pp. 17-21.

131. MARTIN P., MUTEL B, and DRAPIER J. P., (1974) Influence of lathe tool wear on the vibrations sustained in cutting, IMTDR conf. proc., pp. 251-257.

132. TAGLIA D., PORTUNATO S. and TONI P. (1976) An approach to on-line measurement of tool wear by spectrum analysis, IMTDR conf. proc. pp. 141-147.

133. MILNER D. A. (1975) An introduction to adaptive control, the Production Engineer, 3 pp. 176-180.

134. CENTNER R. M. and IDELSOHN J. M. (1966) Application of adaptive control to manufacturing processes, Machine tool and materials sorting conf. proc. paper 27.C.

135. MEYER J. and SAUTTER G. (1970) Sinumeric with adaptive control for machine tools, Siemens Review, 4 pp. 236-241.

136. GIESEKE E. (1976) Adaptive Control Constraint and automatic cut distribution system for turning operations, IMTDR conf. proc. pp. 71-77.

137. NACHTIGAL C. (1972) Design of a force feed-back chatter control system, J. of Dynamic systems, measurement and control, trans. ASME, 3, pp 5-10.

138. COMSTOCK T. R., TSE F. S. and LEMON J. R. (1969) Application of controlled mechanical impedence for reducing machine tool vibrations, J. of Engineering for industry, transactions of ASME, 11, 1057-1062.

139. SRINIVASAN K. and NACHTIGAL C. L. (1978) Analysis and Design of machine tool chatter control systems using the regeneration spectrum, J. of dynamics systems, measurement and control, trans. ASME, 9, pp. 191-200.